Dissertation zur Erlangung des Doktorgrades

der Fakultät für Chemie und Pharmazie

der Ludwig-Maximilians-Universität München

Investigations on Cyclic Esters and Amides in Superacidic Media

Stefanie Beck

aus

Hannover, Deutschland

2022

Erklärung

Diese Dissertation wurde im Sinne von § 7 der Promotionsordnung vom 28. November 2011 von Herrn Prof. Dr. Andreas J. Kornath betreut.

Eidesstattliche Versicherung

Diese Dissertation wurde selbstständig und ohne unerlaubte Hilfe erarbeitet.

München, den 04.05.2022

……

Stefanie Beck

Dissertation eingereicht am	02.02.2022
1. Gutachter:	Prof. Dr. A. J. Kornath
2. Gutachter:	Prof. Dr. T. M. Klapötke
Mündliche Prüfung am	21.03.2022

„Man braucht nichts im Leben zu fürchten,

man muss nur alles verstehen."

Marie Curie

Danksagung

Mein größter Dank gilt Herrn Prof. Dr. Andreas J. Kornath für die Möglichkeit meine Dissertation in seinem Arbeitskreis und unter seiner Anleitung anzufertigen. Ich möchte mich hiermit für die herzliche Aufnahme in seinen Arbeitskreis, sowie die interessante und herausfordernde Themenstellung bedanken. Danke, für die große Forschungsfreiheit, den hilfreichen, fachlichen Austausch und die Unterstützung.

Des Weiteren bedanke ich mich herzlich bei Herrn Prof. Dr. Thomas M. Klapötke für die Übernahme der Zweitkorrektur dieser Arbeit.

Dem gesamten Arbeitskreis gebührt natürlich auch ein riesiges Dankeschön für die unvergessliche Zeit. Danke an Michi, Manu, Domi, Ines, Yvonne, Flo, Fabi, Lukas, Chris, Alan, Marie, Alex, Basti, Dirk, Julian und Valentin für viele schöne, lustige und bereichernde Momente.

Ein spezieller Dank gilt Chris für das Aufnehmen und Lösen von meinen Kristallstrukturen, die dich sicher einige Nerven gekostet haben. Danke für die vielen konstruktiven und vor allem die nicht so konstruktiven Gespräche in unserer Doktorandenzeit und für deine Freundschaft.

Darüber hinaus bedanke ich mich bei meinen PraktikantInnen Thomas, Laura, Vanessa, Milica und Lea für die tolle Mitarbeit an einzelnen Themen meiner Doktorarbeit. Vielen Dank für euren großen Beitrag.

Vielen Dank auch an Gaby, die stets ein offenes Ohr und bei Problemen immer einen guten Rat hatte.

Herzlichen Dank auch an Kathi für die Mühe und Sorgfalt beim Korrekturlesen.

Abschließend möchte ich mich bei meinen Freunden bedanken, die mich während meines gesamten Studiums und meiner Promotion begleitet haben. Danke, für die vielen damit einhergehenden unvergesslichen Erlebnisse (WYB). Ein besonderer Dank gilt Constantin. Danke, für deinen Zuspruch, deine Geduld, deine Unterstützung und dass du mich immer zum Lachen bringst.

Table of Contents

1. Introduction

Simple cyclic esters and amides are referred to as lactones and lactams, respectively. A possibility to build lactones and lactams is the intramolecular cyclodehydration of hydroxyl carboxylic acids or amino carboxylic acids.[1–3] According to the *IUPAC* lactones and lactams are defined as compounds containing an 1-oxacycloalkan-2-one or 1-azacycloalkan-2-one structure, respectively.[4] Since this nomenclature is sometimes complicated, retained names are still very common. Their naming is composed of the ring size together with the retained names of the respective hydroxyl or amino carboxylic acids from which the lactone or lactam can be formally formed.[5] Depending on the ring size, or more precisely the number of carbon atoms that do not belong to the ester or amide group, a distinction is made between e.g. *β*-lactone, *γ*-lactone and *δ*-lactone. To specify the structure, the retained name of the carboxylic acid is added (see Scheme 1).[5]

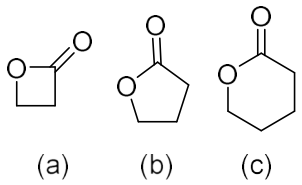

Scheme 1. Lewis structures of *β*-propiolactone (a), *γ*-butyrolactone (b) and *δ*-valerolactone (c).

Higher substituted cyclic esters and amides are usually named as saturated heterocycles according to the revised Hantzsch-Widman system of nomenclature.

In general, the motif of cyclic esters and amides is very common in natural products.[6–10] An example is 2-oxostenine, an alkaloid isolated from the root of *Stemona tuberosa,* which is used in traditional Chinese medicine.[11] In particular, *γ*-butyrolactone is present in about 10% of all natural products known to date.[9,10,12] Common synthetic strategies for five-membered cyclic esters are e.g. the Baeyer-Villiger oxidation, the Beckmann rearrangement and the Ritter reaction.[13–16] An elegant method for synthesis of four-membered lactams and lactones is the Staudinger ketene cycloaddition.[17,18] Although five-membered cyclic esters and amides play an important role in natural products, the four-membered ring systems are of even greater importance. Most important is the *β*-lactam motif in the eponymous class of antibiotics with its best-known representative penicillin.

In 1928 *A. Fleming* discovered an infection on some *Staphylococcus*-inoculated Petri dishes with a fungus called *Penicillium notatum*.[19,20] He observed that the *Staphylococcus* colonies were absent in a circularly pattern around the mold, which he attributed to lysis taking place.[21] In further

experiments *A. Fleming* identified the metabolites of *Penicillium notatum* as antibacterial agents, which he named penicillin.[21,20] This antibacterial, today known as penicillin G, inhibits bacterial cell wall synthesis and thus bacterial growth.[22] More than ten years later, *E. B. Chain* and *Lord H. Florey* succeeded in isolating penicillin and producing it on an industrial scale. [19,20] In 1945 *Fleming*, *Chain* and *Florey* were awarded by the Nobel Prize in Medicine.

D. C. Hodgkin provided in 1945 the X-ray structure analysis of penicillin G and thus proof of the existence of the *β*-lactam motif (see Scheme 2).[19]

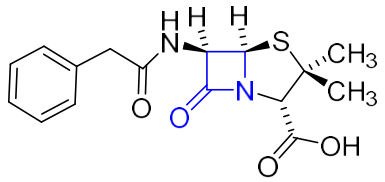

Scheme 2. Lewis structure of penicillin G with highlighted *β*-lactam motif.

This achievement was indispensable for the chemical understanding. At molecular level, the mode of action of penicillin G is based on the irreversible ring opening of the *β*-lactam motif.[20] Due to its importance as an antibacterial agent, several studies have been conducted on the stability of penicillin. Interestingly, the instability towards acidic solutions is also due to the opening of the lactam ring based on a prior protonation of the nitrogen.[23,24] This finding was important because oral application was thus problematic due to gastric acid. Altogether, penicillin and its mode of action is a remarkable example of the importance of ring opening reactions in chemistry.

With this in mind, chemists conducted several studies on ring opening reaction of cyclic esters and amides.[25–28] Under conventional acidic and basic conditions, ring opening reaction occurs for these four- and five-membered ring structures. In these studies, the final reaction products are formed by hydrolysis.[25–28]

The situation is different under superacidic conditions, where hydrolysis itself is not possible. Due to the otherwise strongly decreasing acid strength, superacids are free of water.[29] A superacid was defined, by *R. J. Gillespie* in 1971, as an acid that is stronger or as strong as 100% sulfuric acid.[30] The strengths of such superacids can be classified with the *Hammett* acidity function H_0 (see Equation 1) with K_{BH^+} as equilibrium constant, C as the concentration, a as activity and f as the activity coefficient

$$H_0 = -\log a_{H^+} \cdot \frac{f_B}{f_{BH^+}} = -\log K_{BH^+} + \log \frac{C_B}{C_{BH^+}} \quad (1)$$

based on the equilibrium described in Equation (2).[31]

$$B + H^+ \rightleftharpoons BH^+ \quad (2)$$

Experiments in superacidic media opened up new possibilities for understanding organic chemistry and reaction pathways. Of great importance was the work of *G. A. Olah*, who was awarded the Noble Prize in Chemistry in 1994 for his work on carbocations and their chemical properties.

For synthesis strategy, superacidic systems became a useful tool and found more and more applications. Ring opening reactions were also carried out in superacidic media or by addition of a superacidic catalyst.[32–34] However, these studies focused more on the respective desired reaction products, than on possible reaction intermediates.

For better understanding of reaction pathways, it was again *Olah* who performed an enormous number of studies on the most significant classes of compounds.[29] He investigated higher substituted cyclic esters e.g. ethylene carbonate in the superacidic system $FSO_3H/SbF_5/SO_2$.[35] The prepared protonated species were stable in solution, but were only monitored by ^{1}H-NMR spectroscopy. Later, he investigated numerous of different lactones under same conditions, focusing on whether a ring opening reaction could be observed.[36] All lactones, including γ-butyrolactone and β-propiolactone, were initially protonated on the carbonyl oxygen. Nevertheless the ring structure remained untouched with the exception of protonated β-butyrolactone, where an alkyl-oxygen cleavage occurred at temperatures above −50 °C.[36] Interestingly, it was shown by *Hogeveen* et al. that some β-lactone species, stabilized by methyl groups, are more unstable in protic superacidic media. In this case, the protonated species itself was not observed, since ring cleavage already occurred at −80 °C.[37]

Spurred on by these different results, *Kornath* et. al. investigated γ-butyrolactone in the binary superacidic system HF/MF_5 (M = As, Sb).[38] They succeeded in isolating the respective protonated species for the first time. Under these conditions a monoprotonation occurred exclusively on the carbonyl oxygen and no ring opening reaction was observed.

2. Objectives

This thesis aims at the investigation of cyclic esters and amides in superacidic media and can be divided in two parts. The first issue is the investigation of selected five-membered ring compounds in superacidic media with the aim to examine to what extend it is possible to protonate the respective subjects under preservation of the ring structure. As *γ*-butyrolactam only bears two basic centers, it was initially tested in the binary superacidic media HF/MF_5 (*M* = As, Sb), whether a ring opening reaction could be observed. Subsequently, with an increasing number of potential basic centers, ethylene carbonate and parabanic acid were investigated, with the aim to prepare, isolate and structurally characterize the respective cyclic compounds with the highest possible degree of protonation.

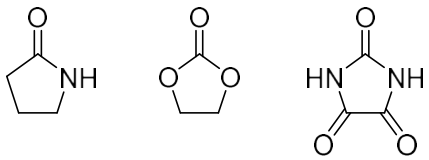

Scheme 3. Lewis structures of *γ*-butyrolactam (left), ethylene carbonate (middle) and parabanic acid (right).

The second issue of this work is the investigation of the ring size at which ring opening reactions can be observed. For this purpose, the four-membered ring compounds *β*-propiolactone and *β*-propiolactam were studied in superacidic media with the aim to examine whether a ring opening reaction occurs and, if so, what kind of cleavage can be observed. Subsequently, it was investigated under which reaction conditions which classes of compounds can be prepared and isolated.

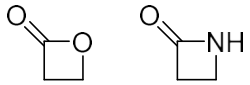

Scheme 4. Lewis structures of *β*-propiolactone (left) and *β*-propiolactam (right).

3. Summary

3.1. Cyclic Five-Membered Esters and Amides

In this part of the thesis, the reaction behavior of five-membered cyclic esters and amides in superacidic media was investigated with regard to the preservation of the cyclic structure and to the extent of protonation. For these studies γ-butyrolactam, ethylene carbonate and parabanic acid were reacted in the binary superacidic systems *X*F/*M*F$_5$ (*X* = H, D; *M* = As, Sb). The obtained salts were characterized by low-temperature infrared and Raman spectroscopy. Additionally, if possible, single-crystal X-ray analyses were conducted. To gain a better understanding of the respective protonated species, quantum chemical calculations were performed. In the following, the results of these investigations are summarized.

3.1.1. γ-Butyrolactam

As the reaction behavior of γ-butyrolactone was already investigated in superacidic media,[38] the isoelectronic species γ-butyrolactam is examined under the same conditions. γ-Butyrolactam reacts in superacidic media according to Equation (3).[39]

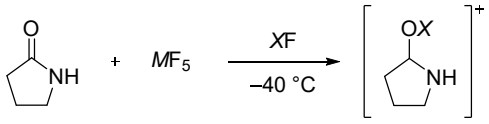

(3)

(*X* = H, D; *M* = As, Sb)

The preservation of the ring structure is confirmed by vibrational spectroscopic analysis. Moreover, only the monoprotonated species of γ-butyrolactam is observed in the vibrational spectra. This finding is confirmed by single-crystal X-ray analysis of $[(CH_2)_3NHCOH][AsF_6]$. An illustration of the interatomic contacts of $[(CH_2)_3NHCOH][AsF_6]$ is displayed in Figure 1. Besides the two hydrogen bonds between cation and anions, a C···F contact is observed in the crystal structure. As these results are in accordance with the investigation of γ-butyrolactone, the nature of these contacts is examined by quantum chemical calculations of the respective cations $[(CH_2)_3OCOH]^+$ and $[(CH_2)_3NHCOH]^+$ on the B3LYP/aug-cc-pVTZ level of theory.

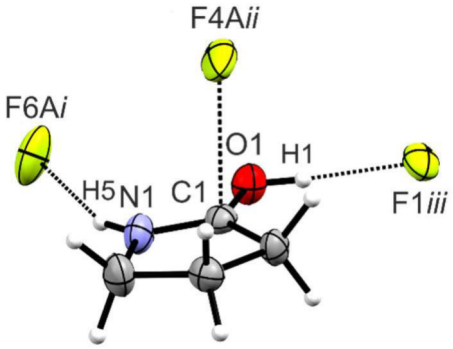

Figure 1. Illustration of interatomic contacts in the $[(CH_2)_3NHCOH][AsF_6]$ crystal (50% probability displacement ellipsoids). Symmetry codes: *i* = −x, −0.5+y, 0.5−z; *ii* = −0.5+x, 0.5−y, −z; *iii* = x, −1+y, z.

As a rate of strength, Mapped Electrostatic Potentials (MEP) are calculated and regions of positive potential are thus located at the respective sp^2-hybridized carbon atoms (see Figure 2). The value for the so-called π-hole is found to be more positive for $[(CH_2)_3OCOH]^+$ compared to $[(CH_2)_3NHCOH]^+$. Interestingly, this leads to the formation of two weaker C···F contacts instead of the formation of one stronger contact.

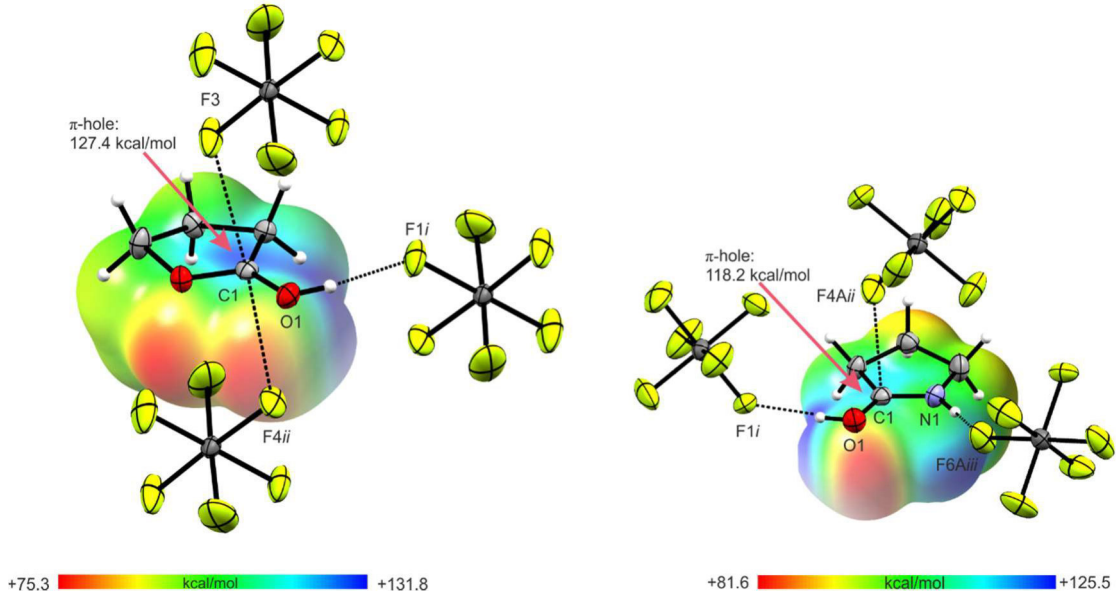

Figure 2. Contacts in the crystal structures of $[(CH_2)_3OCOH][AsF_6]$ (left) and $[(CH_2)_3NHCOH][AsF_6]$ (right) (50% probability displacement ellipsoids). Interatomic contacts are drawn as dashed lines. Behind the cation the respective MEP is illustrated with a color range of 75.3 kcal/mol (red) and 131.8 kcal/mol (blue), isoval. = 0.0004. Symmetry codes: *i* = 1–x, 1–y, –z; *ii* = 1+x, y, z (left) and with a color range of 81.6 kcal/mol (red) and 125.5 kcal/mol (blue), isoval. = 0.0004. Symmetry codes: *i* = x, −1+y, z; *ii* = −0.5+x, 0.5−y, −z; *iii* = −x, −0.5+y, 0.5−z (right).

3.1.2. Ethylene Carbonate

To increase the number of potential basic centers, ethylene carbonate is investigated in superacidic media. Ethylene carbonate reacts according to Equation (4).[40]

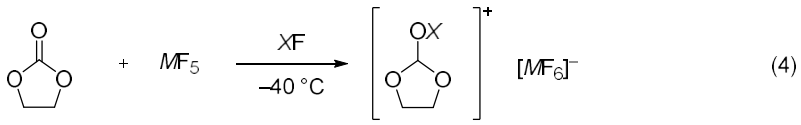

(4)

(*X* = H, D; *M* = As, Sb)

Vibrational spectroscopy confirms the exclusive formation of the monoprotonated species in the form of $[C_3H_5O_3][MF_6]$ (*M* = As, Sb) under preservation of the ring structure. Using an excess of SbF_5 as Lewis acid with respect to ethylene carbonate does not lead to a diprotonated species, but to the formation of $[C_3H_5O_3][Sb_2F_{11}]$. Crystals of this salt were suitable to perform a single-crystal X-ray structure analysis. The structure of the cation is depicted in Figure 3.

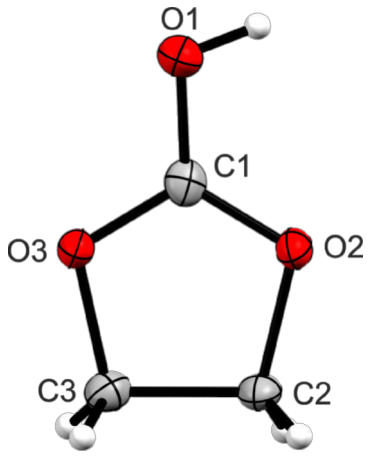

Figure 3. Structure of $[C_3H_5O_3]^+$ (50% probability displacement ellipsoids).

The structural parameters of the crystal structure indicate that all CO bonds belonging to the CO_3 moiety are of equal length within the estimated standard deviations. This can be explained by resonance stabilization, represented by the possible Lewis resonance structures in Scheme 5.

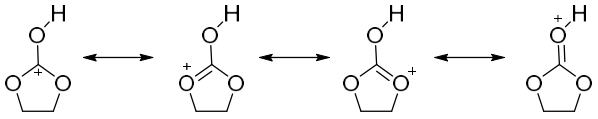

Scheme 5. Lewis resonance structures of monoprotonated ethylene carbonate $[C_3H_5O_3]^+$.

In order to elucidate the bonding situation of the CO_3 moiety, a Natural Bond Orbital (NBO) analysis is carried out on the B3LYP/aug-cc-pVTZ level of theory. As sp^2-hybridization is calculated for both, the central carbon and each oxygen atom, a remarkable 6π-electron delocalization can be assumed. This delocalization is confirmed by ^{13}C NMR spectroscopic measurements. In summary, the protonation of ethylene carbonate leads to a highly resonance stabilized cation.

3.1.3. Parabanic Acid

In order to reach a higher degree of protonation under preservation of the ring structure, parabanic acid is investigated in superacidic media. With its five potential basic centers it reacts according to Equations (5) and (6).[41]

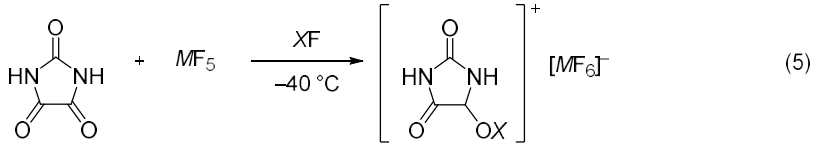

(5)

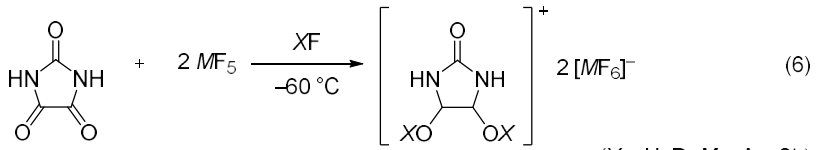

(6)

(*X* = H, D; *M* = As, Sb)

Using an equimolar amount of Lewis acid, with respect to parabanic acid, the monoprotonated species $[C_3H_3N_2O_3][MF_6]$ (*M* = As, Sb) is formed. Vibrational spectroscopy indicates the intact ring structure by revealing the ring breathing mode. This finding is confirmed by single-crystal X-ray structure analysis of the hexafluoridoantimonate of monoprotonated parabanic acid. In addition, the conducted crystal structure analysis shows that the *O*-protonation occurs on one of the neighboring carbonyl groups (see Figure 4).

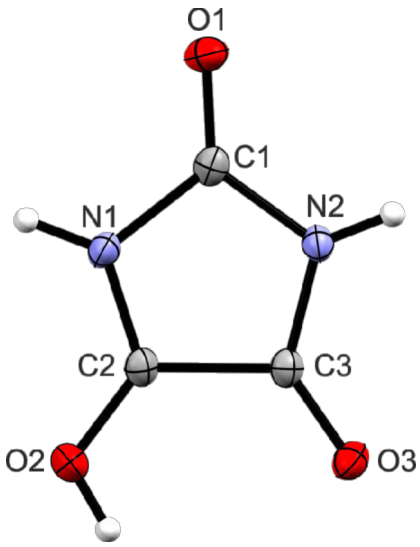

Figure 4. Structure of $[C_3H_3N_2O_3]^+$ (50% probability displacement ellipsoids).

The use of a two-to-one ratio of Lewis acid, with respect to the starting material leads to the formation of the salt $[C_3H_4N_2O_3][MF_6]_2$ (M = As, Sb). Herein, vibrational spectroscopic studies point out that the twofold protonation occurs on the oxygen atoms. The exclusive occurrence of the protonation on the two neighboring carbonyl groups is confirmed by single-crystal X-ray analysis of the hexafluoridoarsenate of diprotonated parabanic acid. In Figure 5, the structure of the dication in $[C_3H_4N_2O_3][AsF_6]_2 \cdot 4HF$ is displayed.

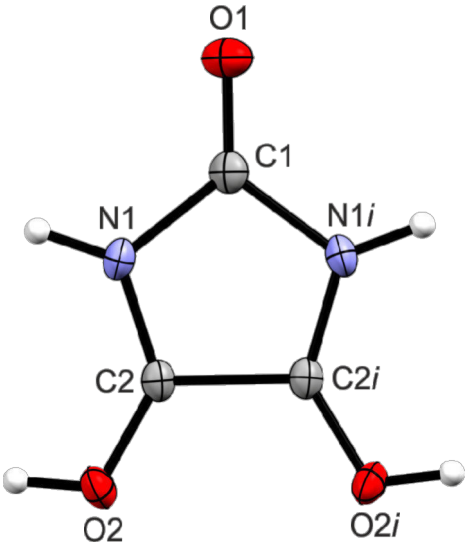

Figure 5. Structure of $[C_3H_4N_2O_3]^{2+}$ (50% probability displacement ellipsoids).

Symmetry code: i = 1 – x, y, 1.5 – z.

Using an eight-to-one ratio of Lewis acid, with respect to the starting material, also leads to the formation of the diprotonated species of parabanic acid. In this study no triprotonated species was observed. With the aim to determine where the positive charges are located, Mapped Electrostatic Potentials (MEP) together with Natural Popular Analysis (NPA) charges are calculated on the B3LYP/aug-cc-pVTZ level of theory. A comparison of parabanic acid with the diprotonated species $[C_3H_4N_2O_3]^{2+}$ is illustrated in Figure 6.

The positive electrostatic potential (blue), which is calculated to be inside the entire five-membered ring structure for parabanic acid, is located between the neighboring carbon atoms after the twofold protonation. In accordance to that, the NPA charges of the positive carbon atoms increase, while the negative charges of oxygen and nitrogen atoms decrease. Diprotonated parabanic acid can be described as a 1,2-*C*,*C* dication, where the positive charges are slightly compensated by the neighboring nitrogen and oxygen atoms.

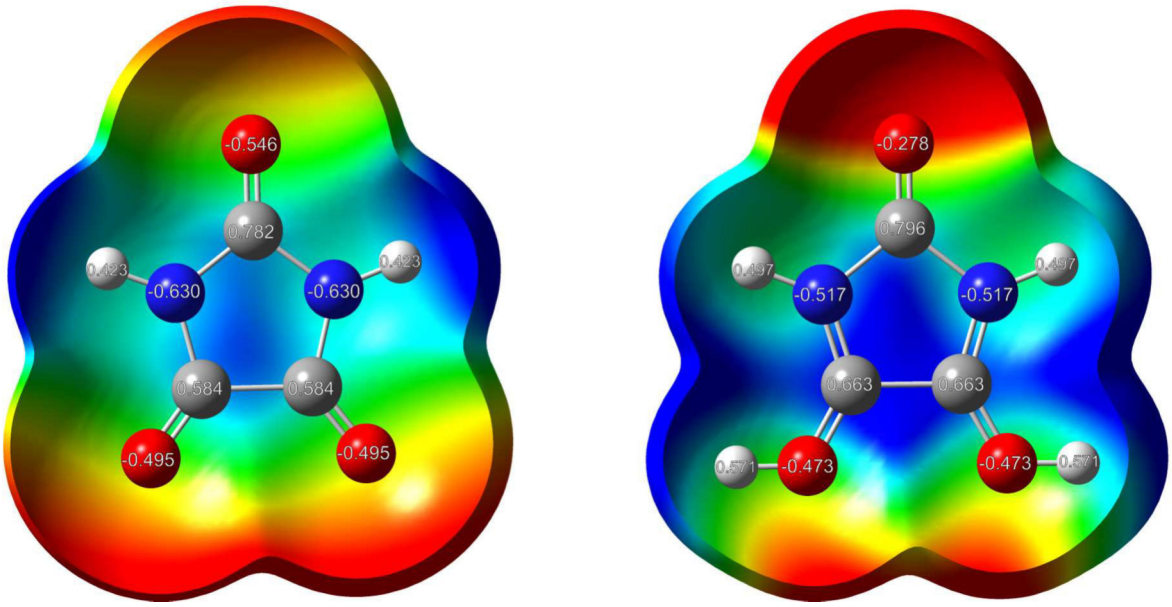

Figure 6. Molecular 0.0004 bohr^{-3} 3D isosurfaces with mapped electrostatic potential as a color scale ranging from −0.03142 a.u. (red) to 0.05124 a.u. (blue) (left) and a color scale ranging from 0.20 a.u. (red) to 0.31 a.u. (blue) (right). The electrostatic potential isosurfaces and the NPA charges have been calculated for $C_3N_2O_3H_2$ (left) and $[C_3H_4N_2O_3]^{2+}$ (right).

3.2. Cyclic Four-Membered Esters and Amides

The second issue of this thesis is focused on the behavior of four-membered cyclic esters and amides in the binary superacidic systems HF/SbF_5 and HF/AsF_5. Therefore, the compounds oxetan-2-one and 2-azetidinone, better known as *β*-propiolactone and *β*-propiolactam, were examined under several conditions. Special attention was paid to possible ring opening reactions and resulting new compounds. For a complete structural understanding vibrational spectroscopic studies and single-crystal X-ray structure analyses were conducted. To gain a better insight into the reaction behavior, quantum chemical calculations were performed additionally. The results of these studies are summarized in the following.

3.2.1. *β*-Propiolactone

β-Propiolactone reacts in the binary superacidic system HF/MF_5 (M = Sb, As) according to Scheme 6.[42]

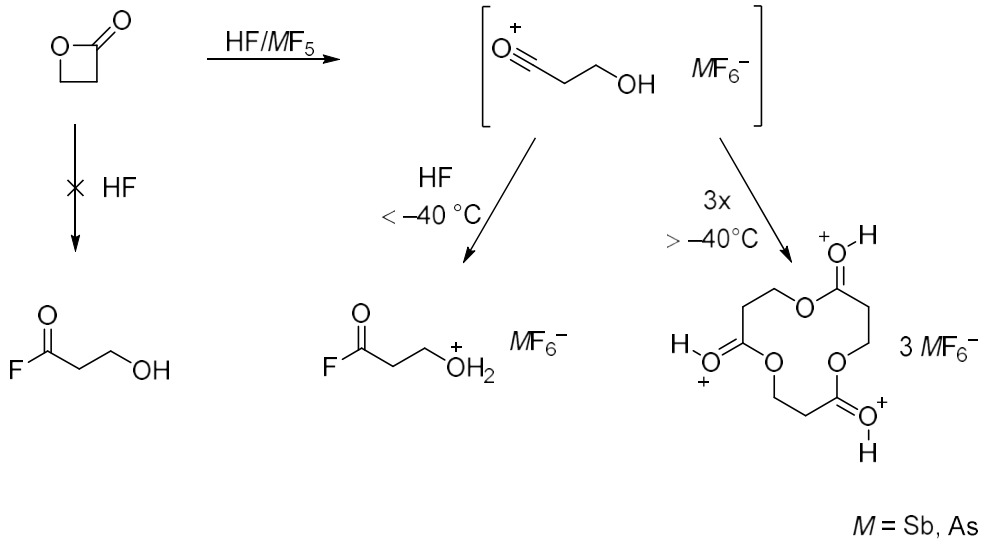

Scheme 6. Reaction scheme of *β*-propiolactone in HF/MF_5 (M = Sb, As).

Choosing reaction conditions with a reaction temperature below −40 °C leads to the formation of salts of monoprotonated 3-hydroxypropanoyl fluoride $[H_2O(CH_2)_2C(O)F][MF_6]$ (M = Sb, As). The formation can be explained by the formal addition of an HF molecule to an assumed acyl cation in the form of $[HO(CH_2)_2CO][MF_6]$ (M = Sb, As). Both, loss of the ring structure as well as the newly formed acyl fluoride group and protonated alcohol group, are evidenced by vibrational

spectroscopy. Single-crystal X-ray structure analysis of the hexafluoridoantimonate of monoprotonated 3-hydroxypropanoyl fluoride confirms the structure of the so far unknown cation. Interestingly, a chain motif is built by the cations in the solid state, which is shown in Figure 7.

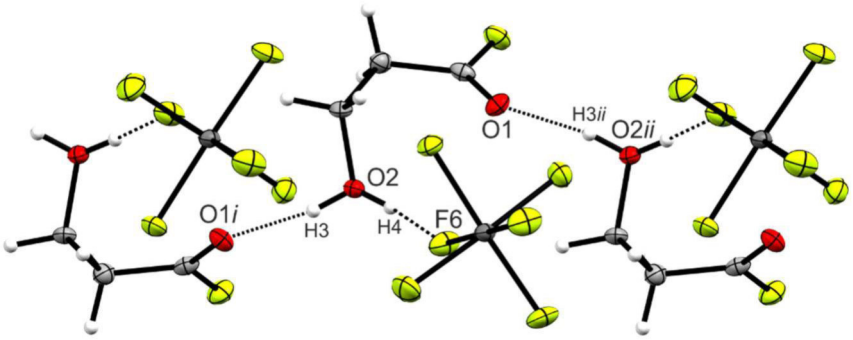

Figure 7. Projection of interatomic contacts in the crystal structure of $[H_2O(CH_2)_2C(O)F][SbF_6]$ (50% probability displacement ellipsoids). Symmetry codes: *i* = −0.5+x, 0.5−y, z; *ii* = 0.5+x, 0.5−y, z.

In contrast, a reaction temperature above −40 °C leads to the exclusive formation of the triprotonated species of 1,5,9-trioxacyclododecane-2,6,10-trione $[C_9H_{15}O_6][MF_6]_3$ (*M* = Sb, As). The formation of this compound can be explained by esterification of three of the assumed acyl cations $[HO(CH_2)_2CO][MF_6]$ (M = Sb, As). Vibrational spectroscopic studies indicate the successful synthesis of the tricationic species by good agreement with reported literature data of protonated esters.[39] The structure is finally clarified by single-crystal X-ray structure analysis of $[C_9H_{15}O_6][SbF_6]_3$. An illustration of the interatomic contacts is shown in Figure 8.

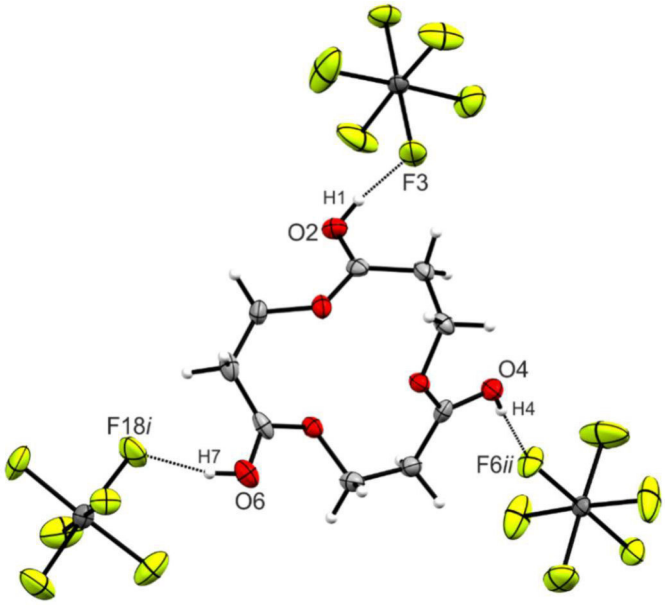

Figure 8. Illustration of interatomic contacts in the $[C_9H_{15}O_6][SbF_6]_3$ crystal (50% probability displacement ellipsoids). Symmetry codes: *i* = −1+x, y, z; *ii* = 2.5−x, 0.5+y, 0.5−z.

It must be emphasized that reacting *β*-propiolactone only with HF does not lead to the formation of the neutral compound 3-hydroxypropanoyl fluoride. Thus, the addition of at least stoichiometric amounts of Lewis acid are required for the ring opening reaction.

In both reactions, the existence of an acyl cation is assumed, which can be formed by an acyl-oxygen cleavage of the protonated species of *β*-propiolactone (proton on the ring oxygen). However, the protonation on the carbonyl oxygen of *β*-propiolactone is calculated to be preferred and its existence was already reported by *Olah*, in a study on different lactones in $FSO_3H/SbF_5/SO_2$.[36] Nevertheless, the protonation of the ring oxygen is needed for the cleavage. A possibility to obtain the protonated species (proton on the ring oxygen) is an intramolecular1,3-proton shift (see Scheme 7).

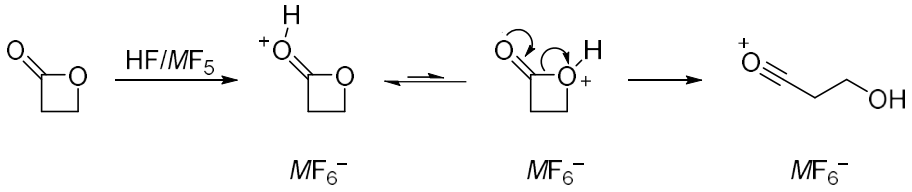

Scheme 7. Possible reaction pathway to obtain acyl cation from *β*-propiolactone.

Therefore, this proton shift along the intrinsic reaction coordinate (IRC) path starting from protonated *β*-propiolactone (protonated on the carbonyl oxygen) is calculated in the gas phase on the MP2/aug-cc-pVTZ level of theory. The calculated energy barrier to overcome the transition state is very high (243 kJ/mol) in the gas phase and more comparable with an aprotic solvent environment. This result leads to the assumption, that protic solvents such as anhydrous HF are required to reduce this barrier and enable the proton transfer.

3.2.2. *β*-Propiolactam

The reactions of *β*-propiolactam in the superacidic system HF/MF_5 (*M* = Sb, As) described in Equations 7 and 8 are observed.[43]

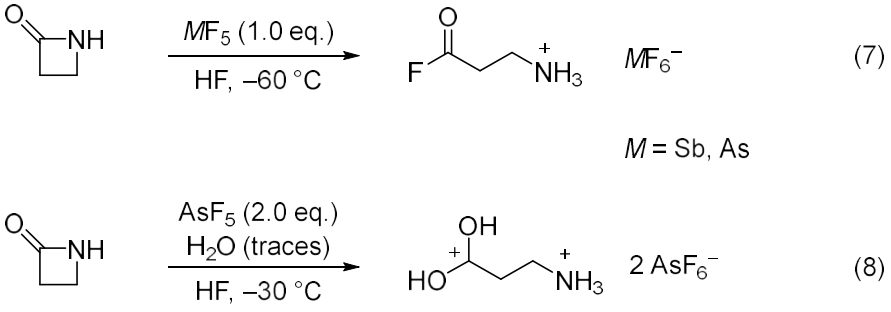

(7)

(8)

Using an equimolar amount of the Lewis acid with respect to *β*-propiolactam, salts of monoprotonated 3-aminopropanoyl fluoride $[C(O)F(CH_2)_2NH_3][SbF_6]$ and $[C(O)F(CH_2)_2NH_3][AsF_6]$ are obtained. The loss of the ring structure, as well as the formation of the acyl fluoride group and the protonated primary amine group are confirmed by vibrational spectroscopy. The final clarification of the structure is achieved by single-crystal X-ray diffraction of the hexafluoridoantimonate of monoprotonated 3-aminopropanoyl fluoride. The structure of the cation of $[C(O)F(CH_2)_2NH_3][SbF_6]$ is shown in Figure 9.

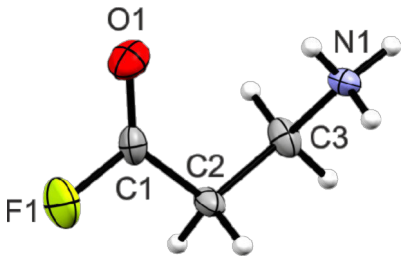

Figure 9. Structure of $[C(O)F(CH_2)_2NH_3]^+$ (50% probability displacement ellipsoids).

The formation of this open-chain compound can be explained by the previous protonation of *β*-propiolactam followed by acyl-nitrogen cleavage to form an assumed acyl cation $[NH_2(CH_2)_2CO]^+$. The formal addition of an HF molecule leads to the formation of monoprotonated 3-aminopropanoyl fluoride.

Using two equivalents of arsenic pentafluoride in presence of water traces leads to the formation of diprotonated *β*-alanine $[C(OH)_2(CH_2)_2NH_3][AsF_6]_2$. The addition of an H_2O molecule to the above-mentioned assumed acyl cation, followed by the protonation of the primary amine group results in the diprotonated species. Vibrational spectroscopy indicates the formation of this so far unknown compound and single-crystal X-ray diffraction confirms it. The structure of the cation of $[C(OH)_2(CH_2)_2NH_3][AsF_6]_2$ is displayed in Figure 10.

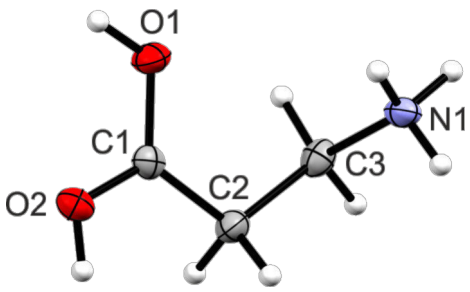

Figure 10. Structure of $[C(OH)_2(CH_2)_2NH_3]^+$ (50% probability displacement ellipsoids).

Interestingly, no protonated species which preserve an intact ring structure was observed by using the protic solvent HF. Changing the solvent from HF to SO_2 does not prevent the ring opening reaction either. Instead, the following reaction is observed (Equation 9).

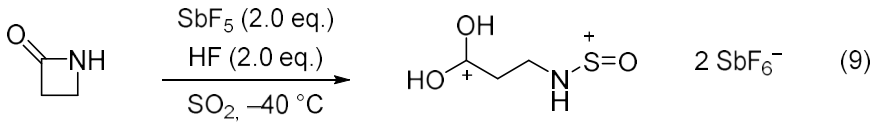

We succeeded in the determination of the structure of the salt $[C(OH)_2(CH_2)_2NHSO][SbF_6]_2 \cdot HF$ by single-crystal X-ray diffraction. The structure of the cation is displayed in Figure 11.

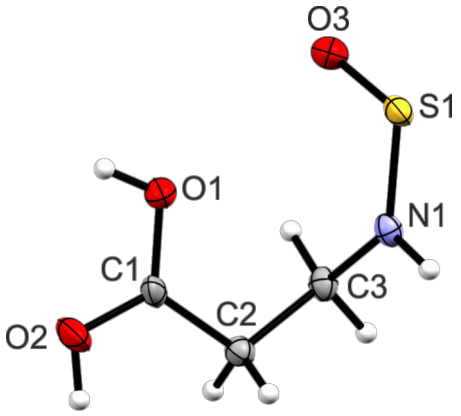

Figure 11. Structure of $[C(OH)_2(CH_2)_2NHSO]^{2+}$ (50% probability displacement ellipsoids).

The formation of this compound, containing a newly formed thionylimide moiety, is not obvious when reacting β-propiolactam with HF/SbF_5 in SO_2. A possible reaction pathway is proposed in Scheme 8.

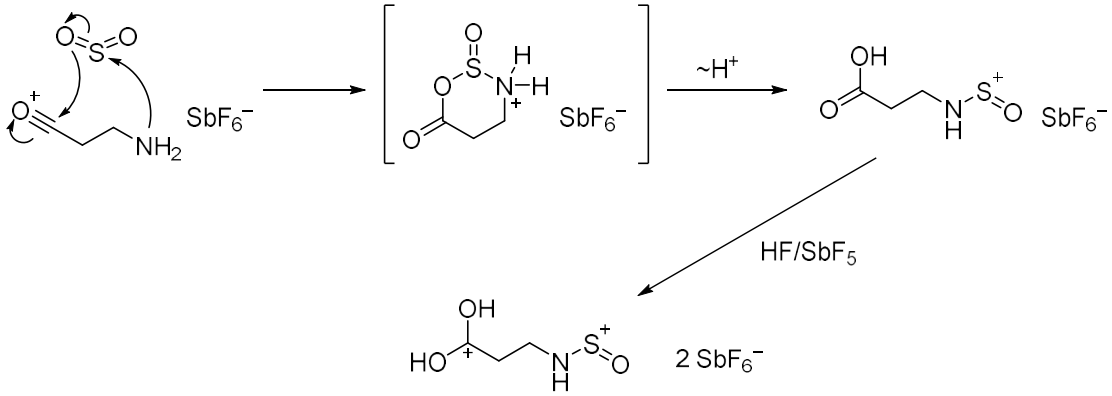

Scheme 8. Possible reaction pathway of formation of $[C(OH)_2(CH_2)_2NHSO][SbF_6]_2$.

Again, this reaction pathway provides an indication for the existence of $[NH_2(CH_2)_2CO]^+$, which is needed for the nucleophilic attack on the sulfur. For a better understanding of this already often postulated, but never isolated acyl cation,[44,27,45] quantum chemical calculations were carried out. In literature, *β*-propiolactam is calculated and described as an oxygen base,[44] which leads us to the calculation of an intramolecular 1,3-proton shift along the intrinsic reaction coordinate (IRC) path starting from oxygen to nitrogen. This calculation showed that the 1,3-proton shift is endothermic and thus unlikely to occur. Consequently, the direct protonation on the nitrogen appears more plausible. To elucidate this assumption, a detailed natural bond orbital (NBO) analysis of both protonated species in comparison with the neutral compound is carried out on the B3LYP/aug-cc-pVTZ level of theory. The results of this calculation show that the *N*-protonated species has a very weak C-N σ bond and is thus the only species that can cause ring opening.

4. Conclusion

The aim of this thesis was to investigate five- and four-membered cyclic esters and amides in the superacidic systems HF/MF_5 (M = Sb, As). In case of the five-membered ring structures, the studies showed the preservation of the ring structure. We succeeded in the monoprotonation of both, a simple representative, γ-butyrolactam, as well as species with more potential basic centers as ethylene carbonate and parabanic acid. In case of parabanic acid, we could also synthesize the diprotonated species in the form of a 1,2-C,C dication.

The studies regarding the simplest representatives of cyclic four-membered esters and amides provided deviating results. By reacting β-propiolactone and β-propiolactam in superacidic media, only open-chain compounds were observed. This way, the ring opening reaction occurs exclusively by acyl-oxygen, or respectively acyl-nitrogen, cleavage. For both compounds, the cleavage is deemed to result in the formation of a highly reactive acyl cationic intermediate which was too reactive for isolation. In a subsequent reaction with the solvent HF, a new synthetic access for acyl fluoride groups was found by preparing protonated 3-hydroxypropanoyl fluoride and protonated 3-aminopropanoyl fluoride. When changing the reaction conditions, a variety of different and so far unknown compounds were synthesized, isolated and structurally characterized.

[1] D. R. Storm, D. E. Koshland, *J. Am. Chem. Soc.* **1972**, *94*, 5805–5814.
[2] A. Bladé-Font, *Tetrahedron Lett.* **1980**, *21*, 2443–2446.
[3] S. Kobayashi, T. Iimori, T. Izawa, M. Ohno, *J. Am. Chem. Soc.* **1981**, *103*, 2406–2408.
[4] V. Gold, *The IUPAC Compendium of Chemical Terminology*, International Union of Pure and Applied Chemistry (IUPAC), Research Triangle Park, NC, **2019**.
[5] T. Schirmeister, C. Schmuck, P. R. Wich, D. N. Bamberger, *Beyer/Walter Organische Chemie*, Hirzel Verlag, Stuttgart, **2016**.
[6] J.-P. Deprés, P. Delair, J.-F. Poisson, A. Kanazawa, A. E. Greene, *Acc. Chem. Res.* **2016**, *49*, 252–261.
[7] T. J. Donohoe, C. J. R. Bataille, G. H. Churchill, *Annu. Rep. Prog. Chem., Sect. B: Org. Chem.* **2006**, *102*, 98.
[8] M. M. Heravi, M. Ghanbarian, V. Zadsirjan, B. Alimadadi Jani, *Monatsh. Chem.* **2019**, *150*, 1365–1407.
[9] H. M. R. Hoffmann, J. Rabe, *Angew. Chem. Int. Ed.* **1985**, *24*, 94–110.
[10] M. Seitz, O. Reiser, *Curr. Opin. Chem. Biol.* **2005**, *9*, 285–292.
[11] J.-P. Hu, D.-H. Yang, W.-H. Lin, S.-Q. Cai, *Helv. Chim. Acta* **2009**, *92*, 2125–2133.
[12] S. S. Canan Koch, A. R. Chamberlin in *Studies in Natural Products Chemistry*, *Vol. 16* (Ed.: A. Rahman), Elsevier, Amsterdam, Lausanne, New-York, **1995**, pp. 687–725.
[13] A. Baeyer, V. Villiger, *Ber. Dtsch. Chem. Ges.* **1899**, *32*, 3625–3633.
[14] E. Beckmann, *Ber. Dtsch. Chem. Ges.* **1886**, *19*, 988–993.
[15] J. J. Ritter, J. Kalish, *J. Am. Chem. Soc.* **1948**, *70*, 4048–4050.
[16] L. Kürti, B. Czakó, E. J. Corey, K. C. Nicolaou, *Strategic applications of named reactions in organic synthesis*, Elsevier Academic Press, Amsterdam, Boston, Heidelberg, **2005**.
[17] C. Palonao, J. M. Aizpurua, *Trends Org. Chem.* **1993**, *4*, 637–659.
[18] J. A. Hyatt, P. W. Raynolds in *Organic Reactions*, John Wiley & Sons, Inc, Hoboken, NJ, USA, **2004**, pp. 159–646.
[19] C. Friedrich, *Pharm. Unserer Zeit* **2006**, *35*, 392–398.
[20] L. M. Lima, B. N. M. Da Silva, G. Barbosa, E. J. Barreiro, *Eur. J. Med. Chem.* **2020**, *208*, 112829.
[21] A. Fleming, *Br. J. Exp. Pathol.* **1929**, *10*, 226–236.
[22] P. M. Blumberg, J. L. Strominger, *Bacteriol. Rev.* **1974**, *38*, 291–335.
[23] R. G. Benedict, W. H. Schmidt, R. D. Coghill, *J. Bacteriol.* **1946**, *51*, 291–292.
[24] R. G. Benedict, W. H. Schmidt, R. D. Coghill, A. P. Oleson, *J. Bacteriol.* **1945**, *49*, 85–95.
[25] H. K. Hall, M. K. Brandt, R. M. Mason, *J. Am. Chem. Soc.* **1958**, *80*, 6420–6427.
[26] P. Imming, B. Klar, D. Dix, *J. Med. Chem.* **2000**, *43*, 4328–4331.
[27] R. A. Cox, K. Yates, *Can. J. Chem.* **1981**, *59*, 2853–2863.
[28] A. R. Olson, J. L. Hyde, *J. Am. Chem. Soc.* **1941**, *63*, 2459–2461.
[29] G. A. Olah, G. K. S. Prakash, J. Sommer, A. Molnar, *Superacid chemistry*, Wiley, Hoboken, NJ, **2009**.
[30] R.J. Gillespie, T.E. Peel, *Adv. Phys. Org. Chem.* **1971**, *9*, 1–24.
[31] L. P. Hammett, A. J. Deyrup, *J. Am. Chem. Soc.* **1932**, *54*, 2721–2739.
[32] K. W. Anderson, J. J. Tepe, *Org. Lett.* **2002**, *4*, 459–461.
[33] S. P. Kotun, D. D. DesMarteau, *Can. J. Chem.* **1989**, *67*, 1724–1728.
[34] Y. Hu, X. Fu, B.-D. Barry, X. Bi, D. Dong, *Chem. Commun. (Cambridge, U. K.)* **2012**, *48*, 690–692.
[35] G. A. Olah, A. M. White, *J. Am. Chem. Soc.* **1968**, *90*, 1884–1889.
[36] G. A. Olah, A. T. Ku, *J. Org. Chem.* **1970**, *35*, 3916–3922.
[37] H. Hogeveen, *Recl. Trav. Chim. Pays-Bas* **1968**, *87*, 1303–1312.
[38] M. Feller, *Dissertation*, LMU Munich **2016**.
[39] S. Beck, M. Feller, L. Spies, K. J. Dietrich, C. Jessen, K. Stierstorfer, A. J. Kornath, *ChemistryOpen* **2021**, *10*, 8–15.

[40] S. Beck, C. Jessen, A. J. Kornath, *ChemistryOpen* **2021**, *10*, 1160–1165.
[41] S. Beck, M. Raljic, C. Jessen, A. J. Kornath, *Eur. J. Org. Chem.* **2020**, *29*, 4521–4527.
[42] S. Beck, C. Jessen, A. J. Kornath, *Eur. J. Org. Chem.* **2021**, *48*, 6628–6635.
[43] S. Beck, V. Rück, L.-V. Pietsch, C. Jessen, A. J. Kornath, *Chem. Eur. J.* **2022,** *in press*.
[44] J. L. M. Abboud, T. Canada, H. Homan, R. Notario, C. Cativiela, M. D. Diaz de Villegas, M. C. Bordeje, O. Mo, M. Yanez, *J. Am. Chem. Soc.* **1992**, *114*, 4728–4736.
[45] P. Wan, T. A. Modro, K. Yates, *Can. J. Chem.* **1980**, *58*, 2423–2432.

5. Appendix

The following appendix contains a list of publications and conference contributions, the manuscripts, supporting information and cover pictures, which are published in the context of this dissertation. All manuscripts have been peer-reviewed and published in scientific journals. The publications are thematically listed, and in the same order as they are summarized in this thesis.

5.1. List of Publications and Conference Contributions

5.1.1. Publications

1. S. Beck, M. Feller, L. Spies, K. J. Dietrich, C. Jessen, K. Stierstorfer, A. J. Kornath, *Protonation of γ-Butyrolactone and γ-Butyrolactam*, *ChemistryOpen* **2021**, *10*, 8–15. (DOI: 10.1002/open.202000220) (Cover Picture)

2. S. Beck, C. Jessen, A. J. Kornath, *Protonated Ethylene Carbonate: A Highly Resonance-Stabilized Cation*, *ChemistryOpen* **2021**, *10*, 1160–1165. (DOI: 10.1002/open.202100229) (Cover Picture)

3. S. Beck. M. Raljic, C. Jessen, A. J. Kornath, *Diprotonated Parabanic Acid: A Vicinal or 1, 3-Dication?, Eur. J. Org. Chem.* **2020**, 4521–4527. (DOI: 10.1002/ejoc.202000656)

4. S. Beck, C. Jessen, A. J. Kornath, *Ring Opening and Closure Reactions of β-Propiolactone in the superacids HF/MF_5 (M = Sb, As), Eur. J. Org. Chem.* **2021**, 6628–6635. (DOI: 10.1002/ejoc.202101351) (Cover Picture)

5. S. Beck. V. Rück, L.-V. Pietsch, C. Jessen, A. J. Kornath, *Ring Opening Reactions of β-Propiolactam in Superacidic Media*, *Chem. Eur. J.* **2022**, *in press*. (DOI: 10.1002/chem.202104086) (Cover Feature)

5.1.2. Conference Contributions

1. Poster presentation
   Investigation of Parabanic Acid in highly acidic Media, S. Beck, A. J. Kornath, *19th European Symposium on Fluorine Chemistry,* Warsaw, Poland.

ChemistryOpen

Chemistry Europe
European Chemical Societies Publishing

Front Cover:
Stefanie Beck et al.
Protonation of γ-Butyrolactone and γ-Butyrolactam

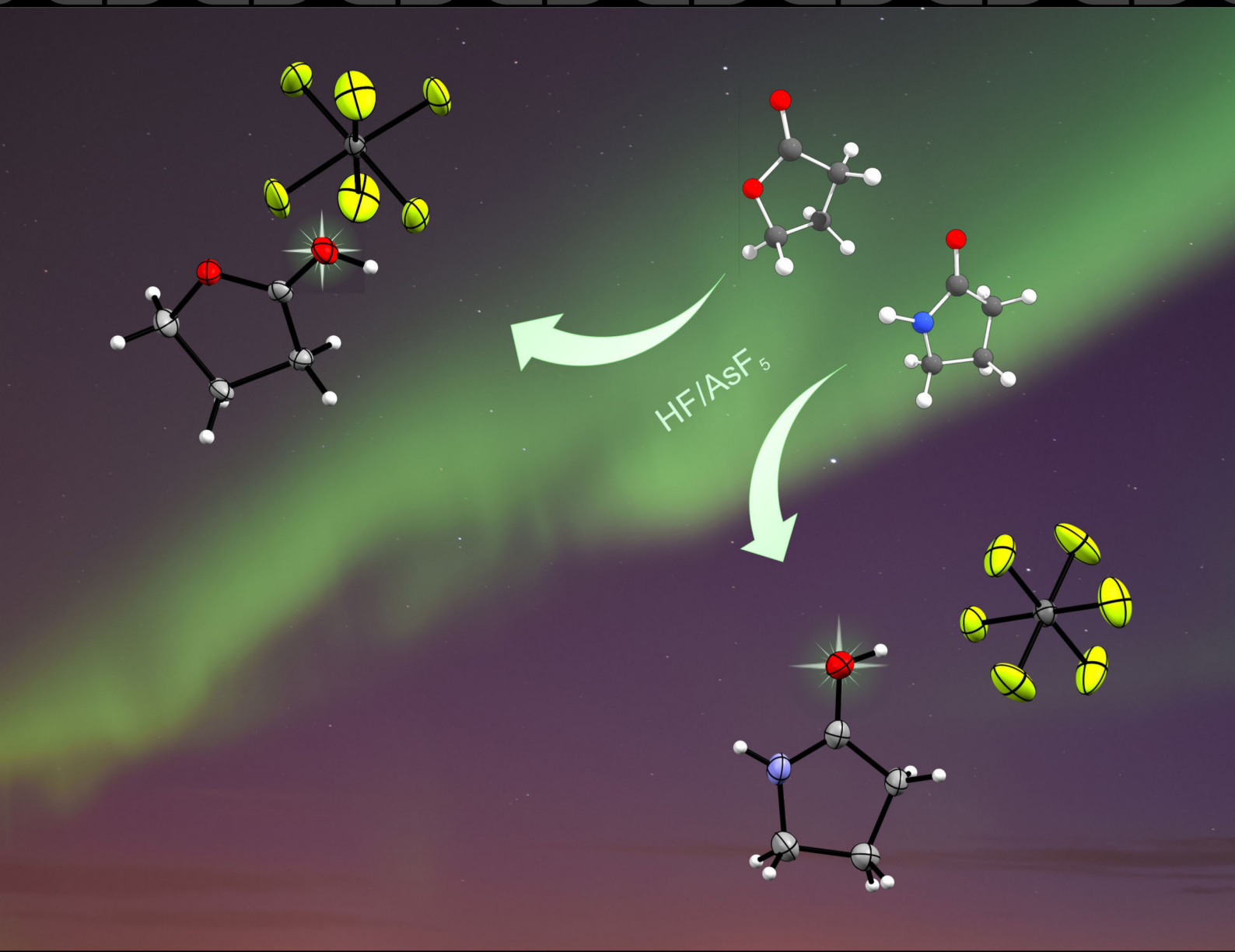

1/2021

WILEY-VCH

Protonation of γ-Butyrolactone and γ-Butyrolactam

Stefanie Beck, Michael Feller, Laura Spies, Kai J. Dietrich, Christoph Jessen, Karin Stierstorfer, and Andreas J. Kornath*[a]

Abstract: γ-Butyrolactone and γ-butyrolactam were reacted in the superacidic systems XF/MF_5 (X = H, D; M = As, Sb). Salts of the monoprotonated species of γ-butyrolactone were obtained in terms of $[(CH_2)_3OCOH]^+[AsF_6]^-$, $[(CH_2)_3OCOH]^+[SbF_6]^-$ and $[(CH_2)_3OCOD]^+[AsF_6]^-$ and the analogous lactam salts in terms of $[(CH_2)_3NHCOH]^+[AsF_6]^-$, $[(CH_2)_3NHCOH]^+[SbF_6]^-$ and $[(CH_2)_3NDCOD]^+[AsF_6]^-$. The salts were characterized by low temperature Raman and infrared spectroscopy and for both protonated hexafluoridoarsenates, $[(CH_2)_3OCOH]^+[AsF_6]^-$ and $[(CH_2)_3NHCOH]^+[AsF_6]^-$, single-crystal X-ray structure analyses were conducted. In addition to the experimental results, quantum chemical calculations were performed on the B3LYP/aug-cc-pVTZ level of theory. As in both crystal structures C···F contacts were observed, the nature of these contacts is discussed with Mapped Electrostatic Potential as a rate of strength.

1. Introduction

Many natural products include a γ-butyrolactone or γ-butyrolactam moiety as structural element.[1,2] Especially the γ-butyrolactone motif is present in about 10% of all natural products.[3–5] In total syntheses, a common strategy to synthesize the γ-butyrolactone motif is the Baeyer-Villinger oxidation.[2,6] Herein, an ester is formed from a ketone by using peroxyacids or peroxides. The Beckmann rearrangement instead, which is used to obtain γ-butyrolactam motifs, is the rearrangement of an oxime into an amide under ring expansion.[2,7] Another synthesis strategy for both cyclic compounds is the catalyzed cyclodehydration of the corresponding hydroxyl acid,[8] respectively amino acid.[9] Interestingly, in case of γ-butyrolactone, both, the lactonization[8] and the hydrolysis,[10] are acid-catalyzed (see Equation 1).

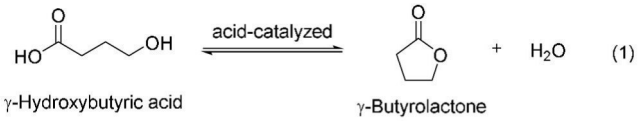

Equation 1. Acid-catalyzed lactonization to γ-butyrolactone or hydrolysis to γ-hydroxybutyric acid.

Since both cyclic compounds are abundant in natural products and their protonated species can occur in syntheses or metabolic cycles, they are of great interest. However, so far, only NMR-spectroscopic investigations of protonated γ-butyrolactone and protonated γ-butyrolactam are reported.[11,12] Under acidic conditions, a ring opening reaction can occur, which prompted us to investigate the reaction behavior of both compounds in superacidic media.

2. Results and Discussion

2.1. Preparation

The synthesis of salts of monoprotonated γ-butyrolactone and γ-butyrolactam was performed according to Equations. (2) and (3)

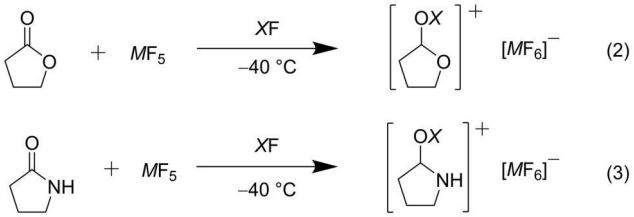

X = H, D
M = As, Sb

Hydrogen or deuterium fluoride, which serve as reagent as well as solvent, were used in excess for preparing the superacidic system. The respective Lewis acids were added, and the resulting mixture was homogenized at −40 °C. After cooling to −196 °C, the starting material γ-butyrolactone, respectively, γ-butyrolactam, was added to the frozen system under nitrogen atmosphere. After warming to −40 °C, all reactants were mixed to form the protonated species, respectively the deuterated species, and the excess of the solvent was removed in a dynamic vacuum at −78 °C. The air- and temperature-sensitive compounds of monoprotonated γ-butyrolactone $[(CH_2)_3OCOH]^+[AsF_6]^-$ (**1**), $[(CH_2)_3OCOH]^+[SbF_6]^-$ (**2**) and the deuterated species $[(CH_2)_3OCOD]^+[AsF_6]^-$ (**3**) were obtained as colorless solids, which decompose at −30 °C. The salts of monoprotonated

[a] S. Beck, Dr. M. Feller, L. Spies, K. J. Dietrich, C. Jessen, Dr. K. Stierstorfer, Prof. Dr. A. J. Kornath
Department of Chemistry
Ludwig-Maximilian University of Munich
Butenandtstr. 5–13, 81377 München (Germany)
E-mail: akoch@cup.uni-muenchen.de
Homepage: http://www.org.chemie.uni-muenchen.de/ac/kornath/

Supporting information for this article is available on the WWW under https://doi.org/10.1002/open.202000220

γ-butyrolactam were obtained in terms of $[(CH_2)_3NHCOH]^+[AsF_6]^-$ (**4**) and $[(CH_2)_3NHCOH]^+[SbF_6]^-$ (**5**). Using the superacidic system DF/AsF_5 led to an H/D exchange at the amide group. The hydrogen atoms were entirely replaced by deuterium and the degree of deuteration reached approximately 98%. The deuterated species is observed in the form of $[(CH_2)_3NDCOD]^+[AsF_6]^-$ (**6**). Salts (**4**), (**5**) and (**6**) are stable up to room temperature. With a larger ratio of Lewis acid, neither for γ-butyrolactone nor for γ-butyrolactam, a diprotonated species was observed.

2.2. Vibrational Spectroscopy

2.2.1. Protonated γ-Butyrolactone

In Figure 1, the Raman and infrared spectra of $[(CH_2)_3OCOH]^+[AsF_6]^-$ (**1**), $[(CH_2)_3OCOH]^+[SbF_6]^-$ (**2**) and $[(CH_2)_3OCOD]^+[AsF_6]^-$ (**3**) are displayed together with the Raman spectrum of γ-butyrolactone. Selected experimental frequencies of (**1**), (**2**) and (**3**) together with quantum-chemically calculated frequencies of the free cations $[(CH_2)_3OCOH]^+$ and $[(CH_2)_3OCOD]^+$ are summarized in Table 1. In Table S1, all observed and calculated frequencies are listed (see Supporting Information). In consequence of the C_1 symmetry of the starting material,[13] no higher symmetry, such as the ideal C_s, is expected for the protonated species. We assumed C_1 symmetry with 33 fundamental vibrations, active in Raman and infrared spectra, for the cation.

A first evidence for a successful protonation is given by the ν(OH) vibration in the infrared spectra of (**1**) and (**2**), which occurs at 3528 cm^{-1} (**1**) and 3460 cm^{-1} (**2**), respectively. In the corresponding Raman spectra, no lines are observed, because of the poor polarizability of the OH stretching vibration. Contrariwise, the OD stretching vibration of $[(CH_2)_3OCOD]^+[AsF_6]^-$ (**3**) is detected at 2239 cm^{-1} (Ra) and 2307 cm^{-1} (IR). The redshift is in good agreement with the Teller-Redlich rule for an H/D isotopic effect.[14] Considering the constitution of the synthesized cation, the ring breathing vibration at about 880 cm^{-1} (Ra, IR) indicates the preservation of the ring structure. Changes in vibrational spectra are observed for the CO stretching vibrations. Due to the protonation, the former CO double bond is weakened and the ν(CO) occurs at 1523 cm^{-1} (Ra) (**1**), at 1522 cm^{-1} (IR) and 1526 cm^{-1} (Ra) (**2**) and at 1510 cm^{-1} (IR and Ra) (**3**).

Compared to the neutral compound,[15] this redshift amounts up to 260 cm^{-1}. In contrast, the former CO single bond, belonging to the lactone moiety, is strengthened and the

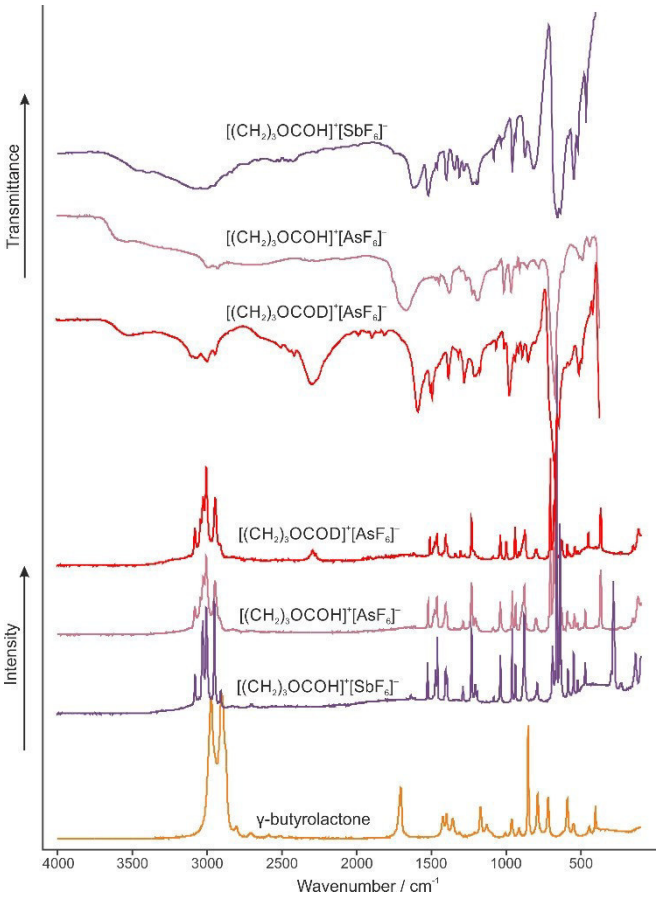

Figure 1. Raman spectrum of γ-butyrolactone, infrared and Raman spectra of $[(CH_2)_3OCOH]^+[AsF_6]^-$ (**1**), $[(CH_2)_3OCOH]^+[SbF_6]^-$ (**2**) and $[(CH_2)_3OCOD]^+[AsF_6]^-$ (**3**).

Table 1. Selected experimental vibrational frequencies [cm^{-1}] of (**1**), (**2**) and (**3**), and calculated vibrational frequencies [cm^{-1}] of $[(CH_2)_3OCOH]^+$ and $[(CH_2)_3OCOD]^+$.

$[(CH_2)_3OCOH]^+[AsF_6]^-$ (1)		$[(CH_2)_3OCOH]^+[SbF_6]^-$ (2)		$[(CH_2)_3OCOD]^+[AsF_6]^-$ (3)		$[(CH_2)_3OCOH]^+$	$[(CH_2)_3OCOD]^+$	Assignment[b]
IR	Raman	IR	Raman	IR	Raman	Calc. (IR/Ra)[a]	Calc. (IR/Ra)[a]	
3528 (vw, br)		3460 (vw, br)		2307 (m)	2293 (14)	3724 (256/61)	2714 (148/29)	ν(O*X*)
1684 (s)	1613 (7)	1616 (m)	1637 (5)	1607 (s)	1619 (12)	1650 (305/0.7)	1635 (383/0.5)	ν(CO)
	1523 (24)	1522 (m)	1526 (14)	1510 (m)	1510 (27)	1523 (161/4)	1515 (74/8)	ν(CO)
1088 (m)	1089 (5)	1084 (w)	1085 (5)	912 (m)	916 (13)	1178 (199/7)	863 (12/1)	δ(CO*X*)
989 (m)		1012 (w)		960 (m)	961 (7)	1029 (3/3)	1029 (6/3)	ν(CC)
955 (m)	959 (33)	959 (m)	961 (24)	1001 (s)	1000 (21)	949 (5/4)	993 (107/6)	ν(CO)
932 (m)	938 (23)	937 (w)	939 (13)	939(m)	941 (35)	934 (1/3)	934 (2/4)	ν(CC)
881 (m)	877 (38)	876 (m)	878 (28)	876 (m)	875 (33)	881 (17/6)	889 (45/5)	ring breathing
806 (m)	800 (13)		793 (8)	800 (m)	799 (15)	796 (11/2)	796 (10/2)	δ(COC)
644 (w)	632 (21)	639 (vs)	633 (50)		450 (30)	611 (77/3)	443 (57/0.2)	$\delta(COX)_{oop}$
515 (m)	525 (9)	525 (s)	524 (3)	523 (m)	523 (13)	517 (25/0.5)	535 (1/0.7)	γ(CCOO)

[a] Calculated on the B3LYP/aug-cc-pVTZ level of theory. IR intensity in km/mol and Raman intensity in $Å^4$/u. Abbreviations for IR intensities: v = very, s = strong, m = medium, w = weak, br = broad. Experimental Raman activities are stated to a scale of 1 to 100. [b] *X* = H, D.

corresponding stretching vibration is detected at 1684 cm^{-1} (IR) and 1613 cm^{-1} (Ra) (**1**), at 1616 cm^{-1} (IR) and 1637 cm^{-1} (Ra) (**2**) and at 1607 cm^{-1} (IR) and 1619 cm^{-1} (Ra) (**3**). The blue shift is up to 306 cm^{-1} compared to γ-butyrolactone.[15] The other CO stretching vibration of the ring skeleton is detected at about 960 cm^{-1} (IR, Ra) for the protonated species (**1** and **2**) and at about 1000 cm^{-1} for the deuterated one (**3**). The δ(COH), respectively the δ(COD), is observed in the range between 1084 cm^{-1} and 1089 cm^{-1} for (**1**) and (**2**) and at 912 cm^{-1} (IR) and 916 cm^{-1} (Ra) for (**3**). More vibrations, which are assigned to the AsF_6^-, respectively the SbF_6^- anion, are observed than were expected for an ideal O_h symmetry. Here, in the Raman spectra more than three lines and in IR spectra more than two bands are detected. The increased number of vibrations indicates a lowered symmetry of the structure of the anions.

2.2.2. Protonated γ-Butyrolactam

The Raman spectrum of γ-butyrolactam together with Raman and IR spectra of $[(CH_2)_3NHCOH]^+[AsF_6]^-$ (**4**), $[(CH_2)_3NHCOH]^+[SbF_6]^-$ (**5**) and $[(CH_2)_3NDCOD]^+[AsF_6]^-$ (**6**) are illustrated in Figure 2. In Table 2, selected experimental frequencies of (**4**), (**5**), and (**6**) with calculated frequencies of the free cations $[(CH_2)_3NHCOH]^+$ and $[(CH_2)_3NDCOD]^+$ are summarized. All observed and calculated frequencies are listed in Table S2 (see Supporting Information).

For protonated γ-butyrolactam, C_1 symmetry with 36 IR and Raman active vibrations, is expected. The assumption of retaining the ring structure is confirmed by the ring breathing vibration at about 900 cm^{-1} (Ra, IR).

The OH stretching vibration, which is the first evidence for a successful protonation, is observed in the IR spectra at 3238 cm^{-1} (**4**) and 3242 cm^{-1} (**5**). In the corresponding Raman spectra, these lines are not observable, due to the poor polarizability of this vibration. In contrast, the ν(NH) vibration occurs in both IR (3364 cm^{-1} (**4**) and 3358 cm^{-1} (**5**)) and Raman spectra (3369 cm^{-1} (**4**) and 3359 cm^{-1} (**5**)). In the spectra of the deuterated species (**6**), the OD stretching vibration occurs at 2492 cm^{-1} (IR) and 2494 cm^{-1} (Ra). The ν(ND) is observed at

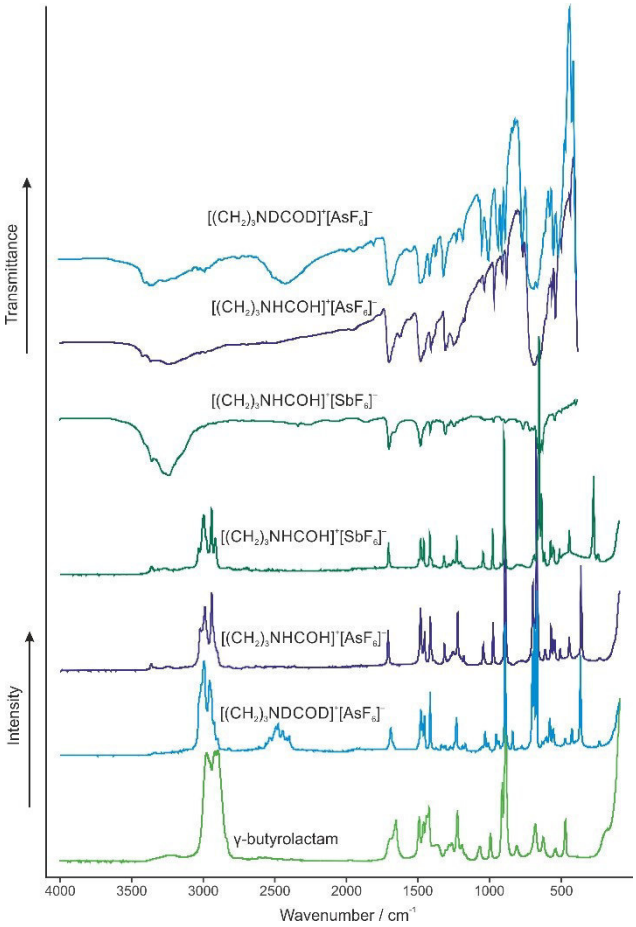

Figure 2. Raman spectrum of γ-butyrolactam, infrared and Raman spectra of $[(CH_2)_3NHCOH]^+[AsF_6]^-$ (**4**), $[(CH_2)_3NHCOH]^+[SbF_6]^-$ (**5**) and $[(CH_2)_3NDCOD]^+[AsF_6]^-$ (**6**).

2430 cm^{-1} (IR) and 2445 cm^{-1} (Ra). These redshifts are in accordance with the Teller-Redlich rule for an H/D isotopic effect.[14] The δ(CO*X*) are observed at about 1190 cm^{-1} for the protonated species (**4** and **5**) and at about 955 cm^{-1} for the deuterated species (**6**). δ(CN*X*) occurs at about 1390 cm^{-1} (**4** and **5**) and at 1180 cm^{-1} (**6**). Due to the protonation, the CO

Table 2. Selected experimental vibrational frequencies [cm^{-1}] of (**4**), (**5**) and (**6**), and calculated vibrational frequencies [cm^{-1}] of $[(CH_2)_3NHCOH]^+$ and $[(CH_2)_3NDCOD]^+$.

$[(CH_2)_3NHCOH]^+[AsF_6]^-$ (4) IR	Raman	$[(CH_2)_3NHCOH]^+[SbF_6]^-$ (5) IR	Raman	$[(CH_2)_3NDCOD]^+[AsF_6]^-$ (6) IR	Raman	$[(CH_2)_3NHCOH]^+$ Calc. (IR/Ra)[a]	$[(CH_2)_3NDCOD]^+$ Calc. (IR/Ra)[a]	Assignment[b]
3238 (w)		3242 (vs)		2492 (w)	2494 (18)	3750 (235/67)	2732 (137/33)	ν(O*X*)
3364 (w)	3369 (3)	3358 (s)	3359 (4)	2430 (w)	2445 (16)	3553 (139/82)	2609 (89/37)	ν(N*X*)
1711 (m)	1716 (16)	1711 (m)	1711 (14)	1691 (m)	1691 (17)	1729 (251/3)	1703 (278/5)	ν(CN)
1462 (w)	1461 (16)	1464 (vw)	1464 (14)	1462 (m)	1456 (24)	1500 (103/7)	1474 (140/5)	ν(CO)
1390 (w)	1393 (4)	1393 (vw)		1186 (w)	1172 (7)	1404 (3/0.7)	1176 (6/2)	δ(CN*X*)
1186 (w)	1189 (5)		1189 (4)	954 (w, sh)	956 (13)	1198 (138/8)	915 (28/9)	δ(CO*X*)
1049 (w)	1052 (10)		1048 (9)	1055 (m)	1056 (6)	1042 (2/2)	1032 (0.3/3)	ν(CN)
982 (m)	983 (20)	982 (vw)	982 (20)	943 (m)	938 (9)	971 (10/3)	938 (11/5)	ν(CC)
926 (w)	924 (sh)	928 (vw)	928 (5)	775 (s)	778 (6)	929 (3/0.2)	809 (6/0.4)	ν(CC)
895 (w)	897 (73)	903 (vw)	902 (58)	895 (m)	895 (79)	896 (5/17)	889 (52/8)	ring breathing
517 (m)	518 (9)	515 (vw)	517 (11)	559 (s)	560 (16)	497 (24/0.6)	665 (21/1)	γ(CCON)

[a] Calculated on the B3LYP/aug-cc-pVTZ level of theory. IR intensity in km/mol and Raman intensity in $Å^4$/u. Abbreviations for IR intensities: v = very, s = strong, m = medium, w = weak. Experimental Raman activities are stated to a scale of 1 to 100. [b] *X* = H, D.

bond is weakened and the vibration occurs at 1462 cm^{-1} (IR) and 1461 cm^{-1} (Ra) (**4**), 1464 cm^{-1} (IR, Ra) (**5**), and at 1462 cm^{-1} (IR) and 1456 cm^{-1}(Ra) (**6**). Compared to the neutral compound, this vibration is redshifted by up to 194 cm^{-1}.[15] Contrariwise, the CN bond is strengthened and its stretching vibration is observed at 1711 cm^{-1} (IR (**4**) and IR and Ra (**5**)), 1716 cm^{-1} (Ra) (**4**) and 1691 cm^{-1} (IR, Ra) (**6**). This blue shift amounts up to 222 cm^{-1} compared to γ-butyrolactam.[15] The remaining stretching modes for the ring bonds nearly are unaffected by the protonation.

For the anions with ideal O_h symmetry, three lines in Raman and two bands in IR spectra are expected, but more are observed for (**4**–**6**). The increased number of vibrations indicates a lowered symmetry of the structure of the AsF_6^- and SbF_6^- anions.

2.3. Crystal Structure of $[(CH_2)_3OCOH]^+[AsF_6]^-$ (1)

The $[AsF_6]^-$ salt of protonated γ-butyrolactone $[(CH_2)_3OCOH]^+$ $[AsF_6]^-$ (**1**) crystallizes in the monoclinic space group $P2_1/c$ with four formula units per unit cell. In Figure 3, the asymmetric unit is shown. Corresponding selected bond lengths and angles are listed in Table 3.

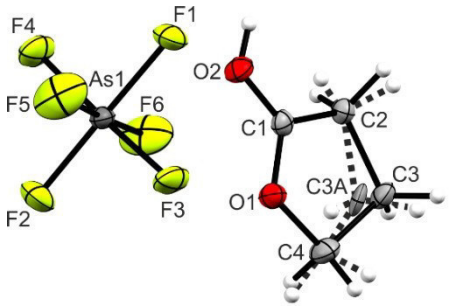

Figure 3. Asymmetric unit of $[(CH_2)_3OCOH]^+[AsF_6]^-$ (**1**) (50% probability displacement ellipsoids). Dashed lines mark disordered position of the C3 atom (C3A).

Table 3. Selected bond lengths [Å] and angles [°] of $[(CH_2)_3OCOH]^+[AsF_6]^-$ (**1**).

Bond lengths [Å]			
C1–O2	1.280(3)	C4–C3A	1.45(1)
C1–O1	1.273(3)	C3–C2	1.543(8)
O1–C4	1.494(3)	C3A–C2	1.54(2)
C4–C3	1.520(8)	C1–C2	1.471(3)
Bond angles [°]			
O2–C1–C2	128.3(2)	O1–C4–C3	105.6(4)
C1–O1–C4	109.3(2)	C4–C3–C2	103.5(5)
O2–C1–O1	116.0(2)	C4–C3A–C2	107(1)
C2–C1–O1	115.7(2)	C3–C2–C1	102.9(4)
Dihedral angles [°]			
O2–C1–O1–C2	−179.8(4)	O2–C1–C2–C3A	−169.0(7)
O2–C1–O1–C4	177.3(2)	C2–C3–C4–O1	−17.0(5)
O2–C1–C2–C3	171.6(4)	C2–C3A–C4–O1	14(1)
Interatomic contacts [Å]			
O2–H1···F1*i*	2.581(2)	C1···F3	2.875(3)
C1···F4*ii*	2.957(3)		

The C3 atom of the cation is disordered, with a 67% occupancy of the C3 position, whereas position C3A is occupied by 33%. The bond lengths between C3A and the adjacent carbon atoms (C4–C3A and C3A–C2) are in parts significantly shorter compared to C4–C3 and C3–C2. In the following, only the main species is described in the text, but bond lengths and angles for the other disordered species are given in Table 3. Due to the protonation, the C1–O2 bond is elongated (1.280(3) Å), compared to the neutral compound,[13] whereas the C1–O1 bond length is shortened (1.273(3) Å). These bond lengths are not significantly different and in the range between a formal single (1.43 Å) and double bond (1.19 Å).[16] The C–C bond lengths are in a range between 1.471(3) Å (C1–C2) and 1.543(8) Å (C2–C3). Thus, the C1–C2 bond is significantly shortened compared to γ-butyrolactone (1.530(1) Å).[13] In consequence of the protonation, the O1–C1–C2 angle is significantly larger (115.7(2)°), compared to the starting material (99.0(3)°).[13] Around the planar lactone moiety (with a dihedral angle of −179.8(4)°), the other angles amount to 116.0(2)° (O1–C1–C2) and 128.3(2)° (O2–C1–C2).

In Figure 4, a projection of observed interatomic contacts in the $[(CH_2)_3OCOH]^+[AsF_6]^-$ (**1**) crystal is illustrated. A moderate hydrogen bond is observed between the cation and anion O2–H1···F1*i* (2.581(2) Å). The strength of hydrogen bonds is classified by *Jeffrey*.[17] Additionally, two interatomic contacts between C1 and F3 (2.875(3) Å) and between C1 and F4*ii* (2.957(3) Å) are found, which are below of the sum of the van der Waals radii (3.17 Å).[18]

The bond lengths of the AsF_6^- anion range from 1.691(2) Å (As1–F5) to 1.757(2) Å (As1–F1). The obtained angles are between 88.3(1)° (F3–As1–F1) and 91.9(1)° (F2–As1–F5). For opposite fluorine atoms, an angle of 180° is expected and values from 177.2(1)° (F3–As1–F4) to 179.3(1)° (F1–As1–F2) are observed. All these values are in accordance with reported literature data for AsF_6^- anions.[19–21]

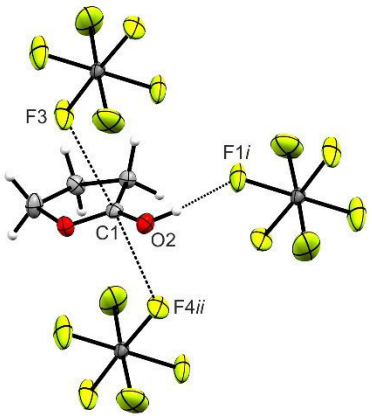

Figure 4. Projection of interatomic contacts in the $[(CH_2)_3OCOH]^+[AsF_6]^-$ (**1**) crystal (50% probability displacement ellipsoids). Symmetry codes: *i* = 1−x, 1−y, −z; *ii* = 1+x, y, z.

2.4 Crystal Structure of $[(CH_2)_3NHCOH]^+[AsF_6]^-$ (4)

$[(CH_2)_3NHCOH]^+[AsF_6]^-$ (**4**) crystallizes in the orthorhombic space group $P2_12_12_1$ with four formula units per unit cell. The asymmetric unit is illustrated in Figure 5. Selected bond lengths and angles of $[(CH_2)_3NHCOH]^+[AsF_6]^-$ are summarized in Table 4.

For the neutral compound γ-butyrolactam, a lactam-lactim tautomerism is observed.[22] Therefore, the C1–O1 bond length is, with a value of 1.238(2) Å,[23] in the range between a formal single and double bond.[16] The C1–N1 bond length (1.335(2) Å)[23] is also found to be in between a formal C–N single (1.47 Å) and double bond (1.22 Å).[16] Due to the protonation, the C1–N1 bond length is significantly shortened (1.283(4) Å) and can be considered as a C–N double bond. In contrast, the C1–O1 bond length is elongated (1.301(4) Å), compared to the neutral compound.[23] The N1–C4 and C2–C3 bond lengths nearly are unaffected by the protonation, whereas the C1–C2 and C3–C4 bond lengths are significantly shortened (1.479(5) Å and 1.519(6) Å, respectively). Changes of bond angles are only observed around the planar lactam moiety. The C2–C1–N2 angle is enlarged to 112.3(3)° and the O1–C1–N1 angle is reduced to 120.9(3)°. All other bond angles remain nearly unaffected by the protonation. Figure 6 shows the projection of interatomic contacts in the $[(CH_2)_3NHCOH]^+[AsF_6]^-$ (**4**) crystal.

The hydrogen bonds N1–H5···F6A*i* (2.906(6) Å) and O1–H1···F1*iii* (2.656(4) Å) are classified as moderate by *Jeffrey*.[17] Another cation-anion contact is detected between C1 and F4A*ii*. With a value of 2.787(7) Å, this distance is below the sum of the van der Waals radii (3.17 Å).[18]

The AsF_6^- anion exhibits a disorder of four fluorine atoms. The A positions are occupied by 61% and the B positions by 39%. The bond lengths of the AsF_6^- anion range from 1.675(6) Å to 1.740(2) Å. For neighboring fluorine atoms, values for bond angles between 85.9(2)° (F6A–As1–F2) and 94.2(2)° (F6A–As1–F2) are observed. The bond angles between opposite fluorine atoms nearly measure 180°, as it is expected for O_h symmetry. All values are in good agreement with data reported in literature.[19–21]

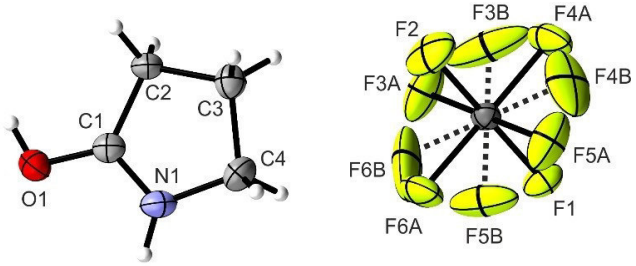

Figure 5. Asymmetric unit of $[(CH_2)_3NHCOH]^+[AsF_6]^-$ (**4**) (50% probability displacement ellipsoids). Dashed lines mark disordered positions of F3B, F4B, F5B and F6B.

Table 4. Selected bond lengths [Å] and angles [°] of $[(CH_2)_3NHCOH]^+[AsF_6]^-$ (**4**) with estimated standard deviations in parentheses. Symmetry codes: *i* = −x, $-^1/_2+$y, $^1/_2-$z; *ii* = $-^1/_2+$z, $^1/_2-$y, −z; *iii* = x, −1+y, z.

Bond lengths [Å]			
C1–N1	1.283(4)	C4–C3	1.519(6)
C1–O1	1.301(4)	C3–C2	1.529(5)
N1–C4	1.465(5)	C1–C2	1.479(5)
Bond angles [°]			
O1–C1–N1	120.9(3)	C2–C3–C4	106.0(3)
C2–C1–N1	112.3(3)	C3–C4–N1	103.5(3)
O1–C1–C2	126.7(3)	C4–N1–C1	113.7(3)
C1–C2–C3	103.4(3)		
Dihedral angles [°]			
O1–C1–N1–C4	179.0(3)	O1–C1–C2–N1	−179.0(6)
O1–C1–C2–C3	174.4(3)	C2–C3–C4–N1	−10.2(4)
Interatomic contacts [Å]			
N1–H5···F6A*i*	2.906(6)	O1–H1···F1*iii*	2.656(4)
C1···F4A*ii*	2.787(7)		

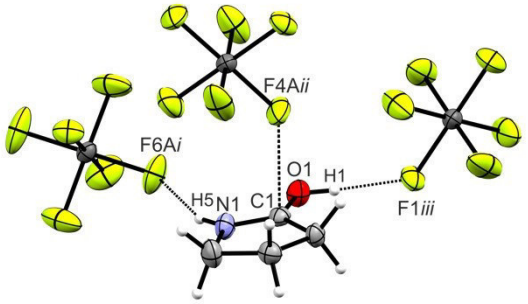

Figure 6. Projection of interatomic contacts in the $[(CH_2)_3NHCOH]^+[AsF_6]^-$ (**4**) crystal (50% probability displacement ellipsoids). Symmetry codes: *i* = −x, $-^1/_2+$y, $^1/_2-$z; *ii* = $-^1/_2+$z, $^1/_2-$y, −z; *iii* = x, −1+y, z.

2.5. Theoretical Calculations

All quantum chemical calculations were carried out on the B3LYP/aug-cc-pVTZ level of theory. In both crystal structures C···F contacts are observed. Usually, organic cations of hexafluoridometalates only possess hydrogen bonds as interionic interactions. In the case of protonated γ-butyrolactone and γ-butyrolactam, we found C···F contacts. Such contacts, which differ from hydrogen bonds, have only rarely been observed.[24–26] To investigate the nature of these contacts, Mapped Electrostatic Potentials (MEP) of the free cations $[(CH_2)_3OCOH]^+$ and $[(CH_2)_3NHCOH]^+$ were calculated. The cation-anion contacts together with the respective MEPs are illustrated in Figures 7 and 8. MEP calculations together with Natural Population Analysis charges (NPA) for the neutral compounds as well as for the protonated species of γ-butyrolactone (Figure S1) and γ-butyrolactam (Figure S2) are displayed in the Supporting Information.

Both MEPs show that the electron deficient moiety (region of higher positive potential) of each cation is located in the region of the sp^2-hybridized carbon atom. The so-called π-

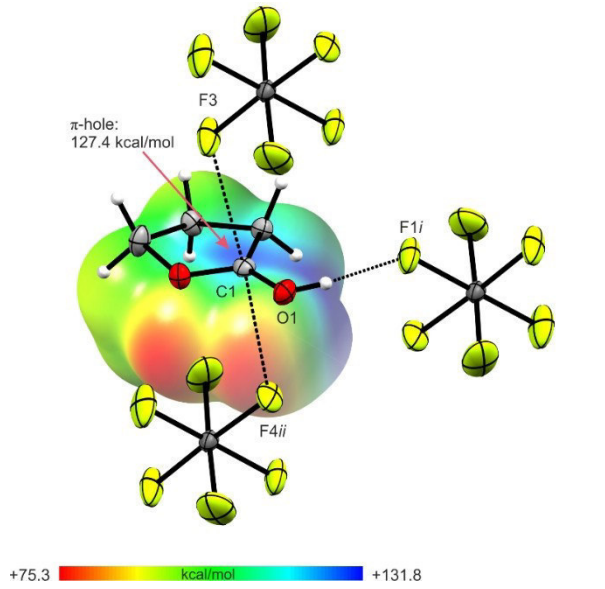

Figure 7. Contacts in the crystal structure (**1**) (50% probability displacement ellipsoids). Interatomic contacts are drawn as dashed lines. In the background of the cation, the MEP is illustrated with a color range of 75.3 kcal/mol (red) and 131.8 kcal/mol (blue), isoval. = 0.0004. Symmetry codes: *i* = 1−x, 1−y, −z; *ii* = 1+x, y, z.

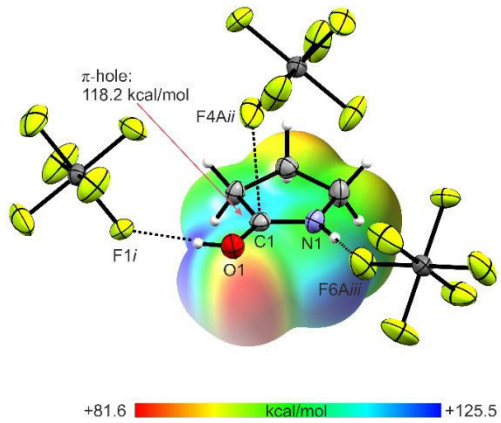

Figure 8. Contacts in the crystal structure (**4**) (50% probability displacement ellipsoids). Interatomic contacts are drawn as dashed lines. In the background of the cation, the MEP is illustrated with a color range of 81.6 kcal/mol (red) and 125.5 kcal/mol (blue), isoval. = 0.0004. Symmetry codes: *i* = x, −1+y, z; *ii* = $-^1/_2+$x, $^1/_2-$y, −z; *iii* = −x, $-^1/_2+$y, $^1/_2-$z.

hole[27] indicates that the positive charge is located at this atom. This assumption is confirmed by comparing the NPA charges of the neutral compound and the protonated species. For both γ-butyrolactone and γ-butyrolactam, the same trend is observed. Due to the protonation, changes of the NPA charges are detected only for the OCO group, respectively the OCN group. For all other atoms NPA charges remain nearly unaffected. Compared to the respective neutral compound, the positive charge of the carbon atom is increased, while the negative charges of the O (or N) atoms are decreased. For electron deficient sp^2-hybridized carbon atoms, especially carbonyl groups, investigations on their ability to develop interatomic contacts were performed.[28,29] The associated MEP value at the π-hole of $[(CH_2)_3OCOH]^+$ (127.4 kcal/mol) is calculated to be more positive compared to the value of $[(CH_2)_3NHCOH]^+$ (118.2 kcal/mol). The analysis predicts a stronger C···F contact in protonated γ-butyrolactone than in protonated γ-butyrolactam. This prediction is confirmed by the crystal structure of (**1**), exhibiting the formation of two C···F contacts (C1–F3: 2.875(3) Å and C1–F4*ii*: 2.957(3) Å), which are below the sum of the van der Waals radii.[18] In contrast, only one C···F contact (C1–F4A*ii*: 2.787(7) Å) is found in (**4**). The more positive MEP value of $[(CH_2)_3OCOH]^+$ represents the ability to form two contacts, which are therefore slightly weaker than that in (**4**). Summarizing these results, it can be stated that in protonated γ-butyrolactone, the localization of the positive charge on the sp^2-hybridized carbon atom is even stronger than in protonated γ-butyrolactam.

3. Conclusions

In this work, the reaction behaviors of γ-butyrolactone and γ-butyrolactam in the superacidic systems *X*F/*M*F$_5$ (*X* = H, D; &bk,*M* = As, Sb) were investigated. Only salts of the respective monoprotonated species were obtained and no ring opening reaction was observed. The salts were characterized by Raman and IR spectroscopy. In case of $[(CH_2)_3OCOH]^+[AsF_6]^-$ (**1**) and $[(CH_2)_3NHCOH]^+[AsF_6]^-$ (**4**), single-crystal X-ray analyses were performed. In both crystal structures C···F contacts between anion and cation, formed from the sp^2-hybridized carbon atoms, were observed. In order to investigate the nature of these contacts, Mapped Electrostatic Potentials (MEP) of the cations were calculated. For both cations, regions of positive potential (π-holes) are located on the sp^2-hybridized carbon atoms. The more positive π-hole MEP value was found for $[(CH_2)_3OCOH]^+$ compared to $[(CH_2)_3NHCOH]^+$. Interestingly, this did not lead to the formation of a stronger C···F contact in (**1**), but to the formation of two weaker ones. In contrast, a stronger C···F contact is observed in (**4**), where the less positive MEP value is calculated for $[(CH_2)_3NHCOH]^+$.

Experimental Section

General

Caution! The hydrolysis of AsF_5, SbF_5 and the prepared salts (**1**–**6**) might form HF which burns skin and causes irreparable damage. Safety precautions must be taken while using and handling these materials.

Apparatus and Materials

The reactions were conducted in standard Schlenk technique using a stainless steel vacuum line. FEP/PFA reactors, closed with a stainless steel valve, were used to perform all reactions in superacidic media. The vacuum line, as well as the reactors, were dried with fluorine prior to use. Low temperature Raman spectroscopic

investigations were carried out on a Bruker MultiRAM FT-Raman spectrometer with Nd:YAG laser excitation ($\lambda = 1064\ cm^{-1}$) in vacuum at −196 °C. For a measurement, the synthesized compounds were transferred into a cooled glass cell. Low temperature IR spectra were recorded on a Bruker Vertex-80 V FTIR spectrometer ($\tilde{\nu} = 350$ to $4000\ cm^{-1}$). A small amount of the synthesized samples was placed on a CsBr single-crystal plate in a cooled cell for the measurement. The low temperature single-crystal X-ray diffractions of $[(CH_2)_3OCOH]^+[AsF_6]^{-1}$ (**1**) and $[(CH_2)_3NHCOH]^+[AsF_6]^{-1}$ (**4**) were performed on an Oxford XCalibur 3 diffractometer equipped with a Kappa CCD detector, operating with Mo-α (0.71073 Å) radiation and a Spellman generator (voltage 50 kV, current 40 mA). Data collection was performed at 100 K using the CrystalAlis CCD software[30] and the reduction was carried out using CrysAlis RED software.[31] The structures were solved and refined utilizing SHELXS-97[32] and SHELXL-97,[33] belonging to the WinGX software package. Afterwards, the structures were verified by PLATON software.[34] The absorption correction was accomplished by using the SCALE3 ABSPACK multiscan method.[35] Selected data and parameters of the single-crystal X-ray structure analyses are summarized in Table S3 for (**1**), and Table S4 for (**4**), respectively (see Supporting Information). Crystallographic data (excluding structure factors) for the structures in this paper were deposited with the Cambridge Crystallographic Data Centre, CCDC, 12 Union Road, Cambridge CB21EZ, UK. Copies of the data can be obtained free of charge on quoting the depository number CCDC-2013823 for $[(CH_2)_3OCOH]^+[AsF_6]^-$ (**1**) and CCDC-2013703 for $[(CH_2)_3NHCOH]^+[AsF_6]^-$ (**4**) (Fax: +44-1223-336-033; E-Mail: deposit@ccdc.cam.ac.uk, http://www.ccdc.cam.ac.uk). The quantum chemical calculations were performed on the B3LYP/aug-cc-pVTZ level of theory.[36] For visualization and illustration of the MEP calculations GaussView 6.0 was used.[37]

Synthesis of $[(CH_2)_3OCOH]^+[AsF_6]^-$ (1), $[(CH_2)_3OCOD]^+[AsF_6]^-$ (3), $[(CH_2)_3NHCOH]^+[AsF_6]^-$ (4) and $[(CH_2)_3NDCOD]^+[AsF_6]^-$ (6)

Approximately 2 mL anhydrous hydrogen fluoride (*a*HF), respectively deuterium fluoride (*a*DF), were condensed into a FEP tube-reactor at −196 °C. Additionally, arsenic pentafluoride (85 mg, 0.5 mmol) was condensed under the same conditions. In order to form the superacidic system, a*X*F (*X*=H, D) and AsF_5 were warmed to −40 °C and subsequently homogenized. After cooling to −196 °C again, the starting material γ-butyrolactone, respectively γ-butyrolactam (43 mg, 0.5 mmol), was added under inert gas atmosphere. The respective reaction mixture was warmed to −40 °C and homogenized until the salt was completely dissolved. Excess *aX*F was removed at −78 °C overnight in a dynamic vacuum. For crystallization of compounds (**1**) and (**4**), the reactors were left in an ethanol bath at −50 °C until the salts recrystallized. Compounds $[(CH_2)_3OCOH]^+[AsF_6]^-$ (**1**) and $[(CH_2)_3OCOD]^+[AsF_6]^-$ (**3**) were obtained as colorless solids, which decompose at −30 °C. Compounds $[(CH_2)_3NHCOH]^+[AsF_6]^-$ (**4**) and $[(CH_2)_3NDCOD]^+[AsF_6]^-$ (**6**), likewise colorless solids, are stable up to room temperature.

Synthesis of $[(CH_2)_3OCOH]^+[SbF_6]^-$ (2) and $[(CH_2)_3NHCOH]^+[SbF_6]^-$ (5)

First, antimony pentafluoride (108 mg, 0.5 mmol) was condensed into a FEP tube-reactor at −196 °C. Subsequently, anhydrous hydrogen fluoride (2 mL) was condensed into the reactor under the same conditions. To form the superacidic system, both compounds were allowed to warm to −40 °C and homogenized. After cooling to −196 °C again, the respective starting material, γ-butyrolactone (43 mg, 0.5 mmol) or γ-butyrolactam (43 mg, 0.5 mmol), was added under inert gas atmosphere. For the desired protonation, the mixture was warmed to −40 °C and homogenized until the respective salts were completely dissolved. Excess *a*HF was removed at −78 °C in a dynamic vacuum overnight. $[(CH_2)_3OCOH]^+[SbF_6]^-$ (**2**) and $[(CH_2)_3NHCOH]^+[SbF_6]^-$ (**5**) were obtained as colorless solids, with a decomposition temperature of −30 °C (**2**), while compound (**5**) is stable up to room temperature.

Acknowledgements

We are grateful to the Department of Chemistry of the Ludwig Maximilian University of Munich, the Deutsche Forschungsgesellschaft (DFG) and the F-Select GmbH for their financial support.

Conflict of Interest

The authors declare no conflict of interest.

Keywords: γ-butyrolactone · γ-butyrolactam · interatomic contacts · mapped electrostatic potentials · superacidic systems

[1] T. J. Donohoe, C. J. R. Bataille, G. H. Churchill, *Annu. Rep. Prog. Chem., Sect. B: Org. Chem.* **2006**, *102*, 9.
[2] J.-P. Deprés, P. Delair, J.-F. Poisson, A. Kanazawa, A. E. Greene, *Acc. Chem. Res.* **2016**, *49*, 252.
[3] M. Seitz, O. Reiser, *Curr. Opin. Chem. Biol.* **2005**, *9*, 285.
[4] H. M. R. Hoffmann, J. Rabe, *Angew. Chem. Int. Ed.* **1985**, *24*, 94.
[5] S. S. Canan Koch, A. R. Chamberlin in *Studies in Natural Products Chemistry, Vol. 16* (Ed.: A.-u. Rahman), Elsevier, Amsterdam, Lausanne, New-York, **1995**, pp. 687–725.
[6] B. Wang, Y.-M. Shen, Y. Shi, *J. Org. Chem.* **2006**, *71*, 9519.
[7] H. J. Kiely-Collins, I. Sechi, P. E. Brennan, M. G. McLaughlin, *Chem. Commun.* **2018**, *54*, 654.
[8] D. R. Storm, D. E. Koshland, *J. Am. Chem. Soc.* **1972**, *94*, 5805.
[9] A. Bladé-Font, *Tetrahedron Lett.* **1980**, *21*, 2443.
[10] M. T. Pérez-Prior, J. A. Manso, M. del Pilar García-Santos, E. Calle, J. Casado, *J. Org. Chem.* **2005**, *70*, 420.
[11] G. A. Olah, A. T. Ku, *J. Org. Chem.* **1970**, *35*, 3916.
[12] P. Behmel, P. G. Jones, G. M. Sheldrick, M. Ziegler, *J. Mol. Struct.* **1980**, *69*, 41.
[13] R. J. Papoular, H. Allouchi, A. Chagnes, A. Dzyabchenko, B. Carré, D. Lemordant, V. Agafonov, *Acta Crystallogr. Sect. B* **2005**, *61*, 312.
[14] J. Weidlein, K. Dehnicke, U. Müller, *Schwingungsspektroskopie. Eine Einführung*, Thieme, Stuttgart, **1988**.
[15] D. P. McDermott, *J. Phys. Chem.* **1986**, *90*, 2569.
[16] A. F. Holleman, E. Wiberg, N. Wiberg, *Anorganische Chemie*, De Gruyter, Berlin, Boston, **2017**.
[17] G. A. Jeffrey, *An Introduction to hydrogen bonding*, Oxford University Press, New York, **1997**.
[18] A. Bondi, *J. Phys. Chem.* **1964**, *68*, 441.
[19] R. Minkwitz, F. Neikes, U. Lohmann, *Eur. J. Inorg. Chem.* **2002**, *2002*, 27.
[20] R. Minkwitz, S. Schneider, *Angew. Chem. Int. Ed.* **1999**, *38*, 210.
[21] M. Schickinger, C. Jessen, Y. Morgenstern, K. Muggli, F. Zischka, A. Kornath, *Eur. J. Org. Chem.* **2018**, *2018*, 6223.
[22] Q. Liu, X. Lu, X. Sun, X. Zhao, *Org. Chem. Front.* **2015**, *2*, 961.
[23] R. Goddard, O. Heinemann, C. Krüger, I. Magdó, F. Mark, K. Schaffner, *Acta Crystallogr., Sect. C: Cryst. Struct. Commun.* **1998**, *54*, 501.
[24] C. C. Dörtbudak, *München, Ludwig-Maximilians-Universität, Diss., 2014*, Universitätsbibliothek der Ludwig-Maximilians-Universität, München, **2014**.
[25] N. R. Götz, *München, Ludwig-Maximilians-Universität, Diss., 2011*, Universitätsbibliothek der Ludwig-Maximilians-Universität, München, **2011**.
[26] D. Leitz, A. Virmani, Y. Morgenstern, F. Zischka, A. J. Kornath, *Eur. J. Inorg. Chem.* **2018**, *2018*, 5053.
[27] I. Alkorta, J. Elguero, A. Frontera, *Crystals* **2020**, *10*, 180.

[28] H. B. Burgi, J. D. Dunitz, E. Shefter, *J. Am. Chem. Soc.* **1973**, *95*, 5065.
[29] M. Naeem Ahmed, K. A. Yasin, S. Aziz, S. U. Khan, M. N. Tahir, D. M. Gil, A. Frontera, *CrystEngComm* **2020**.
[30] *CrysAlisCCD, Version 1.171.35.11 (release 16.05.2011 CrysAlis 171.NET)*, Oxford Diffraction Ltd., **2011**.
[31] *CrysAlisRED, Version 1.171.35.11 (release 16.05.2011 CrysAlis 171.NET)*, Oxford Diffraction Ltd., **2011**.
[32] G. Sheldrick, *SHELXS-97, Program for Crystal Structure Solution*, University of Göttingen, Germany, **1997**.
[33] G. Sheldrick, *SHELXL-97, Program for the Refinement of Crystal Structures*, University of Göttingen, Germany, **1997**.
[34] A. Spek, *PLATON, A Multipurpose Crystallographic Tool*, Utrecht University, Utrecht (The Netherlends), **1999**.
[35] *SCALE3 ABSPACK – An Oxford Diffraction Program*, Oxford Diffraction Ltd., UK, **2005**.
[36] M. J. Frisch, G. W. Trucks, H. B. Schlegel, G. E. Scuseria, M. A. Robb, J. R. Cheeseman, G. Scalmani, V. Barone, B. Mennucci, G. A. Petersson, H. Nakatsuji, M. Caricato, X. Li, H. P. Hratchian, A. F. Izmaylov, J. Bloino, G. Zheng, J. L. Sonnenberg, M. Hada, M. Ehara, K. Toyota, R. Fukuda, J. Hasegawa, M. Ishida, T. Nakajima, Y. Honda, O. Kitao, H. Nakai, T. Vreven, J. A. Montgomery, Jr., J. E. Peralta, F. Ogliaro, M. Bearpark, J. J. Heyd, E. Brothers, K. N. Kudin, V. N. Staroverov, R. Kobayashi, J. Normand, K. Raghavachari, A. Rendell, J. C. Burant, S. S. Iyengar, J. Tomasi, M. Cossi, N. Rega, J. M. Millam, M. Klene, J. E. Knox, J. B. Cross, V. Bakken, C. Adamo, J. Jaramillo, R. Gomperts, R. E. Stratmann, O. Yazyev, A. J. Austin, R. Cammi, C. Pomelli, J. W. Ochterski, R. L. Martin, K. Morokuma, V. G. Zakrzewski, G. A. Voth, P. Salvador, J. J. Dannenberg, S. Dapprich, A. D. Daniels, Ö. Farkas, J. B. Foresman, J. V. Ortiz, J. Cioslowski, D. J. Fox, *Gaussian 09, Revision A.02*, Gaussian Inc., Wallingford CT, **2009**.
[37] R. Dennington, T. A. Keith, J. M. Millam, *GaussView, Version 6.0*. Semichem Inc. Shawnee Mission, KS, **2016**.

Manuscript received: September 7, 2020
Revised manuscript received: November 9, 2020

ChemistryOpen

Supporting Information

Protonation of γ-Butyrolactone and γ-Butyrolactam

Stefanie Beck, Michael Feller, Laura Spies, Kai J. Dietrich, Christoph Jessen, Karin Stierstorfer, and Andreas J. Kornath*

Supporting Information

Table S1. Experimental vibrational frequencies [cm^{-1}] of (**1**), (**2**) and (**3**), and calculated vibrational frequencies [cm^{-1}] of $[(CH_2)_3OCOH]^+$ and $[(CH_2)_3OCOD]^+$.

Table S2. Experimental vibrational frequencies [cm^{-1}] of (**4**), (**5**) and (**6**), and calculated vibrational frequencies [cm^{-1}] of $[(CH_2)_3NHCOH]^+$ and $[(CH_2)_3NDCOD]^+$.

Table S3. Crystal data and structure refinement for $[(CH_2)_3OCOH]^+[AsF_6]^-$ (**1**).

Table S4. Crystal data and structure refinement for $[(CH_2)_3NHCOH]^+[AsF_6]^-$ (**4**).

Figure S1. Electrostatic potential isosurfaces and the NPA charges have been calculated for $C_4H_6O_2$ (left) with a color range of –0.055 a.u. (red) to 0.036 a.u. (blue), isoval = 0.0004; and for $[C_4H_7O_2]^+$ (right) with a color range of 0.12 a.u. (red) and 0.21 a.u. (blue), isoval. = 0.0004.

Figure S2. Electrostatic potential isosurfaces and the NPA charges have been calculated for C_4H_7NO (left) with a color range of –0.061 a.u. (red) to 0.045 a.u. (blue), isoval = 0.0004; and for $[C_4H_8NO]^+$ (right) with a color range of 0.13 a.u. (red) and 0.20 a.u. (blue), isoval. = 0.0004.

Table S1. Experimental vibrational frequencies [cm^{-1}] of (**1**), (**2**) and (**3**), and calculated vibrational frequencies [cm^{-1}] of $[(CH_2)_3OCOH]^+$ and $[(CH_2)_3OCOD]^+$.

$[(CH_2)_3OCOH]^+[AsF_6]^-$ (**1**)		$[(CH_2)_3OCOH]^+[SbF_6]^-$ (**2**)		$[(CH_2)_2OCOD]^+[AsF_6]^-$ (**3**)		$[(CH_2)_3OCOH]^+$	$[(CH_2)_3OCOD]^+$	Assignment[b]
IR	**Raman**	**IR**	**Raman**	**IR**	**Raman**	**Calc. (IR/Ra)[a]**	**Calc. (IR/Ra)[a]**	
				3518 (vw, br)				ν(OH)
3528 (vw, br)		3460 (vw, br)		2307 (m)	2293 (14)	3724 (256/61)	2714 (148/29)	ν(O*X*)
	3078 (22)	3078 (m)	3077 (10)	3072 (m)	3078 (34)	3181 (0.4/57)	3181 (0.4/57)	$\nu_{as}(CH_2)$
	3040 (28)				3040 (42)	3143 (0.2/59)	3143 (0.2/59)	$\nu_{as}(CH_2)$
	3022 (44)		3024 (26)		3023 (62)	3108 (1/114)	3108 (1/114)	$\nu_{s}(CH_2)$
2995 (m)	3004 (60)	3005 (m)	3004 (30)	3001 (m)	3004 (89)	3102 (3/77)	3102 (3/77)	$\nu_{as}(CH_2)$
2930 (m)	2946 (42)	2951 (m)	2950 (31)	2945 (m)	2945 (61)	3089 (2/84)	3089 (2/84)	$\nu_{s}(CH_2)$
	2912 (13)		2905 (6)		2909 (19)	3030 (12/106)	3030 (12/107)	$\nu_{s}(CH_2)$
		2833 (w)						?
		2544 (vw)		2511 (w)				?
		2457 (vw)		2422 (w)				?
				1909 (w)				?
1684 (s)	1613 (7)	1616 (m)	1637 (5)	1607 (s)	1619 (12)	1650 (305/0.7)	1635 (383/0.5)	ν(CO)
	1523 (24)	1522 (m)	1526 (14)	1510 (m)	1510 (27)	1523 (161/4)	1515 (74/8)	ν(CO)
1487 (m)	1476 (18)	1481 (w, sh)	1471 (12)	1524 (m)		1518 (33/6)	1521 (64/3)	$\delta(CH_2)$
1464 (m)	1463 (29)	1460 (w)		1460 (m)	1462 (29)	1502 (13/6)	1500 (17/6)	$\delta(CH_2)$
	1408 (23)		1407 (12)	1404 (m)	1406 (28)	1446 (30/8)	1445 (32/8)	$\delta(CH_2)$
1396 (m)	1397 (17)	1400 (m)	1396 (11)			1371 (2/0.5)	1369 (3/0.8)	$\omega(CH_2)$
		1342 (m)		1337 (m)	1338 (11)			?
1319 (m)		1311 (m)				1340 (30/0.7)	1333 (39/2)	$\omega(CH_2)$
1284 (m)	1286 (10)	1283 (m)	1288 (8)	1298 (m)	1304 (13)	1310 (8/1)	1307 (3/0.8)	$\omega(CH_2)$
1244 (m)	1232 (40)	1227 (m)	1231 (23)	1229 (m)	1231 (43)	1245 (7/5)	1245 (4/5)	$\tau(CH_2)$
1213 (s)	1204 (13)	1205 (m)	1206 (8)		1217 (13)	1235 (65/2)	1231 (19/2)	$\tau(CH_2)$
	1191 (7)	1192 (m)	1194 (6)	1192 (m)	1191 (9)	1207 (20/0.3)	1206 (8/0.4)	$\tau(CH_2)$
1088 (m)	1089 (5)	1084 (w)	1085 (5)	912 (m)	916 (13)	1178 (199/7)	863 (12/1)	δ(CO*X*)
1036 (m)	1038 (25)	1036 (w)	1038 (16)	1034 (m)	1038 (28)	1104 (2/0.2)	1104 (0.6/0.3)	$\rho(CH_2)$
989 (m)		1012 (w)		960 (m)	961 (7)	1029 (3/3)	1029 (6/3)	ν(CC)
955 (m)	959 (33)	959 (m)	961 (24)	1001 (s)	1000 (21)	949 (5/4)	993 (107/6)	ν(CO)
932 (m)	938 (23)	937 (w)	939 (13)	939(m)	941 (35)	934 (1/3)	934 (2/4)	ν(CC)
						896 (7/4)	895 (6/4)	$\rho(CH_2)$
881 (m)	877 (38)	876 (m)	878 (28)	876 (m)	875 (33)	881 (17/6)	889 (45/5)	ring breathing
822 (m)		820 (m)		834 (m)				?
806 (m)	800 (13)		793 (8)	800 (m)	799 (15)	796 (11/2)	796 (10/2)	δ(COC)
	723 (6)			729 (s, sh)	723 (8)	684 (10/3)	682 (9/3)	δ(CCC)
	683 (65)		674 (8)	630 (s)	630 (23)	639 (29/3)	626 (10/5)	δ(CCC)
644 (w)	632 (21)	639 (vs)	633 (50)		450 (30)	611 (77/3)	443 (57/0.2)	$\delta(COX)_{oop}$

515 (m)	525 (9)	525 (s)	524 (3)	523 (m)	523 (13)	517 (25/0.5)	535 (1/0.7)	γ(CCOO)
469 (w)	471 (17)	467 (s)	473 (7)			435 (13/0.8)	411 (13/0.8)	δ(OCO)
	238 (6)		234 (2)			218 (5/0.2)	216 (6/0.1)	skeletal vibration
	154 (12)		137 (8)			137 (2/0.3)	137 (2/0.3)	skeletal vibration
	120 (30)							?
698 (vs)	704 (93)	658 (vs)	691 (16)	675 (vs)	704 (97)			[*M*F$_6$]$^-$
536 (m)	673 (100)	584 (m)	661 (100)	696 (vs)	682 (56)			[*M*F$_6$]$^-$
392 (m)	589 (18)	550 (s)	642 (53)	540 (s)	673 (100)			[*M*F$_6$]$^-$
	545 (15)		587 (8)	447 (w)	589 (20)			[*M*F$_6$]$^-$
	403 (6)		297 (12)		541 (17)			[*M*F$_6$]$^-$
	375 (44)		285 (37)		375 (46)			[*M*F$_6$]$^-$
	368 (49)				367 (53)			[*M*F$_6$]$^-$

[a] Calculated on the B3LYP/aug-cc-pVTZ level of theory. IR intensity in km/mol and Raman intensity in Å^4/u. Abbreviations for IR intensities: v = very, s = strong, m = medium, w = weak. Experimental Raman activities are stated to a scale of 1 to 100. [b] *X* = H, D.

Table S2. Experimental vibrational frequencies [cm^{-1}] of (**4**), (**5**) and (**6**), and calculated vibrational frequencies [cm^{-1}] of [(CH$_2$)$_3$NHCOH]$^+$ and [(CH$_2$)$_3$NDCOD]$^+$.

[(CH$_2$)$_3$NHCOH]$^+$[AsF$_6$]$^-$ (4)		**[(CH$_2$)$_3$NHCOH]$^+$[SbF$_6$]$^-$ (5)**		**[(CH$_2$)$_2$NDCOD]$^+$[AsF$_6$]$^-$ (6)**		**[(CH$_2$)$_3$NHCOH]$^+$**	**[(CH$_2$)$_3$NDCOD]$^+$**	**Assignment[b]**
IR	**Raman**	**IR**	**Raman**	**IR**	**Raman**	**Calc. (IR/Ra)[a]**	**Calc. (IR/Ra)[a]**	
				3391 (w)				ν(OH)
				3358 (w)	3334 (2)			ν(NH)
3238 (w)		3242 (vs)		2492 (w)	2494 (18)	3750 (235/67)	2732 (137/33)	ν(O*X*)
					2477 (19)			?
3364 (w)	3369 (3)	3358 (s)	3359 (4)	2430 (w)	2445 (16)	3553 (139/82)	2609 (89/37)	ν(N*X*)
					2402 (12)			?
3024 (vw)	3026 (17)	3059 (w)	3033 (11)	3024 (vw)	3028 (36)	3148 (0.3/58)	3148 (0.3/58)	ν$_{as}$(CH$_2$)
	3015 (sh)				3015 (43)	3131 (0.4/78)	3131 (0.4/78)	ν$_{as}$(CH$_2$)
2982 (vw)	2991 (27)	2995 (vw)	3000 (25)	2982 (vw)	2995 (58)	3098 (0.04/106)	3098 (0.06/106)	ν$_{as}$(CH$_2$)
2947 (vw)	2945 (33)		2944 (27)	2949 (vw)	2947 (40)	3089 (4/48)	3089 (4/48)	ν$_s$(CH$_2$)
	2931 (sh)	2918 (vw)	2919 (15)		2923 (20)	3074 (3/139)	3074 (3/139)	ν$_s$(CH$_2$)
	2907 (sh)				2901 (11)	3037 (7/121)	3037 (7/122)	ν$_s$(CH$_2$)
				2748 (vw)				?
				1807 (vw)				?
1711 (m)	1716 (16)	1711 (m)	1711 (14)	1691 (m)	1691 (17)	1729 (251/3)	1703 (278/5)	ν(CN)
			1498 (6)	1485 (m)	1482 (28)	1525 (2/8)	1524 (0.9/9)	δ(CH$_2$)
1491 (m)	1489 (26)	1489 (m)	1485 (15)	1472 (m)	1469 (19)	1511 (108/4)	1508 (30/5)	δ(CH$_2$)
1462 (w)	1461 (16)	1464 (vw)	1464 (14)	1462 (m)	1456 (24)	1500 (103/7)	1474 (140/5)	ν(CO)
1419 (w)	1421 (22)	1423 (w)	1421 (17)	1417 (m)	1417 (39)	1460 (207/10)	1460 (21/10)	δ(CH$_2$)
1390 (w)	1393 (4)	1393 (vw)		1186 (w)	1172 (7)	1404 (3/0.7)	1176 (6/2)	δ(CN*X*)

				1375 (w)	1337 (7)	1351 (6/0.3)	1368 (7/1)	ω(CH_2)
1319 (w)	1323 (10)	1317 (w)	1323 (8)	1321 (m)	1325 (6)	1343 (23/3)	1346 (19/2)	ω(CH_2)
1307 (w)		1296 (vw)	1288 (5)			1312 (5/1)	1311 (3/0.9)	ω(CH_2)
1261 (m)	1263 (7)	1256 (vw)	1259 (6)	1279 (vw)	1279 (5)	1254 (2/5)	1263 (11/1)	τ(CH_2)
1229 (w)	1230 (24)	1230 (vw)	1233 (17)	1231 (w)	1233 (23)	1235 (21/2)	1253 (3/4)	τ(CH_2)
			1204 (6)			1208 (10/0.5)	1207 (4/0.4)	τ(CH_2)
1186 (w)	1189 (5)		1189 (4)	954 (w, sh)	956 (13)	1198 (138/8)	915 (28/9)	δ(CO*X*)
1078 (vw)	1079 (2)		1083 (4)	1078 (vw)	1078 (4)	1099 (0.4/0.2)	1098 (0.09/0.2)	ρ(CH_2)
1049 (w)	1052 (10)		1048 (9)	1055 (m)	1056 (6)	1042 (2/2)	1032 (0.3/3)	ν(CN)
				1011 (s)	1009 (8)			?
982 (m)	983 (20)	982 (vw)	982 (20)	943 (m)	938 (9)	971 (10/3)	938 (11/5)	ν(CC)
926 (w)	924 (sh)	928 (vw)	928 (5)	775 (s)	778 (6)	929 (3/0.2)	809 (6/0.4)	ν(CC)
				920 (m)		905 (3/2)	905 (3/2)	ρ(CH_2)
895 (w)	897 (73)	903 (vw)	902 (58)	895 (m)	895 (79)	896 (5/17)	889 (52/8)	ring breathing
824 (vw)		820 (vw)	815 (4)	839 (vw)	842 (14)	817 (3/0.9)	831 (3/4)	δ(CCC)
783 (w)		777 (vw)	782 (4)	476 (m)	476 (10)	761 (65/0.8)	463 (25/0.4)	δ(CN*X*)$_{oop}$
		708 (vw)	694 (8)	584 (m)	583 (23)	702 (6/4)	694 (3/4)	δ(CCN)
620 (s)	620 (8)	617 (vw, sh)	620 (10)	619 (s, sh)	608 (11)	619 (9/3)	598 (9/3)	δ(CCC)
555 (s)	554 (12)	554 (vw)	556 (11)			552 (132/0.7)	391 (66/0.2)	δ(CO*X*)$_{oop}$
517 (m)	518 (9)	515 (vw)	517 (11)	559 (s)	560 (16)	497 (24/0.6)	665 (21/1)	γ(CCON)
453 (w)	454 (13)		447 (19)			420 (9/1)	392 (10/0.9)	δ(OCN)
	240 (4)		248 (9)		237 (9)	224 (0.3/0.2)	219 (0.4/0.1)	skeletal vibration
						122 (0.9/0.3)	121 (0.8/0.3)	skeletal vibration
704 (vs)	705 (35)	667 (s)	671 (18)		700 (63)			[*M*F_6]$^-$
671 (vs)	679 (100)	642 (m)	658 (100)		689 (80)			[*M*F_6]$^-$
579 (s)	580 (18)	563 (vw)	642 (34)		673 (100)			[*M*F_6]$^-$
	561 (12)		579 (14)		430 (17)			[*M*F_6]$^-$
	371 (43)		565 (12)		370 (61)			[*M*F_6]$^-$
			280 (42)					[*M*F_6]$^-$

[a] Calculated on the B3LYP/aug-cc-pVTZ level of theory. IR intensity in km/mol and Raman intensity in $Å^4$/u. Abbreviations for IR intensities: v = very, s = strong, m = medium, w = weak. Experimental Raman activities are stated to a scale of 1 to 100. [b] *X* = H, D.

Table S3. Crystal data and structure refinement for $[(CH_2)_3OCOH]^+[AsF_6]^-$ (**1**).

	$[(CH_2)_3OCOH]^+[AsF_6]^-$ (**1**)
Empirical formular	C4 H7 F6 O2 As
M_r	276.02
Crystal system	monoclinic
Space group	$P2_1/c$
a [Å]	8.2327(5)
b [Å]	9.7948(4)
c [Å]	10.8507(8)
α [°]	90
β [°]	109.891(6)
γ [°]	90
V [Å^3]	822.78(9)
Z	4
ρ_{calcd} [gcm^{-3}]	2.228
μ[mm^{-1}]	4.203
$\lambda_{Moκα}$	0.71073
F(000)	536
T[K]	100(2)
hkl range	–8:10; –11:12;–13:14
refl. measured	3644
refl. unique	1883
R_{int}	0.0187
parameters	132
R(F)/*w*R(F^2)[a)]	0.0317/0.0680
weighting scheme[b)]	0.0356/0.2308
S(GoF)[c)]	1.058
residual density [eÅ^{-3}]	0.548/ –0.517
devide type	Oxford XCalibur
solution/refinement	SHELXS-97
CCDC	2013823

a) $R_1 = \Sigma||F_o|-|F_c||/\Sigma|F_o|$; b) $wR_2 = [\Sigma[w(F_o^2-F_c^2)^2]/\Sigma[w(F_o)^2]]^{1/2}$; $w = [\sigma_c^2(F_o^2)+(xP)^2+yP]^{-1}$; $P = (F_o^2+2F_c^2)/3$ c) GoF = $\{\Sigma[w(F_o^2-F_c^2)^2]/(n-p)\}^{1/2}$ (*n* = number of reflexions; p = total number of parameters).

Table S4. Crystal data and structure refinement for $[(CH_2)_3NHCOH]^+[AsF_6]^-$ (**4**).

	$[(CH_2)_3NHCOH]^+[AsF_6]^-$ (**4**)
Empirical formular	C4 H8 F6 N O As
M_r	275.03
Crystal system	orthorhombic
Space group	$P2_12_12_1$
a [Å]	7.7533(3)
b [Å]	10.1067(4)
c [Å]	10.9203(5)
α [°]	90
β [°]	90
γ [°]	90
V [Å^3]	855.72(6)
Z	4
ρ_{calcd} [gcm^{-3}]	2.135
μ[mm^{-1}]	4.035
$\lambda_{Moκα}$	0.71073
F(000)	536
T[K]	109(2)
hkl range	–11:11; –11:15;–16:16
refl. measured	9417
refl. unique	2827
R_{int}	0.0345
parameters	162
R(F)/*w*R(F^2)[a)]	0.0392/0.0679
weighting scheme[b)]	0.0318/0.0614
x(Flack)	0.022(16)/ 0.0679
S(GoF)[c)]	1.044
residual density [eÅ^{-3}]	0.482/-0.322
devide type	Oxford XCalibur
solution/refinement	SHELXS-97
CCDC	2013703

a) $R_1 = \Sigma||F_o|-|F_c||/\Sigma|F_o|$; b) $wR_2 = [\Sigma[w(F_o^2-F_c^2)^2]/\Sigma[w(F_o)^2]]^{1/2}$; $w = [\sigma_c^2(F_o^2)+(xP)^2+yP]^{-1}$; $P = (F_o^2+2F_c^2)/3$ c) GoF = $\{\Sigma[w(F_o^2-F_c^2)^2]/(n-p)\}^{1/2}$ (*n* = number of reflexions; p = total number of parameters).

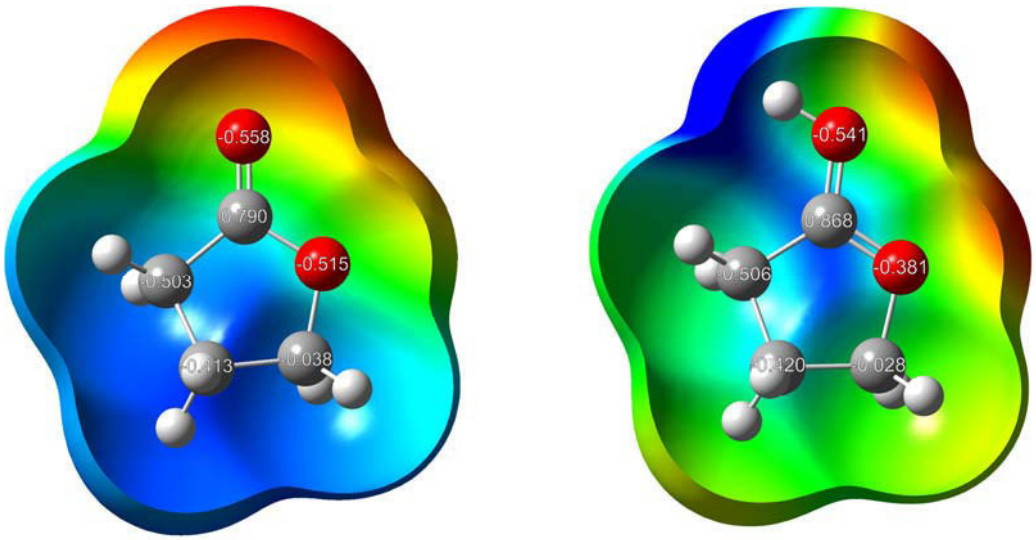

Figure S1. Electrostatic potential isosurfaces and the NPA charges have been calculated for $C_4H_6O_2$ (left) with a color range of –0.055 a.u. (red) to 0.036 a.u. (blue), isoval = 0.0004; and for $[C_4H_7O_2]^+$ (right) with a color range of 0.12 a.u. (red) and 0.21 a.u. (blue), isoval. = 0.0004.

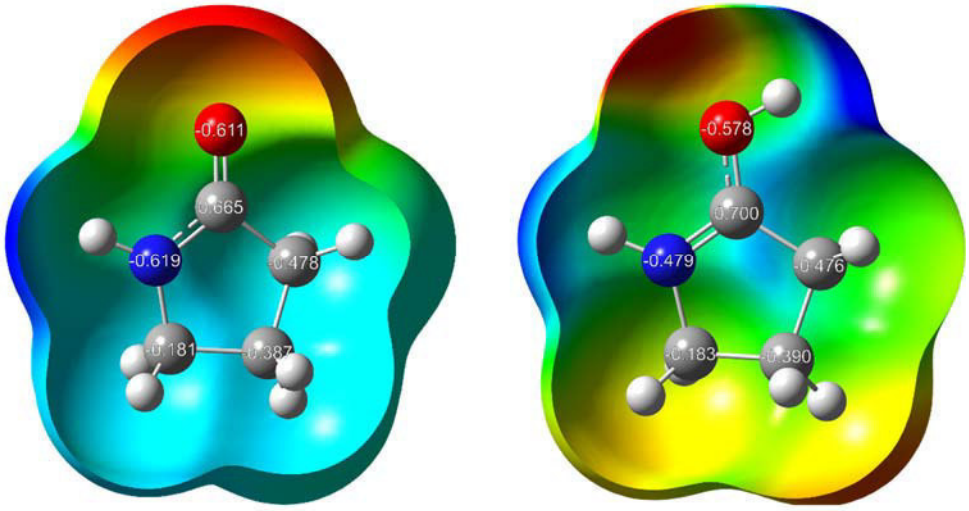

Figure S2. Electrostatic potential isosurfaces and the NPA charges have been calculated for C_4H_7NO (left) with a color range of –0.061 a.u. (red) to 0.045 a.u. (blue), isoval = 0.0004; and for $[C_4H_8NO]^+$ (right) with a color range of 0.13 a.u. (red) and 0.20 a.u. (blue), isoval. = 0.0004.

ChemistryOpen

Chemistry Europe
European Chemical Societies Publishing

Front Cover:
Stefanie Beck et al.
Protonated Ethylene Carbonate: A Highly Resonance-Stabilized Cation

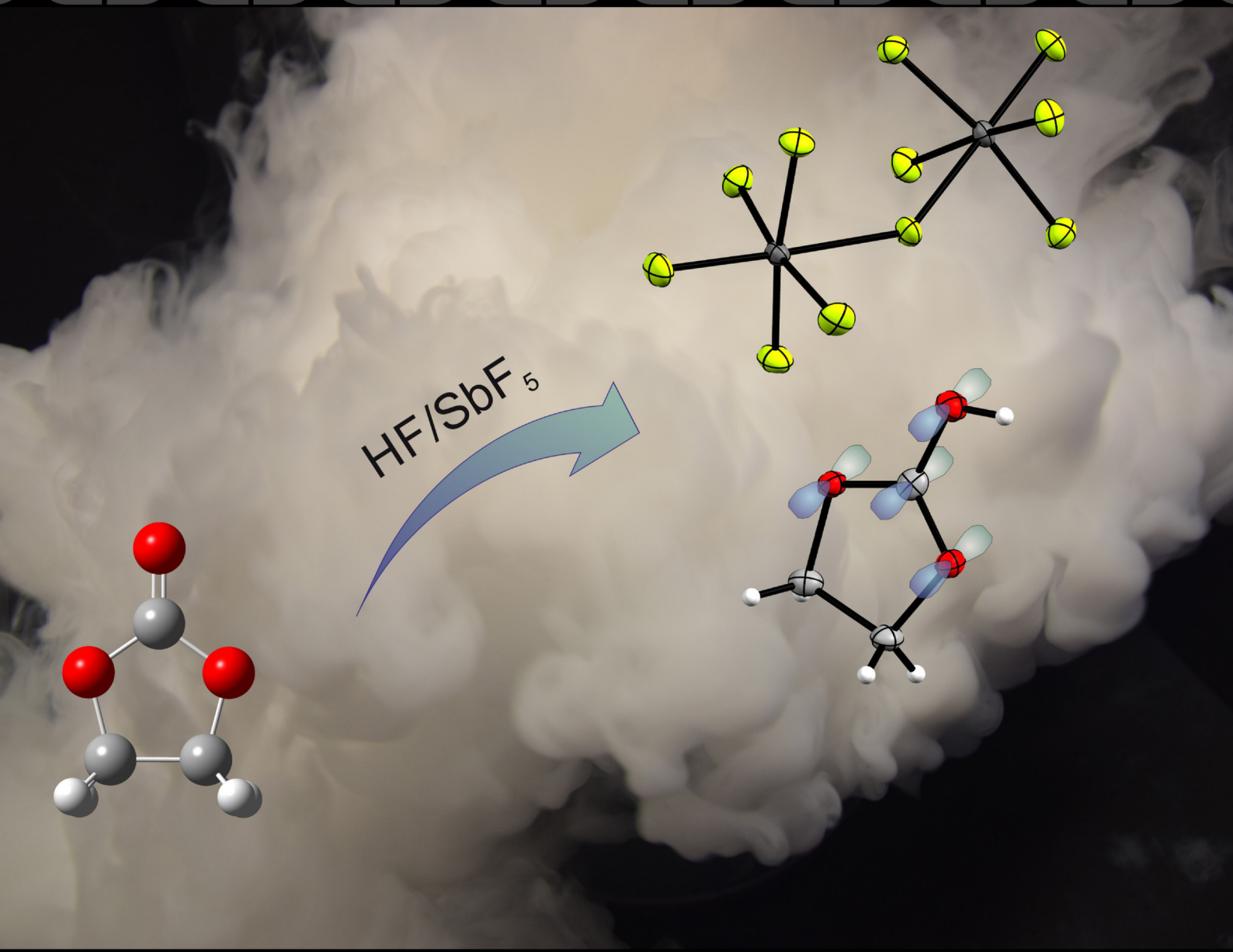

12/2021

WILEY-VCH

ChemistryOpen

Research Article
doi.org/10.1002/open.202100229

Chemistry Europe
European Chemical Societies Publishing

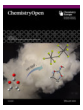

Protonated Ethylene Carbonate: A Highly Resonance-Stabilized Cation

Stefanie Beck, Christoph Jessen, and Andreas J. Kornath*[a]

Salts containing the monoprotonated ethylene carbonate species of were obtained by reacting it with the superacidic systems *X*F/*M*F$_5$ (*X* = H, D; *M* = Sb, As). The salts in terms of $[C_3H_5O_3]^+[SbF_6]^-$, $[C_3H_5O_3]^+[AsF_6]^-$ and $[C_3H_4DO_3]^+[AsF_6]^-$ were characterized by low-temperature infrared and Raman spectroscopy. In order to generate the diprotonated species of ethylene carbonate, an excess of Lewis acid was used. However, this only led to the formation of $[C_3H_5O_3]^+[Sb_2F_{11}]^-$, which was characterized by a single-crystal X-ray structure analysis. Quantum chemical calculations on the B3LYP/aug-cc-PVTZ level of theory were carried out for the $[C_3H_5O_3]^+$ cation and the results were compared with the experimental data. A Natural Bond Orbital (NBO) analysis revealed sp^2 hybridization of each atom belonging to the CO_3 moiety, thus containing a remarkably delocalized 6π-electron system. The delocalization is confirmed by a ^{13}C NMR-spectroscopic study of $[C_3H_5O_3]^+[SbF_6]^-$.

Introduction

Lithium ion batteries play an important role in our everyday life. They are applied in mobile phones, notebooks or other battery-operated tools.[1] A lithium ion battery consists of two electrodes, which are typically separated by a semipermeable membrane, or similar separators, immersed in an ion-conducting electrolyte. Throughout a charge process, or discharge process respectively, lithium ions are transported by an electrolyte from one electrode to the other and are intercalated in the respective layers.[1–6] Cathode materials are commonly transition metal oxides in the form of $LiMO_2$ (M = Co, Ni, Mn, Fe) or $LiMn_2O_4$ (spinel type), whereas the anode consists of carbonic materials. The electrolyte is a mixture of organic solvents, such as propylene carbonate, wherein Li salts are dissolved.[7] Graphite was one of the first anode materials, which was not only able to intercalate the Li^+ ions but also solvent molecules.[4] This problem of co-intercalation made the improvement of anode materials a greater challenge. Replacing graphite by petroleum coke prevented the solvent intercalation. Interestingly, adding ethylene carbonate to the solvent also blocked co-intercalation into the anode material for both graphite and petroleum coke.[4,8] This fact led to the establishment of ethylene carbonate, together with a dialkyl carbonate, as a useful electrolyte.[1] Hence, many investigations on ethylene carbonate were performed, for example on the transportability of binary ethylene carbonate/ propylene carbonate systems[7,9] or cation-solvent interactions.[10] So far, very little is known about the base properties of ethylene carbonate in literature. The only evidence for a protonated species of ethylene carbonate is given by ^1H NMR[11,12] and mass spectroscopic studies.[13] This prompted us to study ethylene carbonate in superacidic solutions.

Results and Discussion

Synthesis of $[C_3H_4XO_3]^+[AsF_6]^-$ and $[C_3H_5O_3]^+[SbF_6]^-$

Ethylene carbonate reacts in the superacidic solutions HF/*M*F$_5$ according to Scheme 1.

The superacidic solutions were prepared using an excess of anhydrous hydrogen or deuterium fluoride, which serves as a reagent as well as a solvent. In order to obtain a complete solvation of the Lewis acid, the mixture was homogenized at −40 °C. Afterwards, ethylene carbonate was added to the frozen mixture under nitrogen atmosphere. The reaction mixture was allowed to warm up to −40 °C and salts of monoprotonated ethylene carbonate were formed. The excess of the solvent was removed in a dynamic vacuum at −78 °C overnight. The air- and temperature-sensitive compounds $[C_3H_5O_3]^+[SbF_6]^-$ (**1**), $[C_3H_5O_3]^+[AsF_6]^-$ (**2**) and $[C_3H_4DO_3]^+[AsF_6]^-$ (**3**) were obtained as colorless salts. Salts **2** and **3** are stable up to room temperature,

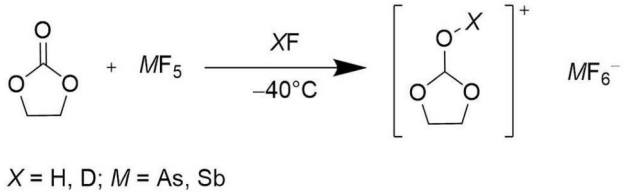

Scheme 1. Reaction of ethylene carbonate with *M*F$_5$ (*M* = As, Sb) in superacidic solutions HF/*M*F$_5$.

[a] *S. Beck, C. Jessen, Prof. Dr. A. J. Kornath*
Department of Chemistry, Ludwig-Maximilians-Universität München
Butenandstr. 5–13
81377 München (Germany)
E-mail: andreas.kornath@cup.uni-muenchen.de

Supporting information for this article is available on the WWW under https://doi.org/10.1002/open.202100229

whereas **1** (containing the SbF_6^- anion) decomposes at −20 °C. In consideration of the fact that ethylene carbonate bears three potential basic centers, a larger amount of Lewis acid (SbF_5) was used in order to obtain a diprotonated compound. The excess of SbF_5 only leads to the formation of $[C_3H_5O_3]^+[Sb_2F_{11}]^-$ (**4**).

Vibrational Spectra of $[C_3H_4XO_3]^+[MF_6]^-$ (M = As, Sb and X = H, D)

The infrared and Raman spectra of $[C_3H_5O_3]^+[SbF_6]^-$ (**1**), $[C_3H_5O_3]^+[AsF_6]^-$ (**2**) and $[C_3H_4DO_3]^+[AsF_6]^-$ (**3**) are shown in Figure 1. Selected observed frequencies of **1**, **2** and **3** are summarized together with quantum-chemically calculated frequencies of the free cations $[C_3H_5O_3]^+$ and $[C_3H_4DO_3]^+$ in Table 1. All observed and calculated frequencies are listed in Table S1 (see Supporting Information).

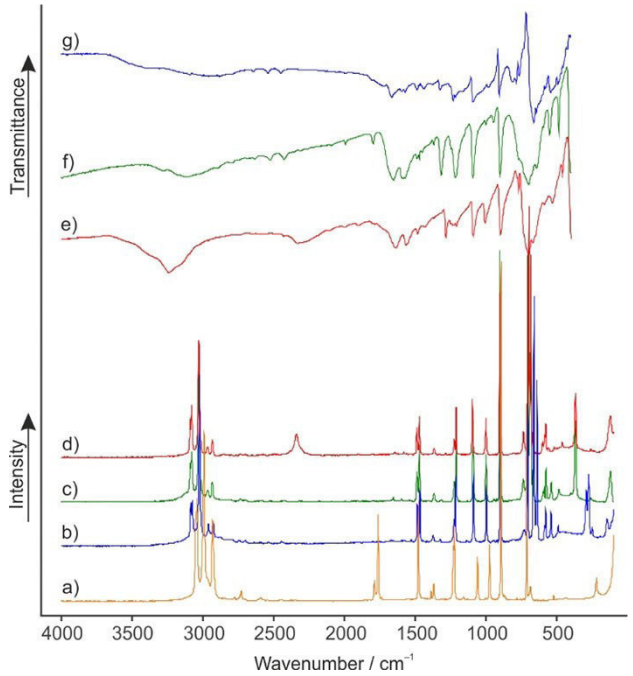

Figure 1. Raman spectra (a) of ethylene carbonate, (b) of $[C_3H_5O_3]^+[SbF_6]^-$ (**1**), (c) of $[C_3H_5O_3]^+[AsF_6]^-$ (**2**), and (d) of $[C_3H_4DO_3]^+[AsF_6]^-$ (**3**); IR spectra (e) of $[C_3H_4DO_3]^+[AsF_6]^-$ (**3**), (f) of $[C_3H_5O_3]^+[AsF_6]^-$ (**2**), and (g) of $[C_3H_5O_3]^+[SbF_6]^-$ (**1**).

For the free cations $[C_3H_5O_3]^+$ and $[C_3H_4DO_3]^+$ with C_s symmetry, 27 fundamental vibrations are expected, active in both Raman and infrared spectra.

Due to the poor polarizability of the OH stretching vibration, the corresponding Raman lines usually are of low Raman intensity ((b) and (c)). Contrariwise, the OD stretching vibration in (d) is detected at 2339 cm^{-1}. The IR spectra (f) and (g) display a broad ν(OH) band at 3406 cm^{-1} and 3278 cm^{-1}, respectively. In comparison, the corresponding ν(OD) of (e) is observed at 2325 cm^{-1}. The red shift is in good agreement with the Teller-Redlich rule for an H/D isotopic effect.[14] These are the most meaningful vibrational modes for providing evidence for a successful protonation. Due to the *O*-protonation, the CO double bond of ethylene carbonate is weakened, whereas the CO single bonds are strengthened. The stretching vibrations of the CO_3 group display this tendency. Compared to the starting material, the vibration of the former CO double bond is red-shifted by about 100 cm^{-1}. In contrast, the former CO single bonds are blue-shifted by up to 400 cm^{-1}.[15] The COX deformation vibration is observed between 1212 cm^{-1} (c) and 1218 cm^{-1} (b) for the protonated and at 826 cm^{-1} (e) for the deuterated species. The most intense line in the Raman spectra (b–d) occurs at about 900 cm^{-1} and is assigned to the skeletal breathing mode. In comparison to ethylene carbonate (a), this mode is nearly unaffected by the protonation.[15,16] This also applies to the rest of the skeletal vibration modes (except for the CO_3 moiety), such as ν(CO), ν(CC), δ(COC), and δ(OCO), respectively. For the anions (M = Sb, As) with an ideal O_h symmetry, three Raman lines and two IR bands are expected. In the Raman spectra (b–d), more than three lines are observed and likewise the IR spectra (d–f) show more than two bands for the anions. The increased numbers of vibrations indicate a lowered symmetry of the hexafluoridometalate anions.

Crystal Structure of $[C_3H_5O_3]^+[Sb_2F_{11}]^-$ (4)

$[C_3H_5O_3]^+[Sb_2F_{11}]^-$ (**4**) crystallizes in the monoclinic space group $P2_1/n$ with four formula units per unit cell. The asymmetric unit is illustrated in Figure 2. Selected bond lengths and angles are

Table 1. Selected experimental vibrational frequencies [cm^{-1}] of **1–3** and calculated vibrational frequencies [cm^{-1}] of $[C_3H_5O_3]^+$ and $[C_3H_4DO_3]^+$.

$[C_3H_5O_3]^+[SbF_6]^-$ (**1**) IR	Raman	$[C_3H_5O_3]^+[AsF_6]^-$ (**2**) IR	Raman	$[C_3H_4DO_3]^+[AsF_6]^-$ (**3**) IR	Raman	$[C_3H_5O_3]^+$ Calc.[a] (IR/Raman)	$[C_3H_4DO_3]^+$ Calc.[a] (IR/Raman)	Assignment[b]
3405(vw, br)		3278(w, br)		2325 (vw, br)	2339 (9)	3694 (305/63)	2690 (176/30)	ν(O*X*)
1663 (w)	1674 (0.9)	1653 (s)	1656 (2)	1640 (w)	1646 (0.8)	1680 (461/0.8)	1667 (559/0.6)	$\nu_{as}(CO_3)$
1591 (vw)		1587 (m)	1597 (0.7)	1567 (w)	1581 (1)	1597 (323/0.5)	1587 (253/0.6)	$\nu_{as}(CO_3)$
1213 (w)	1218 (27)	1216 (s)	1212 (23)	826 (vw, sh)		1174 (182/1)	866 (95/0.3)	δ(CO*X*)
1086 (w)	1090 (26)	1092 (s)	1094 (32)	1092 (m)	1098 (23)	1104 (68/7)	1103 (43/6)	ν(CO)
	1000 (21)	1001 (vw)	1002 (19)	996 (w, sh)	1002 (15)	993 (2/4)	993 (18/3)	ν(CC)
902 (m)	899 (100)	901 (s)	904 (100)	900 (m)	905 (66)	897 (86/14)	899 (50/14)	skeletal breathing
784 (m)		771 (s, sh)	778 (0.5)	771 (w)		775 (28/0.006)	775 (30/0.01)	$\gamma(CO_3)$
731 (w)	735 (3)		740 (5)	735 (s, sh)	739 (8)	743 (10/3)	740 (14/3)	δ(COC)
704 (w, sh)	707 (54)		706 (99)		710 (3)	700 (12/8)	689 (6/8)	δ(OCO)

[a] Calculated on the B3LYP/aug-cc-pVTZ level of theory. IR intensity in km mol^{-1} and Raman intensity in $Å^4 u^{-1}$. Abbreviations for IR intensities: v = very, s = strong, m = medium, w = weak. Experimental Raman activities are stated to a scale of 1 to 100. [b] X = H, D.

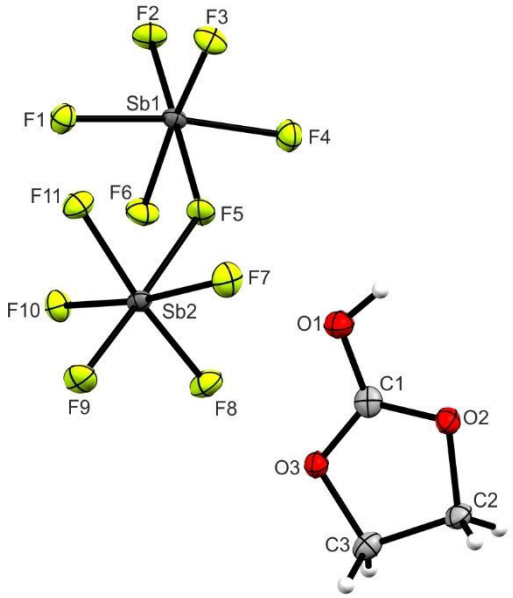

Figure 2. Asymmetric unit of $[C_3H_5O_3]^+[Sb_2F_{11}]^-$ (**4**) (50% probability displacement ellipsoids).

summarized together with crystal structure of ethylene carbonate in Table 2.[17]

Due to the protonation, the C1–O1 bond length is significantly elongated (1.266(3) Å) compared to the neutral compound.[17] In contrast, the bond lengths from C1 to the ring oxygens (C1–O2 and C1–O3) are significantly shortened (1.280(4) Å and 1.283(3) Å). All these bond lengths are in a range between a formal single (1.43 Å) and a double bond (1.19 Å)[18] and are not significantly different. The recently reported crystal structure of ethylene carbonate shows C_2 symmetry with CH_2 groups deviating out of plane. Interestingly, the CO_3 moiety is absolutely planar.[17] In consequence of the protonation, the symmetry changes to approximately C_s symmetry with dihedral angles of 175.6(2)° (O1–C1–O3–C3) and 176.8(3)° (O1–C1–O2–C2). The planarity of the CO_3 group remains nearly unaffected (178.5(4)°). Moreover, the angles of the CO_3 moiety approximate 120° with values in the range between 118.1(2)° (O3–C1–O2) and 123.4(3)°(O1–C1–O2). By comparing the C(H_2)–O bond lengths (C2–O2 and C3–O3) with the neutral species, an elongation to 1.471(3) Å and 1.474(3) Å, respectively, is observed. The C–C bond length is also elongated compared with the neutral compound.[17] In Figure 3, hydrogen bonds and interatomic contacts are illustrated. Cation and anion are connected by moderate hydrogen bonds O1–H1···F11*iii* (2.663(3) Å).[19] Moreover, a C···F contact between C1 and F9, with a value of 2.753(3) Å below the sum of the van der Waals radii, is observed.[20]

The Sb–F bond lengths of the $Sb_2F_{11}^-$ anion are all in a range between 1.847(2) Å and 1.887(2) Å, except the bridging Sb–F bonds. These distances are significantly longer (2.026(1) Å to 2.051(1) Å). With a Sb1–F5–Sb2 bond angle of 140.7(1)°, the $Sb_2F_{11}^-$ anion possesses an angulated conformation. All these bond lengths, as well as the angles are in accordance with previously reported $Sb_2F_{11}^-$ anions.[21,22]

Table 2. Comparison of selected bond lengths [Å] and angles [°] of ethylene carbonate and (**4**) with estimated standard deviations in parentheses. For (**4**), interatomic contacts are listed. Symmetry codes: *i* = ½ + x, ½ − y, −½ + z; *iii* = ½ − x, ½ + y, ½ − z.

	ethylene carbonate[17]	(**4**)
Bond lengths [Å]		
C1–O1	1.188(3)	1.266(3)
C1–O2	1.328(2)	1.280(4)
C1–O3	1.328(2)	1.283(3)
C2–O2	1.474(3)	1.474(3)
C3–O3	1.474(3)	1.471(3)
C3–C2	1.482(3)	1.526(4)
Bond angles [°]		
O1–C1–O3	124.2(1)	118.5(2)
O1–C1–O2	124.2(1)	123.4(3)
O3–C1–O2	111.6(2)	118.1(2)
C1–O3–C3	109.0(2)	107.8(2)
O3–C3–C2	103.2(1)	103.1(2)
C3–C2–O2	103.2(1)	103.3(2)
C2–O2–C1	109.0(2)	107.7(2)
Dihedral angles [°]		
O2–O3–C1–O1	180.00	178.5(4)
O1–C1–O2–C2	173.17	176.8(3)
O1–C1–O3–C3	173.17	175.6(2)
Interatomic contacts D-A [Å]		
O1–H1···F11*iii*		2.663(3)
C1–F9*i*		2.753(3)

Theoretical Calculations

Structure optimization of the free $[C_3H_5O_3]^+$ cation was carried out on the B3LYP/aug-cc-pVTZ level of theory. IR and Raman intensities as well as vibrational frequencies were calculated in the harmonic approximation. Figure 4 shows the comparison of the cation of the single-crystal X-ray structure (4) and the calculated structure of $[C_3H_5O_3]^+$ together with bond lengths and angles.

Comparing the values of the experimentally obtained geometric parameters with those obtained from the calculation

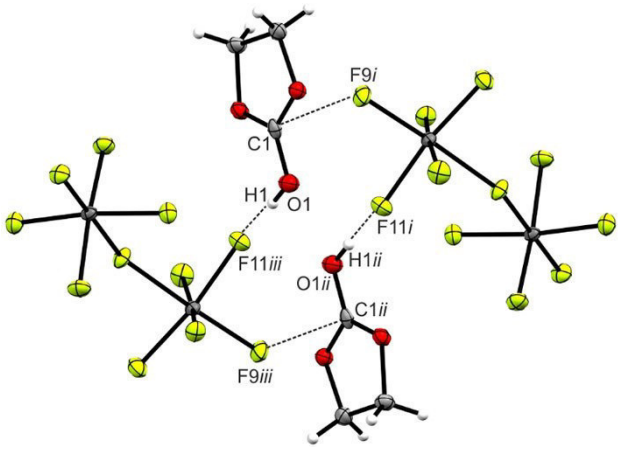

Figure 3. Projection of the interatomic contacts in the $[C_3H_5O_3]^+[Sb_2F_{11}]^-$ (**4**) crystal. (50% probability displacement ellipsoids). Symmetry codes: *i* = ½ + x, ½ − y, −½ + z; *ii* = 1 − x, 1 − y, −z; *iii* = ½ − x, ½ + y, ½ − z.

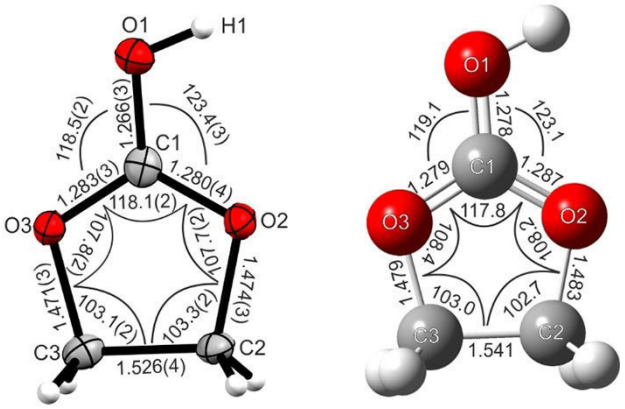

Figure 4. Geometric parameters of the cation of the single crystal X-ray analysis of **4** (left) and the calculated structure of $[C_3H_5O_3]^+$. Bond lengths are given in Å and angles in °.

shows that all values are in good agreement. Only the C1–O1 bond length is overestimated by the calculation. The crystal structure analysis as well as the quantum chemical calculation indicate that all CO bond lengths of the CO_3 moiety are of approximately equal length. This is caused by the resonance stabilization of this group and can be expressed by the Lewis resonance structures shown in Scheme 2.

Despite the protonation, the sp^2 hybridization of the central carbon atom is conserved compared to the neutral compound. Even more interesting is the hybridization of the oxygen atoms. In order to investigate the hybridization situation of the CO_3 group, a Natural Bond Orbital (NBO) analysis was performed on the B3LYP/aug-cc-pVTZ level of theory. In Figure 5, the calculated NBOs of the lone pairs on the oxygen atoms together with the calculated electron occupancy are illustrated.

All oxygen lone pairs are located in the molecule plane, which suggests sp^2 hybridization on each oxygen atom in the protonated species. In order to confirm this hybridization, the corresponding p-orbitals were considered. Figure 6 shows the calculated NBOs of the corresponding p-orbitals together with the calculated electron occupancy. The p-orbital of the central carbon atom as well as every p-orbital of the oxygen atoms are oriented perpendicular to the molecule plane. The NBO analysis shows a π-bond between O3 and C1 with approximately two electrons, whereas the residual p-orbitals on O2 and O1 are occupied with 1.74 and 1.76 electrons, respectively. Additionally, the NBO of the antibonding π-bond of O3 and C1 is occupied with 0.48 electrons. In Table S3, selected NBOs (concerning the CO_3 group) are listed, together with calculated values for electron occupancy and s- and p-character given in percentage (see Supporting Information). In summary, the NBO

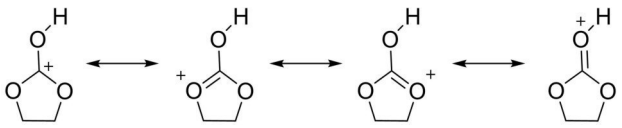

Scheme 2. Lewis resonance structures of monoprotonated ethylene carbonate.

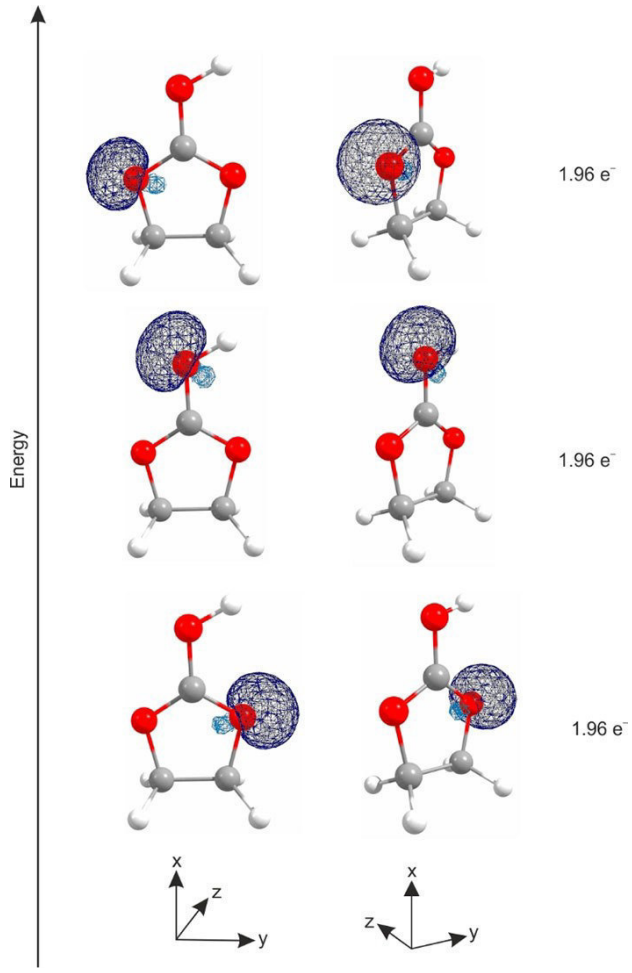

Figure 5. Calculated NBOs (view: frontal and perspective) of the oxygen atoms; here: lone pairs, together with electron occupancy.

analysis indicates that a strong delocalization of the electrons over the Y-shaped CO_3 group is possible.

NMR Spectroscopy of $[C_3H_5O_3]^+[SbF_6]^-$ (1)

The NMR spectroscopic study of $[C_3H_5O_3]^+[SbF_6]^-$ (**1**) was carried out in anhydrous HF (*a*HF). For better comparability, a reference of neutral ethylene carbonate was measured in *a*HF as well. The chemical shifts obtained by ^1H, ^{13}C and ^{19}F NMR spectroscopy are listed in Table 3.

Table 3. ^1H, ^{13}C and ^{19}F chemical shifts of ethylene carbonate and $[C_3H_5O_3]^+[SbF_6]^-$ (**1**) recorded in *a*HF at room temperature for the neutral compound and at −40 °C for **1**, respectively.

	ethylene carbonate	$[C_3H_5O_3]^+[SbF_6]^-$ (**1**)
δ^1H [ppm]	4.54 (CH_2) 7.80 (HF)	4.75 (CH_2) 8.04 (HF)
δ ^{13}C [ppm]	69.73 (CH_2) 165.58 (CO_3)	73.11 (CH_2) 168.16 (CO_3)
δ ^{19}F [ppm]	−197.97 (HF)	−196.41 (HF) −123.24 (SbF_6^-)

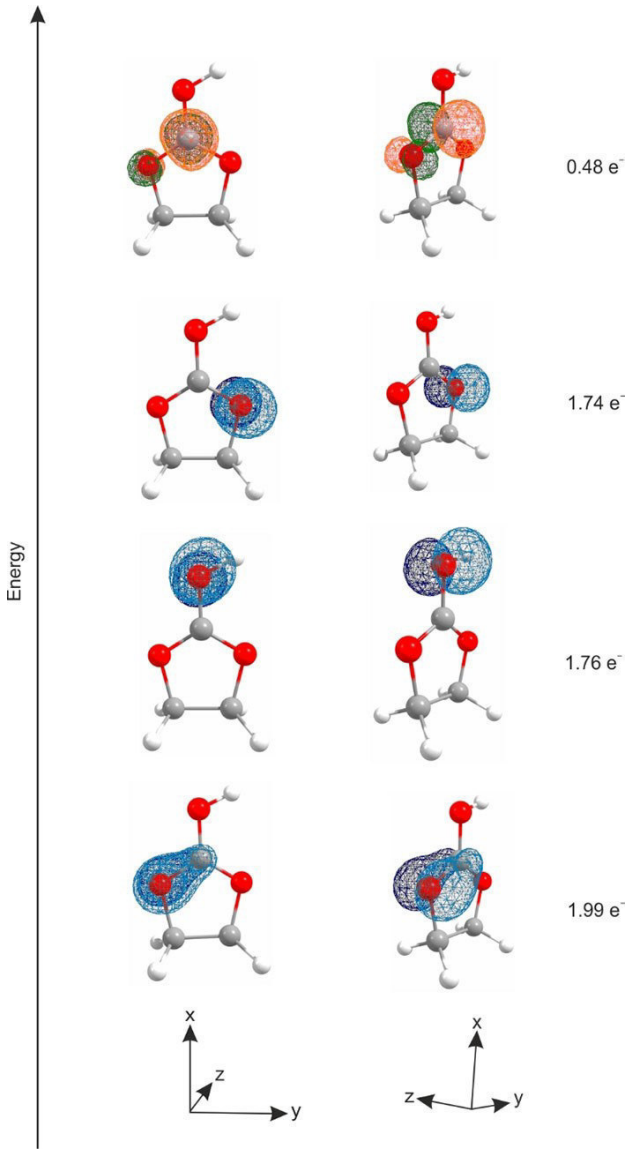

Figure 6. Calculated NBOs (view frontal and perspective) of oxygen atoms and the central carbon atom; here: p-orbitals, together with calculated electron occupancy.

Due to the large excess of *a*HF, the resonance of the proton on the oxygen atom is not observable. Nevertheless, the observation of the anion confirms the formation of the $[C_3H_5O_3]^+$ cation. The ^{19}F signal at −123.24 ppm is attributed to the SbF_6^- anion, which is in accordance with literature.[23] In the ^1H NMR spectrum, the signal of the protons of the CH_2 groups, which appears as a multiplet, is slightly shifted to higher frequencies compared to ethylene carbonate. The same trend is observed for the corresponding C signal in the ^{13}C NMR spectrum. Interestingly, the C atom, belonging to the CO_3 group, is also only slightly deshielded. The signal is shifted by about 2.58 ppm. This leads to the conclusion that protonated ethylene carbonate is a cation where the positive charge is strongly delocalized over the CO_3 moiety.

Conclusion

The protonation of ethylene carbonate succeeded for the first time in the superacidic systems HF/MF_5 (M = As, Sb) and the salts $[C_3H_5O_3]^+[SbF_6]^-$ (**1**), $[C_3H_5O_3]^+[AsF_6]^-$ (**2**), $[C_3H_4DO_3]^+[AsF_6]^-$ (**3**) and $[C_3H_5O_3]^+[Sb_2F_{11}]^-$ (**4**) were isolated. The compounds were characterized by IR and Raman spectroscopy and, in the case of **4**, by an X-ray structure analysis. For compound **1**, an NMR-spectroscopic study in *a*HF was carried out. The experimental results were compared with quantum chemical calculations on the B3LYP/aug-cc-pVTZ level of theory. To elucidate the bonding situation of the CO_3 moiety, a NBO analysis was performed. This calculation indicates a sp^2 hybridization on the central carbon atom as well as on the oxygen atoms, thus leading to the conclusion that protonated ethylene carbonate is a compound with a remarkable 6π-electron delocalization, located on the CO_3 group.

Experimental Section

General

Caution! Avoid contact with any of these compounds. The hydrolysis of all these salts might form HF, which burns skin and causes irreparable damage. Safety arrangements should be taken while using and handling these materials.

All reactions were performed by standard Schlenk technique using a stainless steel vacuum line. All reactions in superacidic media were carried out in FEP/PFA reactors closed with a stainless steel valves. The vacuum line as well as the reactors were dried with fluorine prior to use. Detailed Information about the used apparatus and materials as well as analytic measurement methods are described in the Supporting Information.

Deposition Number 1978961 (for **4**) contains the supplementary crystallographic data for this paper. These data are provided free of charge by the joint Cambridge Crystallographic Data Centre and Fachinformationszentrum Karlsruhe Access Structures service.

Synthesis of $[C_3H_5O_3]^+[SbF_6]^-$ (1) and $[C_3H_5O_3]^+[Sb_2F_{11}]^-$ (4)

First, antimony pentafluoride SbF_5 (140 mg, 0.65 mmol, 1.0 eq. for **1** and 170 mg, 0.78 mmol, 2.0 eq. for **4**) was condensed into a FEP tube reactor at −196 °C. Afterwards, 2 mL anhydrous hydrogen fluoride *a*HF (2 mL) were also condensed in the reactor. To form the superacidic system, both compounds (SbF_5 and HF) were allowed to warm up to −40 °C. The reaction mixture was cooled to −196 °C and under inert gas atmosphere ethylene carbonate was added (57 mg, 0.65 mmol, 1.0 eq. for **1** and 34 mg, 0.39 mmol, 1.0 eq. for **4**). For the desired protonation of ethylene carbonate, the reaction mixture was warmed up again to −40 °C and homogenized until the salt was completely dissolved. To obtain salt **1**, the solution was again cooled (−196 °C) and excess HF was removed overnight at −78 °C in a dynamic vacuum. For the crystallization of compound **4**, the reactor was left in an ethanol bath (T = −50 °C) until the salt recrystallized. Both salts $[C_3H_5O_3]^+[SbF_6]^-$ (**1**) and $[C_3H_5O_3]^+[Sb_2F_{11}]^-$ (**4**) were obtained as colorless solids, which are stable under inert gas atmosphere up to −20 °C.

Synthesis of $[C_3H_5O_3]^+[AsF_6]^-$ (2) and $[C_3H_4DO_3]^+[AsF_6]^-$ (3)

Anhydrous hydrogen fluoride *a*HF (2 mL) for **2**, respectively deuterium fluoride *a*DF for **3**, was condensed into a FEP tube-reactor at −196 °C. Under the same conditions, arsenic pentafluoride (85 mg, 0.5 mmol, 1.0 eq.) was also condensed into the reactor. Both compounds were warmed up to −40 °C, blended to form the superacidic system and cooled to −196 °C. Ethylene carbonate (44 mg, 0.5 mmol, 1.0 eq.) was added under inert gas atmosphere and the reaction mixture was again allowed to warm up to −40 °C. After homogenizing all compounds until the salt was completely dissolved, the solution was again cooled to −196 °C and excess *a*HF/*a*DF was removed in a dynamic vacuum overnight at −78 °C. $[C_3H_5O_3]^+[AsF_6]^-$ (**2**) and $[C_3H_4DO_3]^+[AsF_6]^-$ (**3**) were obtained as colorless solids, which are stable up to room temperature.

Acknowledgements

We are grateful to the Department of Chemistry of the Ludwig Maximilian University of Munich, the Deutsche Forschungsgemeinschaft (DFG), and the F-Select GmbH for their financial support.

Conflict of Interest

The authors declare no conflict of interest.

[1] K. Ozawa, *Lithium Ion Rechargeable Batteries*, Wiley, Weinheim, **2009**.
[2] D. W. Murphy, J. Broadhead, B. C. H. Steele, *Materials for Advanced Batteries*, Springer, Boston, MA, **1980**.
[3] M. Lazzari, *J. Electrochem. Soc.* **1980**, *127*, 773.
[4] G. E. Blomgren, *J. Electrochem. Soc.* **2017**, *164*, A5019-A5025.
[5] K. Mizushima, P. C. Jones, P. J. Wiseman, J. B. Goodenough, *Mater. Res. Bull.* **1980**, *15*, 783–789.
[6] J. C. Hunter, *J. Solid State Chem.* **1981**, *39*, 142–147.
[7] B. Klassen, R. Aroca, M. Nazri, G. A. Nazri, *J. Phys. Chem. B* **1998**, *102*, 4795–4801.
[8] R. Fong, *J. Electrochem. Soc.* **1990**, *137*, 2009.
[9] D. Battisti, G. A. Nazri, B. Klassen, R. Aroca, *J. Phys. Chem.* **1993**, *97*, 5826–5830.
[10] S.-A. Hyodo, K. Okabayashi, *Electrochim. Acta* **1989**, *34*, 1557–1561.
[11] H. Hart, D. A. Tomalia, *Tetrahedron Lett.* **1966**, *7*, 3383–3388.
[12] G. A. Olah, A. M. White, *J. Am. Chem. Soc.* **1968**, *90*, 1884–1889.
[13] M. N. Eberlin, R. G. Cooks, *Org. Mass Spectrom.* **1993**, *28*, 679–687.
[14] J. Weidlein, K. Dehnicke, U. Müller, *Schwingungsspektroskopie. Eine Einführung*, Thieme, Stuttgart, **1988**.
[15] B. Fortunato, P. Mirone, G. Fini, *Spectrochim. Acta Part A* **1971**, *27*, 1917–1927.
[16] J. R. Durig, J. W. Clark, J. M. Casper, *J. Mol. Struct.* **1970**, *5*, 67–84.
[17] S. Atterberry, M. R. Bond, *CCDC 1965649: Experimental Crystal Structure Determination*, Cambridge Crystallographic Data Centre, **2019**.
[18] A. F. Holleman, E. Wiberg, N. Wiberg, *Anorganische Chemie*, De Gruyter, Berlin, Boston, **2017**.
[19] G. A. Jeffrey, *An Introduction to hydrogen bonding*, Oxford University Press, New York, **1997**.
[20] A. Bondi, *J. Phys. Chem.* **1964**, *68*, 441–451.
[21] J. F. Lehmann, G. J. Schrobilgen, K. O. Christe, A. Kornath, R. J. Suontamo, *Inorg. Chem.* **2004**, *43*, 6905–6921.
[22] D. Leitz, M. Hopfinger, K. Stierstorfer, Y. Morgenstern, J. Axhausen, A. Kornath, *Z. Anorg. Allg. Chem.* **2017**, *643*, 1202–1207.
[23] J.-C. Culmann, M. Fauconet, R. Jost, J. Sommer, *New J. Chem.* **1999**, *23*, 863–867.

Manuscript received: October 11, 2021
Revised manuscript received: October 18, 2021

ChemistryOpen

Supporting Information

Protonated Ethylene Carbonate: A Highly Resonance-Stabilized Cation

Stefanie Beck, Christoph Jessen, and Andreas J. Kornath*

Table of Contents

Apparatus and Materials

Low-temperature IR spectra were recorded by a Bruker Vertex-80V FTIR spectrometer ($\tilde{\nu}$ = 350 to 4000 cm^{-1}). For the measurement, small amounts of the synthesized compounds were placed on a CsBr single-crystal plate in a cooled cell.

Raman measurements were carried out on a Bruker MultiRAM FT-Raman spectrometer with Nd:YAG laser excitation (λ = 1064 nm) in vacuum at –196 °C. Therefore, the samples were transferred into cooled glass cells.

The low-temperature X-ray diffraction of $[C_3H_5O_3]^+[Sb_2F_{11}]^-$ (**4**) was performed with an Oxford XCalibur3 diffractometer equipped with a Kappa CCD detector, operated with Mo-κ_α radiation (λ = 0.71073 Å) and a Spellman generator (voltage 50 kV, current 40 mA). The collection of the data was performed at 113 K using the CrysAlis CCD software,[1] while the reduction were carried out using CrysAlis RED software.[2] Programs SHELXS[3] and SHELXL-97,[4] belonging to the WinGX software package, were used for performing the solution and refinement of the crystal structure. Afterwards the structure was checked by PLATON software.[5] The absorption correction was accomplished by using the SCALE3 ABSPACK multiscan method.[6] In Table S2 selected data and parameters of the X-ray structure analysis are listed. Crystallographic data (excluding structure factors) for the structure in this paper have been deposited with the Cambridge Crystallographic Data Centre, CCDC, 12 Union Road, Cambridge CB21EZ, UK. Copies of the data can be obtained free of charge on quoting the depository number CCDC-1978961 for $[C_3H_5O_3]^+[Sb_2F_{11}]^-$ (**4**) (Fax: +44-1223-336-033; E-Mail: deposit@ccdc.cam.ac.uk, http:// www.ccdc.cam.ac.uk).

Quantum chemical calculations were carried out on the B3LYP/aug-cc-PVTZ level of theory by Gaussian 09.[7]

NMR spectra were recorded on a Jeol ECX400 NMR. The spectrometer were externally referenced to $CFCl_3$ for ^{19}F and to tetramethylsilane for ^1H and ^{13}C NMR spectra. The spectra were recorded inside 4 mm FEP NMR tube inliners. Acetone-d_6 was employed for external shimming, when *a*HF was used as solvent for the respective compounds. The NMR samples were prepared by dissolving ethylene carbonate, and the protonated species $[C_3H_5O_3]^+[SbF_6]^-$ (**1**) respectively, in *a*HF. The solutions were transferred into a 4 mm FEP NMR tube inliner. The inliner was than frozen and flame sealed.

[1] *CrysAlisCCD, Version 1.171.35.11 (release 16-05-2011 CrysAlis 171.NET)*, Oxford Diffraction Ltd., **2011**.
[2] *CrysAlisRED, Version 1.171.35.11 (release 16.05.2011 CrysAlis 171.NET)*, Oxford Diffraction Ltd., **2011**.
[3] G. Sheldrick, *SHELXS-97, Program for Crystal Structure Solution*, University of Göttingen, Germany, **1997**.
[4] G. Sheldrick, *SHELXL-97, Program for the Refinement of Crystal Structures*, University of Göttingen, Germany, **1997**.
[5] A. Spek, *PLATON, A Multipurpose Crystallographic Tool*, Utrecht University, Utrecht (The Netherlends), **1999**.
[6] *SCALE3 ABSPACK - An Oxford Diffraction Program*, Oxford Diffraction Ltd., UK, **2005**.
[7] M. J. Frisch, G. W. Trucks, H. B. Schlegel, G. E. Scuseria, M. A. Robb, J. R. Cheeseman, G. Scalmani, V. Barone, B. Mennucci, G. A. Petersson, H. Nakatsuji, M. Caricato, X. Li, H. P. Hratchian, A. F. Izmaylov, J. Bloino, G. Zheng, J. L. Sonnenberg, M. Hada, M. Ehara, K. Toyota, R. Fukuda, J. Hasegawa, M. Ishida, T. Nakajima, Y. Honda, O. Kitao, H. Nakai, T. Vreven, J. A. Montgomery, Jr., J. E. Peralta, F. Ogliaro, M. Bearpark, J. J. Heyd, E. Brothers, K. N. Kudin, V. N. Staroverov, R. Kobayashi, J. Normand, K. Raghavachari, A. Rendell, J. C. Burant, S. S. Iyengar, J. Tomasi, M. Cossi, N. Rega, J. M. Millam, M. Klene, J. E. Knox, J. B. Cross, V. Bakken, C. Adamo, J. Jaramillo, R. Gomperts, R. E. Stratmann, O. Yazyev, A. J. Austin, R. Cammi, C. Pomelli, J. W. Ochterski, R. L. Martin, K. Morokuma, V. G. Zakrzewski, G. A. Voth, P. Salvador, J. J. Dannenberg, S. Dapprich, A. D. Daniels, Ö. Farkas, J. B. Foresman, J. V. Ortiz, J. Cioslowski, D. J. Fox, *Gaussian 09, Revision A.02*, Gaussian Inc., Wallingford CT, **2009**.

Table S1. Experimental vibrational frequencies [cm^{-1}] of **1**-**3** and calculated vibrational frequencies [cm^{-1}] of free cations $[C_3H_5O_3]^+$ and $[C_3H_4DO_3]^+$.

$[C_3H_5O_3]^+[SbF_6]^-$		$[C_3H_5O_3]^+[AsF_6]^-$		$[C_3H_4DO_3]^+[AsF_6]^-$		$[C_3H_5O_3]^+$	$[C_3H_4DO_3]^+$	Assignment[b]
IR	**Raman**	**IR**	**Raman**	**IR**	**Raman**	**Calc.[a] (IR/Raman)**	**Calc.[a] (IR/Raman)**	
3405(vw, br)		3278 (vw)		2325 (vw, br)	2339 (9)	3694 (305/63)	2690 (176/30)	ν(O*X*)
3083 (vw)	3085 (5)	3108 (w)	3089 (3)	3089 (w, sh)	3090 (5)	3189 (3/42)	3189 (3/42)	$\nu_{as}(CH_2)$
	3074 (12		3078 (16)		3079 (18)	3174 (0.01/48)	3174 (0.01/48)	$\nu_{as}(CH_2)$
						3118 (0.3/52)	3118 (0.3/52)	$\nu_{s}(CH_2)$
	3024 (68)		3028 (54)	3031 (vw, sh)	3028 (47)	3117 (0.4/161)	3117 (0.4/161)	$\nu_{s}(CH_2)$
	2961 (4)		2966 (3)	2961 (vw)	2968 (3)			?
	2924 (6)		2932 (6)		2931 (6)			?
2637 (vw)		2630 (vw)						?
2534 (vw)		2522 (vw)						?
2442 (vw)	2445 (0.8)	2424 (vw)						?
1663 (w)	1674 (0.9)	1653 (s)	1656 (2)	1640 (w)	1646 (0.8)	1680 (461/0.8)	1667 (559/0.6)	$\nu_{as}(CO_3)$
1591 (vw)		1587 (m)	1597 (0.7)	1567 (w)	1581 (1)	1597 (323/0.5)	1587 (253/0.6)	$\nu_{as}(CO_3)$
	1531 (1)		1539 (0.5)			1529 (0.9/4)	1528 (1/4)	$\delta(CH_2)$
1483 (vw)	1487 (13)		1489 (8)	1483 (w)	1490 (9)			?
1468 (vw)	1470 (20)	1471 (w)	1473 (23)	1469 (vw)	1473 (16)	1514 (3/6)	1514 (1/6)	$\delta(CH_2)$
1371 (vw)	1376 (3)	1370 (w)	1369 (4)	1369 (w)	1369 (3)	1394 (1/0.7)	1394 (0.5/0.7)	$\omega(CH_2)$
1320 (vw)	1325 (1)	1316 (s)	1317 (0.8)	1284 (w)	1289 (0.7)	1330 (90/0.4)	1314 (89/0.2)	$\omega(CH_2)$
1250 (vw, sh)		1247(w, sh)				1244 (0.05/2)	1244 (0.03/2)	$\rho(CH_2)$
1227 (w)	1229 (4)		1226 (3)	1228 (w)	1227 (5)	1229 (5/3)	1229 (5/3)	$\tau(CH_2)$
1213 (w)	1218 (27)	1216 (s)	1212 (23)	826 (vw, sh)		1174 (182/1)	866 (95/0.3)	δ(CO*X*)
1164 (vw)		1133 (vw)				1145 (0.04/0.06)	1145 (0.004/0.05)	$\tau(CH_2)$
1086 (w)	1090 (26)	1092 (s)	1094 (32)	1092 (m)	1098 (23)	1104 (68/7)	1103 (43/6)	ν(CO)
	1000 (21)	1001 (vw)	1002 (19)	1007 (w)	1002 (15)	993 (2/4)	993 (18/3)	ν(CC)
977 (w)		947 (vw)		992 (w, sh)		931 (7/0.7)	991(29/1))	ν(CO)
902 (m)	899 (100)	901 (s)	904 (100)	900 (m)	905 (66)	897 (86/14)	899 (50/14)	skeletal breathing
806 (m, sh)				826 (vw, sh)		847 (0.2/0.1)	847 (0.2/0.1)	$\rho(CH_2)$
784 (m)		771 (s, sh)	778 (0.5)	771 (w)		775 (28/0.006)	775 (30/0.01)	$\gamma(CO_3)$
762 (m)								?
731 (w)	735 (3)		740 (5)	735 (s, sh)	739 (8)	743 (10/3)	740 (14/3)	δ(COC)
704 (w, sh)	707 (54)		706 (99)		710 (3)	700 (12/8)	689 (6/8)	δ(OCO)
						565 (135/0.8)	418 (63/0.2)	$\delta(CO X)_{oop}$
						451 (14/0.3)	424 (15/0.3)	δ(OCO)
	253 (3)		264 (1)		263 (1)	229 (9/0.1)	226 (11/0.08)	skeletal vibration
	148 (5)		124 (12)		124 (8)	36 (0.2/0.02)	36 (0.2/0.02)	skeletal vibration

658 (vs)	662 (97)	699 (vs)	692 (28)	700 (vs)	699 (100)	$[MF_6]^-$
641 (vs)	642 (59)	676 (vs, sh)	685 (75)	672 (vs)	686 (65)	$[MF_6]^-$
621 (vs)	581 (12)	642 (vs)	671 (7)	589 (m)	672 (6)	$[MF_6]^-$
611 (vs)	543 (10)	595 (m, sh)	634 (0.5)	587 (m, sh)	601 (3)	$[MF_6]^-$
596 (vs)	493 (5)	551 (m)	590 (5)	532 (m)	587 (1)	$[MF_6]^-$
578 (vs)	294 (8)	487 (s)	579 (13)	464 (w)	580 (12)	$[MF_6]^-$
542 (m)	278 (26)		541 (7)		565 (1)	$[MF_6]^-$
491 (vs)			488 (4)		519 (1)	$[MF_6]^-$
467 (s)			401 (0.7)		464 (3)	$[MF_6]^-$
452 (s)			372 (32)		372 (24)	$[MF_6]^-$
422 (m)						$[MF_6]^-$

[a] Calculated on the B3LYP/aug-cc-pVTZ level of theory. IR intensity in km/mol and Raman intensity in $Å^4/u$. Abbreviations for IR intensities: v = very, s = strong, m = medium, w = weak. Experimental Raman activities are stated to a scale of 1 to 100. [b] *X* = H, D.

Table S2. Crystal data and structure refinement for $[C_3H_5O_3]^+[Sb_2F_{11}]^-$ (**4**).

	$[C_3H_5O_3]^+[Sb_2F_{11}]^-$ (**4**)
Empirical formula	C3 H5 F11 O3 Sb2
M_r	541.57
Crystal system	monoclinic
Space group	*P* $2_1/n$
a [Å]	9.0783(4)
b [Å]	10.4388(4)
c [Å]	12.3161(4)
α [°]	90
β [°]	93.146(4)
γ [°]	90
V [Å^3]	1165.40(8)
Z	4
ρ_{calcd} [gcm^{-3}]	3.087
μ[mm^{-1}]	4.785
$\lambda_{Moκα}$	0.71073
F(000)	992
T[K]	113(2)
hkl range	–12:12; –12:14;–17:17
refl. measured	12132
refl. unique	3542
R_{int}	0.0311
parameters	178
R(F)/*w*R(F^2)[a)]	0.0348/0.0531
weighting scheme[b)]	0.0157
S(GoF)[c)]	1.071
residual density [eÅ^{-3}]	1.159/ –0.813
devide type	Oxford XCalibur
solution/refinement	SHELXS-97
CCDC	1978961

a) $R_1 = \Sigma||F_o|-|F_c||/\Sigma|F_o|$; b) $wR_2 = [\Sigma[w(F_o^2-F_c^2)^2]/\Sigma[w(F_o)^2]]^{1/2}$; $w = [\sigma_c^2(F_o^2)+(xP)^2+yP]^{-1}$; $P = (F_o^2+2F_c^2)/3$ c) GoF = $\{\Sigma[w(F_o^2-F_c^2)^2]/(n-p)\}^{1/2}$ (*n* = number of reflexions; p = total number of parameters).

Table S3. Selected NBOs (BD = 2-center bond; LP = 1-center valence lone pair; BD* = 2-center antibond) together with calculated values for occupancy and s- and p-character.[a]

Bond	Occupancy	s-, p-character
BD(1) C1–O3	1.99	O3 s (30.19%), p 2.29 (69.24%)
		C1 s (33.29%), p 2.00 (66.57%)
BD(2) C1–O3	1.99	O3 s (0.00%), p 1.00 (99.55%)
		C1 s (0.00%), p 1.00 (99.47%)
BD(1) O2–C1	2.00	O2 s (29.69%), p 2.35 (69.76%)
		C1 s (32.95%), p 2.03 (66.91%)
BD(1) C1–O1	1.99	C1 s (33.65%), p 1.97 (66.24%)
		O1 s (32.76%), p 2.03 (66.63%)
LP(1) O3	1.96	s (44.68%), p 1.23 (55.13%)
LP(1) O2	1.96	s (44.70%), p 1.23 (55.13%)
LP(2) O2	1.74	s (0.00%), p 1.00 (99.56%)
LP(1) O1	1.96	s (44.28%), p 1.25 (55.48%)
LP(2) O1	1.76	s (0.00%), p 1.00 (99.55%)
BD*(1) O3–C1	0.05	O3 s (30.19%), p 2.29 (69.24%)
		C1 s (33.29%), p 2.00 (66.57%)
BD*(2) O3–C1	0.48	O3 s (0.00%), p 1.00 (99.55%)
		C1 s (0.00%), p1.00 (99.47%)

[a] Calculated on the B3LYP/aug-cc-pVTZ level of theory.

Table S4. Cartesian coordinates of calculated minimum structures of protonated ethylene carbonate at the B3LYP/aug-cc-pVTZ level of theory.

Atoms	x	y	z
C	-1.399518	-0.742857	-0.000086
C	-1.363250	0.798016 0	0.000090
H	-1.832686	-1.179328	0.893609
H	-1.832406	-1.179118	-0.894021
H	-1.772339	1.255483	0.894512
H	-1.772615	1.255698	-0.894092
O	0.033739	-1.108557	0.000084
O	0.090864	1.088526	-0.000089
C	0.724734	-0.031504	-0.000002
O	2.000313	-0.111526	-0.000008
H	2.438917	0.757801	0.000079

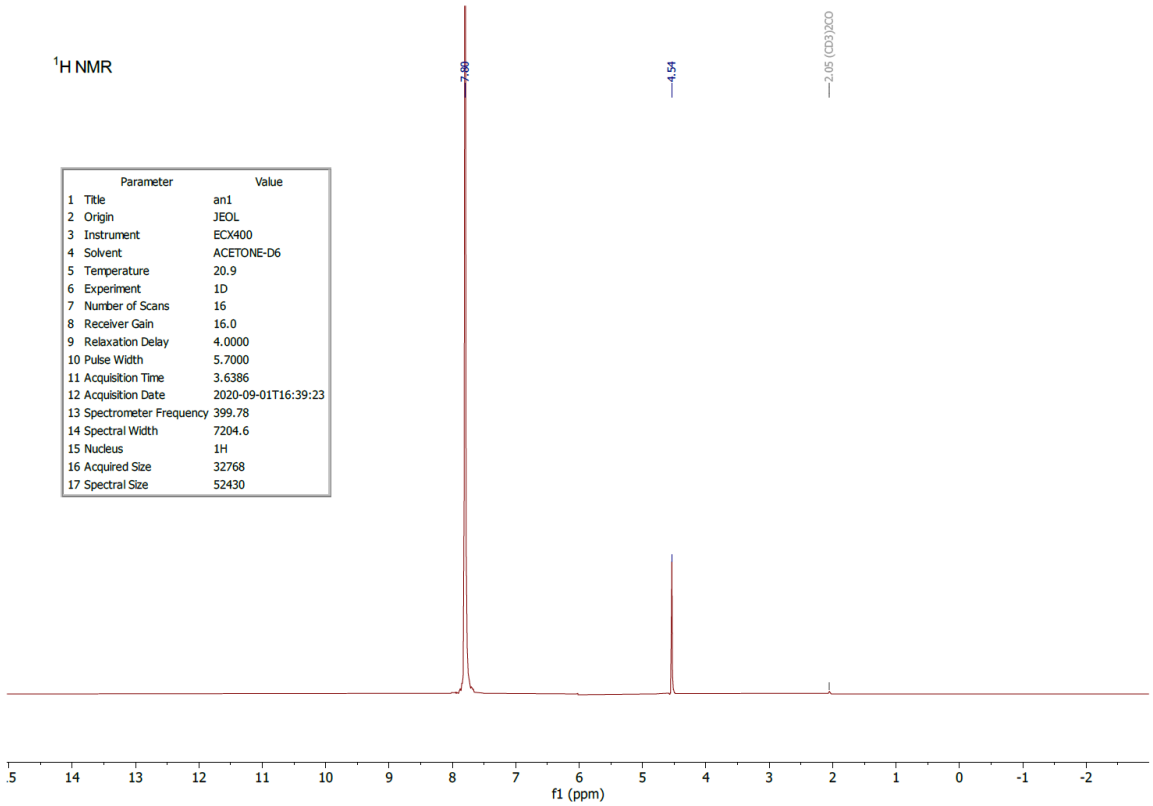

Figure S1. 400 MHz ^{1}H NMR spectrum of ethylene carbonate.

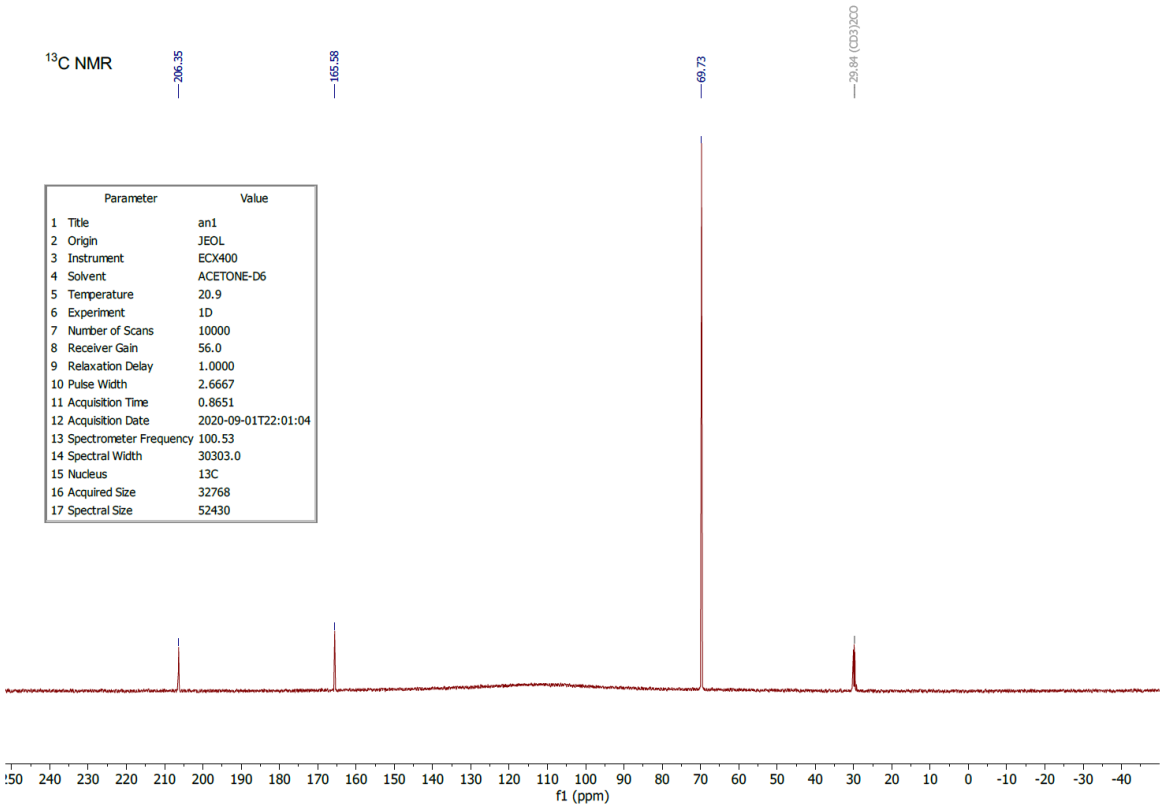

Figure S2. 100 MHz ^{13}C NMR spectrum of ethylene carbonate.

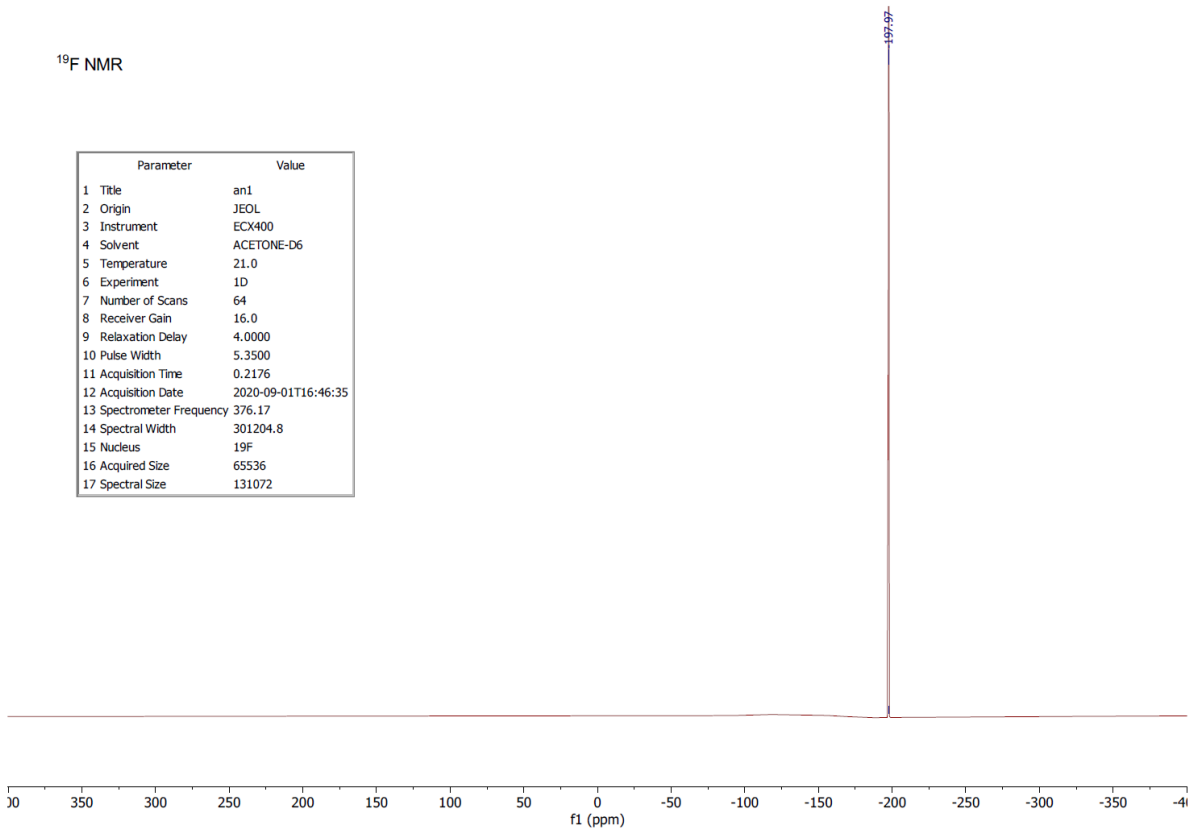

Figure S3. 376 MHz ^{19}F NMR spectrum of ethylene carbonate.

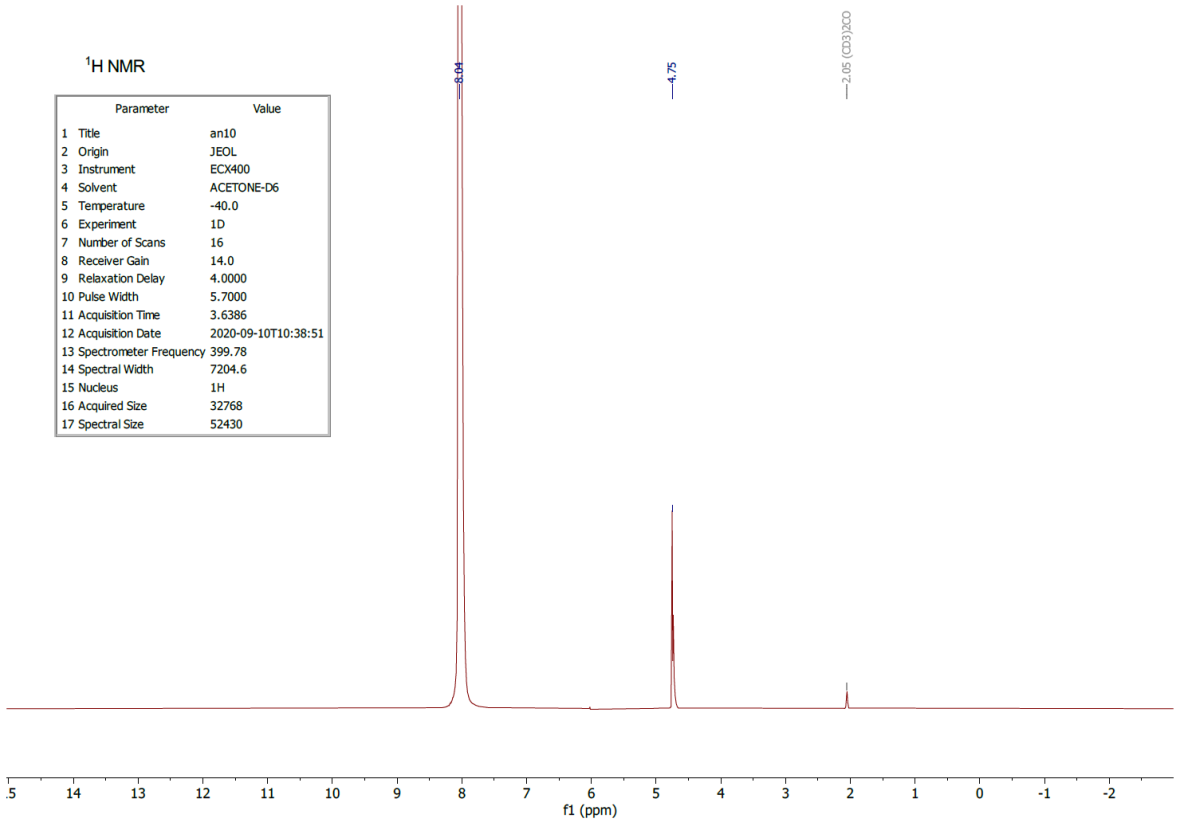

Figure S4. 400 MHz ^{1}H NMR Spectrum of $[C_3H_5O_3]^+[SbF_6]^-$ (**1**).

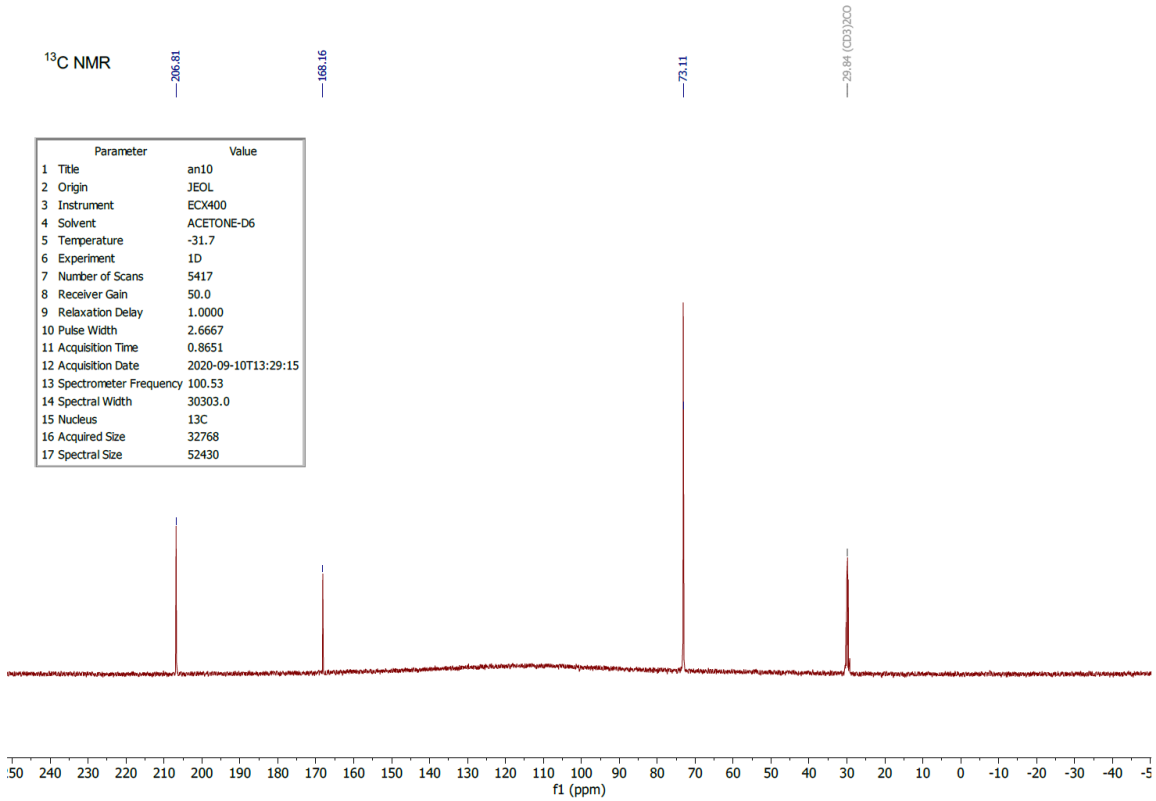

Figure S5. 100 MHz ^{13}C NMR spectrum of $[C_3H_5O_3]^+[SbF_6]^-$ (**1**).

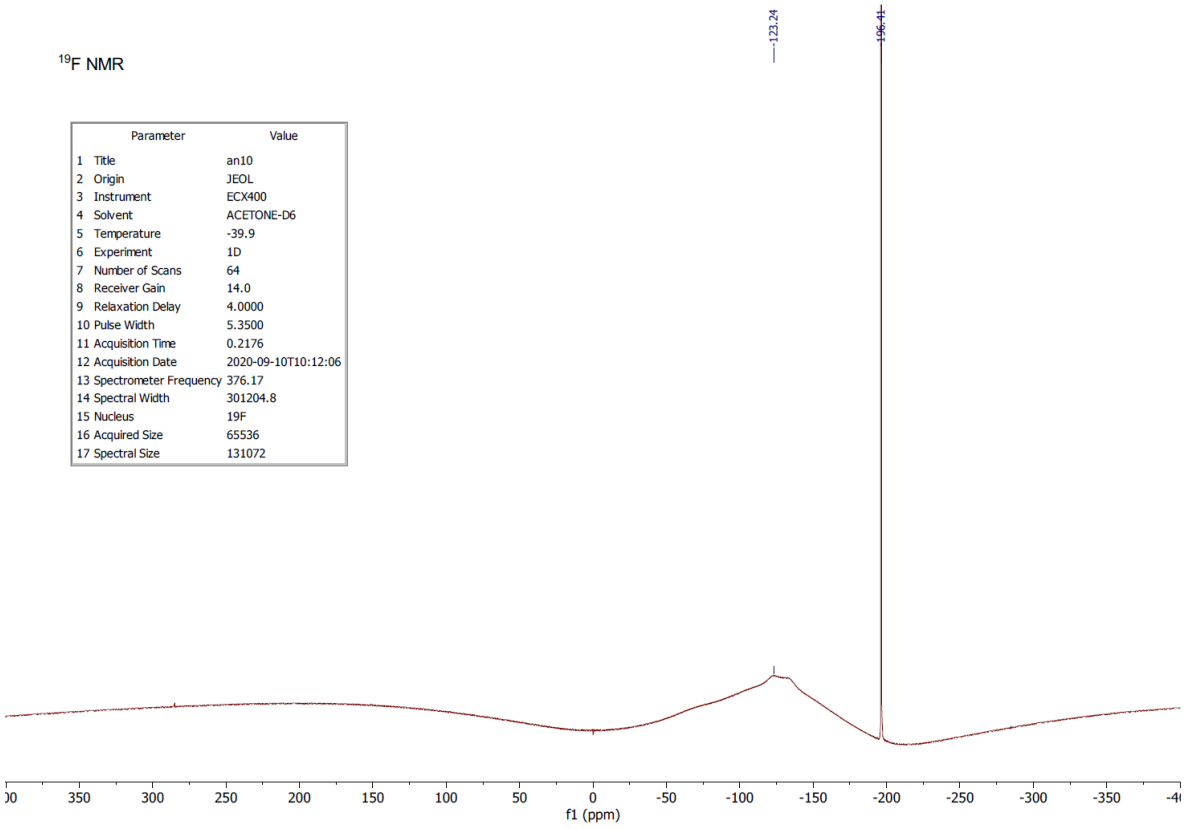

Figure S6. 376 MHz ^{19}F Spectrum of $[C_3H_5O_3]^+[SbF_6]^-$ (**1**).

EurJOC
European Journal of Organic Chemistry

Full Paper
doi.org/10.1002/ejoc.202000656

Chemistry Europe
European Chemical Societies Publishing

Check for updates

Superacid Chemistry

Diprotonated Parabanic Acid: A Vicinal or 1,3-Dication?

Stefanie Beck,[a] Milica Raljic,[a] Christoph Jessen,[a] and Andreas J. Kornath*[a]

Abstract: Reacting parabanic acid with the superacidic systems XF/MF_5 (X = H, D; M = As, Sb) in different ratios, led to the formation of the mono- and diprotonated species. Salts in terms of $[C_3H_3N_2O_3][AsF_6]$, $[C_3H_3N_2O_3][SbF_6]$, $[C_3H_4N_2O_3][AsF_6]_2$, $[C_3H_4N_2O_3][SbF_6]_2$, $[C_3D_3N_2O_3][AsF_6]$ and $[C_3D_4N_2O_3][AsF_6]_2$ were obtained and characterized by low-temperature infrared and Raman spectroscopy. Single-crystal X-ray structure analyses were performed for $[C_3H_3N_2O_3][SbF_6]$ and $[C_3H_4N_2O_3][AsF_6]_2 \cdot 4HF$. Additionally, quantum chemical calculations were carried out on the B3LYP/aug-cc-pVTZ level of theory for the mono- and dication. Mapped Electrostatic Potentials together with Natural Population Analysis charges were calculated in order to localize the two positive charges of the diprotonated parabanic acid. The diprotonated parabanic acid can be described as an 1,2-*C*,*C*-dication, stabilized by electron delocalization over the five-membered ring.

Introduction

Imidazolidine-2,4,5-trione, better known as parabanic acid, was prepared for the first time by *Woehler* and *Liebig* in 1838.[1] An established synthesis route is the reaction of urea with diethyl oxalate [Equation (1)].[2,3]

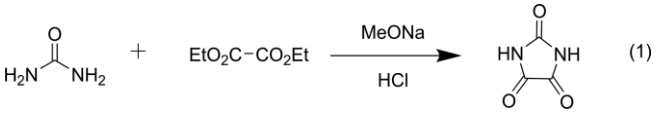

(1)

In a biological context, parabanic acid can be considered as the oxidation product of uric acid, which is the end-product of the nucleotide metabolism.[4,5] Parabanic acid is a heterocyclic compound with an imidazolidine skeletal structure, where the CH_2 groups are replaced by carbonyl groups. Thus, the molecule bears five potential basic centers. In this context, *Arca* et al. reported theoretical investigations on the electron delocalization and charge distribution.[6] Their results led to the assumption that protonations were possible on the carbonyl groups, as well as on the amine groups.

To the best of our knowledge, no isolated protonated species of parabanic acid has been reported in literature. In the course of our investigations on multiple protonations, we focus on two questions. First, to what extent it would be possible to protonate parabanic acid, and second, where the positive charges, in case of a higher protonated species, are located.

[a] *S. Beck, M. Raljic, C. Jessen, Prof. Dr. A. J. Kornath*
Department of Chemistry, Ludwig-Maximilian University München
Butenandtstr. 5–13, 81377 München, Germany
E-mail: andreas.kornath@cup.uni-muenchen.de
http://www.org.chemie.uni-muenchen.de/ac/kornath/

Supporting information and ORCID(s) from the author(s) for this article are available on the WWW under https://doi.org/10.1002/ejoc.202000656.

Results and Discussion

Synthesis of $[C_3H_3N_2O_3][MF_6]$ and $[C_3H_4N_2O_3][MF_6]_2$ (M = As, Sb)

The salts of the mono- and diprotonated parabanic acid were prepared according to Equations (2) and (3):

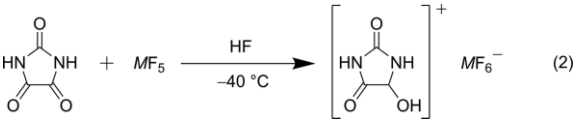

(2)

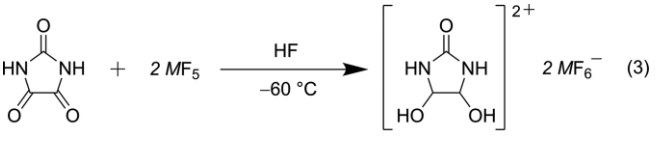

(3)

M = As, Sb

Firstly, the superacidic systems HF/AsF_5 and HF/SbF_5 were prepared using an excess of anhydrous hydrogen fluoride (*a*HF). Both mixtures were warmed up to –40 °C and homogenized to achieve complete solvation of the respective Lewis acid. After cooling down to –196 °C, parabanic acid was added to the frozen superacidic system under nitrogen atmosphere. The reaction mixture was warmed up to –40 °C (–60 °C, respectively), resulting in the formation of the protonated species. Excess *a*HF was removed at –78 °C under dynamic vacuum overnight. The salts were obtained as colorless solids, stable at room temperature under inert gas atmosphere.

The monoprotonated salts of parabanic acid $[C_3H_3N_2O_3][AsF_6]$ (**1**) and $[C_3H_3N_2O_3][SbF_6]$ (**2**) were obtained by using an equimolar amount of the starting material with respect to the Lewis acid.

Using a two-to-one ratio of Lewis acid, in terms of parabanic acid, the diprotonated species $[C_3H_4N_2O_3][AsF_6]_2$ (**3**) and

Full Paper
doi.org/10.1002/ejoc.202000656

$[C_3H_4N_2O_3][SbF_6]_2$ (**4**) were obtained. The salts (**3**) and (**4**) are stable up to –20 °C.

For vibrational spectroscopic studies, the deuterium isotopomers of both cations were prepared. The superacidic system DF/AsF_5 led to the formation of the corresponding deuterated species $[C_3D_3N_2O_3][AsF_6]$ (**5**) and $[C_3D_4N_2O_3][AsF_6]_2$ (**6**), respectively. The hydrogen atoms of the amine groups were entirely replaced by deuterium, as deuterium fluoride was used in large excess (100:1). The degree of deuteration approximates 98 %.

Even with an eight-to-one ratio of the stronger Lewis acid SbF_5, only the diprotonated species was obtained and, in this work, no triprotonated species was observed.

Crystal Structure of $[C_3H_4N_2O_3][AsF_6]_2$·4 HF (3)

The diprotonated species of parabanic acid $[C_3H_4N_2O_3][AsF_6]_2$·4HF (**3**) crystallizes in the monoclinic space group *C*2/*c* with four formula units per unit cell. Figure 1 depicts the formula unit, with selected bond lengths and angles being summarized in Table 1.

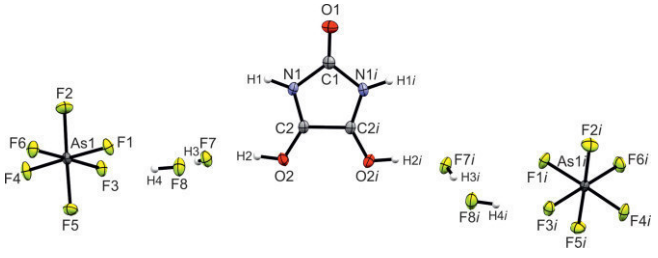

Figure 1. Formula unit of $[C_3H_4N_2O_3][AsF_6]_2$·4HF (50 % probability displacement ellipsoids). Symmetry code: *i* = 1 – *x*, *y*, 1.5 – *z*.

Table 1. Selected bond lengths [Å] and angles [°] of $[C_3H_4N_2O_3][AsF_6]_2$·4HF (**3**) with estimated standard deviations in parentheses.[a]

Bond lengths [Å]			
O1–C1	1.167(3)	C2–C2*i*	1.511(3)
C1–N1	1.434(2)	C2–O2	1.253(2)
N1–C2	1.305(2)		
Bond angles [°]			
N1–C1–N1*i*	104.9(2)	O1–C1–N1	127.6(10)
C1–N1–C2	110.6(15)	O2–C2–N1	132.8(15)
N1–C2–C2*i*	106.9(9)	O2–C2–C2*i*	120.2(10)
Interatomic contacts D–A [Å]			
N1–(H1)···F4*ii*	2.765(2)	F7–(H3)···F8	2.449(2)
O2–(H2)···F7	2.479(2)	F8–(H4)···F3	2.511(1)

[a] Symmetry codes: *i* = 1 – *x*,*y*,1.5 – *z*; *ii* = 0.5 + *x*,0.5 + *y*,1 + *z*.

Due to the twofold protonation, the C_{2v} symmetry of parabanic acid is conserved in the resulting dication. Both protonations are located on the respective neighboring carbonyl groups, O2/O2*i*. The protons were found in the difference Fourier synthesis and refined isotropically. However, the localization of the protons is not very meaningful. In consequence of the significant elongation of the C2–O2 (C2*i*–O2*i* respectively) bond length [1.253(2) Å], compared to the starting material,[7] the *O*-protonations are clearly confirmed. In contrast, the N1–C2 bond length becomes significantly shorter [1.305(2) Å]. The third remaining carbonyl bond is significantly shortened, compared to the neutral compound,[7] and is, with a value of 1.167(3) Å, shorter than a formal CO double bond (1.19 Å).[8] Moreover, the C2–C2*i* bond length [1.511(3) Å] is significantly shortened compared to the neutral compound [1.541(4) Å]. This value is comparable to the C–C distance of the vicinal dication of diprotonated oxalic acid [1.528(3) Å].[9] The interatomic contacts of $[C_3H_4N_2O_3][AsF_6]_2$·4HF (**3**) are illustrated in Figure 2. The cation is connected with the anions, N1–(H1)···F4*ii* [2.765(2) Å], and HF molecules via moderate hydrogen bonds according to the classification by *Jeffrey*.[10] The hydrogen bonds via the HF molecules range between 2.449(2) Å and 2.511(1) Å, and are classified as strong to moderate.[10]

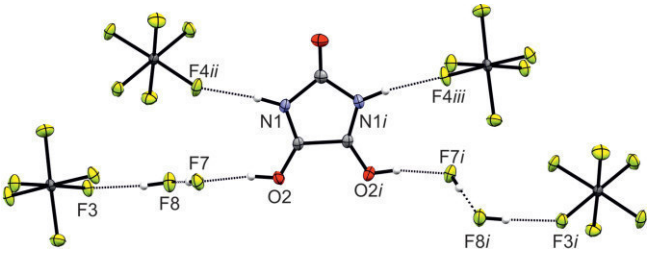

Figure 2. Projection of interatomic contacts in the $[C_3H_4N_2O_3][AsF_6]_2$·4HF (**3**) crystal (50 % probability displacement ellipsoids). Symmetry codes: *i* = 1 – *x*, *y*, 1.5 – *z*; *ii* = 0.5 + *x*, 0.5 + *y*, 1 + *z*; *iii* = 0.5 – *x*, – 0.5 + *y*, 0.5 – *z*. All contacts are drawn as dashed lines.

The As–F bond lengths of the AsF_6^- anions are in a range between 1.701(9) and 1.740(9) Å, which is in accordance with the literature.[11–13]

Crystal Structure of $[C_3H_3N_2O_3][SbF_6]$ (2)

The monoprotonated species of parabanic acid $[C_3H_3N_2O_3][SbF_6]$ (**2**) crystallizes in the monoclinic space group $P2_1/c$ with four formula units per unit cell. Figure 3 shows the asymmetric unit and Table 2 summarizes selected bond lengths and angles.

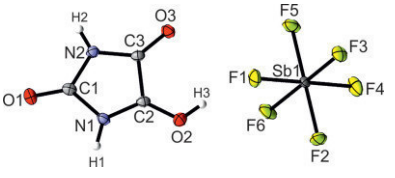

Figure 3. Asymmetric unit of $[C_3H_3N_2O_3][SbF_6]$ (**2**) (50 % probability displacement ellipsoids).

Even if the proton is not of great significance, it was found in the difference Fourier synthesis and refined isotropically. Compared to the neutral compound the C2–O2 bond length is significantly elongated [1.264(4) Å], which confirms the *O*-protonation.[7] Consequently, the N1–C2 distance [1.303(4) Å] is significantly shorter and in the range of the bond length of the diprotonated species. The other bond lengths of the two carbonyl groups are shortened to 1.183(4) Å for O1–C1 and 1.194(4) Å for C3–O3. A comparison of the most important bond lengths of parabanic acid, the monocation (**2**) and the dication (**3**) are summarized in Table 3.

Full Paper
doi.org/10.1002/ejoc.202000656

Table 2. Selected bond lengths [Å] and angles [°] of (**2**). The estimated standard deviation is marked in parentheses.[a]

Bond lengths [Å]			
O1–C1	1.183(4)	N2–C3	1.361(4)
C1–N1	1.438(3)	C3–O3	1.194(4)
C1–N2	1.390(4)	C2–O2	1.264(4)
N1–C2	1.303(4)	C2–C3	1.524(4)
Bond angles [°]			
O1–C1–N1	125.6(3)	O2–C2–C3	126.2(3)
C1–N1–C2	110.6(2)	C2–C3–N2	103.4(2)
N1–C2–C3	108.1(2)	O3–C3–C2	124.9(3)
O2–C2–N1	125.6(3)	O3–C3–N2	131.6(3)
Interatomic contacts D–A [Å]			
O2–(H3)···F1	2.555(3)	N1–(H1)···F6*i*	2.927(3)
N2–(H2)···F2*ii*	2.840(3)		

[a] Symmetry codes: *i* = 1 – *x*, – *y*, 1 – *z*; *ii* = 1 + *x*, 0.5 – *y*, 0.5 + *z*.

Table 3. Comparison of selected bond lengths [Å] of parabanic acid, (**2**) and (**3**) with estimated standard deviation in parentheses.[a]

	Parabanic acid[7]	(**2**)	(**3**)
O1–C1	1.212(4)	1.183(4)	1.167(3)
C1–N1	1.381(3)	1.438(3)	1.434(2)
N1–C2	1.360(3)	1.303(4)	1.305(2)
C2–O2	1.212(3)	1.264(4)	1.253(2)
C2–C(3/*i*)	1.541(4)	1.524(4)	1.511(3)

[a] Symmetry code: *i* = 1 – *x*, *y*, 1.5 – *z*.

The Sb–F bond lengths of the SbF_6^- anion are in a range between 1.866(2) and 1.895(2) Å. The angles are between 88.36(8) and 92.83(8)°, and between 176.47(8) and 179.77(8)°. These values are in good agreement with those reported in literature.[13,14] Deviations from perfect octahedron symmetry are explained by interatomic contacts, which are depicted in Figure 4.

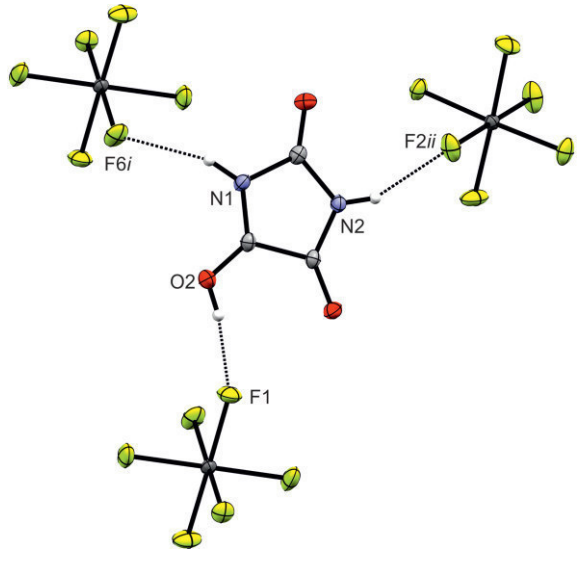

Figure 4. Projection of interatomic contacts in the $[C_3H_3N_2O_3][SbF_6]$ (**2**) crystal (50 % probability displacement ellipsoids). Symmetry codes: *i* = 1 – *x*, – *y*, 1 – *z*; *ii* = 1 + *x*, 0.5 – *y*, 0.5 + *z*.

The monocation is connected to the anions via moderate hydrogen bonds [O2–(H3)···F1, N2–(H2)···F2*ii*] with a distance of 2.555(3) Å, respectively 2.840(3) Å and via a weak hydrogen bond [N1–(H1)···F6*i*] of 2.927(3) Å.

Vibrational Spectra of $[C_3X_4N_2O_3][MF_6]_2$ (*M* = As, Sb and *X* = H, D)

The infrared and Raman spectra of $[C_3H_4N_2O_3][AsF_6]_2$ (**3**), $[C_3H_4N_2O_3][SbF_6]_2$ (**4**) and $[C_3D_4N_2O_3][AsF_6]_2$ (**6**) as well as the Raman spectrum of parabanic acid are displayed in Figure 5.

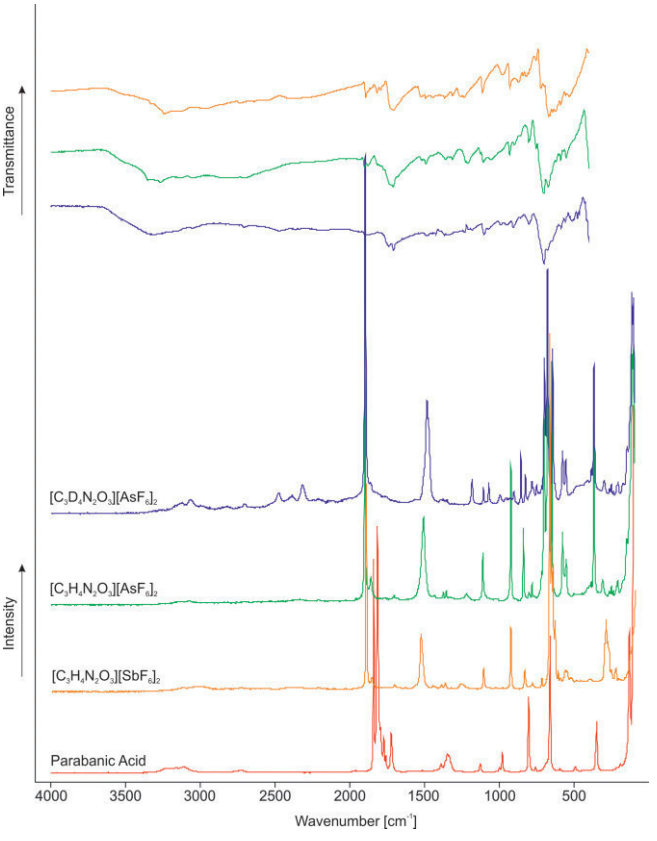

Figure 5. Raman spectrum of parabanic acid (red), Raman and IR spectra of $[C_3H_4N_2O_3][SbF_6]_2$ (**4**) (orange), $[C_3H_4N_2O_3][AsF_6]_2$ (**3**) (green) and $[C_3D_4N_2O_3][AsF_6]_2$ (**6**) (blue).

Table 4 lists selected observed frequencies of (**3**), (**4**) and (**6**) together with quantum-chemically calculated frequencies of $[C_3H_4N_2O_3]^{2+}$·4HF and $[C_3D_4N_2O_3]^{2+}$·4HF. In Table S1 all observed and calculated frequencies are summarized (see Supporting Information). For better accordance of the calculated frequencies with observed ones, four HF molecules were added to the gas-phase structure, to simulate hydrogen bonding in the solid state.

According to the quantum chemical calculations, which are discussed later, the dication possesses C_{2v} symmetry with 30 fundamental vibrations. The successful diprotonation of parabanic acid is confirmed by the OH stretching vibrations in the infrared spectra [3128 cm^{-1}, 3043 cm^{-1} (**3**) and 3138 cm^{-1}, 2964 cm^{1} (**4**)]. In the corresponding Raman spectra, these vibrations are not observable due to the poor polarizability. In contrast, the OD stretching vibrations are detected at 2322 cm^{-1}

Table 4. Selected experimental vibrational frequencies [cm^{-1}] of (**3**), (**4**) and (**6**), and calculated vibrational frequencies [cm^{-1}] of $[C_3H_4N_2O_3]^{2+}$·4HF and $[C_3D_4N_2O_3]^{2+}$·4HF.

$[C_3H_4N_2O_3][AsF_6]_2$ (**3**)		$[C_3H_4N_2O_3][SbF_6]_2$ (**4**)		$[C_3D_4N_2O_3][AsF_6]_2$ (**6**)		$[C_3H_4N_2O_3]^{2+}$·4HF	$[C_3D_4N_2O_3]^{2+}$·4HF	Assignment[b]
IR	Raman	IR	Raman	IR	Raman	Calc.[a] (IR/Raman)	Calc.[a] (IR/Raman)	
3348 (w)		3327 (vw)		2476 (sh)	2474 (6)	3141 (305/272)	2333 (197/110)	ν(N*X*)
3267 (w)		3236 (w)		2382 (s)	2387 (5)	3103 (2937/44)	2293 (1533/21)	ν(N*X*)
3128 (w)		3138 (w)		2322 (s)	2318 (8)	2854 (1023/154)	2092 (563/69)	ν(O*X*)
3043 (w)		2964 (vw)				2823 (3999/88)	2071 (2017/39)	ν(O*X*)
1902 (vw)	1902 (100)	1894 (w)	1898 (58)	1898 (vw)	1899 (100)	1953 (132/114)	1948 (120/121)	ν(CO)
1772 (vw)		1774 (vw)				1768 (161/1)	1756 (180/2)	ν(CN)
1711 (m)	1707 (2)	1709 (m)	1709 (2)	1732 (w)		1764 (888/0.08)	1744 (906/0.4)	ν(CN)
1516 (vw)	1510 (19)	1518 (vw)	1533 (16)	1487 (vw)	1487 (32)	1507 (175/60)	1449 (29/71)	ν(CO)
	1379 (3)		1395 (2)	1182 (w)	1186 (10)	1417 (0.9/2)	1182 (66/5)	δ(CN*X*)
1452 (vw)		1448 (w)	1450 (2)		1377 (4)	1455 (0.7/1)	1385 (0.06/0.5)	ν(CO)
1360 (vw)	1359 (3)	1365 (w)	1371 (2)	995 (vw)	997 (5)	1280 (336/6)	968 (225/2)	δ(CO*X*)
1225 (vw)	1224 (2)	1234 (w)	1265 (2)	959 (vw)	958 (5)	1269 (110/2)	956 (30/2)	δ(COX)
1107 (w)	1115 (11)	1113 (w)	1115 (7)	1107 (vw)	1110 (8)	1093 (218/9)	1016 (165/5)	ν(CN)
932 (w)	927 (30)	930 (w)	933 (18)	858 (w)	859 (w)	942 (70/13)	839 (34/10)	ν(CN)

[a] Calculated on the B3LYP/aug-cc-pVTZ level of theory. IR intensity in km/mol and Raman intensity in Å^4/u. Abbreviations for IR intensities: v = very, s = strong, m = medium, w = weak. Experimental Raman activities are stated to a scale of 1 to 100. [b] *X* = H, D.

(Ra) and 2318 cm^{-1} (IR) (**6**). Other than the mentioned ν(OD), also ν(ND) vibrations are observed [2476 cm^{-1}, 2382 cm^{-1} (IR) and 2474 cm^{-1}, 2387 cm^{-1} (Ra)], which is explained by H/D exchange at the NH groups. The H/D-red-shifts are in good agreement with the Teller-Redlich rule for an H/D isotopic effect.[15] Due to the twofold protonation on the neighboring carbonyl groups, the corresponding CO stretching vibrations are red shifted up to 342 cm^{-1} compared to the neutral compound.[16] They occur between 1448 cm^{-1} [IR, (**4**)] and 1533 cm^{-1} [Ra, (**4**)]. In contrast to the CO stretching vibrations, a blue shift of about 420 cm^{-1} is detected for the ν(CN) vibrations, compared to parabanic acid[16] {1707 cm^{-1} [Ra, (**3**)] and 1774 cm^{-1} [IR, (**4**)]}. The most intense line in the Raman spectra belongs to the remaining unprotonated carbonyl group, which occurs at approximately 1900 cm^{-1}. This value is remarkably high for a carbonyl group and is based on the strengthening of the bond, which is also observed in the crystal structure. For the anions AsF_6^- and SbF_6^-, more than three lines are observed in the Raman spectra and likewise more than two bands in the infrared spectra. This is explained by a distortion of the ideal O_h symmetry, caused by solid state interactions.

The Raman and infrared spectra of the monoprotonated species $[C_3H_3N_2O_3][AsF_6]$ (**1**), $[C_3H_3N_2O_3][SbF_6]$ (**2**) and $[C_3D_3N_2O_3][AsF_6]$ (**5**) are shown in Figure S1 and the observed and calculated frequencies are listed in Table S2 (see Supporting Information).

Theoretical Calculations

All theoretical calculations were carried out on the B3LYP/aug-cc-pVTZ level of theory with the Gaussian program package. Figure 6 shows the comparison of the calculated structure of $[C_3H_3N_2O_3]^+$ and the cation of the single-crystal X-ray structure of (**2**) together with bond lengths and angles. Comparing the values of the experimentally obtained geometric parameters of the $[C_3H_3N_2O_3]^+$ cation with the calculated ones, shows that almost all bond lengths and angles are in accordance. Only the N1–C1, as well as the C3–N2 bond lengths are calculated slightly longer, compared to the experimental values. The C2–C3 distance is also predicted to be slightly longer by the calculation, than it is observed in the crystal structure.

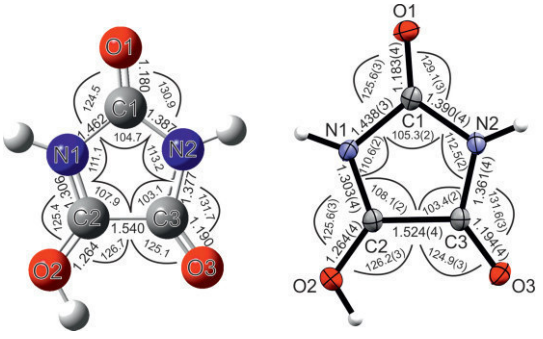

Figure 6. Calculated structure of $[C_3H_3N_2O_3]^+$ (left) and the $[C_3H_3N_2O_3]^+$ cation of the single-crystal X-ray structure (right) together with bond lengths [Å] and angles [°].

In Figure 7, the calculated structure of $[C_3H_4N_2O_3]^{2+}$ and the dication of the single-crystal X-ray structure are illustrated. In general, the calculated and experimentally obtained parameters of $[C_3H_4N_2O_3]^{2+}$ are in good agreement. As observed in the monocationic species, the same bond lengths (C1–N1 and

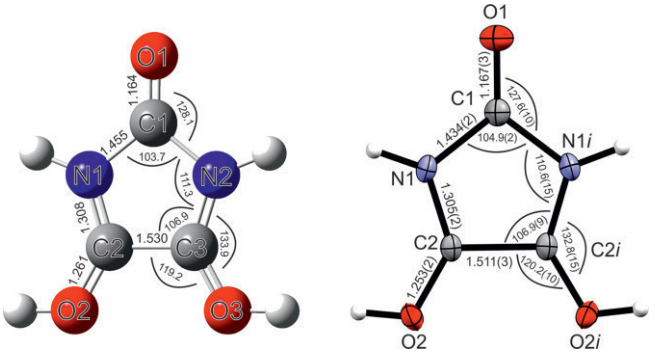

Figure 7. Calculated structure of $[C_3H_4N_2O_3]^{2+}$ (left) and the $[C_3H_4N_2O_3]^{2+}$ cation of the single-crystal X-ray structure (right) together with bond lengths [Å] and angles [°].

Full Paper
doi.org/10.1002/ejoc.202000656

C2–C3) are slightly elongated in the calculated structure of $[C_3H_4N_2O_3]^{2+}$ compared to the single-crystal X-ray structure.

Mapped Electrostatic Potentials (MEPs) together with Natural Population Analysis charges (NPA) are calculated to analyze where the positive charges of the diprotonated species are located. Figures 8, 9 and 10 depict the MEPs together with the NPA of parabanic acid, $[C_3H_4N_2O_3]^{2+}$ and $[C_3H_4N_2O_3]^{2+}$·4HF. The calculation for parabanic acid shows that the positive electrostatic potential is located inside the entire five-membered ring structure. The negative electrostatic potential is located exclusively on the oxygen atoms (red), which highlights the carbonyl groups as the more attractive functional group for protonation compared to the amide groups. Positive NPA charges are found at all carbon atoms, whereas the negative ones are observed for all oxygen and nitrogen atoms. Twofold protonation of parabanic acid leads to a change of the electrostatic potential distribution. The positive potential (blue) is now located between the two neighboring carbon atoms. In contrast, the negative potential is strongly compacted at the unprotonated oxygen atom. The influence on the NPA charges is describable as an increase of the positive carbon atom charges and a decrease of the negative oxygen and nitrogen atom charges. This leads to the assumption that both positive charges are delocalized over the individual OCNCO site of the molecule. The addition of four HF molecules for the simulation of hydrogen bonds in the solid-state results in a similar delocalization of the positive charges. Interestingly, a different trend is observed for the NPA charges of O2 and O3 atoms, which are decreased compared to the values of parabanic acid. Consequently, the NPA charges for the carbon atoms increase, whilst they decrease for the nitrogen atoms, however slightly weaker. By adding four HF molecules, the positive electrostatic potential is more distributed over the ring structure, but nevertheless compacted at C2 and C3. In conclusion, these calculations show that the two positive charges are located on the two carbon atoms C2 and C3, even though the charges are slightly compensated by the neighboring oxygen and nitrogen atoms. Albeit a 1,3-*N*,*N* dication would appear more stable due to the larger distance of the positive charges, a 1,2-*C*,*C* dication is generated by the twofold protonation of parabanic acid. The synthesized dicarbenium dication represents a new compound, which is to classify into 1,2 dications in organic main group systems.[17]

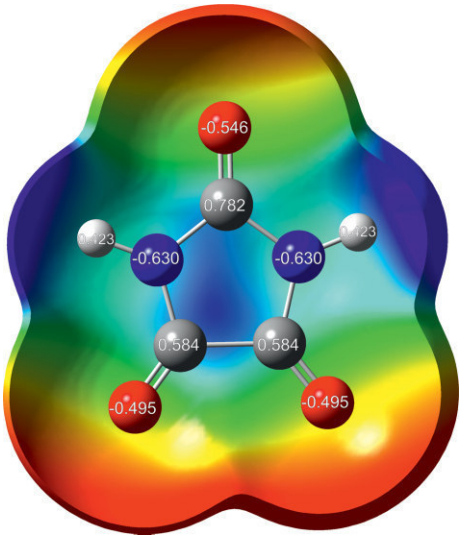

Figure 8. Molecular 0.0004 bohr^{-3} 3D isosurfaces with mapped electrostatic potential as a color scale ranging from –0.03142 a.u. (red) to 0.05124 a.u. (blue). The electrostatic potential isosurfaces and the NPA charges have been calculated for $C_3N_2O_3H_2$.

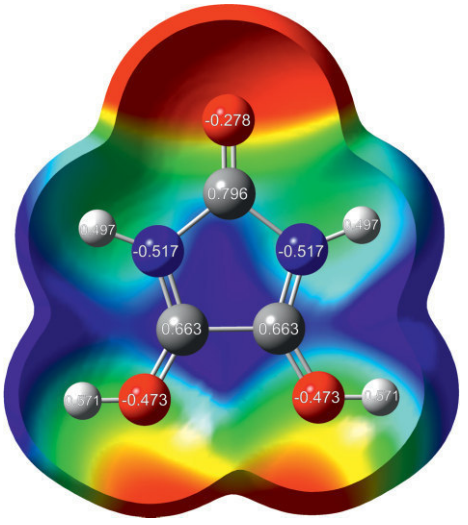

Figure 9. Molecular 0.0004 bohr^{-3} 3D isosurfaces with mapped electrostatic potential as a color scale ranging from 0.28 a.u. (red) to 0.37 a.u. (blue). The electrostatic potential isosurfaces and the NPA charges have been calculated for $[C_3H_4N_2O_3]^{2+}$.

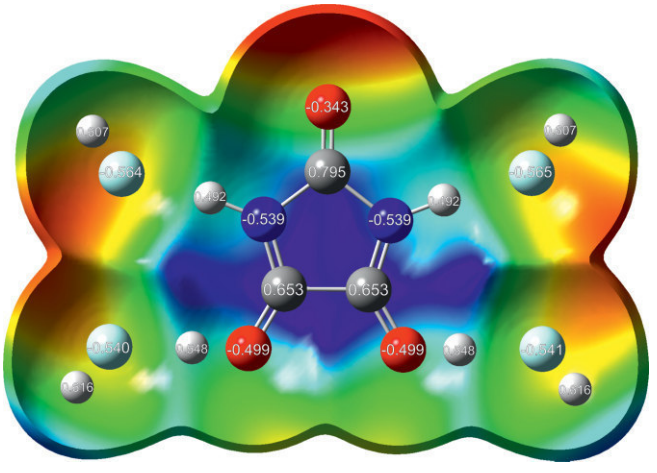

Figure 10. Molecular 0.0004 bohr^{-3} 3D isosurfaces with mapped electrostatic potential as a color scale ranging from 0.20 a.u. (red) to 0.31 (blue). The electrostatic potential isosurfaces and the NPA charges have been calculated for $[C_3H_4N_2O_3]^{2+}$·4HF.

Conclusion

Parabanic acid was investigated in the superacidic systems *X*F/*M*F$_5$ (*X* = H, D; *M* = As, Sb) for the first time. Using an equimolar amount of Lewis acid with respect to the starting material, the formation of the monoprotonated species in terms of $[C_3H_3N_2O_3][AsF_6]$ (**1**), $[C_3H_3N_2O_3][SbF_6]$ (**2**) and the correspond-

ing deuterated compound $[C_3D_3N_2O_3][AsF_6]$ (**5**) is observed. A twofold or larger amount of Lewis acid generates the compounds $[C_3H_4N_2O_3][AsF_6]_2$ (**3**), $[C_3H_4N_2O_3][SbF_6]_2$ (**4**) and $[C_3D_4N_2O_3][AsF_6]_2$ (**6**). The compounds were isolated and characterized by IR and Raman spectroscopy. The spectroscopical results are supported by calculated vibrational frequencies on the B3LYP/aug-cc-pVTZ level of theory. In case of $[C_3H_3N_2O_3][SbF_6]$ (**2**) and $[C_3H_4N_2O_3][AsF_6]_2$·4HF (**3**) single-crystal X-ray structure analyses were performed. In the dicationic species both protonations were determined on the neighboring carbonyl groups. For determining where the two positive charges are located, Mapped Electrostatic Potentials and Natural Popular Analysis charges were calculated. The positive charges of the 1,2-*C*,*C* dication are slightly compensated by the neighboring nitrogen and oxygen atoms.

Experimental Section

General

Caution! Avoid contact with any of these compound. Hydrolysis might form HF, which burns skin and causes irreparable damage.

Apparatus and Materials

Standard Schlenk technique with a stainless steel vacuum line was used to perform all reactions. All reactions in superacidic media were carried out in FEP/PFA reactors closed with a stainless steel valve. The reactors as well as the vacuum line were dried with fluorine prior to use. A Bruker Vertex-80V FT-IR spectrometer ($\tilde{\nu}$ = 350 to 4000 cm^{-1}) was used for recording low-temperature IR spectra. Small amounts of the synthesized compounds were placed on a CsBr single-crystal plate in a cooled cell for the measurement. For Raman measurements, the samples were transferred into cooled glass cells (–196 °C), which were evacuated afterwards. The measurements were performed by a Bruker MultiRAM FT-Raman spectrometer with Nd:YAG laser excitation (λ = 1064 nm). The low-temperature X-ray diffraction of $[C_3H_3N_2O_3][SbF_6]$ (**2**) and $[C_3H_4N_2O_3][AsF_6]_2$·4HF (**3**) was performed with an Oxford X-Calibur3 equipped with a Kappa CCD detector, operating with Mo-K_α radiation (λ = 0.71073 Å) and a Spellman generator (voltage 50 kV, current 40 mA). The CrysAlis CCD software was used to collect the data at 130 K,[18] while the reduction was carried out using CrysAlis RED software.[19] Solution and refinement of the crystal structures were performed with programs SHELXS[20] and SHELXL-97,[21] belonging to the WinGX software package. Subsequently, the structure was verified by PLATON software.[22] SCALE ABSPACK multiscan method was used for absorption correction.[23] In Table S3 and S4 (see Supporting Information) selected data and parameters of the X-ray analysis are listed. The quantum chemical calculations were carried out on the B3LYP/aug-cc-pVTZ level of theory by Gaussian 09.[24]

Deposition Numbers 1995038 for $[C_3H_3N_2O_3]^+[SbF_6]^-$ (**2**) and 1995041 for $[C_3H_4N_2O_3][AsF_6]_2$·4HF (**4**) contain the supplementary crystallographic data for this paper. These data are provided free of charge by the joint Cambridge Crystallographic Data Centre and Fachinformationszentrum Karlsruhe Access Structures service www.ccdc.cam.ac.uk/structures.

Synthesis of $[C_3H_3N_2O_3][AsF_6]$ (1), $[C_3H_4N_2O_3][AsF_6]_2$ (3) $[C_3D_3N_2O_3][AsF_6]$ (5) and $[C_3D_4N_2O_3][AsF_6]_2$ (6): Anhydrous hydrogen fluoride (2 mL) was condensed into an FEP tube-reactor at –196 °C. For compounds (**5**) and (**6**) deuterium fluoride was used instead. Afterwards, arsenic pentafluoride [85 mg, 0.5 mmol for (**1**) and (**5**), and 170 mg, 1.0 mmol for (**3**) and (**6**)] was condensed in the tube-reactor under same conditions. To form the superacidic systems, the mixtures were warmed up to –40 °C and homogenized, subsequently. After cooling down again to –196 °C, parabanic acid (57 mg, 0.5 mmol) was added under nitrogen atmosphere. After warming up to –40 °C [(**1**), (**5**)], or –60 °C [(**3**), (**6**)] respectively, the reaction mixture was homogenized until the resulted salt was completely dissolved. The solution was again cooled to –196 °C and excess HF or DF was removed under dynamic vacuum overnight at –78 °C. For crystallization of compound (**3**), the reactor was left in an ethanol bath (T = –70 °C) without removing HF until the salt recrystallized. All salts were obtained as colorless solids. $[C_3H_3N_2O_3][AsF_6]$ (**1**), and $[C_3D_3N_2O_3][AsF_6]$ (**5**) are stable up to room temperature, whereas $[C_3H_4N_2O_3][AsF_6]_2$ (**3**) and $[C_3D_4N_2O_3][AsF_6]_2$ (**6**) were decomposed at –20 °C.

Synthesis of $[C_3H_3N_2O_3][SbF_6]$ (2) and $[C_3H_4N_2O_3][SbF_6]_2$ (4): Antimony pentafluoride [110 mg, 0.51 mmol (**2**); 213 mg, 0.98 mmol (**4**)] was condensed into an FEP tube-reactor at –196 °C. Subsequently, 2 mL of anhydrous hydrogen fluoride were condensed into the reactor at –196 °C. For homogenizing these compounds, the reaction mixtures were warmed up to –40 °C. Under nitrogen atmosphere, parabanic acid [58 mg, 0.51 mmol (**2**), 56 mg, 0.49 mmol (**4**)], was added to the refrozen superacidic system. The complete reaction mixture was warmed up to –40 °C (**2**), –60 °C respectively (**4**), and was homogenized until the salt was completely dissolved. Excess HF was removed under dynamic vacuum at –78 °C, after the solution had been cooled down to –196 °C. Both compounds were obtained as colorless solids with decomposition temperatures of 20 °C for $[C_3H_3N_2O_3][SbF_6]$ (**2**) and –20 °C for $[C_3H_4N_2O_3][SbF_6]_2$ (**4**). For crystallization of compound (**2**), the reactor was left in an ethanol bath (T = –50 °C) until the salt recrystallized.

Acknowledgments

We are grateful to the Department of Chemistry of the Ludwig Maximilian University of Munich and the Deutsche Forschungsgemeinschaft (DFG), and the F-Select GmbH for their support. 2020 Open access funding enabled and organized by Projekt DEAL.

Keywords: Protonated parabanic acid · Vibrational spectroscopy · Single-crystal X-ray diffraction · Theoretical calculations · Superacidic media

[1] F. Woehler, J. Liebig, *Ann. Pharm.* **1838**, *26*, 256.
[2] P. H. Laursen, W. A. Thews, B. E. Christensen, *J. Org. Chem.* **1957**, *22*, 274.
[3] J. I. Murray, *Org. Synth.* **1957**, *37*, 71.
[4] E. S. Canellakis, A. L. Tuttle, P. P. Cohen, *J. Biol. Chem.* **1955**, *213*, 397.
[5] M. d. D. M. C. Ribeiro da Silva, M. A. V. Ribeiro da Silva, V. L. S. Freitas, M. V. Roux, P. Jiménez, J. Z. Dávalos, P. Cabildo, R. M. Claramunt, J. Elguero, *J. Chem. Thermodyn.* **2008**, *40*, 1378.
[6] M. Arca, F. Demartin, F. A. Devillanova, F. Isaia, F. Lelj, V. Lippolis, G. Verani, *Can. J. Chem.* **2000**, *78*, 1147.
[7] D. R. Davies, J. J. Blum, *Acta Crystallogr.* **1955**, *8*, 129.
[8] A. F. Holleman, E. Wiberg, N. Wiberg, *Anorganische Chemie*, De Gruyter, Berlin, Boston, **2017**.
[9] M. Schickinger, T. Saal, F. Zischka, J. Axhausen, K. Stierstorfer, Y. Morgenstern, A. J. Kornath, *ChemistrySelect* **2018**, *3*, 12396.
[10] G. A. Jeffrey, *An Introduction to hydrogen bonding*, Oxford University Press, New York, **1997**.
[11] R. Minkwitz, F. Neikes, U. Lohmann, *Eur. J. Inorg. Chem.* **2002**, *2002*, 27.
[12] K. O. Christe, X. Zhang, R. Bau, J. Hegge, G. A. Olah, G. K. S. Prakash, J. A. Sheehy, *J. Am. Chem. Soc.* **2000**, *122*, 481.

[13] M. Schickinger, C. Jessen, Y. Morgenstern, K. Muggli, F. Zischka, A. Kornath, *Eur. J. Org. Chem.* **2018**, *2018*, 6223.
[14] R. Minkwitz, S. Schneider, *Angew. Chem. Int. Ed.* **1999**, *38*, 210; *Angew. Chem.* **1999**, *111*, 229.
[15] J. Weidlein, K. Dehnicke, U. Müller, *Schwingungsspektroskopie. Eine Einführung*, Thieme, Stuttgart, **1988**.
[16] L. Coclers, A. Vanclef, R. Bouché, *Spectrosc. Lett.* **1978**, *11*, 799.
[17] V. G. Nenajdenko, N. E. Shevchenko, E. S. Balenkova, I. V. Alabugin, *Chem. Rev.* **2003**, *103*, 229.
[18] *CrysAlisCCD*, Version 1.171.35.11 (release 16–05–**2011** CrysAlis 171.NET), Oxford Diffraction Ltd., **2011**.
[19] *CrysAlisRED*, Version 1.171.35.11 (release 16.05.**2011** CrysAlis 171.NET), Oxford Diffraction Ltd., **2011**.
[20] G. Sheldrick, *SHELXS-97, Program for Crystal Structure Solution*, University of Göttingen, Germany, **1997**.
[21] G. Sheldrick, *SHELXL-97, Program for the Refinement of Crystal Structures*, University of Göttingen, Germany, **1997**.
[22] A. Spek, *PLATON, A Multipurpose Crystallographic Tool*, Utrecht University, Utrecht (The Netherlends), **1999**.
[23] *SCALE3 ABSPACK* - An Oxford Diffraction Program, Oxford Diffraction Ltd., UK, **2005**.
[24] M. J. Frisch, G. W. Trucks, H. B. Schlegel, G. E. Scuseria, M. A. Robb, J. R. Cheeseman, G. Scalmani, V. Barone, B. Mennucci, G. A. Petersson, H. Nakatsuji, M. Caricato, X. Li, H. P. Hratchian, A. F. Izmaylov, J. Bloino, G. Zheng, J. L. Sonnenberg, M. Hada, M. Ehara, K. Toyota, R. Fukuda, J. Hasegawa, M. Ishida, T. Nakajima, Y. Honda, O. Kitao, H. Nakai, T. Vreven, J. A. Montgomery Jr., J. E. Peralta, F. Ogliaro, M. Bearpark, J. J. Heyd, E. Brothers, K. N. Kudin, V. N. Staroverov, R. Kobayashi, J. Normand, K. Raghavachari, A. Rendell, J. C. Burant, S. S. Iyengar, J. Tomasi, M. Cossi, N. Rega, J. M. Millam, M. Klene, J. E. Knox, J. B. Cross, V. Bakken, C. Adamo, J. Jaramillo, R. Gomperts, R. E. Stratmann, O. Yazyev, A. J. Austin, R. Cammi, C. Pomelli, J. W. Ochterski, R. L. Martin, K. Morokuma, V. G. Zakrzewski, G. A. Voth, P. Salvador, J. J. Dannenberg, S. Dapprich, A. D. Daniels, Ö. Farkas, J. B. Foresman, J. V. Ortiz, J. Cioslowski, D. J. Fox, *Gaussian 09, Revision A.02*, Gaussian, Inc., Wallingford CT, **2009**.

Received: May 11, 2020

Supporting Information

Diprotonated Parabanic Acid: A Vicinal or 1,3-Dication?

Stefanie Beck, Milica Raljic, Christoph Jessen, Andreas J. Kornath*

Supporting Information

Figure S1. Infrared spectra of $[C_3D_3N_2O_3][AsF_6]$ (**5**) (green) (a), $[C_3H_3N_2O_3][AsF_6]$ (**1**) (blue) (b), $[C_3H_3N_2O_3][SbF_6]$ (**2**) (red) (c) and corresponding Raman spectra (d–f).

Table S1. Experimental vibrational frequencies [cm^{-1}] of (**3**), (**4**) and (**6**), and calculated vibrational frequencies [cm^{-1}] of $[C_3H_4N_2O_3]^{2+} \cdot 4$ HF and $[C_3D_4N_2O_3]^{2+} \cdot 4$ HF.

Table S2. Experimental vibrational frequencies [cm^{-1}] of (**1**), (**2**) and (**5**), and calculated vibrational frequencies [cm^{-1}] of $[C_3H_3N_2O_3]^{+} \cdot$ HF and $[C_3D_3N_2O_3]^{+} \cdot$ HF.

Table S3. Crystal data and structure refinement for $[C_3H_3N_2O_3][SbF_6]$ (**2**).

Table S4. Crystal data and structure refinement for $[C_3H_4N_2O_3][AsF_6]_2 \cdot 4$ HF (**3**).

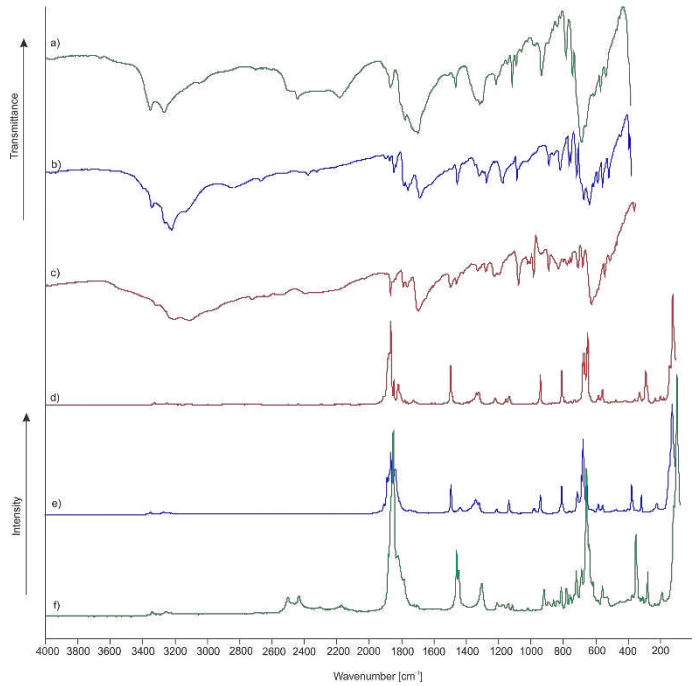

Figure S1. Infrared spectra of $[C_3D_3N_2O_3][AsF_6]$ (**5**) (green) (a), $[C_3H_3N_2O_3][AsF_6]$ (**1**) (blue) (b), $[C_3H_3N_2O_3][SbF_6]$ (**2**) (red) (c) and corresponding Raman spectra (d–f).

Table S1. Experimental vibrational frequencies [cm^{-1}] of (**3**), (**4**) and (**6**), and calculated vibrational frequencies [cm^{-1}] of $[C_3H_4N_2O_3]^{2+} \cdot 4$ HF and $[C_3D_4N_2O_3]^{2+} \cdot 4$ HF.

$[C_3H_4N_2O_3][AsF_6]_2$ (3)		$[C_3H_4N_2O_3][SbF_6]_2$ (4)		$[C_3D_4N_2O_3][AsF_6]_2$ (6)		$[C_3H_4N_2O_3]^{2+} \cdot 4HF$	$[C_3D_4N_2O_3]^{2+} \cdot 4HF$	Assignment[b]
IR	Raman	IR	Raman	IR	Raman	Calc.[a] (IR/Raman)	Calc.[a] (IR/Raman)	
3348 (w)		3327 (vw)			3123 (3)	3141 (305/272)		ν(NH)
3267 (w)		3236 (w)			3070(4)	3103 (2937/44)		ν(NH)
				2476 (sh)	2474 (6)		2333 (197/110)	ν(ND)
				2382 (s)	2387 (5)		2293 (1533/21)	ν(ND)
3128 (w)		3138 (w)		3138 (w)		2854 (1023/154)		ν(OH)
				2322 (s)	2318 (8)		2092 (563/69)	ν(OD)
3043 (w)		2964 (vw)				2823 (3999/88)	2071 (2017/39)	ν(O*X*)
2797 (w)		2727 (vw)						?
2712 (w)				2708 (vw)	2709 (3)			?
1902 (vw)	1902 (100)	1894 (w)	1898 (58)	1898 (vw)	1899 (100)	1953 (132/114)	1948 (120/121)	ν(CO)
1887 (vw)	1862 (6)		1860 (4)		1866 (9)			?
		1817 (vw)						?
		1796 (vw)						?
1772 (vw)		1774 (vw)				1768 (161/1)	1756 (180/2)	ν(CN)
1711 (m)	1707 (2)	1709 (m)	1709 (2)	1732 (w)		1764 (888/0.08)	1744 (906/0.4)	ν(CN)
1516 (vw)	1510 (19)	1518 (vw)	1533 (16)	1487 (vw)	1487 (32)	1507 (175/60)	1449 (29/71)	ν(CO)
1491 (vw)		1493 (w)						?
1452 (vw)		1448 (w)	1450 (2)		1377 (4)	1455 (0.7/1)	1385 (0.06/0.5)	ν(CO)
1313 (vw)		1313 (w)						?
1225 (vw)	1224 (2)	1234 (w)	1265 (2)	959 (vw)	958 (5)	1269 (110/2)	956 (30/2)	δ(CO*X*)
1211 (w)				930 (w)	932 (4)			?
1128 (vw)				906 (w)	906 (6)			?
1107 (w)	1115 (11)	1113 (w)	1115 (7)	1107 (vw)	1110 (8)	1093 (218/9)	1016 (165/5)	ν(CN)
				1072 (vw)	1075 (9)			?
1056 (w)		1049 (vw)	1032 (1)		754 (8)	949 (215/0.1)	713 (82/0.05)	$\delta(COX)_{oop}$
987 (sh)		980 (vw)		698 (vs)[c]	703 (44)[c]	947 (86/0.1)	691 (0.05/0.01)	$\delta(COX)_{oop}$
932 (w)	927 (30)	930 (w)	933 (18)	858 (w)	859 (16)	942 (70/13)	839 (34/10)	ν(CN)
899 (vw)				662 (s)		904 (61/0.1)	647 (2/0.08)	$\delta(CNX)_{oop}$
862 (vw)		872 (w)				866 (0.2/0.02)	635 (0.2/0.8)	$\delta(CNX)_{oop}$
	844 (17)	841 (w)	841 (6)	789 (w)	787 (9)	831 (5/9)	768 (24/9)	ring breathing
		820 (w)						?
795 (w)	786 (5)	795 (w)	789 (3)		831 (11)	812 (0.01/0.2)	816 (0.002/0.2)	γ(OCCN)
754 (w)		756 (vw)			723 (8)			?
	723 (7)	721 (m)	727 (4)	778 (vw)	778 (7)	739 (3/0.7)	768 (86/2)	γ(NCON)

671 (vs)	674 (sh)	669 (vs)[c]	674 (100)[c]		648 (46)	683 (11/2)	640 (3/8)	δ(CCO)
650 (s)	653 (53)	646 (vs)[c]	652 (35)[c]		634 (8)	648 (0.9/11)	639 (5/2)	δ(NCN)
590 (s)	582 (16)	590 (vs)	600 (4)	586 (w)	582 (18)	610 (28/0.4)	590 (40/0.2)	δ(CCN)
552 (m)	557 (10)	555 (s)	558 (6)	500 (m)		524 (0.7/0.01)	487 (6/0.06)	skeletal vibration
	398 (4)	405 (vw)	401 (4)		389 (13)[c]	401 (198/0.2)	391 (206/0.2)	δ(OCN)
	254 (4)		260 (6)		373 (42)[c]	371 (58/0.2)	358 (44/0.2)	δ(CCO)
	212 (5)		212 (4)		210 (9)	200 (0.02/0.01)	195 (0.1/0.03)	skeletal vibration
	153 (14)		172 (4)		150 (19)	187 (8/0.5)	186 (6/0.5)	δ(CCO)
	118 (54)				119 (62)			?
	109 (57)				109 (60)			?
704 (vs)	704 (40)	702 (m)	674 (100)[c]	698 (vs)[c]	703 (44)[c]			$[MF_6]^-$
673 (vs)	682 (50)	669 (vs)[c]	661 (41)	679 (s)	683 (68)			$[MF_6]^-$
621 (s)	390 (5)	662 (vs)	652 (35)[c]	557 (w)	559 (15)			$[MF_6]^-$
575 (m)	374 (39)	646 (vs)[c]	638 (20)	519 (m)	389 (13)[c]			$[MF_6]^-$
501 (w)	314 (6)	627 (vs)	616 (6)	467 (w)	373 (42)[c]			$[MF_6]^-$
482 (w)	270 (3)	534 (s)	571 (6)	457 (vw)	304 (9)			$[MF_6]^-$
442 (vw)		473 (m)	296 (20)		267 (7)			$[MF_6]^-$
			286 (14)		255 (8)			$[MF_6]^-$
			278 (12)		243 (6)			$[MF_6]^-$
			230 (7)					$[MF_6]^-$

[a] Calculated on the B3LYP/aug-cc-pVTZ level of theory. IR intensity in km/mol and Raman intensity in $Å^4/u$. Abbreviations for IR intensities: v = very, s = strong, m = medium, w = weak. Experimental Raman activities are stated to a scale of 1 to 100. [b] *X* = H, D. [c] vibrational frequencies of cation and anion interfere with each other.

Table S2. Experimental vibrational frequencies [cm^{-1}] of (**1**), (**2**) and (**5**), and calculated vibrational frequencies [cm^{-1}] of $[C_3H_3N_2O_3]^+ \cdot HF$ and $[C_3D_3N_2O_3]^+ \cdot HF$.

$[C_3H_3N_2O_3][AsF_6]$ (1)		$[C_3H_3N_2O_3][SbF_6]$ (2)		$[C_3D_3N_2O_3][AsF_6]$ (5)		$[C_3H_3N_2O_3]^+ \cdot HF$	$[C_3D_3N_2O_3]^+ \cdot HF$	Assignment[b]
IR	Raman	IR	Raman	IR	Raman	Calc.[a] (IR/Raman)	Calc.[a] (IR/Raman)	
3350 (m)	3347 (2)	3327 (w)	3323 (3)	3352 (w)	3347 (2)	3575 (185/85)		ν(NH)
3267 (s)	3263 (2)	3248 (sh)	3246 (2)	3267 (w)	3264 (2)	3532 (195/78)		ν(NH)
3227 (s)		3217 (m)						ν(OH)
3148 (m)		3122 (m)		3049 (vw)		3141 (1743/125)		ν(OH)
		2741 (vw)						?
2687 (vw)		2648 (vw)						?
		2561 (vw)						?
2401 (vw)		2415 (vw)			2319 (4)			?
				2512 (sh)	2513 (8)		2628 (101/46)	ν(ND)
				2446 (w)	2446 (9)		2598 (138/30)	ν(ND)
				2187 (w)	2185 (4)		2296 (914/53)	ν(OD)
1904 (vw)	1902 (10)							?
1880 (w)	1883 (33)	1896 (vw)	1871 (47)	1877 (w)	1888 (sh)	1936 (190/129)	1933 (161/136)	ν(CO)
1863 (vw)	1862 (56)	1863 (vw)	1861 (76)	1864 (sh)	1865 (77)	1868 (529/17)	1863 (508/15)	ν(CO)
	1834 (42)		1842 (22)		1834 (25)			?
1817 (m)		1817 (w)	1816 (19)					?
1790 (m)		1794 (w)	1775 (5)	1786 (m)	1799 (15)			?
1718 (s)	1714 (2)	1726 (s)	1725 (4)	1707 (m)	1712 (4)	1749 (458/0.09)	1728 (533/0.3)	ν(CN)
		1529 (w)						?
1493 (m)	1490 (28)	1495 (m)	1493 (35)	1477 (vw)	1477 (27)	1491 (135/15)	1456 (36/22)	ν(CO)
	1434 (7)				1462 (19)			?
1383 (w)								?
1360 (w)		1365 (w)		1227 (w)	1224 (6)	1380 (71/0.8)	1232 (88/2)	δ(CN*X*)
					1193 (5)			
				1160 (vw)	1158 (5)			?
1329 (w)	1334 (14)		1332 (11)	1130 (w)	1134 (5)	1340 (3/2)	1149 (72/5)	δ(CN*X*)
1313 (w)	1316 (11)	1313 (w)	1318 (12)	1327 (w)	1320 (13)	1300 (220/14)	1288 (212/13)	ν(CN)
		1263 (m)						?
		1236 (m)						?
1215 (m)	1207 (5)		1217 (6)	1036 (vw)	1035 (3)	1246 (265/13)	988 (39/0.2)	δ(CO*X*)
1128 (m)	1131 (13)	1115 (s)	1130 (8)	949 (w)	937 (11)	1108 (51/2)	926 (84/3)	ν(CN)
		1059 (w)		1105 (vw)				?
		1024 (m)		1072 (vw)				?
	977 (6)	980 (w)		995 (vw)				?

933 (w)	936 (18)	932 (m)	936 (27)	833 (vw)	834 (12)	918 (45/12)	814 (64/9)	ν(CN)
906 (vw)					910 (6)			?
864 (m)		872 (m)	881 (2)	638 (s)	644 (14)	889 (67/0.04)	649 (14/0.01)	$\delta(CO\mathit{X})_{oop}$
		843 (w)		851 (vw)	879 (7)			?
		822 (w)			780 (9)			?
806 (w)	805 (25)	806 (w)	806 (31)	800 (w)	801 (12)	812 (8/0.3)	812 (0.8/0.4)	γ(OCCN)
795 (w)	797 (9)	795 (w)	796 (8)	700 (vs)[c]	708 (20)[c]	782 (22/5)	724 (2/10)	ring breathing
758 (m)	760 (3)	754 (w)	756 (3)	758 (m)	740 (19)	755 (91/0.5)	750 (31/0.4)	γ(NCON)
710 (vs)[c]	708 (21)[c]	725 (w)	726 (6)	586 (s)	577 (13)	718 (108/0.4)	577 (107/0.1)	$\delta(CN\mathit{X})_{oop}$
675 (vs)[c]	674 (69)[c]	671 (vs)[c]	674 (47)[c]	677 (vs)[c]	677 (61)[c]	675 (0.2/6)	652 (0.8/8)	δ(CCO)
650 (s)	648 (26)	648 (vs)[c]	649 (50)[c]	623 (s)[c]	636 (14)[c]	641 (2/8)	600 (4/3)	δ(CNC)
590 (s)	589 (sh)	590 (s)	589 (4)	469 (vw)	468 (6)	599 (62/0.7)	454 (15/0.2)	$\delta(CN\mathit{X})_{oop}$
552 (s)	553 (8)	559 (m)[c]	554 (13)[c]	554 (m)	551 (8)	586 (34/0.2)	563 (28/0.1)	δ(CCN)
471 (w)	469 (5)		471 (5)		421 (7)	463 (0.003/0.04)	411 (19/0.03)	skeletal vibration
420 (w)	419 (4)	409 (vw)	415 (4)		397 (9)[c]	393 (68/1)	390 (58/1)	δ(OCN)
	314 (16)		326 (11)		302 (19)	300 (16/1)	290 (15/1)	δ(CCO)
	218 (10)		212 (4)		210 (10)	194 (8/0.8)	187 (12/0.06)	skeletal vibration
			174 (7)					?
			138 (35)		140 (46)	162 (42/0.04)	161 (40/0.04)	skeletal vibration
	124 (100)		119 (100)		122 (100)			?
710 (vs)[c]	708 (21)[c]	671 (vs)[c]	674 (47)[c]	700 (vs)[c]	708 (20)[c]			$[\mathit{M}F_6]^-$
675 (vs)[c]	684 (36)[c]	648 (vs)[c]	662 (47)	677 (vs)[c]	677 (61)[c]			$[\mathit{M}F_6]^-$
621 (s)	674 (69)[c]	559 (m)[c]	649 (50)[c]	623 (s)[c]	660 (30)			$[\mathit{M}F_6]^-$
	626 (5)		643 (62)		636 (14)[c]			$[\mathit{M}F_6]^-$
	578 (9)		577 (9)		607 (7)			$[\mathit{M}F_6]^-$
	398 (6)		554 (13)[c]		565 (8)			$[\mathit{M}F_6]^-$
			353 (6)		397 (9)[c]			$[\mathit{M}F_6]^-$
			285 (30)		389 (8)			$[\mathit{M}F_6]^-$
			278 (17)		373 (34)			$[\mathit{M}F_6]^-$
			226 (6)		365 (17)			$[\mathit{M}F_6]^-$
					329 (8)			$[\mathit{M}F_6]^-$

[a] Calculated on the B3LYP/aug-cc-pVTZ level of theory. IR intensity in km/mol and Raman intensity in $Å^4/u$. Abbreviations for IR intensities: v = very, s = strong, m = medium, w = weak. Experimental Raman activities are stated to a scale of 1 to 100. [b] *X* = H, D. [c] vibrational frequencies of cation and anion interfere with each other.

Table S3. Crystal data and structure refinement for $[C_3H_3N_2O_3]^+[SbF_6]^-$ (**2**).

	$[C_3H_3N_2O_3]^+[SbF_6]^-$ (**2**)
Empirical formular	C3 H3 F6 N2 O3 Sb
M_r	350.82
Crystal system	monoclinic
Space group	$P\,2_1/c$
a [Å]	10.1642(4)
b [Å]	8.5371(3)
c [Å]	10.5093(4)
α [°]	90
β [°]	108.489(4)
γ [°]	90
V [Å^3]	864.85(6)
Z	4
ρ_{calcd} [gcm^{-3}]	2.694
μ[mm^{-1}]	3.285
λ_{Moka}	0.71073
F(000)	656
T[K]	130(2)
hkl range	–15:14; –12:7;–15:15
refl. measured	9840
refl. unique	2891
R_{int}	0.0402
parameters	148
R(F)/*w*R(F^2)[a)]	0.0404/0.0612
weighting scheme[b)]	0.0212
S(GoF)[c)]	1.073
residual density [eÅ^{-3}]	0.990/ –1.095
devide type	Oxford XCalibur
solution/refinement	SHELXS-97
CCDC	1995038

a) $R_1 = \Sigma||F_o|-|F_c||/\Sigma|F_o|$; b) $wR_2 = [\Sigma[w(F_o^2-F_c^2)^2]/\Sigma[w(F_o)^2]]^{1/2}$; $w = [\sigma_c^2(F_o^2)+(xP)^2+yP]^{-1}$; $P = (F_o^2+2F_c^2)/3$ c) GoF = $\{\Sigma[w(F_o^2-F_c^2)^2]/(n-p)\}^{1/2}$ (*n* = number of reflexions; p = total number of parameters).

Table S4. Crystal data and structure refinement for $[C_3H_4N_2O_3][AsF_6]_2 \cdot 4\ HF$.

	$[C_3H_4N_2O_3][AsF_6]_2 \cdot 4\ HF$
Empirical formular	C3 H4 F12 N2 O3 As2
M_r	573.95
Crystal system	monoclinic
Space group	*C*2/*c*
a [Å]	13.5733(7)
b [Å]	8.1318(4)
c [Å]	14.6499(8)
α [°]	90
β [°]	112.502(6)
γ [°]	90
V [Å^3]	1493.88(15)
Z	4
ρ_{calcd} [gcm^{-3}]	2.552
μ[mm^{-1}]	4.670
$\lambda_{Moκα}$	0.71073
F(000)	1096
T[K]	130(2)
hkl range	–19:15; –12:9;–21:21
refl. measured	7782
refl. unique	2455
R_{int}	0.0289
parameters	135
R(F)/*w*R(F^2)[a)]	0.0287/0.0495
weighting scheme[b)]	0.0194
S(GoF)[c)]	1.048
residual density [eÅ^{-3}]	0.447/ –0.673
devide type	Oxford XCalibur
solution/refinement	SHELXS-97
CCDC	1995041

a) $R_1 = \Sigma||F_o|-|F_c||/\Sigma|F_o|$; b) $wR_2 = [\Sigma[w(F_o^2-F_c^2)^2]/\Sigma[w(F_o)^2]]^{1/2}$; $w = [\sigma_c^2(F_o^2)+(xP)^2+yP]^{-1}$; $P = (F_o^2+2F_c^2)/3$ c) GoF = $\{\Sigma[w(F_o^2-F_c^2)^2]/(n-p)\}^{1/2}$ (*n* = number of reflexions; p = total number of parameters).

EurJOC

European Journal of Organic Chemistry

Chemistry Europe

European Chemical Societies Publishing

Front Cover:
A. J. Kornath et al.
Ring Opening and Closure Reactions of β-Propiolactone in the Superacids HF/MF_5 (*M*=Sb, As)

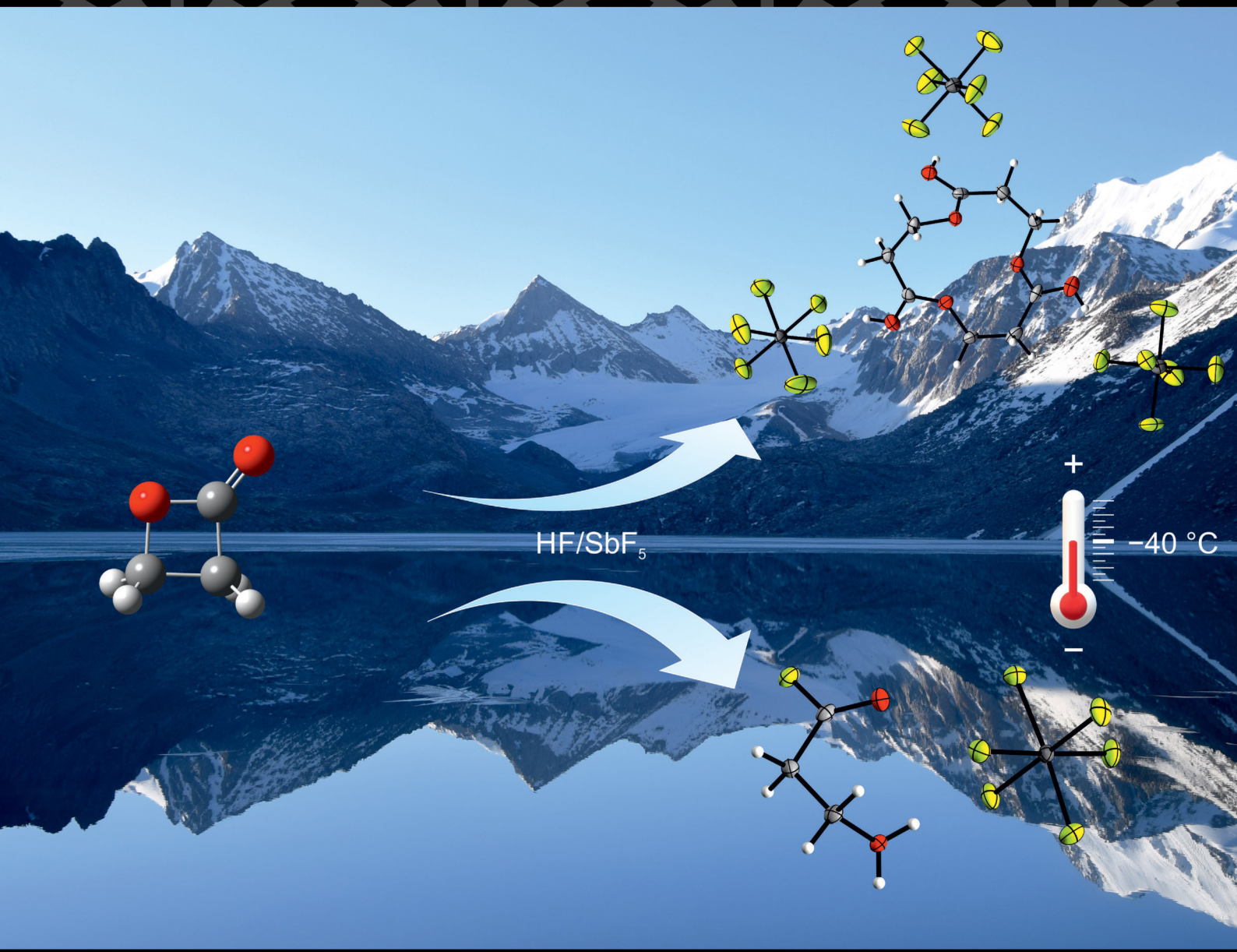

48/2021

WILEY-VCH

EurJOC
European Journal of Organic Chemistry

Research Article
doi.org/10.1002/ejoc.202101351

Chemistry Europe
European Chemical Societies Publishing

VIP *Very Important Paper*

Ring Opening and Closure Reactions of β-Propiolactone in the Superacids HF/MF_5 (M = Sb, As)

Stefanie Beck,[a] Christoph Jessen,[a] and Andreas J. Kornath*[a]

Transformations of β-propiolactone in the binary superacidic systems HF/MF_5 (M = Sb, As) were investigated at different temperatures. Salts of monoprotonated 3-hydroxypropanoyl fluoride $[H_2O(CH_2)_2C(O)F][SbF_6]$ (**1**) and $[H_2O(CH_2)_2C(O)F][AsF_6]$ (**2**) were obtained by performing the reactions at temperatures lower than −40 °C. In contrast, temperatures higher than −40 °C yield the respective salts $[C_9H_{15}O_6][SbF_6]_3$ (**3**) and $[C_9H_{15}O_6][AsF_6]_3$ (**4**) containing a cyclic trication. The protonated species of β-propiolactone was not observed. All salts were characterized by low temperature Raman and IR spectroscopy. In addition, single-crystal X-ray analyses were performed for (**1**) and (**3**). For both cations the existence of a cationic acyl species as a reactive intermediate in the form of $[HO(CH_2)_2CO][MF_6]$ is assumed. The formation of the acyl cation, based on protonated β-propiolactone, was investigated by quantum chemical calculations on the MP2/aug-cc-pVTZ level of theory.

Introduction

The ring opening of β-lactones by hydrolysis, which leads to the formation of the corresponding acid is well investigated.[1–5] Therefore, neutral, basic and acidic conditions were examined theoretically and experimentally. Even a theoretical study of the hydrolysis in strongly acidic media was performed, in which it is concluded that the ring opening reaction undergoes an unimolecular mechanism.[4] In superacidic media, where the hydrolysis itself is not possible, only a few studies of the reaction behavior of β-lactones are reported in literature. In 1967, an investigation of α,α-dimethyl-β-propiolactone (a) in the superacidic system HF/BF_3 at −80 °C was carried out by *Hogeveen* et al.[6] Under these conditions, an acyl-oxygen cleavage was observed but the protonated cyclic species was not detected. Compared to that, *Olah* et al. obtained contrary results by a study of different lactones in $FSO_3H/SbF_5/SO_2$ solution.[7] This study showed that the protonation occurs exclusively on the carbonyl oxygen of the respective cyclic compound and no cleavage was observed at −80 °C. For example, the protonated species of β-butyrolactone (b) was stable up to −50 °C and at higher temperature an alkyl-oxygen cleavage occurred and led to the formation of protonated crotonic acid. Interestingly, the protonated species of the simplest β-lactone, β-propiolactone (c), was reported to be stable up to room temperature and no cleavage was observed at all.[7] The compounds a–c together with their respective cleavages are shown in Scheme 1.

On the one hand both, β-butyrolactone and α,α-dimethyl-β-propiolactone have one or two methyl groups on the four-membered ring skeleton, which are potentially able to stabilize cleavage intermediates. On the other hand, the protic solvent HF might be necessary to enable the acyl-oxygen cleavage. These studies led us to investigate β-propiolactone in the binary superacidic systems HF/MF_5 (M = Sb, As).

Results and Discussion

Preparation

β-Propiolactone reacts in the superacidic systems HF/MF_5 according to Scheme 2.

The superacidic systems were prepared using an excess of anhydrous HF (*a*HF), which serves as solvent as well as reagent. The Lewis acid was added in an equimolar amount and was completely solvated, by homogenizing the mixture at −40 °C. β-Propiolactone was added to the frozen mixture under nitrogen atmosphere. Depending on the reaction temperature, two different species were obtained, after removing the excess of *a*HF in a dynamic vacuum overnight at −78 °C. Warming up and homogenizing the reaction mixture without exceeding −40 °C, only salts of monoprotonated 3-hydroxypropanoyl fluoride were formed. Due to the ring opening reaction of β-propiolactone, induced by the reaction in the superacidic

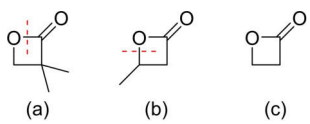

Scheme 1. Structures of α,α-dimethyl-β-propiolactone (a), β-butyrolactone (b) and β-propiolactone (c) with highlighted localizations of the respective cleavages.

[a] *S. Beck, C. Jessen, Prof. Dr. A. J. Kornath*
Department of Chemistry,
Ludwig-Maximilian University of Munich
Butenandtstr. 5–13, 81377 München, Germany
E-mail: akoch@cup.uni-muenchen.de
http://www.org.chemie.uni-muenchen.de/ac/kornath/

Supporting information for this article is available on the WWW under https://doi.org/10.1002/ejoc.202101351

Research Article
doi.org/10.1002/ejoc.202101351

Chemistry Europe
European Chemical Societies Publishing

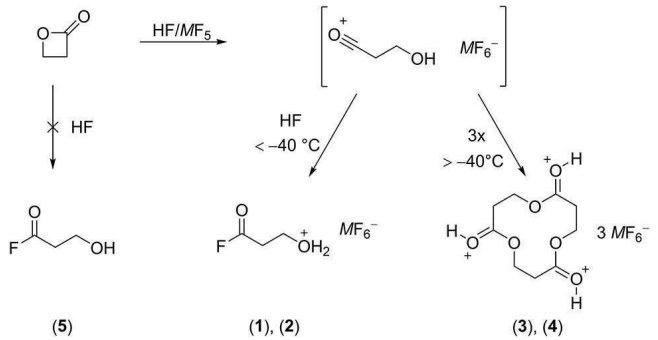

Scheme 2. Reaction scheme of β-propiolactone in HF/MF_5.

system HF/MF_5 (M = Sb, As), an acyl cation in the form of $[HO(CH_2)_2CO][MF_6]$ is assumed. The formal addition of an HF molecule led to the formation of the air- and temperature-sensitive compounds $[H_2O(CH_2)_2C(O)F][SbF_6]$ (**1**) and $[H_2O(CH_2)_2C(O)F][AsF_6]$ (**2**). Salt (**1**) is stable up to −40 °C, while (**2**) decomposes at −60 °C. Decomposition temperatures were determined by detecting gas release. In case of a higher reaction temperature (> −40 °C), the formation of the triprotonated species of 1,5,9-trioxacyclododecane-2,6,10-trione was observed. The formation can be explained by esterification of three of the assumed acyl cations $[HO(CH_2)_2CO][MF_6]$. The salts $[C_9H_{15}O_6][SbF_6]_3$ (**3**) and $[C_9H_{15}O_6][AsF_6]_3$ (**4**) are air- and temperature-sensitive, stable up to −15 °C.

Reacting β-propiolactone only with *a*HF does not lead to the formation of the neutral compound 3-hydroxypropanoyl fluoride (**5**), thus the addition of Lewis acid is required for the ring opening reaction.

Crystal structure of $[H_2O(CH_2)_2C(O)F][SbF_6]$ (1)

The salt $[H_2O(CH_2)_2C(O)F][SbF_6]$ (**1**) crystallizes in the orthorhombic space group $Pna2_1$ with four formula units per unit cell. Selected bond lengths and angles are listed in Table 1 and in Figure 1 the asymmetric unit is displayed.

The C1–O1 bond length of 1.183(6) Å is in the range of CO bonds in acyl fluoride groups.[8–10] The C1–F1 bond length (1.329(6) Å) is in accordance with typical CF bond lengths in acyl fluoride groups.[8–10] Moreover, the C–C bond distances are in the range of formal C–C single bonds (1.54 Å).[11] Since the alcohol group is protonated, the C3–O2 bond length (1.485(5) Å) corresponds to the CO bonds of protonated primary alcohol groups reported in literature.[12] Both functional groups are twisted with respect to each other by a dihedral angle of −64.1(5)° (C1–C2–C3–O2). In Figure 2 interatomic contacts of $[H_2O(CH_2)_2C(O)F][SbF_6]$ (**1**) are displayed. A chain structure of the cations is formed by moderate hydrogen bonds.[13] The connection occurs between the oxygen atom of the acyl fluoride group and the oxygen atom of the protonated alcohol group (O1*i*···H3–O2 with 2.577(5) Å). In addition, the anions are connected to the cation chain by moderate hydrogen bonds O2–H4···F6 (2.550(5) Å).[13]

Table 1. Selected bond lengths [Å] and angles [°] of $[H_2O(CH_2)_2C(O)F][SbF_6]$ (**1**) with estimated standard deviations in parentheses. Symmetry codes: *i* = −½ + x, ½ − y, z; *ii* = ½ + x, ½ − y, z.

Bond lengths [Å]			
O1–C1	1.183(6)	C2–C3	1.505(7)
C1–F1	1.329(6)	C3–O2	1.485(5)
C1–C2	1.495(6)		
Bond angles [°]			
F1–C1–O1	119.8(4)	C1–C2–C3	112.6(4)
O1–C1–C2	127.7(4)	C3–C3–O2	108.6(4)
F1–C1–F2	112.5(4)		
Dihedral angles [°]			
F1–C1–C2–C3	172.4(4)	C1–C2–C3–O2	−64.1(5)
O1–C1–C2–C3	−7.5(7)		
Interatomic contacts [Å]			
O2–(H3)···O1*i*	2.577(5)	O2–(H4)···F6	2.550(5)

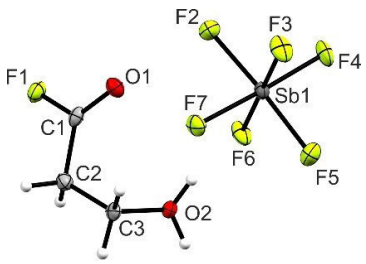

Figure 1. Asymmetric unit of $[H_2O(CH_2)_2C(O)F][SbF_6]$ (**1**) (50% probability displacement ellipsoids).

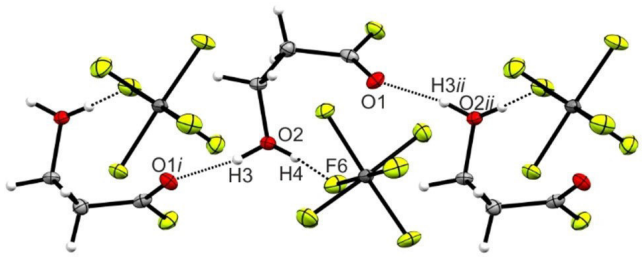

Figure 2. Projection of interatomic contacts in the crystal structure of $[H_2O(CH_2)_2C(O)F][SbF_6]$ (**1**) (50% probability displacement ellipsoids). Symmetry codes: *i* = −½ + x, ½ − y, z; *ii* = ½ + x, ½ − y, z.

The Sb–F bond lengths in the SbF_6^- anion range between 1.859(3) Å and 1.914(4) Å. Bond angles are observed between 87.3(1)° and 92.5(1) °, and between 175.4(1)° and 179.8(1)° respectively. These values are in accordance with reported parameters for SbF_6^- anions.[14,15]

Crystal structure of $[C_9H_{15}O_6][SbF_6]_3$ (3)

Compound (**3**) crystallizes in the monoclinic space group $P2_1/n$ with four formula units per unit cell. Figure 3 shows the asymmetric unit and Table 2 summarizes selected bond lengths

Research Article
doi.org/10.1002/ejoc.202101351

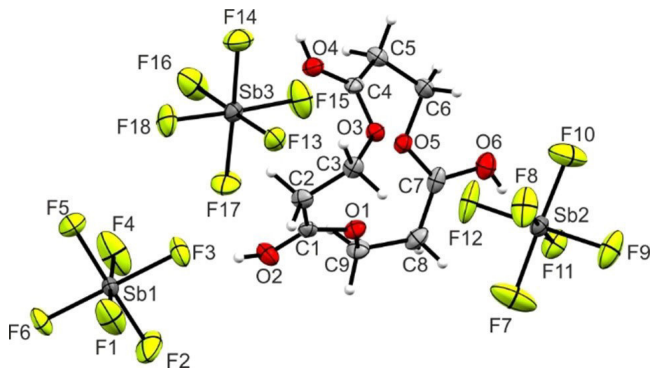

Figure 3. Asymmetric unit of $[C_9H_{15}O_6][SbF_6]_3$ (**3**) (50% probability displacement ellipsoids).

Table 2. Selected bond lengths [Å] and angles [°] of $[C_9H_{15}O_6][SbF_6]_3$ (**3**) with estimated standard deviations in parentheses. Symmetry codes: $i = -1+x, y, z$; $ii = 2.5-x, {}^1/_2+y, {}^1/_2-z$.

Bond lengths [Å]			
O1–C1	1.275(7)	C5–C6	1.529(9)
C1–O2	1.269(7)	C6–O5	1.465(7)
C1–C2	1.473(8)	O5–C7	1.275(7)
C2–C3	1.514(8)	C7–O6	1.265(8)
C3–O3	1.478(7)	C7–C8	1.480(8)
O3–C4	1.275(6)	C8–C9	1.529(9)
C4–O4	1.275(8)	C9–O1	1.475(8)
C4–C5	1.476(8)		
Bond angles [°]			
O1–C1–O2	117.6(5)	C5–C6–O5	107.2(5)
O1–C1–C2	118.7(5)	O5–C7–C8	119.1(5)
O2–C1–C2	123.6(5)	C7–C8–C9	115.5(5)
C1–C2–C3	116.4(5)	C8–C9–O1	107.2(5)
C2–C3–O3	110.1(4)	O3–C4–O4	118.7(5)
O3–C4–C5	117.2(5)	O5–C7–O6	118.3(5)
C4–C5–C6	114.1(5)	C8–C7–O6	122.5(5)
O4–C4–C5	124.1(5)		
Dihedral angles [°]			
C4–C5–C6–O5	56.7(6)	O1–C1–C2–C3	2.9(8)
C4–O3–C3–C2	79.0(6)	O2–C1–O1–C9	10.9(8)
Interatomic contacts [Å]			
O2–H1···F3	2.513(7)	O6–H7···F18*i*	2.668(7)
O4–H4···F6*ii*	2.561(5)		

and angles. The CO bond lengths of the protonated carbonyl groups (C1–O2, C4–O4 and C7–O6), are between 1.265(8) Å and 1.275(8) Å. The adjacent cyclic CO bonds (C1–O1, C4–O3 and C7–O5) are in the same range. These CO bond lengths are all between a formal single (1.43 Å) and double bond (1.19 Å) and in accordance with values of protonated ester groups.[16,17] The C–C bond distances in the trication are between 1.473(8) Å (C1–C2) and 1.529(9) Å (C8–C9). Three C atoms of one $[C_3O_2H_5]^+$ unit span an angle between 114.1(5)° (C4–C5–C6) and 116.4(5)° (C1–C2–C3). The respective O–C–C and O–C–O angles, around each protonated ester moiety, range from 117.2(5)° (O3–C4–C5) to 124.1(5)° (O4–C4–C5).

The contacts between the cation and the anions are displayed in Figure 4. The trication is connected to three anions

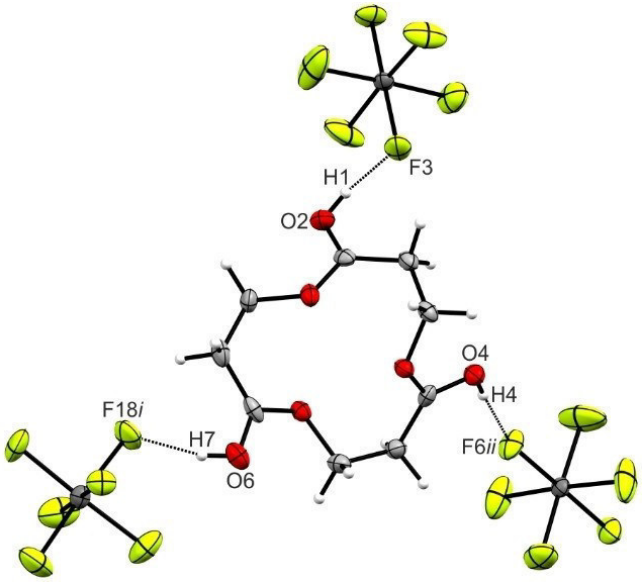

Figure 4. Projection of interatomic contacts in the $[C_9H_{15}O_6][SbF_6]_3$ (**3**) crystal (50% probability displacement ellipsoids). Symmetry codes: $i = -1+x, y, z$; $ii = 2.5-x, {}^1/_2+y, {}^1/_2-z$.

by moderate hydrogen bonds,[13] whereby the strongest hydrogen bond occurs between O2–H1···F3 (2.513(7) Å).The bond lengths and angles of the SbF_6^- anions are in the range of previously reported literature data.[14,15]

Vibrational spectroscopy

$[H_2O(CH_2)_2C(O)F][MF_6]$ (M = Sb, As)

The Raman spectrum of β-propiolactone together with Raman and IR spectra of $[H_2O(CH_2)_2C(O)F][SbF_6]$ (**1**) and $[H_2O(CH_2)_2C(O)F][AsF_6]$ (**2**) are illustrated in Figure 5. Selected experimental frequencies of (**1**) and (**2**) together with calculated frequencies of $[H_2O(CH_2)_2C(O)F]^+ \cdot COF_2 \cdot [H_3O]^+$ are summarized in Table 3.

The O–H···O hydrogen bond connecting the cations has a great influence on the frequency of the CO stretching vibration belonging to the acyl fluoride group. Calculated vibrational frequencies of the free cation show large deviations from the experimentally obtained frequencies. Therefore, a H_3O^+ and a COF_2 molecule were added to the gas-phase structure to simulate the hydrogen bonds in the solid state. According to quantum chemical calculations, which are discussed later, the cation possesses C_1 symmetry with 30 fundamental vibrations. The ring opening reaction of β-propiolactone and subsequently the formation of monoprotonated 3-hydroxypropanoyl fluoride is confirmed by the vibrational spectroscopic study. The most intense line in the Raman spectrum of β-propiolactone and the most characteristic vibration for ring compounds, the ring breathing vibration (here at 1007 cm^{-1}),[18] are not detected in the Raman spectra of (**1**) and (**2**). The stretching vibration ν(CO) of the acyl fluoride group is observed at 1769 cm^{-1} (IR),

Research Article
doi.org/10.1002/ejoc.202101351

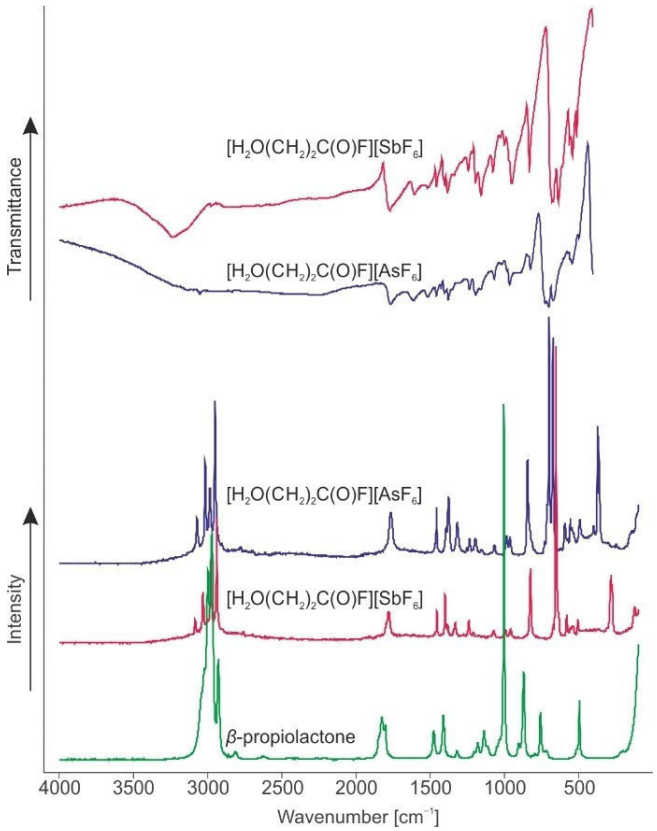

Figure 5. Raman spectrum of β-propiolactone (green), Raman and IR spectra of $[H_2O(CH_2)_2C(O)F][SbF_6]$ (**1**) (red) and $[H_2O(CH_2)_2C(O)F][AsF_6]$ (**2**) (blue).

1781 cm^{-1} (Ra) (**1**) and at 1764 cm^{-1} (IR), 1768 cm^{-1} (Ra) (**2**). Usually, this vibration occurs in a range between 1800 cm^{-1} and 1950 cm^{-1}.[19,20] The fact that this frequency in (**1**) and (**2**) appears lower than expected for this group can be explained by the above-mentioned hydrogen bond between the cations. The ν(CF) vibration occurs at about 1240 cm^{-1} in (**1**) and at 1235 cm^{-1} in (**2**), which is in accordance with reported literature data.[20,21] Due to the protonation, the CO stretching vibration of the alcohol group is red-shifted compared to unprotonated primary alcohols.[22] This vibration is detected at 827 cm^{-1} (IR), 828 cm^{-1} (Ra) (**1**) and at 841 cm^{-1} (IR) and 847 cm^{-1} (Ra) (**2**). The ν(OH) stretching vibrations of the protonated alcohol group are not observable in the Raman spectra of (**1**) and (**2**), because of the poor polarizability of this vibration. Contrariwise, in the corresponding IR spectra these vibrations occur at about 3231 cm^{-1} (**1**) and 3128 cm^{-1} (**2**).

$[C9H15O6][MF6]3\ (M = Sb, As)$

The Raman and corresponding IR spectra of $[C_9H_{15}O_6][SbF_6]_3$ (**3**) and $[C_9H_{15}O_6][AsF_6]_3$ (**4**) are displayed in Figure 6. Selected experimentally observed and calculated frequencies of the free trication $[C_9H_{15}O_6]^{3+}$ are summarized in Table 4. All observed frequencies of (**3**) and (**4**) are listed in Table S4 (see Supporting Information). An ideal C_{3h} symmetry is expected for the trication, but C_1 symmetry with 84 IR and Raman active vibrations, is quantum-chemically calculated. The calculated structure differs only slightly from C_{3h} symmetry in which degeneracy of vibrations occurs, which explains why less vibrations are observed in the spectra of (**3**) and (**4**) than calculated. The Raman and IR spectra show that the single

Table 3. Selected experimental vibrational frequencies [cm^{-1}] of (**1**) and (**2**) and calculated vibrational frequencies [cm^{-1}] of $[H_2O(CH_2)_2C(O)F]^+ \cdot COF_2 \cdot [H_3O]^+$.

$[H_2O(CH_2)_2C(O)F][SbF_6]$ (**1**)		$[H_2O(CH_2)_2C(O)F][AsF_6]$ (**2**)		$[H_2O(CH_2)_2C(O)F]^+ \cdot COF_2 \cdot [H_3O]^+$	Assignment
IR	Raman	IR	Raman	Calc.[a] (IR/Raman)	
3231 (w)		3128 (vw)		3700 (224/50)	ν(OH)
1769 (w)	1781 (11)	1764 (w)	1768 (21)	1771 (1389/34)	ν(CO)
1238 (vw)	1242 (7)	1234 (vw)	1236 (10)	1230 (147/1)	ν(CF)
1153 (w)		1157 (vw)	1157 (6)	1095 (78/2)	δ(COH)
1074 (vw)	1076 (4)	1067 (vw)	1069 (8)	1008 (21/0.5)	ν(CC)
995 (vw)	997 (5)	982 (vw)	987 (11)	1000 (57/1)	ν(CC)
827 (m)	828 (25)	841 (vw)	847 (42)	852 (19/3)	ν(CO)

[a] Calculated on the B3LYP/aug-cc-pVTZ level of theory. IR intensity in km/mol and Raman intensity in $Å^4/u$. Abbreviations for IR intensities: v = very, m = medium, w = weak. Experimental Raman activities are stated to a scale of 1 to 100.

Table 4. Selected experimental vibrational frequencies [cm^{-1}] of (**3**) and (**4**) and calculated vibrational frequencies [cm^{-1}] of $[C_9H_{15}O_6]^{3+}$.

$[C_9H_{15}O_6][SbF_6]_3$ (**3**)		$[C_9H_{15}O_6][AsF_6]_3$ (**4**)		$[C_9H_{15}O_6]^{3+}$	Assignment
IR	Raman	IR	Raman	Calc.[a] (IR/Raman)	
3232 (vs)		3229 (w)		3636 (323/82), 3628 (341/85), 3625(546/51)	ν(OH)
1609 (w)	1648 (10)	1608 (w)	1626 (16)	1627 (226/1), 1619 (238/0.8), 1616 (477/0.9)	ν(CO)
1508 (w)	1510 (12)	1508 (w)	1515 (25)	1510 (330/0.4), 1507 (244/1), 1497 (10/16)	ν(CO)
1213 (vw)	1239 (11)	1213 (w)	1237 (20)	1157 (200/8), 1155 (249/4), 1153 (276/7)	δ(COH)
1090 (vw)	1093 (10)	1084 (vw)	1095 (21)	1080(8/0.4), 1073 (2/0.3), 1068 (6/3)	ν(CC)
1024 (vw)	1026 (8)	1026 (vw)	1021 (17)	1024 (37/0.7), 1022 (19/0.5), 1002 (3/0.3)	ν(CC)
968 (w)	971 (12)	966 (w)	967 (23)	959 (3/2), 953 (73/0.8), 942 (66/2)	ν(CO)

[a] Calculated on the B3LYP/aug-cc-pVTZ level of theory. IR intensity in km/mol and Raman intensity in $Å^4/u$. Abbreviations for IR intensities: v = very, s = strong, m = medium, w = weak. Experimental Raman activities are stated to a scale of 1 to 100.

Research Article
doi.org/10.1002/ejoc.202101351

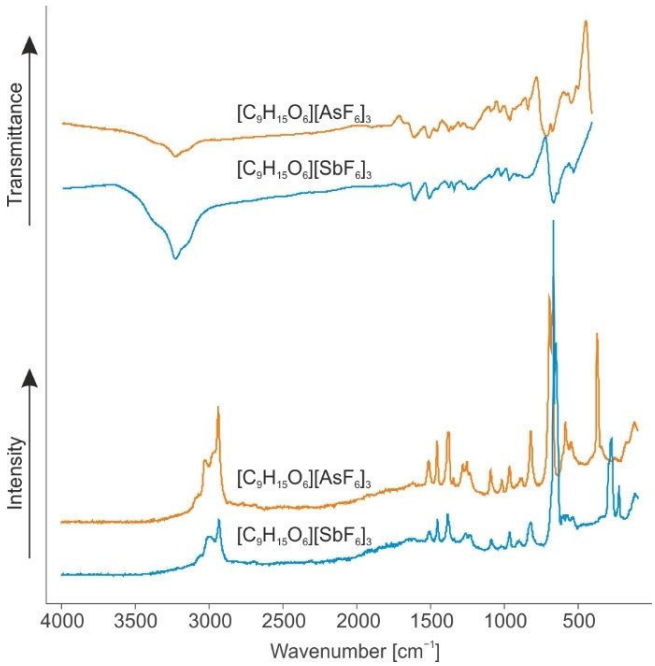

Figure 6. Raman and IR spectra of $[C_9H_{15}O_6][SbF_6]_3$ (**3**) (blue) and $[C_9H_{15}O_6][AsF_6]_3$ (**4**) (orange).

crystal of (**3**) (discussed above) is representative for the bulk sample and the trication is formed exclusively. The ν(OH) stretching vibration occurs at about 3230 cm^{-1} in both IR spectra of (**3**) and (**4**). Due to the poor polarizability of this vibration, it is not observable in the corresponding Raman spectra.

The ν(CO) vibration of the protonated carbonyl group occurs at 1609 cm^{-1} (IR), 1648 cm^{-1} (Ra) (**3**) and 1608 cm^{-1} (IR), 1626 cm^{-1} (Ra) (**4**). The neighboring CO stretching vibration, belonging to the ester group, is detected at 1508 cm^{-1} in the respective IR spectra of (**3**) and (**4**) and in the Raman spectra at 1510 cm^{-1} (**3**) and 1515 cm^{-1} (**4**), respectively. All these frequencies are in good agreement, with reported literature data of protonated esters.[17] The ν(CC) vibrations are observed at approximately 1090 cm^{-1} and 1025 cm^{-1} in (**3**) and (**4**), which is in fair agreement to values reported in literature.[22] The COH deformation vibration occurs at 1213 cm^{-1} in the respective IR spectra of (**3**) and (**4**) and in the Raman spectra at 1239 cm^{-1} (**3**) and 1237 cm^{-1} (**4**), respectively.

Theoretical calculations

The quantum chemical calculations for geometry optimization and vibrational frequency analysis were carried out on the B3LYP/aug-cc-pVTZ level of theory. The optimization of the free cation $[H_2O(CH_2)_2C(O)F]^+$ leads to the formation of an intramolecular hydrogen bond between the protonated hydroxyl group and the carbonyl oxygen. This hydrogen bond has a significant influence on the calculated vibrational frequencies and leads to large deviations from the experimentally obtained frequencies. The optimized structure of the free cation is displayed in the Supporting Information (Figure S1). To overcome this discrepancy to the geometry of the $[H_2O(CH_2)_2C(O)F]^+$ cation observed in the crystal structure of (**1**), a H_3O^+ ion and a COF_2 molecule were added. As described above, a chain structure is formed by the cations and anions in the solid state. The H_3O^+ simulates the protonated hydroxyl group, while COF_2 simulates the neighboring acyl fluoride group. In Figure 7, the calculated structure of $[H_2O(CH_2)_2C(O)F]^+{\cdot}H_3O^+{\cdot}COF_2$ and the cation of the single-crystal X-ray structure analysis are displayed together with selected bond lengths and angles. Almost all calculated bond lengths and angles are in good accordance with the parameters, observed in the crystal structure of (**1**). Only the C1–F1 bond is calculated shorter than observed in the crystal structure. Contrariwise, the C1–O1 bond is calculated longer compared to the bond lengths determined in the solid state.

The obtained experimental data lead to the assumption of the cationic acyl species $[HO(CH_2)_2CO]^+MF_6^-$ as an intermediate. However, the isolation of this compound was not possible. In order to quantify where the protonation occurs initially, Natural Population Analysis (NPA) charges were calculated for β-propiolactone and are illustrated in the Supporting Information (Figure S2). The protonation of the carbonyl oxygen appears more likely, due to the more negative NPA charge of this oxygen compared to the ring oxygen atom. Nevertheless, the protonation on the ring oxygen is necessary for the formation of the acyl species. In Scheme 3, a possible reaction pathway is illustrated for the formation of the cationic acyl species.

The reaction pathway includes an intramolecular 1,3-proton shift. For the isoelectronic species β-propiolactam, such an equilibrium is reported in literature.[23] Calculations of the proton transfer in the gas phase together with corresponding

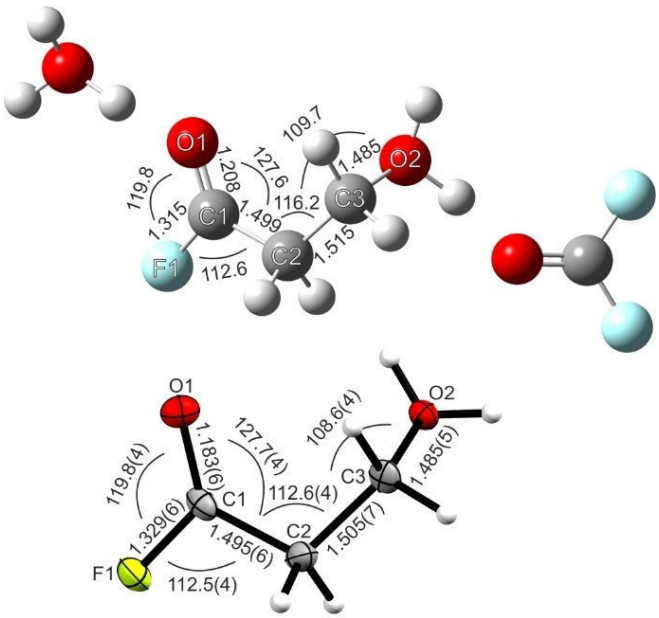

Figure 7. Calculated structure of $[H_2O(CH_2)_2C(O)F]^+{\cdot}H_3O^+{\cdot}COF_2$ (top) and cation of the single-crystal X-ray structure (bottom).

Research Article
doi.org/10.1002/ejoc.202101351

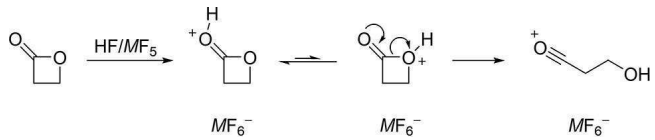

Scheme 3. Reaction pathway to obtain the acyl cation from β-propiolactone.

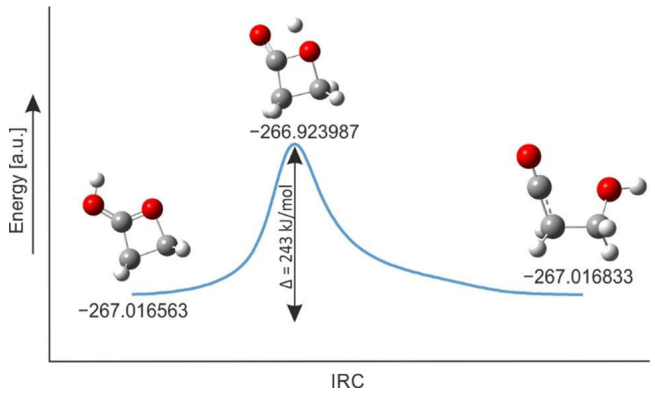

Figure 8. Calculated intrinsic reaction coordinate (IRC) path of the proton shift based on protonated β-propiolactone together with corresponding single point energy values.

single point energy values were performed on the MP2/aug-cc-pVTZ level of theory for the protonated β-propiolactone. Based on the optimized structure of protonated β-propiolactone (proton on carbonyl oxygen), the proton transfer from the carbonyl to the ring oxygen was calculated and a transition state was determined. Starting from this transition state, the potential energy curve along the intrinsic reaction coordinates was calculated. Interestingly, the optimization of the cyclic compound (proton on ring oxygen) does not provide an energetic minimum and leads directly to the formation of the cationic acyl species instead. Figure 8 shows the optimized structures of protonated β-propiolactone, the transition state and the acyl cation, together with the calculated intrinsic reaction coordinate (IRC) path of the proton shift.

The energy gain of the system by ring opening appears quite small with only 0.7 kJ/mol, but the energy barrier of the intramolecular proton transfer is very high (243 kJ/mol). For proton transfers several theoretical studies have been performed to investigate the influence of solvents on these calculations.[24–27] These studies concluded that in particular protic solvents are able to decrease calculated intrinsic barriers compared to the gas phase and facilitate proton transfer.[24–27] *Yu* et al. compared the effects of protic and aprotic solvent on an intramolecular proton transfer with the result, that the intrinsic barrier decreases rapidly under the influence of protic solvents, while the influence of aprotic solvents are more comparable to gas phase calculations in their studies.[27] With this in mind, the herein performed gas phase calculations show more similarity to an aprotic solvent environment, such as SO_2. In this solvent, the intrinsic barrier could be high enough to prevent the 1,3-proton transfer. This assumption is consistent with the results of *Olah*, where no ring opening reaction was observed.[7] Under the condition that protic solvents are able to reduce this barrier enough to enable ring opening, a possible explanation for the results of *Hogeveen*[6] and the results of this study has emerged.

Conclusion

In this work, the reaction behavior of β-propiolactone in the binary superacidic systems HF/MF_5 (M = Sb, As) was investigated. Depending on the reaction temperature, two different products were obtained. Salts of monoprotonated 3-hydroxypropanoyl fluoride $[H_2O(CH_2)_2C(O)F][SbF_6]$ (**1**) and $[H_2O(CH_2)_2C(O)F][AsF_6]$ (**2**) were obtained by performing the reaction at temperatures lower than −40 °C. In contrast, temperatures higher than −40 °C lead to the formation of a trication in the form of $[C_9H_{15}O_6][SbF_6]_3$ (**3**) and $[C_9H_{15}O_6][AsF_6]_3$ (**4**). All salts were characterized by Raman and IR spectroscopy. In case of the respective SbF_6^- salts (**1**) and (**3**) single-crystal X-ray analyses were performed. For the formation of both, the monoprotonated 3-hydroxypropanoyl fluoride and the trication, the existence of the acyl cationic species $[HO(CH_2)_2CO]^+MF_6^-$ as an intermediate is assumed. As protonated β-propiolactone was not observed, the proton transfer from the carbonyl to the ring oxygen was calculated. Interestingly, the optimization of the protonated ring compound (proton on the ring oxygen) leads directly to a ring opening and formation of the acyl cation. An intrinsic reaction coordinate (IRC) path of the proton shift showed that the energy barrier to overcome the transition state is very high (243 kJ/mol) in the gas phase. As this calculation is more comparable to a calculation in an aprotic solvent environment, it provides an explanation that a ring opening reaction is not observed in *Olah*'s studies in SO_2.[7] We conclude that protic solvents, such as *a*HF, are required to reduce this barrier and enable proton transfer, which is supported by the results of *Hogeveen*[6] and this study.

Experimental Section

General information

Caution! The hydrolysis of AsF_5, SbF_5 and the prepared salts (**1**–**4**) might form HF which burns skin and causes irreparable damage. Safety precautions should be taken while using and handling these materials.

Apparatus and materials

All reactions were conducted in standard Schlenk technique using a stainless-steel vacuum line. As reaction vessels FEP/PFA reactors, closed with a stainless-steel valve were used. Prior to use, the vacuum line as well as the reaction vessels were dried with fluorine. A Bruker MultiRAM FT-Raman spectrometer with Nd:YAG laser excitation (λ = 1064 nm) was used for all low temperature Raman spectroscopic measurements in vacuum at −196 °C. For the measurements, the synthesized compounds were transferred into a cooled glass cell. The low temperature IR spectra were recorded on

a Bruker Vertex-80V FTIR spectrometer ($\tilde{\nu}$ = 400–4000 cm^{-1}). Small amounts of the synthesized samples were placed on a CsBr single-crystal plate in a cooled cell. The low-temperature single-crystal X-ray diffractions of $[H_2O(CH_2)_2C(O)F][SbF_6]$ (**1**) and $[C_9H_{15}O_6][SbF_6]_3$ (**3**) were performed on an Oxford XCalibur 3 diffractometer equipped with a Kappa CCD detector, operating with Mo-Kα (0.71073 Å) radiation and a Spellman generator (voltage 50 kV, current 40 mA). The program CrysAlisPro 1.171.38.46 (Rigaku OD, 2015)[28] were employed for the data collection and reduction. The structures were solved utilizing SHELXT[29] and SHELXL-2018/3[30] of the WINGX software package.[31] The structures were checked using the software PLATON.[32] The absorption correction was performed using the SCALE3 ABPSACK multiscan method.[33] Selected parameters and data are listed in Table S1 for (**1**) and Table S2 for (**3**) (see Supporting Information). The quantum chemical calculations were performed on the B3LYP/aug-cc-pVTZ level of theory or on the MP2/aug-cc-pVTZ level of theory, respectively.

Synthesis of $[H_2O(CH_2)_2C(O)F][SbF_6]$ (1) and $[C_9H_{15}O_6][SbF_6]_3$ (3)

SbF_5 (140 mg, 0.65 mmol) was condensed into a FEP tube-reactor at −196 °C. Afterwards, approximately 2 mL *a*HF was also condensed in the reactor at −196 °C. Both compounds were warmed up to −40 °C and homogenized in order to form the superacidic system. The system was cooled down to −196 °C and β-propiolactone (46 mg, 0.65 mmol) was added under inert gas atmosphere. In order to form (**1**), the reaction mixture was warmed up, not exceeding −40 °C. For the formation of (**3**), the reaction temperature was kept between −40 °C and −20 °C. The homogenization was performed until the respective salts were completely dissolved. Excess *a*HF was removed overnight in a dynamic vacuum at −78 °C. For crystallization of compound (**1**) and (**3**) the reactors were left in an ethanol bath at −70 °C for (**1**), and at −40 °C for (**3**) respectively, until the salts recrystallized. Compounds $[H_2O(CH_2)_2C(O)F][SbF_6]$ (**1**) and $[C_9H_{15}O_6][SbF_6]_3$ (**3**) were obtained as colorless solids. Compound (**1**) is stable up to −40 °C, while (**3**) decomposes at −15 °C.

Synthesis of $[H_2O(CH_2)_2C(O)F][AsF_6]$ (2) and $[C_9H_{15}O_6][AsF_6]_3$ (4)

Anhydrous hydrogen fluoride (2 mL) and subsequently arsenic pentafluoride (85 mg, 0.50 mmol) were condensed into a FEP tube-reactor at −196 °C. In order to form the superacidic system, both compounds were warmed up to −40 °C and homogenized. After cooling down to −196 °C, β-propiolactone (36 mg, 0.50 mmol) was added to the frozen system under inert gas atmosphere. The formation of salt (**2**) was carried out by warming up all compounds not exceeding −40 °C and homogenizing until the salt was completely dissolved. The suitable reaction temperature for the formation of compound (**4**) was between −40 °C and −20 °C. All compounds were warmed up to this temperature range and homogenized until the salt was completely dissolved. For (**2**) and (**4**), excess *a*HF was removed at −78 °C overnight. Salts $[H_2O(CH_2)_2C(O)F][AsF_6]$ (**2**) and $[C_9H_{15}O_6][AsF_6]_3$ (**4**) were obtained in form of colorless solids. The respective decomposition temperatures are −40 °C for (**2**) and −15 °C for (**4**) and consequently in accordance with the respective antimony species (**1**) and (**3**).

Crystallographic data

Deposition numbers 2040260 for $[H_2O(CH_2)_2C(O)F][SbF_6]$ (**1**) and 2040261 for $[C_9H_{15}O_6][SbF_6]_3$ (**3**) contain the supplementary crystallographic data for this paper. These data are provided free of charge by the joint Cambridge Crystallographic Data Centre and Fachinformationszentrum Karlsruhe Access Structures service www.ccdc.cam.ac.uk/structures.

Acknowledgements

We are grateful to the Department of Chemistry of the Ludwig Maximilian University of Munich, the Deutsche Forschungsgemeinschaft (DFG) and the F-Select GmbH for their financial support. Open Access funding enabled and organized by Projekt DEAL.

Conflict of Interest

The authors declare no conflict of interest.

Data Availability Statement

The data that support the findings of this study are available in the supplementary material of this article.

Keywords: β-Propiolactone · Ring opening · Trication · IRC Calculations · Single-crystal X-ray analysis

[1] A. R. Olson, J. L. Hyde, *J. Am. Chem. Soc.* **1941**, *63*, 2459–2461.
[2] A. R. Olson, R. J. Miller, *J. Am. Chem. Soc.* **1938**, *60*, 2687–2692.
[3] A. R. Olson, P. V. Youle, *J. Am. Chem. Soc.* **1951**, *73*, 2468–2471.
[4] R. Gómez-Bombarelli, E. Calle, J. Casado, *J. Org. Chem.* **2013**, *78*, 6880–6889.
[5] R. Gómez-Bombarelli, E. Calle, J. Casado, *J. Org. Chem.* **2013**, *78*, 6868–6879.
[6] H. Hogeveen, *Recl. Trav. Chim. Pays-Bas* **1968**, *87*, 1303–1312.
[7] G. A. Olah, A. T. Ku, *J. Org. Chem.* **1970**, *35*, 3916–3922.
[8] A. F. Baxter, K. O. Christe, R. Haiges, *Struct. Chem.* **2017**, *28*, 303–307.
[9] *NATO ASI series Series C, Mathematical and physical sciences*, *Vol. 410*, Kluwer, Dordrecht, **1993**.
[10] N. V. Belova, H. Oberhammer, X. Zeng, M. Gerken, H. Willner, R. J. F. Berger, S. A. Hayes, N. W. Mitzel, *Phys. Chem. Chem. Phys.* **2010**, *12*, 11445–11453.
[11] A. F. Holleman, E. Wiberg, N. Wiberg, *Anorganische Chemie*, De Gruyter, Berlin, Boston, **2017**.
[12] R. Minkwitz, S. Schneider, *Z. Anorg. Allg. Chem.* **1998**, *624*, 1989–1993.
[13] G. A. Jeffrey, *An Introduction to hydrogen bonding*, Oxford University Press, New York, **1997**.
[14] M. Schickinger, C. Jessen, Y. Morgenstern, K. Muggli, F. Zischka, A. Kornath, *Eur. J. Org. Chem.* **2018**, *2018*, 6223–6229.
[15] R. Minkwitz, S. Schneider, *Angew. Chem. Int. Ed.* **1999**, *38*, 210–212; *Angew. Chem.* **1999**, *111*, 229–231.
[16] M. S. Yusubov, N. S. Soldatova, P. S. Postnikov, R. R. Valiev, A. Yoshimura, T. Wirth, V. N. Nemykin, V. V. Zhdankin, *Chem. Commun. (Camb.)* **2019**, *55*, 7760–7763.
[17] S. Beck, M. Feller, L. Spies, K. J. Dietrich, C. Jessen, K. Stierstorfer, A. J. Kornath, *ChemistryOpen* **2021**, *10*, 8–15.
[18] J. R. Durig, *Spectrochim. Acta* **1963**, *19*, 1225–1233.
[19] A. H. Nielsen, T. G. Burke, P. J. H. Woltz, E. A. Jones, *J. Chem. Phys.* **1952**, *20*, 596–604.
[20] J. A. Ramsey, J. A. Ladd, *J. Chem. Soc. B* **1968**, 118.
[21] M. C. Bayer, C. Jessen, A. J. Kornath, *Z. Anorg. Allg. Chem.* **2020**, *646*, 1688–1695.
[22] J. Weidlein, K. Dehnicke, U. Müller, *Schwingungsspektroskopie. Eine Einführung*, Thieme, Stuttgart, **1988**.
[23] R. A. Cox, K. Yates, *Can. J. Chem.* **1981**, *59*, 2853–2863.
[24] W. Chansen, N. Kungwan, *J. Phys. Chem. A* **2021**, *125*, 5314–5325.
[25] H. Tavakol, *J. Phys. Chem. A* **2013**, *117*, 6809–6816.

Research Article
doi.org/10.1002/ejoc.202101351

[26] H. Tavakol, F. Keshavarzipour, *Struct. Chem.* **2015**, *26*, 1049–1057.
[27] B. Xiao, Y. Li, X. Yu, J. Cheng, *J. Phys. Chem. A* **2015**, *119*, 11882–11890.
[28] *CrysAlisPro Software System*, Rigaku Oxford Diffraction, Rigaku Corpoation, Oxford, UK, **2015**.
[29] G. M. Sheldrick, *Acta. Crystallogr., Sect. A: Found. Adv.* **2015**, *71*, 3–8.
[30] G. M. Sheldrick, *Acta. Crystallogr., Sect. C: Struct. Chem.* **2015**, *71*, 3–8.
[31] L. J. Farrugia, *J. Appl. Crystallogr.* **1999**, *32*, 837–838.
[32] A. L. Spek, *J. Appl. Crystallogr.* **2003**, *36*, 7–13.
[33] *SCALE3 ABSPACK – An Oxford Diffraction Program*, Oxford Diffraction Ltd., UK, **2005**.

Manuscript received: November 5, 2021
Revised manuscript received: November 22, 2021
Accepted manuscript online: November 24, 2021

European Journal of Organic Chemistry

Supporting Information

Ring Opening and Closure Reactions of β-Propiolactone in the Superacids HF/MF_5 (M = Sb, As)

Stefanie Beck, Christoph Jessen, and Andreas J. Kornath*

Supporting Information

Table S1. Crystal data and structure refinement for $[H_2O(CH_2)_2C(O)F][SbF_6]$ (**1**).

Table S2. Crystal data and structure refinement for $[C_9H_{15}O_6][SbF_6]_3$ (**3**).

Table S3. Experimental vibrational frequencies [cm^{-1}] of (**1**) and (**2**) and calculated vibrational frequencies [cm^{-1}] of $[H_2O(CH_2)_2C(O)F]^+ \cdot COF_2 \cdot [H_3O]^+$.

Table S4. Experimental vibrational frequencies [cm^{-1}] of (**3**) and (**4**) and calculated vibrational frequencies [cm^{-1}] of $[C_9H_{15}O_6]^{3+}$.

Figure S1. Optimized structure of $[H_2O(CH_2)_2C(O)F]^+$ at the B3LYP/aug-cc-pVTZ level of theory.

Figure S2. NPA charges calculated for *β*-propiolactone.

Table S5. Cartesian coordinates of calculated minimum structure of $[H_2O(CH_2)_2C(O)F]^+ \cdot H_3O^+ \cdot COF_2$ at the B3LYP/aug-cc-pVTZ level of theory.

Table S6. Cartesian coordinates of calculated minimum structure of $[C_9H_{15}O_6]^{3+}$ at the B3LYP/aug-cc-pVTZ level of theory.

Table S7. Cartesian coordinates of calculated minimum structure of *β*-propiolactone at the B3LYP/aug-cc-pVTZ level of theory.

Table S8. Cartesian coordinates of calculated minimum structure of the transition state and concurrently starting point for IRC calculations at the MP2/aug-cc-pVTZ level of theory.

Table S9. Cartesian coordinates of calculated minimum structures of $[H_2O(CH_2)_2C(O)F]^+$ at the B3LYP/aug-cc-pVTZ level of theory.

Table S1. Crystal data and structure refinement for $[H_2O(CH_2)_2C(O)F][SbF_6]$ (**1**).

	$[H_2O(CH_2)_2C(O)F][SbF_6]$ (**1**)
Empirical formular	C3 H6 F7 O2 Sb
M_r	328.83
Crystal system	orthorhombic
Space group	*Pna*2$_1$
a [Å]	9.9712(5)
b [Å]	10.9087(4)
c [Å]	7.5038(3)
α [°]	90
β [°]	90
γ [°]	90
V [Å^3]	816.21(6)
Z	4
ρ_{calcd} [gcm^{-3}]	2.676
μ[mm^{-1}]	3.472
$\lambda_{Moκα}$	0.71073
F(000)	616
T[K]	109(2)
hkl range	–13:14; –15:14;–10:10
refl. measured	8295
refl. unique	2470
R_{int}	0.0271
parameters	127
R(F)/*w*R(F^2)[a)]	0.0268/ 0.0579
weighting scheme[b)]	0.0341
S(GoF)[c)]	1.064
residual density [eÅ^{-3}]	2.024/ -0.518
devide type	Oxford XCalibur
solution/refinement	SHELXT
CCDC	2040260

a) $R_1 = \Sigma||F_o|-|F_c||/\Sigma|F_o|$; b) $wR_2 = [\Sigma[w(F_o^2-F_c^2)^2]/\Sigma[w(F_o)^2]]^{1/2}$; $w = [\sigma_c^2(F_o^2)+(xP)^2+yP]^{-1}$; $P = (F_o^2+2F_c^2)/3$ c) GoF = $\{\Sigma[w(F_o^2-F_c^2)^2]/(n-p)\}^{1/2}$ (*n* = number of reflexions; p = total number of parameters).

Table S2. Crystal data and structure refinement for $[C_9H_{15}O_6][SbF_6]_3$ (**3**).

	$[C_9H_{15}O_6][SbF_6]_3$ (**3**)
Empirical formular	C9 H15 F18 O6 Sb3
M_r	926.46
Crystal system	monoclinic
Space group	$P2_1/n$
a [Å]	9.5326(4)
b [Å]	19.8923(9)
c [Å]	12.9377(6)
α [°]	90
β [°]	106.823(5)
γ [°]	90
V [Å^3]	2348.32(19)
Z	4
ρ_{calcd} [gcm^{-3}]	2.620
μ[mm^{-1}]	3.593
$\lambda_{Moκα}$	0.71073
F(000)	1728
T[K]	111(2)
hkl range	–11:5; –24:12;–15:16
refl. measured	10857
refl. unique	4798
R_{int}	0.0177
parameters	334
R(F)/*w*R(F^2)[a)]	0.0430/ 0.0980
weighting scheme[b)]	0.0467 17.2530
S(GoF)[c)]	1.024
residual density [eÅ^{-3}]	3.600 / –1.465
devide type	Oxford XCalibur
solution/refinement	SHELXT
CCDC	2040261

a) $R_1 = \Sigma||F_o|-|F_c||/\Sigma|F_o|$; b) $wR_2 = [\Sigma[w(F_o^2-F_c^2)^2]/\Sigma[w(F_o)^2]]^{1/2}$; $w = [\sigma_c^2(F_o^2)+(xP)^2+yP]^{-1}$; $P = (F_o^2+2F_c^2)/3$ c) GoF = $\{\Sigma[w(F_o^2-F_c^2)^2]/(n-p)\}^{1/2}$ (*n* = number of reflexions; p = total number of parameters).

Table S3. Experimental vibrational frequencies [cm^{-1}] of (**1**) and (**2**) and calculated vibrational frequencies [cm^{-1}] of $[H_2O(CH_2)_2C(O)F]^+ \cdot COF_2 \cdot [H_3O]^+$.

$[H_2O(CH_2)_2C(O)F][SbF_6]$ (1)		$[H_2O(CH_2)_2C(O)F][AsF_6]$ (2)		$[H_2O(CH_2)_2C(O)F]^+ \cdot COF_2 \cdot [H_3O]^+$	Assignment
IR	**Raman**	**IR**	**Raman**	**Calc.[a] (IR/Raman)**	
3231 (w)		3128 (vw)		3700 (224/50)	ν(OH)
	3083 (8)	3049 (vw)	3070 (18)	3167 (3/28)	$\nu_{as}(CH_2)$
	3031 (17)		3015 (41)	3106 (0.5/80)	$\nu_{s}(CH_2)$
2974 (vw)	2978 (28)		2984 (31)	3076 (8/70)	$\nu_{as}(CH_2)$
2933 (vw)	2939 (42)		2951 (66)	3025 (22/105)	$\nu_{s}(CH_2)$
				2289 (3418/103)	ν(OH)
1769 (w)	1781 (11)	1764 (w)	1768 (21)	1771 (1389/34)	ν(CO)
1603 (vw)		1612 (w)		1706 (135/4)	$\delta(OH_2)$
1510 (vw)					?
1452 (vw)	1456 (11)	1456 (vw)	1459 (23)	1494 (19/4)	$\delta(CH_2)$
1406 (vw)		1423 (vw)		1445 (107/3)	$\omega(CH_2)$
1398 (vw)	1401 (16)	1402 (vw)	1393 (15)	1420 (197/7)	$\delta(CH_2)$
1379 (w)	1387 (6)	1377 (w)	1379 (27)	1417 (15/3)	$\delta(CH_2)$
1333 (vw)	1333 (7)		1321 (17)	1343 (22/7)	$\tau(CH_2)$
			1256 (7)	1290 (6/3)	$\tau(CH_2)$
1238 (vw)	1242 (7)	1234 (vw)	1236 (10)	1230 (147/1)	ν(CF)
1213 (vw)	1212 (4)				?
1190 (vw)		1190 (w)	1197 (10)	1193 (45/2)	δ(COH)
1153 (w)		1157 (vw)	1157 (6)	1095 (78/2)	δ(COH)
1074 (vw)	1076 (4)	1067 (vw)	1069 (8)	1008 (21/0.5)	ν(CC)
1022 (vw)		1015 (vw)			?
995 (vw)	997 (5)	982 (vw)	987 (11)	1000 (57/1)	ν(CC)
962 (vw)	961 (5)	964 (w)	967 (11)	970 (41/2)	δ(CCC)
945 (w)		895 (vw)			?
827 (m)	828 (25)	841 (vw)	847 (42)	852 (19/3)	ν(CO)
		824 (w)	832 (sh)	826 (10/8)	δ(OCF)
675 (vs)	675 (6)	671 (vs)[b]	676 (92)[b]	653 (69/1)	δ(CCO)
557 (s)	560 (5)	554 (m)	558 (18)	573 (14/0.7)	γ(COFC)
	549 (5)	544 (m)	548 (15)	520 (55/0.9)	δ(CCF)
538 (s)	540 (6)		534 (sh)	462 (29/0.9)	δ(COH)
507 (s)	507 (8)	496 (m)	495 (18)	367 (25/0.9)	δ(CCO)
				312 (48/0.1)	Skeletal vibration
				298 (209/0.1)	Skeletal vibration
				199 (27/0.2)	Skeletal vibration
665 (vs)	656 (100)	723 (vs)	734 (9)		MF_6^-

631 (vs)	584 (9)	702 (vs)	713 (25)	MF_6^-
	285 (23)	569 (vs)	701 (100)	MF_6^-
	279 (20)		676 (92)[b]	MF_6^-
			595 (17)	MF_6^-
			577 (10)	MF_6^-
			403 (15)	MF_6^-
			377 (56)	MF_6^-
			367 (52)	MF_6^-

[a] Calculated on the B3LYP/aug-cc-pVTZ level of theory. IR intensity in km/mol and Raman intensity in $Å^4/u$. Abbreviations for IR intensities: v = very, s = strong, m = medium, w = weak, br = broad. Experimental Raman activities are stated to a scale of 1 to 100. [b] Anion and cation interfere with each other.

Table S4. Experimental vibrational frequencies [cm^{-1}] of (**3**) and (**4**) and calculated vibrational frequencies [cm^{-1}] $[C_9H_{15}O_6]^{3+}$.

$[C_9H_{15}O_6][SbF_6]_3$ (**3**)		$[C_9H_{15}O_6][AsF_6]_3$ (**4**)		$[C_9H_{15}O_6]^{3+}$	Assignment
IR	**Raman**		**Raman**	**Calc.[a] (IR/Raman)**	
3232 (vs)		3229 (w)		3636 (323/82)/ 3628 (341/85)/ 3625 (546/51)	ν(OH)
3150 (vs)		3152 (w)		3155 (7/30)/ 3154 (8/32)/ 3153 (11/47)	$\nu_{as}(CH_2)$
	3065 (5)		3090 (10)	3105 (11/47)	$\nu_{as}(CH_2)$
	3006 (11)		3031 (26)	3093 (6/90)/ 3091 (6/83)/ 3086 (6/84)	$\nu_{s}(CH_2)$
			3024 (26)	3056 (24/110)	$\nu_{s}(CH_2)$
			2967 (29)	3050 (21/65)/ 3045 (18/54)	$\nu_{as}(CH_2)$
	2936 (16)		2938 (47)	3013 (46/139)/ 3007 (33/107)	$\nu_{s}(CH_2)$
1701 (vw)		1672 (vw)			?
1609 (w)	1648 (10)	1608 (w)	1626 (16)	1628 (226/1)/ 1619 (238/0.8)/ 1616 (477/0.9)	ν(CO)
1508 (w)	1510 (12)	1508 (w)	1515 (25)	1510 (330/0.4)/ 1507 (244/1)/ 1497 (10/16)	ν(CO)
		1464 (vw)		1487 (5/3)/ 1481 (17/2)/ 1477 (55/4)/	$\delta(CH_2)$
1454 (vw)	1458 (16)	1454 (vw)	1458 (33)	1466 (24/4)/ 1420 (30/6)	$\delta(CH_2)$
1373 (vw)	1388 (17)	1373 (vw)	1387 (37)	1416 (24/9)	$\delta(CH_2)$
	1345 (10)	1346 (vw)	1347 (18)	1410 (78/3) 1402 (143/0.9)/ 1382 (110/5)/	$\omega(CH_2)$
		1331 (vw)	1309 (16)	1374 (131/1)/ 1371 (13/7)/ 1361 (8/3)	$\omega(CH_2)$
1276 (vw)	1268 (12)	1294 (vw)	1284 (23)	1303 (33/6)/ 1289 (17/5)/ 1271 (20/6)	$\tau(CH_2)$
1244 (vw)			1256 (25)	1255 (22/1)/ 1252 (1/2)/ 1233 (55/2)	$\tau(CH_2)$
1213 (vw)	1239 (11)	1213 (w)	1237 (20)	1157 (200/8)/ 1155 (249/4)/ 1153 (276/7)	δ(COH)
1090 (vw)	1093 (10)	1084 (vw)	1095 (21)	1080 (8/0.4)/ 1073 (2/0.3) 1068 (6/3)	ν(CC)
1024 (vw)	1026 (8)	1026 (vw)	1021 (17)	1025 (37/0.7)/ 1022 (19/0.5)/ 1002 (3/0.3)	ν(CC)

968 (w)	971 (12)	966 (w)	967 (23)	959 (3/2)/ 953 (73/0.8)/ 942 (66/2)	ν(CO)
957 (w, sh)		955 (w)		905 (2/6)	δ(OCO)
916 (vw)	907 (10)	924 (vw)	896 (18)	864 (15/0.6)	δ(OCO)
905 (vw)			883 (18)	860 (8/0.6)	δ(OCO)
843 (m)	826 (15)	837 (w)	824 (37)	824 (33/0.7)/ 814 (18/2)/ 790 (16/5)	δ(CCO)
665 (vs)[b]	674 (100)[b]	706 (vs)[b]	695 (91)[b]	759 (10/0.2)	γ(COOC)
640 (vs)[b]	658 (65)[b]	667 (vs)[b]	682 (81)[b]	687 (84/0.7)/ 681 (76/0.9)/ 669 (80/0.7)	$\delta(COH)_{oop}$
583 (m)	615 (16)	575 (w)	673 (100)[b]	634 (58/1)	δ(CCC)
544 (m)	602 (17)	542 (m)	589 (41)	597 (18/4)	δ(CCC)
530 (s)	585 (17)	494 (m)	551 (33)	579 (9/4)	δ(CCO)
	544 (16)		475 (24)	562 (26/1)	γ(COOC)
				548 (5/5)	δ(CCO)
				522 (8/3)/ 494 (6/1) 433 (3/1)	δ(CCC)
				380 (6/0.9)/ 312 (21/2)/ 278 (18/1)	Skeletal vibration
				252 (0.7/1)/ 249 (0.05/1)/ 238 (0.3/1)	Skeletal vibration
				214 (5/0.4)/ 195 (26/0.2)/ 169 (2/0.2)	Skeletal vibration
				156 (2/0.6)/ 137 (0.3/0.7)/ 106 (3/0.8)	Skeletal vibration
				58 (2/0.6)/ 52 (2/2)/ 45 (1/0.4)	Skeletal vibration
	301 (31)		377 (77)		MF_6^-
	282 (38)		346 (31)		MF_6^-
	230 (25)		317 (27)		MF_6^-
	123 (23)		298 (26)		MF_6^-
			264 (26)		MF_6^-
			257 (26)		MF_6^-
			178 (33)		MF_6^-
			122 (41)		MF_6^-

[a] Calculated on the B3LYP/aug-cc-pVTZ level of theory. IR intensity in km/mol and Raman intensity in $Å^4/u$. Abbreviations for IR intensities: v = very, s = strong, m = medium, w = weak, br = broad. Experimental Raman activities are stated to a scale of 1 to 100. [b] Anion and cation interfere with each other.

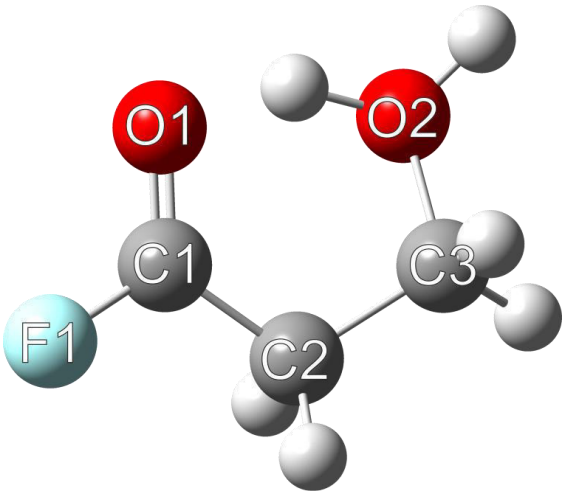

Figure S1. Optimized structure of $[H_2O(CH_2)_2C(O)F]^+$ at the B3LYP/aug-cc-pVTZ level of theory.

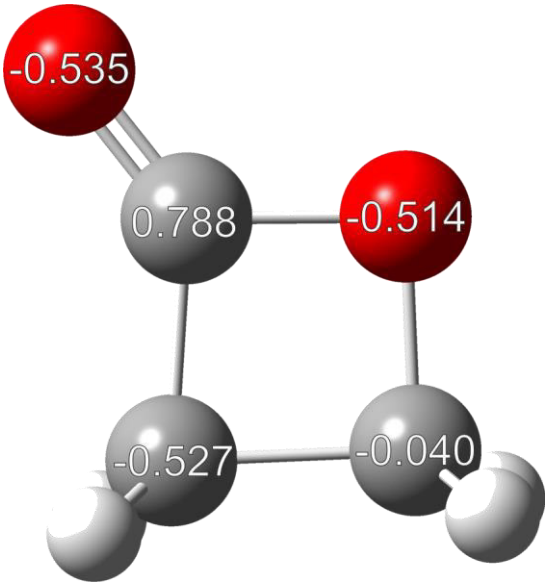

Figure S2. NPA charges calculated for *β*-propiolactone.

Table S5. Cartesian coordinates of calculated minimum structures of $[H_2O(CH_2)_2C(O)F]^{+}\cdot H_3O^{+}\cdot COF_2$ at the B3LYP/aug-cc-pVTZ level of theory.

Atom	x	y	z
O	-0.458609	-0.852904	0.671916
F	2.761553	1.545080	-0.805228
O	2.887355	-0.383332	0.209319
C	2.287871	0.650257	0.033228
C	1.025196	1.099847	0.704044
H	0.371368	1.547654	-0.047950
H	1.310470	1.936384	1.354241
C	0.310984	0.064946	1.549399
H	0.993045	-0.566931	2.110313
H	-0.397149	0.537288	2.224643
H	-1.410473	-0.495968	0.384910
H	-0.521158	-1.755993	1.026844
O	5.038906	-1.212053	-0.826733
H	4.171357	-0.797674	-0.400693
H	5.589592	-0.590746	-1.336718
F	-4.155627	-1.284651	-0.466843
O	-2.605549	0.206633	0.010277
C	-3.719494	-0.078757	-0.345317
H	5.582011	-1.743314	-0.216506
F	-4.607397	0.788991	-0.646311

Table S6. Cartesian coordinates of calculated minimum structures of $[C_9H_{15}O_6]^{3+}$ at the B3LYP/aug-cc-pVTZ level of theory.

Atom	x	y	z
O	-0.000000833	0.000004985	-0.000003521
O	-0.000006084	-0.000004386	0.000001348
O	0.000001130	0.000008827	-0.000004895
O	-0.000016257	0.000028505	0.000004794
O	-0.000000107	0.000003721	-0.000002578
O	0.000005246	0.000001441	0.000004129
C	-0.000008948	-0.000010408	0.000008068
C	0.000022334	-0.000029629	0.000003484
H	-0.000002551	0.000001676	0.000000744
H	-0.000002943	0.000002504	-0.000002732
C	0.000009634	0.000001602	0.000001338
C	0.000006653	0.000001898	-0.000005858
H	-0.000001111	-0.000000734	0.000003025
H	-0.000001370	0.000002540	0.000000997
C	0.000001722	-0.000007185	0.000001536
H	-0.000000726	-0.000000319	-0.000000870
H	-0.000001088	0.000002323	-0.000001199
C	-0.000005536	-0.000015791	-0.000007948
C	0.000006674	0.000010342	-0.000009666
H	-0.000000935	-0.000001696	0.000000414
H	0.000002155	-0.000001326	0.000007433
C	-0.000000163	0.000006920	-0.000000653
H	0.000000547	-0.000002676	-0.000000908
H	-0.000000367	-0.000003645	0.000002812
C	-0.000008758	0.000001324	0.000003220
H	0.000001199	-0.000000785	0.000000764
H	0.000002675	0.000001119	-0.000001084
H	-0.000000925	-0.000001816	-0.000000614
H	-0.000001322	0.000000250	0.000000484
H	0.000000054	0.000000419	-0.000002068

Table S7. Cartesian coordinates of calculated minimum structure *β*-propiolactone at the B3LYP/aug-cc-pVTZ level of theory.

Atom	x	y	z
C	0.000000117	-0.000003424	0.000000790
C	0.000001692	0.000016245	0.000000522
H	0.000002203	0.000001756	0.000000580
H	0.000001823	0.000001725	-0.000001127
H	-0.000000001	-0.000002213	-0.000000053
H	-0.000000352	-0.000002825	0.000000989
O	-0.000001677	0.000026295	0.000002110
C	-0.000009527	-0.000049301	-0.000006139
O	0.000005722	0.000011742	0.000002329

Table S8. Cartesian coordinates of calculated minimum structure of the transition state and concurrently starting point for IRC calculations at the MP2/aug-cc-pVTZ level of theory.

Atom	x	y	z
C	0.000000002	-0.000000029	0.000000574
C	0.000000080	0.000000003	-0.000000206
H	-0.000000134	0.000000107	-0.000000086
H	0.000000115	-0.000000065	0.000000052
H	0.000000027	0.000000027	0.000000019
H	-0.000000038	0.000000060	0.000000050
O	-0.000000893	-0.000000341	-0.000000824
C	0.000000006	-0.000000100	0.000000286
O	0.000000194	-0.000000065	-0.000000448
H	0.000000641	0.000000403	0.000000582

Table S9. Cartesian coordinates of calculated minimum structures of $[H_2O(CH_2)_2C(O)F]^+$ at the B3LYP/aug-cc-pVTZ level of theory.

Atom	x	y	z
O	-0.000008342	0.000105449	-0.000008998
F	-0.000021656	0.000030771	-0.000001764
O	0.000012411	0.000062464	-0.000033109
C	-0.000000748	-0.000101146	0.000049656
C	0.000042751	0.000050053	-0.000025231
H	-0.000006160	0.000012152	0.000005130
H	-0.000017186	-0.000008770	0.000002263
C	-0.000028171	-0.000168210	-0.000028775
H	0.000000441	0.000020969	0.000012480
H	-0.000002507	0.000030574	0.000009322
H	0.000040062	-0.000060606	0.000028553
H	-0.000010894	0.000026300	-0.000009527

Chemistry A European Journal

Chemistry Europe
European Chemical Societies Publishing

Cover Feature:
A. J. Kornath et al.
Ring Opening Reactions of β-Propiolactam in Superacidic Media

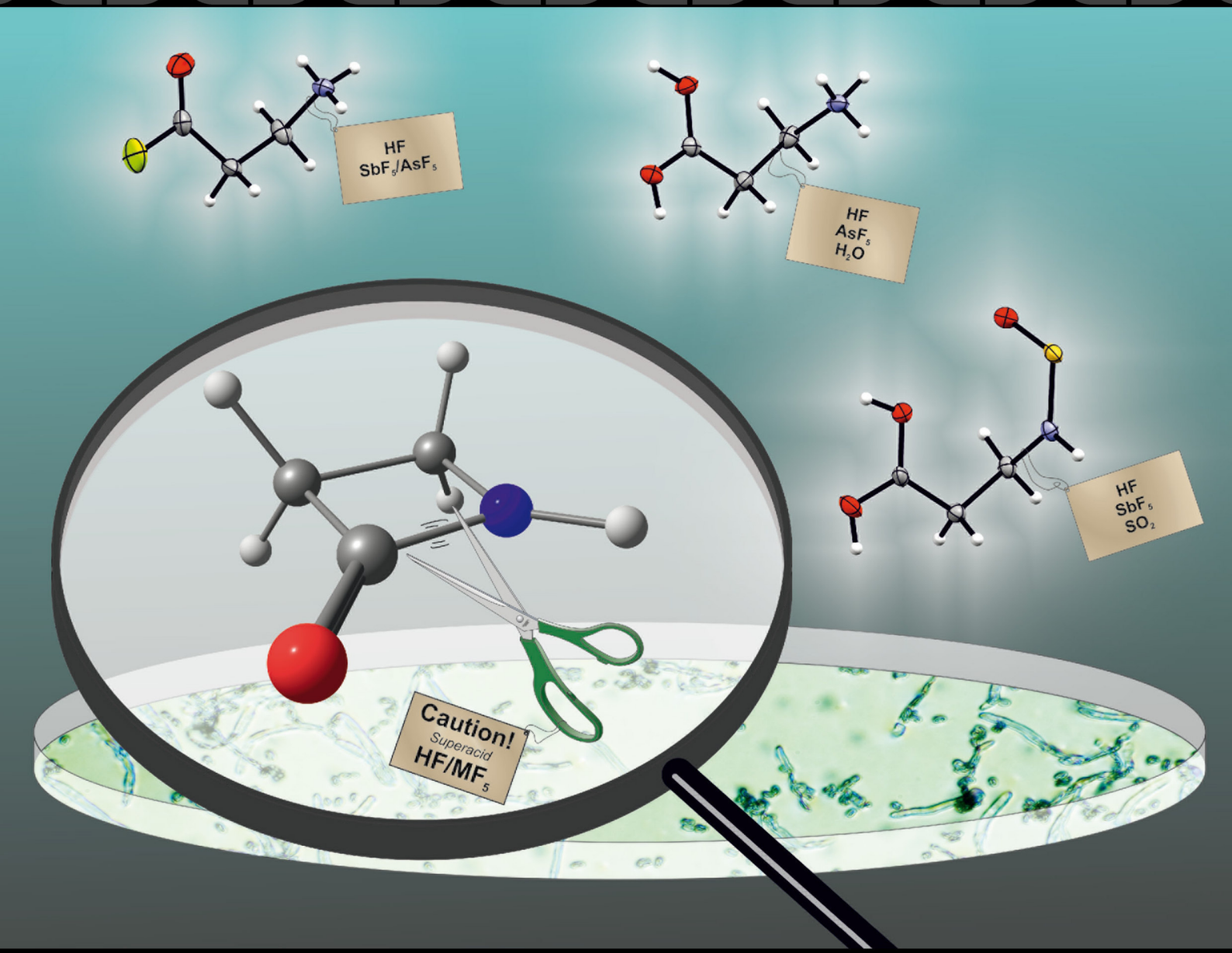

6/2022

WILEY-VCH

Chemistry–A European Journal
Research Article
doi.org/10.1002/chem.202104086
Chemistry Europe
European Chemical Societies Publishing
www.chemeurj.org

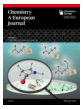

Ring Opening Reactions of β-Propiolactam in Superacidic Media

Stefanie Beck,[a, b] Vanessa Rück,[a] Lea-Viktoria Pietsch,[a] Christoph Jessen,[b] and Andreas J. Kornath*[a]

Abstract: The reaction of β-propiolactam in the superacidic systems HF/MF_5 (M = Sb, As) led to the formation of monoprotonated 3-aminopropanoyl fluoride in the form of $[C(O)F(CH_2)_2NH_3][SbF_6]$ and $[C(O)F(CH_2)_2NH_3][AsF_6]$. In the presence of traces of water, the diprotonated species β-alanine $[C(OH)_2(CH_2)_2NH_3][AsF_6]_2$ was synthesized for the first time. All salts were characterized by low-temperature infrared and Raman spectroscopy. Additionally, single-crystal X-ray analyses were conducted in the case of $[C(O)F(CH_2)_2NH_3][SbF_6]$ and $[C(OH)_2(CH_2)_2NH_3][AsF_6]_2$. By using SO_2 instead of HF as the solvent, the salt $[C(OH)_2(CH_2)_2NHSO][SbF_6]_2$ was obtained, and single-crystal X-ray analysis of this salt containing a thionylimide moiety was conducted. For the formation of these open-chain compounds, an acyl cationic species as intermediate is assumed, which is formed from N-protonated β-propiolactam. Quantum chemical calculations at the B3LYP/aug-cc-pVTZ and MP2/aug-cc-pVTZ levels of theory were carried out to gain a better understanding of the formation and the structural properties of protonated β-propiolactam.

Introduction

The β-lactam motif is of particular importance for the eponymous class of antibiotics,[1] of which the best-known representatives are penicillins and cephalosporins.[1,2] The opening of the β-lactam ring plays a decisive role in the mode of action of these antibiotics and potential resistance to them.[1] Given this importance, many studies on the basic structure of β-propiolactam have been conducted.[3–5] In particular, the mechanism and corresponding kinetics of acid-catalyzed hydrolysis, including ring opening, have been investigated.[3,4] For these kinetic measurements, β-propiolactam (Scheme 1a) was reacted in aqueous sulfuric acid so that the exclusive product of hydrolysis was β-alanine (Scheme 1 b).[3,4] The ring opening is proposed to be subject to a unimolecular mechanism with the formation of an acylium ion as rate-determining step.[4]

For this mechanism the requirement of an N-protonated species was assumed, but the O-protonated species was determined to be the major formed intermediate.[3]

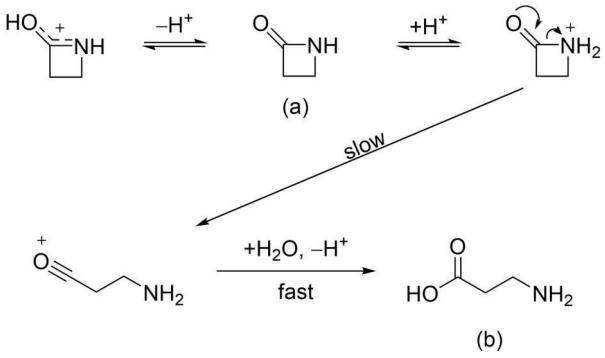

Scheme 1. Postulated reaction mechanism of acid-catalyzed ring opening of β-propiolactam by Yates.[4]

Focusing on its two basic centers and regarding its hydrolysis behavior, calculations of the gas-phase basicity of β-propiolactam were performed.[5] The calculations showed that β-propiolactam is an oxygen base, with the gap between the intrinsic basicities of oxygen and nitrogen being very small.[5]

Taking advantage of the reactivity of β-propiolactam, Tepe et al. performed trifluoromethanesulfonic acid-catalyzed Friedel–Crafts acylations.[6] Interestingly, even in superacidic media the same mechanism for the four-membered ring opening is assumed[6] as described in Scheme 1. This prompted us to study the reaction behavior of β-propiolactam in the superacidic systems HF/MF_5 (M = Sb, As).

[a] S. Beck, V. Rück, L.-V. Pietsch, Prof. Dr. A. J. Kornath
Department of Chemistry
Ludwig-Maximilian University of Munich
Butenandtstr. 5–13, 81377 München (Germany)
E-mail: akoch@cup.uni-muenchen.de
Homepage: http://www.org.chemie.uni-muenchen.de/ac/kornath/
[b] S. Beck, C. Jessen
F-Select GmbH
Semmelweisstraße 5, 82152 Planegg (Germany)

Supporting information for this article is available on the WWW under https://doi.org/10.1002/chem.202104086

Results and Discussion

Preparation

β-Propiolactam reacts in the superacidic system HF/MF_5 (M = Sb, As) according to Equations (1) and (2).

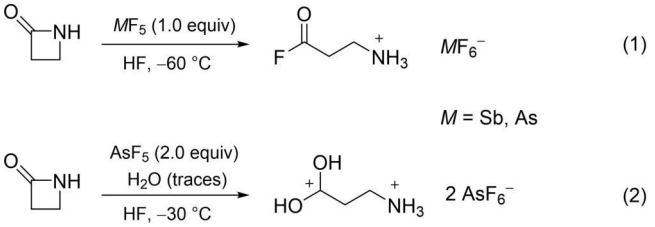

(1)

(2)

Hydrogen fluoride was used in excess and served as reagent as well as solvent. One or two equivalents of the respective Lewis acid were added and completely solvated by homogenizing the mixture at −40 °C. Under nitrogen atmosphere, β-propiolactam was added to the frozen system. Using one equivalent Lewis acid and homogenizing the reaction mixture at −60 °C led to the formation of salts of monoprotonated 3-aminopropanoyl fluoride [Eq. (1)]. As already postulated by Yates et al.,[4] the protonation of β-propiolactam leads to a ring opening reaction, even in superacidic media. In this context, an acyl cation in the form of $[NH_2(CH_2)_2CO][MF_6]$ is expected to be formed. The formal addition of a HF molecule to the acyl cationic species led to the generation of the air- and temperature sensitive compounds $[C(O)F(CH_2)_2NH_3][SbF_6]$ (**1**) and $[C(O)F(CH_2)_2NH_3][AsF_6]$ (**2**), which decompose above −10 °C.

Using two equivalents of the Lewis acid arsenic pentafluoride and increasing the reaction temperature to −30 °C, the diprotonated species of β-alanine, $[C(OH)_2(CH_2)_2NH_3][AsF_6]_2$ (**3**), was obtained [Eq. (2)]. Based on the assumed acyl cation $[NH_2(CH_2)_2CO][MF_6]$, a formal addition of a water molecule, followed by protonation of the amino group yielded compound **3**. For the formation of this compound small amounts of water are needed. They could be traced back to the use of a non-anhydrous reaction set up. The temperature- and air-sensitive salt **3** is stable up to 0 °C.

By reacting β-propiolactam in SO_2 with two equivalents of HF, and SbF_5 respectively, the formation of the air-sensitive salt $[C(OH)_2(CH_2)_2NHSO][SbF_6]_2{\cdot}HF$ (**4**) was observed [Eq. (3)].

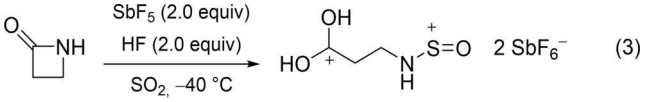

(3)

As the formation process of **4** is not obvious, a possible reaction pathway is given in Scheme 2. In particular, the assumed nucleophilic attack on sulfur suggests the existence of the acyl cationic species $[NH_2(CH_2)_2CO][MF_6]$.

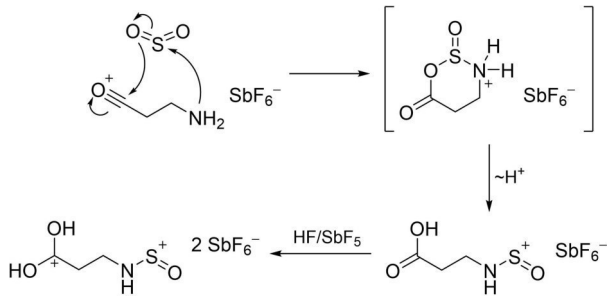

Scheme 2. Possible reaction pathway for the formation of **4**.

Crystal structures

$[C(O)F(CH_2)_2NH_3][SbF_6]$ (1)

The salt **1** crystallizes in the triclinic space group $P\bar{1}$ with two formula units per unit cell. The asymmetric unit of **1** is displayed in Figure 1 and selected bond lengths and angles are summarized in Table 1. Interatomic contacts are illustrated in Figure S1 and the respective values are given in Table S1 (see the Supporting Information).

The C1–O1 bond length measures 1.176(6) Å and is in the typical range for CO bonds in acyl fluoride groups.[7–9] Moreover, the C1–F1 bond distance of 1.340(6) Å exhibits a characteristic CF bond length in acyl fluoride groups.[7–9] The C–C bond lengths, with values of 1.480(6) Å (C1–C2) and 1.508(6) Å (C2–C3), are slightly shorter than a formal C–C single bond (1.54 Å).[10] The C3–N1 bond length (1.484(4) Å) is, due to the protonation, slightly longer than a formal C–N bond (1.47 Å)[10] and in accordance with reported C–NH_3^+ bond lengths.[11,12] The bond angles around the acyl fluoride moiety are in the range between 111.9(3)° (F1–C1–C2) and 128.8(4)° (O1–C1–C2). The molecule skeleton spans an dihedral angle of 66.2(4)° (C1–C2–C3–N1).

The Sb–F bond lengths of the SbF_6^- anion are in the range between 1.865(2) Å (Sb1–F2) and 1.883(2) Å (Sb1–F5). Bond angles are between 87.08(9)° (F5–Sb1–F6) and 91.8(1)° (F3–Sb1–F2) or between 177.4(1)° (F6–Sb1–F2) and 178.4(1)° (F7–Sb1–F4), respectively. All of these values are in accordance with reported literature for SbF_6^- anions.[13,14]

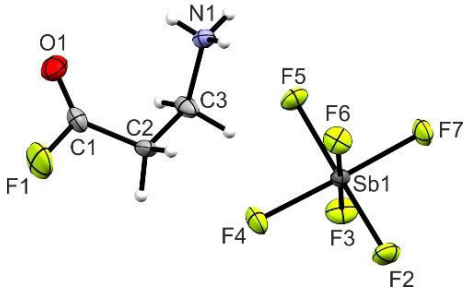

Figure 1. Asymmetric unit of **1** with 50% probability displacement ellipsoids.

Table 1. Comparison of selected bond lengths and angles of **1**, **3** and **4** with estimated standard deviations in parentheses.

	1	3	4
Bond lengths [Å]			
C1–F1	1.340(6)		
C1–O1	1.176(6)	1.270(3)	1.268(6)
C1–O2		1.264(3)	1.270(6)
C1–C2	1.480(6)	1.481(3)	1.489(8)
C2–C3	1.508(6)	1.518(3)	1.513(6)
C3–N1	1.484(4)	1.498(4)	1.488(7)
N1–S1			1.563(4)
S1–O3			1.431(4)
Bond angles [°]			
O1–C1–F1	119.4(4)		
F1–C1–C2	111.9(3)		
O1–C1–O2		118.4(2)	117.7(5)
O1–C1–C2	128.8(4)	117.7(2)	119.4(5)
O2–C1–C2		123.9(2)	122.9(5)
C1–C2–C3	112.8(3)	114.9(2)	114.2(4)
C2–C3–N1	112.6(3)	112.3(2)	112.4(4)
C3–N1–S1			127.8(4)
N1–S1–O3			111.4(2)
Dihedral angles [°]			
F1–C1–C2–C3	173.9(3)		
O1–C1–C2–C3	−6.4(6)	4.9(3)	−5.6(7)
O2–C1–C2–C3		−174.7(2)	175.2(5)
C1–C2–C3–N1	66.2(4)	76.7(3)	71.0(6)
C2–C3–N1–S1			−115.7(5)
C3–N1–S1–O3			3.1(5)

$[C(OH)_2(CH_2)_2NH_3][AsF_6]_2$ (3)

Compound **3** crystallizes in the monoclinic space group $P2_1/n$ with four formula units per unit cell. In Figure 2 the formula unit is illustrated and in Table 1 selected bond lengths and angles are listed. Interatomic contacts are displayed in Figure S2 and corresponding values are listed in Table S2.

In **3** both C–O bond lengths (C1–O1: 1.270(3) Å, C1–O2: 1.264(3) Å) are between a formal single (1.43 Å)[10] and double bond (1.19 Å).[10] The angles around the protonated acid moiety are between 117.7(2)° (O1–C1–C2) and 123.9(2)° (O2–C1–C2). These values are in good agreement with those reported in literature for this moiety.[15,16] The C1–C2 bond (1.481(3) Å) next to the protonated acid group is comparable with the C1–C2 bond length in **1** (1.480(6) Å). In contrast, the bond lengths of C2–C3 (1.518(3) Å) and C3–N1 (1.498(4) Å) are slightly elongated compared to **1**. With a value of 76.7(3)°, the dihedral angle C1–C2–C3–N1 of **3** is about 10° wider than in **1**.

The As–F bond lengths of the two AsF_6^- anions are between 1.693(2) Å (As2–F9) and 1.748(2) Å (As2–F8) and in the typical range for AsF_6^- anions.[13,14,17] Additionally, the F–As–F angles, which are in the range between 87.9(8)° (F8–As2–F12) and 92.5(9)° (F11–As2–F10), and between 175.6(1)° (F10–As2–F7) and 179.0(9)° (F3–As1–F6), are in accordance with reported AsF_6^- anions.[13,14,17]

$[C(OH)_2(CH_2)_2NHSO][SbF_6]_2 \cdot HF$ (4)

Salt **4** crystallizes in the triclinic space group $P\bar{1}$ with two units per unit cell. In Figure 3, the formula unit of **4** is displayed and in Table 1 selected bond lengths and angles of **4** together with those of **1** and **3** are summarized. A projection of interatomic contacts of **4** is illustrated in Figure S3 and respective values are listed in Table S3.

Both C–O bond lengths of **4** (C1–O1: 1.268(6) Å, C1–O2: 1.270(6) Å) are closely comparable with those of **3**, as the C1–O1 and C1–O2 bond lengths are not significantly different. The same accordance is observed for both C–C bonds (1.489(8) Å (C1–C2), 1.513(6) Å (C2–C3)) as well as for the C3–N1 bond, with a value of 1.488(7) Å. The bond angles of **4** are in good agreement with those of **3**, as their molecular skeletons are comparable (Table 1).

The bond lengths of the thionylimide moiety (HNSO) are comparable with reported crystal data for H–NSO trapped by adduct formation with bulky Lewis acids.[18] The N1–S1 bond length of **4**, with a value of 1.563(4) Å, is significantly longer than the bond length of the free thionylimide (1.530(2) Å).[18] Both bond lengths are between a formal S–N single (1.73 Å) and double bond (1.49 Å).[10] In contrast, greater agreement between **4** and the free thionylimide is observed for the S1–O3 bond (1.431(4) Å (**4**) and 1.427(2) Å[18]). These bond lengths are in the range of SO double bonds (S=O: 1.46 Å, S=2O: 1.34 Å).[10]

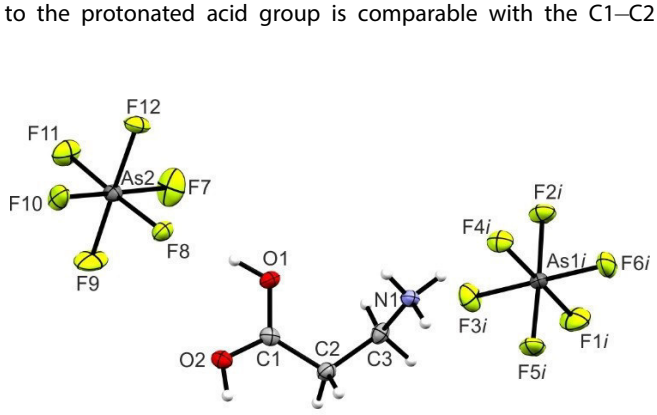

Figure 2. Formula unit of **3** with 50% probability displacement ellipsoids. Symmetry code: $i = {}^1/_2-x,-{}^1/_2+y,{}^1/_2-z$.

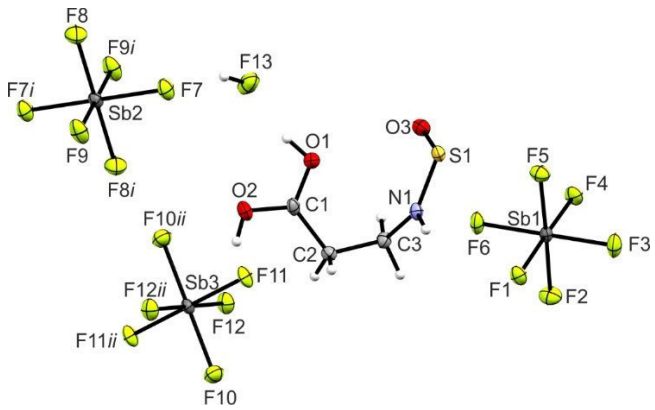

Figure 3. Formula unit of **4** with 50% probability displacement ellipsoids. Symmetry codes: $i = 2-x,-y,2-z$; $ii = 2-x,-y,1-z$.

The N1–S1–O3 angle 111.4(2)° is comparable to that observed in the free HNSO (114.3(2)°).[18]

The Sb–F bond lengths are between 1.860(3) Å (Sb2–F8) and 1.891(3) Å (Sb2–F7). F–Sb–F angles are between 88.5(1)° (F4–Sb1–F2) and 92.8(1)° (F5–Sb1–F4) and between 178.1(1)° (F4–Sb1–F1) and 180.0(1)° (F11–Sb3–F11*ii*), respectively. All bond lengths and angles found in both SbF_6^- anions are in good agreement with data reported in literature.[13,14]

Vibrational spectroscopy

Monoprotonated 3-aminopropanoyl fluoride

The infrared and Raman spectra of **1** and **2** together with the Raman spectrum of β-propiolactam are displayed in Figure 4.

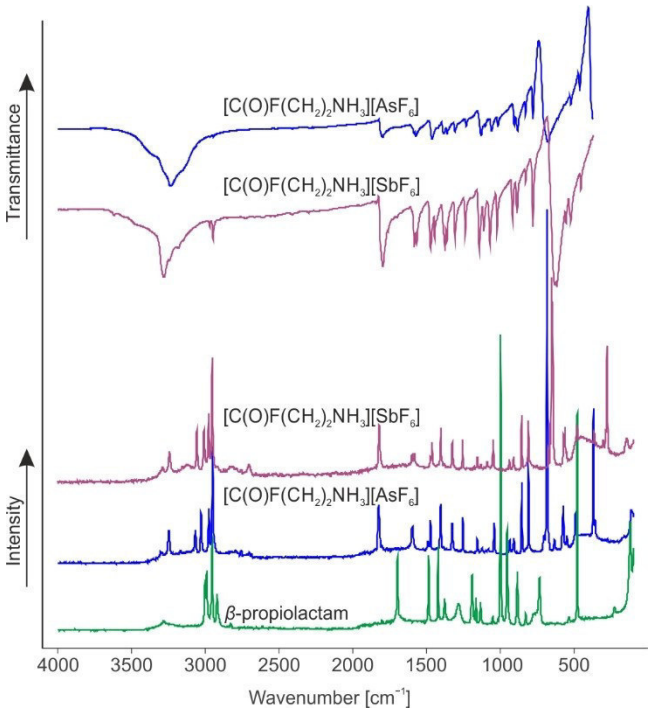

Figure 4. Raman spectrum of β-propiolactam (green), Raman and IR spectra of **1** (violet) and **2** (blue).

Selected experimental and calculated vibrational frequencies are listed in Table 2. The $[C(O)F(CH_2)_2NH_3]^+$ cation possesses C_1 symmetry with 33 fundamental vibrations, active in both Raman and infrared spectra. A complete list of all experimentally obtained and calculated frequencies is given in Table S4. For better accordance of the calculated and experimental frequencies one HF molecule was added to the gas phase structure, to simulate the hydrogen bonding in the solid state. The most characteristic vibration of β-propiolactam, the ring breathing vibration at 962 cm^{-1},[19] is not detectable in the Raman spectra of **1** and **2**. Moreover, the CO stretching vibration is blue-shifted compared to the starting material[19] and occurs in the range between 1812 cm^{-1} (IR of **1**) and 1826 cm^{-1} (Ra of **2**). This range for ν(CO) is typical for acyl fluoride groups.[20,21] At 1157 cm^{-1} in both Raman spectra and at 1165 (**1**) and 1155 cm^{-1} (**2**) in the IR spectra, the corresponding ν(CF) vibrations are observed. For the NH_3 group three NH stretching vibrations are expected. They occur in the range between 3158 (IR of **2**) and 3303 cm^{-1} (Ra of **2**). The ν(CN) vibration of the formed protonated primary amine is detected at about 856 cm^{-1} for **1** and **2**. However, the typical range for primary amines is between 1030 and 1090 cm^{-1}.[22] This red-shift can be explained by the protonation and is in accordance with reported literature data of protonated primary amines.[11] To conclude, the vibrational spectroscopy confirms the results of the X-ray diffraction analysis.

For both anions, SbF_6^- and AsF_6^-, more vibrations than expected for ideal O_h symmetry are observed. In the Raman spectra of **1** and **2** more than three lines and in the corresponding infrared spectra more than two bands are detected. The increased number of vibrations indicates a lowered symmetry of the anion structures, which is in accordance with the results of the X-ray study.

Diprotonated β-alanine

In Figure 5, the Raman and infrared spectra of diprotonated β-alanine in the form of **3** are illustrated. Table 3 summarizes selected calculated and observed vibrational frequencies of **3** together with experimental frequencies of the neutral compound β-alanine for comparison.[23] The complete table is given in the Supporting Information (Table S5). In order to simulate

Table 2. Selected experimental vibrational frequencies [cm^{-1}] of **1** and **2** and calculated vibrational frequencies [cm^{-1}] of $[C(O)F(CH_2)_2NH_3]^+ \cdot HF$.

1 IR	Raman	**2** IR	Raman	$[C(O)F(CH_2)_2NH_3]^+ \cdot HF$ Calc.[a] (IR/Raman)	Assignment
3283 (w)	3290 (8)	3303 (w, sh)	3302 (3)	3482 (122/56)	$\nu_{as}(NH_3)$
3244 (w)	3244 (15)	3238 (m)	3247 (9)	3355 (381/71)	$\nu_{as}(NH_3)$
3186 (vw)		3158 (w, sh)	3166 (4)	3242 (203/54)	$\nu_{s}(NH_3)$
1812 (w)	1822 (28)	1814 (vw)	1826 (17)	1842 (228/13)	ν(CO)
1165 (w)	1157 (13)	1155 (w)	1157 (7)	1208 (174/2)	ν(CF)
1045 (w)	1050 (21)	1041 (vw)	1043 (12)	1024 (9/2)	ν(CC)
912 (vw)	913 (13)	908 (w)	910 (7)	917 (37/1)	ν(CC)
854 (vw)	857 (33)	854 (w)	856 (23)	843 (2/8)	ν(CN)

[a] Calculated at the B3LYP/aug-cc-pVTZ level of theory. IR intensity in km/mol and Raman intensity in $Å^4$/u. Abbreviations for IR intensities: v = very, m = medium, w = weak. Experimental Raman activities are stated to a scale of 1 to 100.

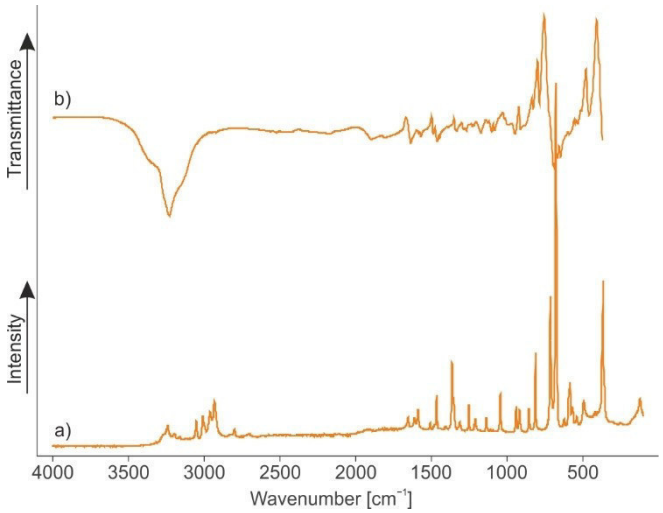

Figure 5. a) Raman and b) infrared spectra of **3**.

the interatomic contacts in the solid state, three HF molecules were added to the calculated gas phase structure.

For the cation, C_1 symmetry with 36 fundamental vibrations, active in Raman and IR, is expected. The first evidence for the diprotonated β-alanine is the ν(CO) vibration at 1605 cm^{-1} (IR). This vibration is red-shifted by approximately 165 cm^{-1} compared to the neutral compound.[23] As β-alanine turned out to be a nitrogen base and the N-protonated species is already known,[12] this shift indicates a second protonation on the oxygen. The ν(CN) vibration, which occurs at 856 (IR) and 858 cm^{-1} (Ra), shows the same trend, with a red-shift of about 194 (IR) and 192 cm^{-1} (Ra). Furthermore, the ν(OH) vibrations are detected as broad bands at about 3125 cm^{-1} (IR). Due to the poor polarizability of this bond, no lines are observed in the corresponding Raman spectra. In contrast, the NH stretching vibrations occur in the IR and Raman spectra in the range between 3159 and 3242 cm^{-1}. The second CO stretching vibration occurs at 1589 (IR) and 1590 cm^{-1} (Ra). These values are in good agreement with reported literature data for protonated carbon acid groups.[15,16]

For the AsF_6^- anion, more than three lines in the Raman spectrum and more than two bands in the IR spectrum are observed, which would be the numbers of vibrations for an ideal O_h symmetry. The increased number of vibrations indicates a lowered symmetry for the structure of this anion and is in accordance with X-ray diffraction analysis.

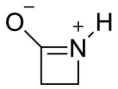

Scheme 3. Lewis structure of amide resonance structure of β-propiolactam.

Theoretical calculations

In this study, the performed experiments led exclusively to the formation of open-chained compounds. Herein, it is assumed that the protonated species of β-propiolactam is necessary for the ring opening reaction. Gas-phase calculations on whether β-propiolactam is an oxygen or nitrogen base were carried out with the result that the protonation will preferably occur on the oxygen atom.[5] However, the gap between oxygen and nitrogen intrinsic basicities is very small.[5] This can be explained by the lack of amide resonance (Scheme 3), due to the steric strain in the four-membered ring.

To elucidate if a proton transfer (from oxygen to nitrogen) is likely, the intrinsic reaction coordinate (IRC) path was calculated for β-propiolactam at the MP2/aug-cc-pVTZ level of theory.[24] In Figure 6, the optimized structures of the O- and N-protonated species, the transition state and the calculated intrinsic reaction coordinate path of the possible proton shift is displayed. The 1,3-proton shift for β-propiolactam is calculated to be endothermic (+17.99 kJ mol^{-1}) in the gas phase. This result leads to the assumption that a direct N-protonation appears more likely than the proton transfer. As there is no clear contradiction to the calculated intrinsic basicities,[5] natural bond orbital (NBO) analyses were performed to gain closer insights into the different species.[24] In Table S6–S8 selected NBOs together with calculated values for occupancy and s- and p-character of the different species are summarized. Additionally, a comparison of the most meaningful NBOs is given in Table S9.

Table 3. Selected experimental vibrational frequencies [cm^{-1}] of **3** and calculated vibrational frequencies [cm^{-1}] of $[C(OH)_2(CH_2)_2NH_3]^{2+}\cdot 3\,HF$.

3 IR	Raman	$[C(OH)_2(CH_2)_2NH_3]^{2+}\cdot 3\,HF$ Calcd.[a] (IR/Raman)	β-Alanine[23]	Assignment
3234 (vs)	3242 (6)	3467 (103/17)	3408	$\nu_{as}(NH_3)/\nu_{as}(NH_2)$[23]
3159 (vs, sh)	3161 (3)	3206 (544/156)		$\nu_{s}(NH_3)/\nu_{as}(NH_2)$[23]
3125 (s,sh)		3161 (1589/121)	3559	ν(OH)
1605 (w)		1653 (310/0.7)	1770	ν(CO)
1589 (w)	1590 (11)	1568 (212/5)	1159	ν(CO)
1312 (w)	1316 (8)	1329 (111/0.2)	1267	δ(COH)
1196 (w)	1214 (8)	1275 (214/5)		δ(COH)
856 (m)	858 (10)	841 (11/3)	1050	ν(CN)

[a] Calculated at the B3LYP/aug-cc-pVTZ level of theory. IR intensity in km/mol and Raman intensity in $Å^4/u$. Abbreviations for IR intensities: v = very, s = strong, m = medium, w = weak, sh = shoulder. Experimental Raman activities are stated to a scale of 1 to 100.

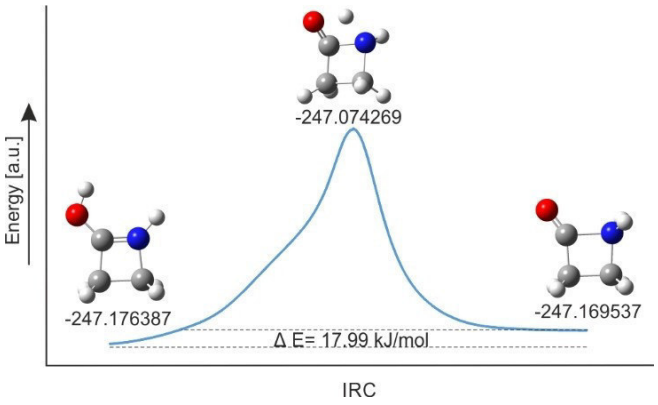

Figure 6. Calculated intrinsic reaction coordinate (IRC) path of the proton shift from O-protonated to N-protonated β-propiolactam together with respective single-point energy values.

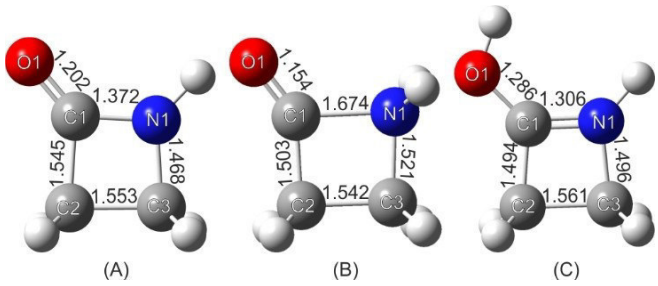

Figure 7. Optimized structures of the A) β-propiolactam, B) N-protonated species and C) O-protonated species, together with calculated bond lengths at the B3LYP/aug-cc-pVTZ level of theory.

The optimized structures of β-propiolactam, and both the O- and N-protonated species are illustrated in Figure 7 together with calculated bond lengths.

Due to the respective protonation, both the C1–O1 and C1–N1 bonds are affected the most. In Figure 8, the calculated NBOs for the C–O bond of the different species are displayed. Concerning the C1–O1 bond in β-propiolactam (A), two types of bonds (one σ and one π bond) are calculated, both occupied with 2.00 e^-. The corresponding antibonding orbitals are occupied with 0.02 e^- (σ* bond) and 0.28 e^- (π* bond). Compared to that, in the N-protonated species (B) (also one σ and one π bond), the s character of the σ bond increases while the p character decreases. Moreover, the according π* bond is less occupied than in the neutral compound, with only 0.07 e^-. These two results lead to the conclusion that the bond strength of the C1–O1 bond increases in the N-protonated species, which is confirmed by the calculated shortened bond length (1.154 Å). In the O-protonated species only one σ bond with less s-character than in the two other structures is calculated. This bond is weakened due to the protonation, as it is expected.

The situation is different for the C1–N1 bond. Selected NBOs for the CN bond are illustrated in Figure 9. In the neutral compound (A) the calculation revealed only one σ bond for the C1–N1 bond, whereas two bonds (one σ and one π bond) are determined by the calculation for the O-protonated species (C). The s character of the σ bond herein is slightly increased, compared to β-propiolactam. Moreover, corresponding anti-bonding orbitals are calculated to be occupied with 0.03 e^- (σ* bond) and 0.31 e^- (π* bond). The calculation results show that this bond is strengthened, which is supported by the bond length of 1.306 Å. In summary, O-protonation leads to a strengthening of the C1–N1 bond and makes ring opening impossible. In the N-protonated species (B), the calculation revealed only one σ bond, where the s character is about 20%.

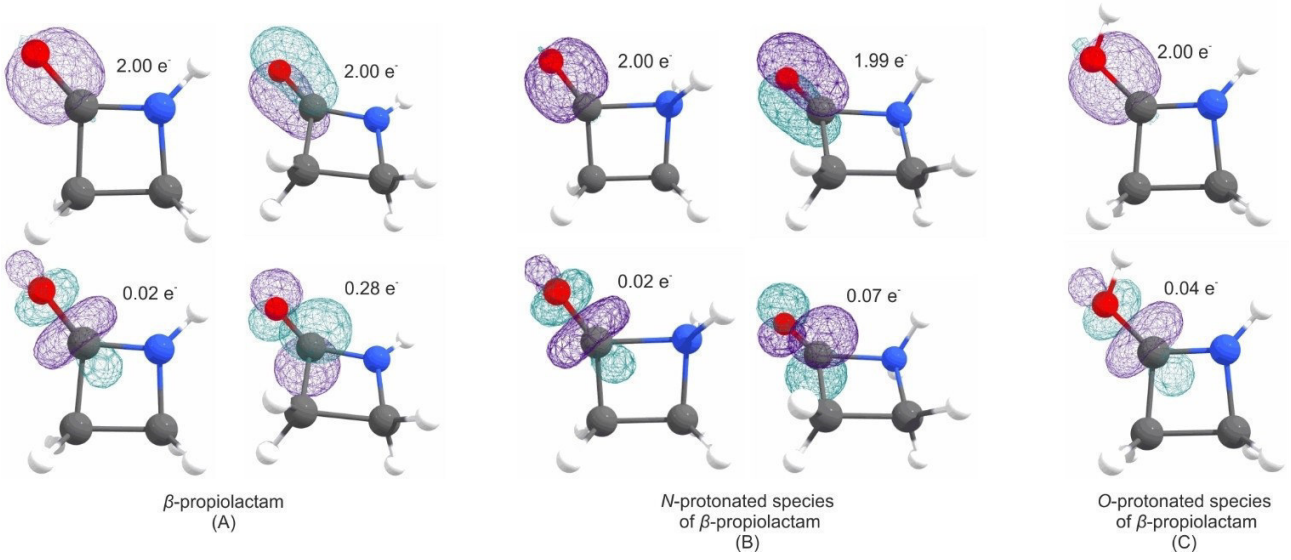

Figure 8. Selected NBOs for the CO bond with corresponding occupancies of the A) β-propiolactam, B) N-protonated species and C) O-protonated species.

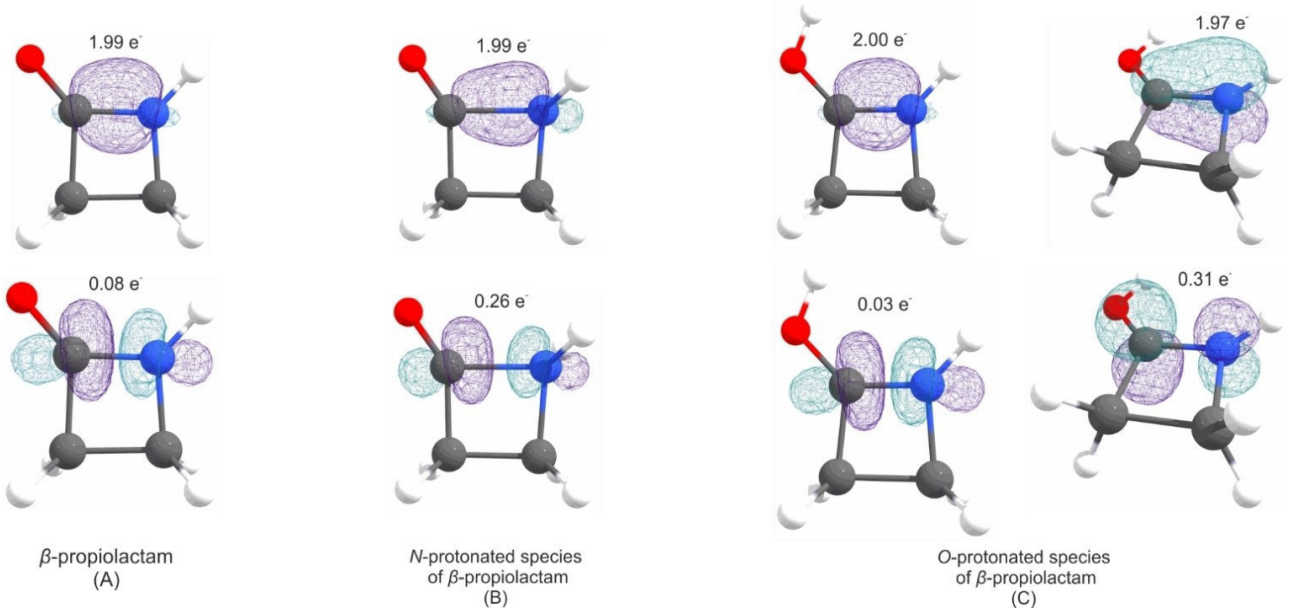

Figure 9. Selected NBOs for the CN bond with the corresponding occupancies of the A) β-propiolactam, B) N-protonated species and C) O-protonated species.

Compared to the other two structures, the s character is decreased while the p character is increased. Additionally, the calculation shows that the corresponding σ* orbital is, with 0.26 e^-, more strongly occupied than the O-protonated species (C). In conclusion, these values show that the strength of the C1–N1 bond is not only decreased in this species, but it also turned out to be a very weak σ bond in general. As these calculations clarify the bonding situation in protonated β-propiolactam, the N-protonated species turned out to be the only species, which is able to form the acyl cation $[NH_2(CH_2)_2CO]^+$.

Conclusion

In this study, the reaction behavior of β-propiolactam in the superacidic systems HF/MF_5 (M = Sb, As) was investigated. With an equimolar amount of Lewis acid, the salts of monoprotonated 3-aminopropanoyl fluoride $[C(O)F(CH_2)_2NH_3][SbF_6]$ (**1**) and $[C(O)F(CH_2)_2NH_3][AsF_6]$ (**2**) were obtained. Changing the reaction conditions to a larger amount of Lewis acid together with traces of water, led to the formation of the hitherto unknown diprotonated species of β-alanine $[C(OH)_2(CH_2)_2NH_3][AsF_6]_2$ (**3**). The salts were characterized by Raman and IR spectroscopy, and, in the case of **1** and **3**, single-crystal X-ray analyses were performed. By changing the solvent from HF to SO_2, the salt $[C(OH)_2(CH_2)_2NHSO][SbF_6]_2$·HF (**4**), which includes a thionylimide moiety, was formed, as detected by single-crystal X-ray analysis. Experimental evidence of these open-chain compounds suggests that they might be formed via the same reactive intermediate $[NH_2(CH_2)_2CO][MF_6]$. This species is proposed to form from N-protonated β-propiolactam. As a protonated cyclic species (O- or N-protonated) of the oxygen base β-propiolactam was neither isolated nor observed. Theoretical calculations were also performed. The calculated intrinsic reaction coordinate path shows that an intramolecular proton shift from oxygen to nitrogen is unlikely, because of its endothermic character (+ 17.99 kJ mol^{-1}) in the gas phase. Subsequently, natural bond orbital analyses were performed to get closer insights into the different protonated species. The analyses could support the assumption that the N-protonated species is responsible for the formation of the highly reactive acyl cationic species.

Experimental Section

General

CAUTION! Avoid contact with any of these compounds. Note that hydrolysis of AsF_5, SbF_5 and the prepared salts might form HF, which burns skin and causes irreparable damage. Safety precautions should be taken while using and handling these materials.

Apparatus and materials: All reactions were conducted by employing standard Schlenk techniques using a stainless-steel vacuum line. FEP/PFA reactors, closed with a stainless steel valve, were used to perform all reactions in superacidic media. Prior to use, all reaction vessels and the stainless steel vacuum line were dried with fluorine (excluding reactions to obtain compound (**3**)). IR spectroscopic investigations were performed on a Vertex-80 V FTIR spectrometer ($\tilde{\nu}$ = 350–4000 cm^{-1}) by placing small amounts of the respective sample on a CsBr single-crystal plate in a cooled cell. Raman measurements were carried out on a Bruker MultiRAM FT-Raman spectrometer with Nd:YAG laser excitation (λ = 1064 cm^{-1}) under vacuum at −196 °C. For measurements, the synthesized compounds were transferred into a cooled glass cell. The low-temperature single-crystal X-ray diffraction of **1**, **3** and **4** were performed on an Oxford XCalibur 3 diffractometer equipped with a Kappa CCD detector operating with $Mo_{K\alpha}$ radiation (λ = 0.71073 Å) and a Spellman generator (voltage 50 kV, current 40 mA). The

program CrysAlisPro 1.171.38.46 (Rigaku OD, 2015)[25] was employed for the data collection and reduction. The structures were solved utilizing SHELXT[26] and SHELXL-2018/3[27] of the WINGX software package.[28] The structures were checked using the software PLATON.[29] The absorption correction was performed using the SCALE3 ABPSACK multiscan method.[30] selected crystallographic parameters and data for **1**, **3** and **4** are listed in Table S10. The quantum chemical calculations were performed at the B3LYP/aug-cc-pVTZ and MP2/aug-cc-pVTZ levels of theory.

Synthesis $[C(O)F(CH_2)_2NH_3][SbF_6]$ (1) and $[C(OH)_2(CH_2)_2NHSO][SbF_6]_2$ (4): Antimony pentafluoride (160 mg, 0.74 mmol, 1.0 equiv. for **1** and 310 mg, 1.43 mmol, 2.0 equiv. for **4**) was condensed at −196 °C into a FEP tube reactor. Afterwards, anhydrous hydrogen fluoride (*a*HF, approximately 2 mL for **1** and 28.6 mg, 1.43 mmol, 2.0 equiv. for **4**) was condensed into the reactor under the same conditions. In the case of **4**, sulfur dioxide (2 mL) was condensed additionally at −196 °C. In order to form the superacidic system, the respective compounds were warmed up to −40 °C and homogenized. The mixture was cooled again to −196 °C and subsequently β-propiolactam (52 mg, 0.74 mmol, 1.0 equiv. (**1**) and 51 mg, 0.72 mmol, 1.0 equiv. (**4**)) was added under nitrogen atmosphere. The reaction mixture was warmed up to −60 (**1**) or −40 °C (**4**) and homogenized until the respective salts were completely dissolved. For crystallization of compounds **1** and **4**, the reactors were left in an ethanol bath at −70 (**1**), or −50 °C (**4**) until the salts recrystallized. For Raman und IR measurements of **1**, the reactor was cooled down to −196 °C again and excess *a*HF was removed at −78 °C in a dynamic vacuum overnight. Compound **1** was obtained as a colorless solid, which is stable up to −10 °C.

Synthesis of $[C(O)F(CH_2)_2NH_3][AsF_6]$ (2): Anhydrous hydrogen fluoride, approximately 2 mL, was condensed into a FEP tube reactor at −196 °C. Subsequently, arsenic pentafluoride (85 mg, 0.5 mmol, 1.0 equiv.) was condensed into the reactor under the same conditions. To form the superacidic system, the compounds were warmed up to −40 °C and homogenized. After cooling down to −196 °C again, β-propiolactam (35 mg, 0.5 mmol, 1.0 equiv.) was added under nitrogen atmosphere. For homogenization, the reaction mixture was warmed up to −60 °C. After cooling down to −196 °C again, excess *a*HF was removed overnight in a dynamic vacuum. Compound **2** was obtained as a colorless solid, which is stable up to −10 °C.

Synthesis of $[C(OH)_2(CH_2)_2NH_3][AsF_6]_2$ (3): As a modification to the reaction procedure of **2**, compound **3** was obtained by using a non-anhydrous reaction set up. Anhydrous hydrogen fluoride (2 mL) and arsenic pentafluoride (170 mg, 1.0 mmol, 2.0 equiv.) were condensed into a FEP tube reactor at −196 °C. Both compounds were warmed up to −30 °C and homogenized. After cooling down again to −196 °C β-propiolactam (35 mg, 0.5 mmol, 1.0 equiv.) was added under nitrogen atmosphere. The reaction mixture was warmed up again to −30 °C and homogenized until the salt was completely dissolved. The mixture was cooled down to −196 °C and excess *a*HF was removed overnight in a dynamic vacuum. Compound **3** was obtained as a colorless solid, with a decomposition temperature of 0 °C. To crystallize compound **3**, the reactor was left in an ethanol bath at −40 °C until the salt recrystallized.

Crystallographic data: Deposition Numbers 2062961 (for **1**), 2062962 (for **3**) and 2062963 (for **4**) contain the supplementary crystallographic data for this paper. These data are provided free of charge by the joint Cambridge Crystallographic Data Centre and Fachinformationszentrum Karlsruhe Access Structures service.

Acknowledgements

We are grateful to the Department of Chemistry of the Ludwig Maximilian University of Munich, the Deutsche Forschungsgemeinschaft (DFG) and the F-Select GmbH for their financial support. Open Access funding enabled and organized by Projekt DEAL.

Conflict of Interest

The authors declare no conflict of interest.

Data Availability Statement

The data that support the findings of this study are available in the supplementary material of this article.

Keywords: beta-propiolactam · natural bond orbital calculations · ring opening · superacidic media · thionylimide moiety

[1] L. M. Lima, B. N. M. Da Silva, G. Barbosa, E. J. Barreiro, *Eur. J. Med. Chem.* **2020**, *208*, 112829.
[2] A. P. Laws, M. I. Page, *J. Chem. Soc. Perkin Trans. 2* **1989**, *10*, 1577–1581.
[3] P. Wan, T. A. Modro, K. Yates, *Can. J. Chem.* **1980**, *58*, 2423–2432.
[4] R. A. Cox, K. Yates, *Can. J. Chem.* **1981**, *59*, 2853–2863.
[5] J. L. M. Abboud, T. Canada, H. Homan, R. Notario, C. Cativiela, M. D. Diaz de Villegas, M. C. Bordeje, O. Mo, M. Yanez, *J. Am. Chem. Soc.* **1992**, *114*, 4728–4736.
[6] K. W. Anderson, J. J. Tepe, *Tetrahedron* **2002**, *58*, 8475–8481.
[7] A. F. Baxter, K. O. Christe, R. Haiges, *Struct. Chem.* **2017**, *28*, 303–307.
[8] H.-G. Mack in *NATO ASI Series, Series C: Mathematical and Physical Sciences* (Eds.: J. Laane, M. Dakkouri, B. Veken, H. Oberhammer), Springer, Dordrecht, **1993**, p. 535.
[9] N. V. Belova, H. Oberhammer, X. Zeng, M. Gerken, H. Willner, R. J. F. Berger, S. A. Hayes, N. W. Mitzel, *Phys. Chem. Chem. Phys.* **2010**, *12*, 11445–11453.
[10] A. F. Holleman, E. Wiberg, N. Wiberg in *Anorganische Chemie*, De Gruyter, Berlin, **2017**, p. 2006.
[11] Y. Morgenstern, F. Zischka, A. Kornath, *Chem. Eur. J.* **2018**, *24*, 17311–17317.
[12] A. Kaiba, M. H. Geesi, P. Guionneau, T. A. Aljohani, L. Bih, H. Bih, S. Kassou, *J. Mol. Struct.* **2020**, *1204*, 127380.
[13] R. Minkwitz, S. Schneider, *Angew. Chem. Int. Ed.* **1999**, *38*, 210–212; *Angew. Chem.* **1999**, *111*, 229–231.
[14] M. Schickinger, C. Jessen, Y. Morgenstern, K. Muggli, F. Zischka, A. Kornath, *Eur. J. Org. Chem.* **2018**, *2018*, 6223–6229.
[15] M. Schickinger, T. Saal, F. Zischka, J. Axhausen, K. Stierstorfer, Y. Morgenstern, A. J. Kornath, *ChemistrySelect* **2018**, *3*, 12396–12404.
[16] M. Schickinger, F. Zischka, K. Stierstorfer, A. Kornath, *Eur. J. Org. Chem.* **2019**, *2019*, 1876–1882.
[17] R. Minkwitz, F. Neikes, U. Lohmann, *Eur. J. Inorg. Chem.* **2002**, *2002*, 27–30.
[18] R. Labbow, D. Michalik, F. Reiß, A. Schulz, A. Villinger, *Angew. Chem. Int. Ed.* **2016**, *55*, 7680–7684; *Angew. Chem.* **2016**, *128*, 7811–7815.
[19] K. Hanai, Y. Maki, A. Kuwae, *BCSJ* **1985**, *58*, 1367–1375.
[20] M. C. Bayer, C. Jessen, A. J. Kornath, *Z. Anorg. Allg. Chem.* **2020**, *646*, 1688–1695.
[21] J. A. Ramsey, J. A. Ladd, *J. Chem. Soc. B* **1968**, 118.
[22] J. Weidlein, K. Dehnicke, U. Müller, *Schwingungsspektroskopie. Eine Einführung*, Thieme, Stuttgart, **1988**.
[23] M. T. S. Rosado, M. L. R. Duarte, R. Fausto, *J. Mol. Struct.* **1997**, *410–411*, 343–348.
[24] M. J. Frisch, G. W. Trucks, H. B. Schlegel, G. E. Scuseria, M. A. Robb, J. R. Cheeseman, G. Scalmani, V. Barone, B. Mennucci, G. A. Petersson, H.

Nakatsuji, M. Caricato, X. Li, H. P. Hratchian, A. F. Izmaylov, J. Bloino, G. Zheng, J. L. Sonnenberg, M. Hada, M. Ehara, K. Toyota, R. Fukuda, J. Hasegawa, M. Ishida, T. Nakajima, Y. Honda, O. Kitao, H. Nakai, T. Vreven, J. A. Montgomery, Jr., J. E. Peralta, F. Ogliaro, M. Bearpark, J. J. Heyd, E. Brothers, K. N. Kudin, V. N. Staroverov, R. Kobayashi, J. Normand, K. Raghavachari, A. Rendell, J. C. Burant, S. S. Iyengar, J. Tomasi, M. Cossi, N. Rega, J. M. Millam, M. Klene, J. E. Knox, J. B. Cross, V. Bakken, C. Adamo, J. Jaramillo, R. Gomperts, R. E. Stratmann, O. Yazyev, A. J. Austin, R. Cammi, C. Pomelli, J. W. Ochterski, R. L. Martin, K. Morokuma, V. G. Zakrzewski, G. A. Voth, P. Salvador, J. J. Dannenberg, S. Dapprich, A. D. Daniels, Ö. Farkas, J. B. Foresman, J. V. Ortiz, J. Cioslowski, D. J. Fox, *Gaussian 09, Revision A.02*, Gaussian Inc., Wallingford CT, **2009**.

[25] *CrysAlisPro Software System*, Rigaku Corpoation, Oxford, UK, **2015**.

[26] G. M. Sheldrick, *Acta Crystallogr. Sect. A Found. Adv.* **2015**, *71*, 3–8.

[27] G. M. Sheldrick, *Acta Crystallogr. Sect. C Struct. Chem.* **2015**, *71*, 3–8.

[28] L. J. Farrugia, *J. Appl. Crystallogr.* **1999**, *32*, 837–838.

[29] A. L. Spek, *J. Appl. Crystallogr.* **2003**, *36*, 7–13.

[30] SCALE3 ABSPACK – An Oxford Diffraction Program, Oxford Diffraction Ltd., UK, **2005**.

Manuscript received: November 12, 2021
Accepted manuscript online: December 16, 2021
Version of record online: January 5, 2022

Chemistry–A European Journal

Supporting Information

Ring Opening Reactions of β-Propiolactam in Superacidic Media

Stefanie Beck, Vanessa Rück, Lea-Viktoria Pietsch, Christoph Jessen, and Andreas J. Kornath*

Table of Contents

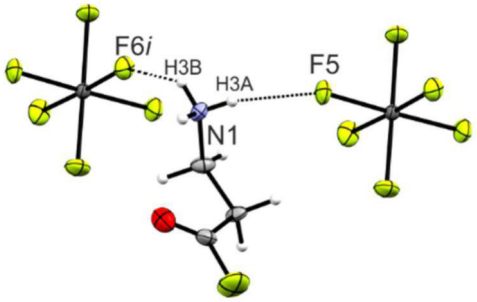

Figure S1. Projection of interatomic contacts in the $[C(O)F(CH_2)_2NH_3][SbF_6]$ (**1**) crystal (50% probability displacement ellipsoids).Symmetry code: *i* = x, −1+y, z.

Table S1. Selected bond lengths [Å] and angles [°] of $[C(O)F(CH_2)_2NH_3][SbF_6]$ (**1**) with estimated standard deviations in parentheses. Symmetry code: *i* = x, −1+y, z.

Bond lengths [Å]			
N1–C3	1.484(4)	C1–F1	1.340(6)
C3–C2	1.508(6)	C1–O1	1.176(6)
C2–C1	1.480(6)		
Bond angles [°]			
N1–C3–C2	112.6(3)	C2–C1–O1	128.8(4)
C1–C2–C3	112.8(3)	O1–C1–F1	119.4(4)
C2–C1–F1	111.9(3)		
Dihedral angles [°]			
N1–C3–C2–C1	66.2(4)	C3–C2–C1–O1	−6.4(6)
C3–C2–C1–F1	173.9(3)		
Interatomic contacts [Å]			
N1–H3A···F5	2.877(4)	N1–H3B···F6*i*	2.894(5)

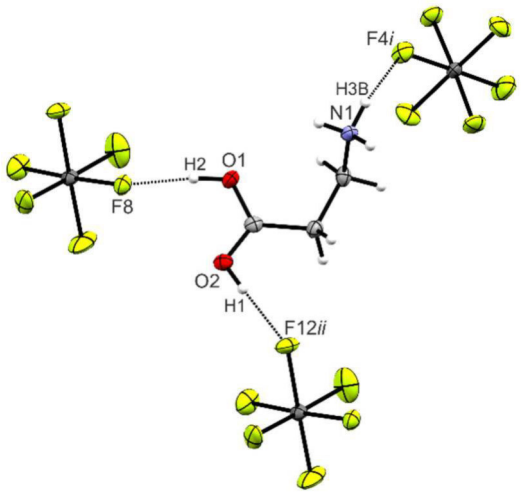

Figure S2. Projection of interatomic contacts in the $[C(OH)_2(CH_2)_2NH_3][AsF_6]_2$ (**3**) crystal (50% probability displacement ellipsoids). Symmetry codes: *i* = ½-x, −½+y, ½−z; *ii* = −1+x, y, z.

Table S2. Selected bond lengths [Å] and angles [°] of $[C(OH)_2(CH_2)_2NH_3][AsF_6]_2$ (**3**) with estimated standard deviations in parentheses. Symmetry codes: *i* = ½−x, −½+y, ½−z; *ii* = −1+x, y, z.

Bond lengths [Å]			
N1–C3	1.498(4)	C1–O1	1.270(3)
C2–C3	1.518(3)	C1–O2	1.264(3)
C1–C2	1.481(3)		
Bond angles [°]			
N1–C3–C2	112.3(2)	O1–C1–O2	118.4(2)
C3–C2–C1	114.9(2)	O2–C1–C2	117.7(2)
C2–C1–O1	123.9(2)		
Dihedral angles [°]			
O1–C1–C2–C3	−174.7(2)	C1–C2–C3–N1	76.7(3)
O2–C1–C2–C3	4.9(3)		
Interatomic contacts [Å]			
N1–H3B···F4*i*	2.865(3)	O2–H2···F8	2.602(2)
O1–H1···F12*ii*	2.616(2)		

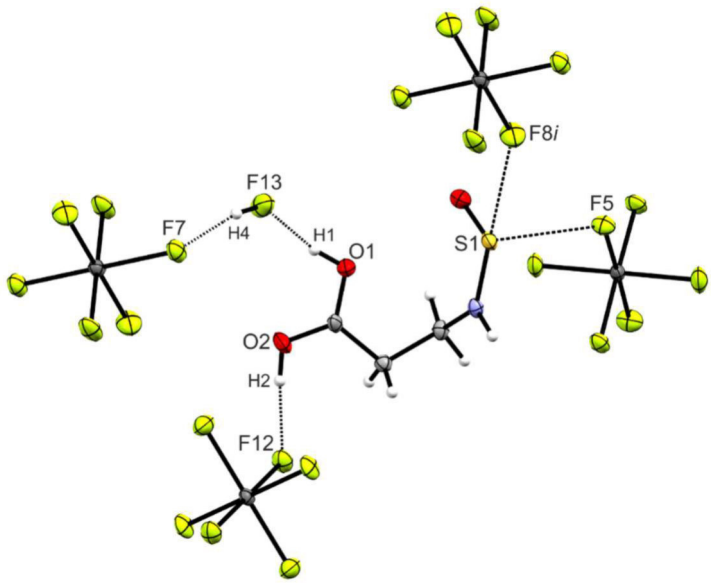

Figure S3. Projection of interatomic contacts in the $[C(OH)_2(CH_2)_2NHSO][SbF_6]_2 \cdot HF$ (**4**) crystal (50% probability displacement ellipsoids). Symmetry code: *i* = 1−x,1−y, 2−z.

Table S3. Selected bond lengths [Å] and angles [°] of $[C(OH)_2(CH_2)_2NHSO][SbF_6]_2 \cdot HF$ (**4**) with estimated standard deviations in parentheses. Symmetry codes: *i* = 1−x,1−y, 2−z.

Bond lengths [Å]			
N1–C3	1.488(7)	C1–O1	1.268(6)
C2–C3	1.513(6)	C1–O2	1.270(6)
C1–C2	1.489(8)	N1–S1	1.563(4)
S1–O3	1.431(4)		
Bond angles [°]			
N1–C3–C2	112.4(4)	O1–C1–O2	117.7(5)
C3–C2–C1	114.2(4)	O2–C1–C2	122.9(5)
C2–C1–O1	128.8(4)	C3–N1–S1	127.8(4)
N1–S1–O3	111.4(2)		
Dihedral angles [°]			
O1–C1–C2–C3	−5.6(7)	C1–C2–C3–N1	71.0(6)
O2–C1–C2–C3	175.2(5)	C2–C3–N1–S1	−115.7(5)
C3–N1–S1–O3	3.1(5)		
Interatomic contacts [Å]			
O2–H1···F12	2.626(4)	O1–H1···F13	2.544(6)
S1···F5	2.811(3)	S1···F8*i*	2.776(4)

Table S4. Experimental vibrational frequencies [cm^{-1}] of (**1**) and (**2**) and calculated vibrational frequencies [cm^{-1}] of $[C(O)F(CH_2)_2NH_3]^+ \cdot HF$.

$[C(O)F(CH_2)_2NH_3][SbF_6]$ (1)		**$[C(O)F(CH_2)_2NH_3][AsF_6]$ (2)**		**$[C(O)F(CH_2)_2NH_3]^+ \cdot HF$**	**Assignment**
IR	**Raman**	**IR**	**Raman**	**Calc.[a] (IR/Raman)**	
3283 (w)	3290 (8)	3303 (w, sh)	3302 (3)	3482 (122/56)	$\nu_{as}(NH_3)$
3244 (w)	3244 (15)	3238 (m)	3247 (9)	3355 (381/71)	$\nu_{as}(NH_3)$
3186 (vw)		3158 (w, sh)	3166 (4)	3242 (203/54)	$\nu_{s}(NH_3)$
3057 (vw)	3057 (26)	3066 (vw)	3067 (10)	3150 (0.6/45)	$\nu_{as}(CH_2)$
	3008 (26)		3028 (14)	3102 (3/91)	$\nu_{as}(CH_2)$
2976 (vw)	2976 (34)	2974 (vw)	2975 (16)	3093 (3/64)	$\nu_{s}(CH_2)$
2953 (vw)	2953 (61)	2951 (vw)	2951 (33)	3046 (3/111)	$\nu_{s}(CH_2)$
	2814 (8)		2795 (4)		?
			2757 (4)		?
	2704 (9)		2701 (3)		?
1812 (w)	1822 (28)	1814 (vw)	1826 (17)	1842 (228/13)	ν(CO)
1603 (w)	1601 (14)	1605 (vw)	1600 (10)	1687 (31/2)	$\delta_{as}(NH_3)$
1587 (w)	1584 (14)	1591 (vw)	1595 (11)	1656 (23/6)	$\delta_{as}(NH_3)$
1493 (w)		1483 (w)	1492 (6)	1509 (122/3)	$\delta_{s}(NH_3)$
	1475 (13)		1476 (12)	1505 (49/4)	$\delta(CH_2)$
1464 (vw)	1466 (20)			1451 (35/7)	$\delta(CH_2)$
1396 (w)	1406 (27)	1402 (vw)	1407 (17)	1427 (3/0.9)	$\omega(CH_2)$
1383 (w)	1385 (10)	1381 (vw)	1386 (5)	1409 (69/0.4)	$\omega(CH_2)$
1327 (w)	1328 (20)	1329 (vw)	1329 (11)	1354 (40/3)	τ(CH2)
1259 (w)	1258 (21)	1256 (vw)	1256 (13)	1284 (15/3)	$\tau(CH_2)$
			1204 (3)		?
1165 (w)	1157 (13)	1155 (w)	1157 (7)	1208 (174/2)	ν(CF)
1134 (w)	1135 (9)	1126 (vw)	1126 (4)	1145 (10/0.4)	$\rho(NH_3)$
1094 (w)	1091 (10)	1084 (w)	1084 (4)	1108 (94/0.7)	$\rho(NH_3)$
1045 (w)	1050 (21)	1041 (vw)	1043 (12)	1024 (9/2)	ν(CC)
943 (vw)	941 (11)	932 (vw)	938 (7)	959 (4/0.5)	$\rho(CH_2)$
912 (vw)	913 (13)	908 (w)	910 (7)	917 (37/1)	ν(CC)
854 (vw)	857 (33)	854 (w)	856 (23)	843 (2/8)	ν(CN)
806 (w)	812 (30)	806 (w)	810 (26)	819 (23/5)	$\rho(CH_2)$
				671 (13/1)	δ(CCO)
582 (s)	575 (24)	576 (s)	577 (16)	561 (7/1)	γ(COFC)
484 (m)	484 (29)	492 (s)	494 (14)	477 (4/2)	δ(CCF)
				353 (13/0.1)	$\tau(NH_3)$

				348 (19/0.9)	δ(CCN)
				262 (37/0.3)	δ(CCC)
				210 (39/0.3)	$\delta(CCN)_{oop}$
				80 (0.4/0.1)	Skeletal vibration
693 (m)	679 (16)	702 (vs)	706 (8)		MF_6^-
659 (vs)	664 (27)	683 (vs, sh)	686 (100)		MF_6^-
646 (vs)	655 (100)	636 (s)	636 (7)		MF_6^-
559 (s)	649 (88)	550 (s)	551 (8)		MF_6^-
550 (s)	565 (27)		373 (44)		MF_6^-
	555 (15)		360 (12)		MF_6^-
	365 (24)		117 (15)		MF_6^-
	305 (21)				MF_6^-
	289 (26)				MF_6^-
	281 (67)				MF_6^-
	146 (22)				MF_6^-

[a] Calculated on the B3LYP/aug-cc-pVTZ level of theory. IR intensity in km/mol and Raman intensity in $Å^4/u$. Abbreviations for IR intensities: v = very, s = strong, m = medium, w = weak, br = broad. Experimental Raman activities are stated to a scale of 1 to 100. *M* = Sb, As.

Table S5. Experimental vibrational frequencies [cm^{-1}] of (**3**) and calculated vibrational frequencies [cm^{-1}] of $[C(OH)_2(CH_2)_2NH_3]^{2+}\cdot 3HF$.

$[C(OH)_2(CH_2)_2NH_3][AsF_6]_2$ (3)		$[C(OH)_2(CH_2)_2NH_3]^{2+}\cdot 3HF$	Assignment
IR	Raman	Calc.[a] (IR/Raman)	
3365 (m)	3268 (3)		?
3234 (vs)	3242 (6)	3467 (103/17)	$\nu_{as}(NH_3)$
	3198 (4)	3415 (86/48)	$\nu_{as}(NH_3)$
3159 (vs, sh)	3161 (3)	3206 (544/156)	$\nu_{s}(NH_3)$
3125 (s,sh)		3161 (1589/121)	ν(OH)
3054 (w, sh)	3053 (8)	3149 (5/33)	$\nu_{as}(CH_2)$
	3008 (10)	3099 (3/90)	$\nu_{s}(CH_2)$
2957 (vw)	2961 (11)	3070 (7/41)	$\nu_{as}(CH_2)$
		3050 (2141/122)	ν(OH)
2928 (vw)	2931 (14)	3021 (57/81)	$\nu_{s}(CH_2)$
	2801 (6)		?
	2701 (5)		?
1657 (m)	1656 (9)	1676 (19/4)	$\delta_{as}(NH_3)$
	1616 (9)	1664 (19/3)	$\delta_{as}(NH_3)$
1605 (w)		1653 (310/0.7)	ν(CO)
1589 (w)	1590 (11)	1568 (212/5)	ν(CO)
1506 (w)	1510 (8)	1552 (123/0.9)	$\delta_{s}(NH_3)$
1481 (m)	1476 (7)	1498 (12/4)	$\delta(CH_2)$
1466 (m)	1467 (16)	1440 (18/1)	$\omega(CH_2)$
1410 (w)	1408 (7)	1428 (27/5)	$\delta(CH_2)$
1366 (w)	1366 (24)	1397 (30/2)	$\omega(CH_2)$
1354 (w)	1357 (15)	1363 (27/3)	$\tau(CH_2)$
1312 (w)	1316 (8)	1329 (111/0.2)	δ(COH)
1292 (w)			?
1254 (vw)	1254 (11)	1292 (10/2)	$\tau(CH_2)$
1242 (vw)			?
1196 (w)	1214 (8)	1275 (214/5)	δ(COH)
1149 (vw)	1139 (8)	1151 (20/0.4)	$\rho(NH_3)$
1107 (w)	1113 (5)	1122 (27/0.3)	$\rho(NH_3)$
1043 (w)	1047 (14)	1032 (11/3)	ν(CC)
1022 (w)			?
974 (w)		962 (54/0.2)	$\delta(COH)_{oop}$
939 (w)	943 (11)	947 (17/0.6)	$\tau(CH_2)$
906 (w)	922 (10)	915 (2/3)	ν(CC)

		888 (128/0.2)	$\delta(COH)_{oop}$
856 (m)	858 (10)	841 (11/3)	ν(CN)
814 (s)	817 (26)	806 (13/9)	δ(OCO)
619 (s)	627 (8)	660 (4/0.7)	δ(OCC)
538 (m)	544 (8)	573 (11/2)	$\gamma(CCO_2)$
490 (s)	497 (13)	496 (16/2)	δ(OCC)
		361 (29/0.8)	δ(CCN)
		324 (19/0.3)	$\tau(NH_3)$
	257 (7)	287 (51/0.5)	δ(CCC)
	127 (13)	98 (8/0.8)	Skeletal vibrations
		52 (8/0.2)	Skeletal vibrations
723 (vs)	717 (41)		AsF_6^-
712 (vs)	683 (100)		AsF_6^-
967 (vs)	588 (18)		AsF_6^-
675 (vs)	576 (11)		AsF_6^-
580 (s)	423 (10)		AsF_6^-
563 (s)	371 (45)		AsF_6^-
424 (m)			AsF_6^-

[a] Calculated on the B3LYP/aug-cc-pVTZ level of theory. IR intensity in km/mol and Raman intensity in $Å^4/u$. Abbreviations for IR intensities: v = very, s = strong, m = medium, w = weak, br = broad. Experimental Raman activities are stated to a scale of 1 to 100.

Table S6. Selected NBOs (BD = 2-center bond; LP = 1-center valence lone pair; BD* = 2-center antibond) of *β*-propiolactam together with calculated values for occupancy and s- and p-character.[a]

Bond	Occupancy	Energy	s-, p- character
BD(1) C3-C2	1.97 e^-	−0.58681	C3 s (26.00%), p 2.84 (73.86%)
			C2 s (24.66%), p 3.05 (75.14%)
BD(1) C3-N1	1.99 e^-	−0.71947	C3 s (22.01%), p 3.54 (77.84%)
			N1 s (31.58%), p 2.16 (68.25%)
BD(1) C2-C1	1.98 e^-	−0.59149	C2 s (23.57%), p 3.24 (76.28%)
			C1 s (33.02%), p 2.02 (66.84%)
BD(1) C1-N1	1.99 e^-	−0.80129	C1 s (30.68%), p 2.25 (69.17%)
			N1 s (35.18%), p 1.84 (64.62%)
BD*(1) C1-N1	0.08 e^-	0.43573	C1 s (30.68%), p 2.25 (69.17%)
			N1 s (35.18%), p 1.84 (64.62%)
BD(1) C1-O1	2.00 e^-	−1.08942	C1 s (36.42%), p 1.74 (63.45%)
			O1 s (41.04%), p 1.42 (58.28%)
BD*(1) C1-O1	0.02 e^-	0.64457	C1 s (36.42%), p 1.74 (63.45%)
			O1 s (41.04%), p 1.42 (58.28%)
BD(2) C1-O1	2.00 e^-	−0.37404	C1 s (0.00%), p 1.00 (99.76%)
			O1 s (0.00%), p 1.00 (99.57%)
BD*(2) C1-O1	0.28 e^-	0.01880	C1 s (0.00%), p 1.00 (99.76%)
			O1 s (0.00%), p 1.00 (99.57%)
LP(1) N1	1.70 e^-	−0.26373	N1 s (0.00%), p 1.00 (99.94%)
LP(1) O1	1.98 e^-	−0.69300	O1 s (58.86%), p 0.70 (41.00%)
LP(2) O1	1.78 e^-	−0.25031	O1 s (0.01%), p 99.99 (99.65%)

[a] Calculated on the B3LYP/aug-cc-pVTZ level of theory.

Table S7. Selected NBOs (BD = 2-center bond; LP = 1-center valence lone pair; BD* = 2-center antibond) of the *N*-protonated species of *β*-propiolactam together with calculated values for occupancy and s- and p-character.[a]

Bond	Occupancy	Energy	s-, p-character
BD(1) C3-C2	1.98 e^-	−0.82163	C3 s (27.43%), p 2.64 (72.43%)
			C2 s (25.85%), p 2.86 (73.93%)
BD(1) C3-N1	1.99 e^-	−0.93087	C3 s (19.52%), p 4.12 (80.33%)
			N1 s (28.01%), p 2.56 (71.84%)
BD(1) C2-C1	1.98 e^-	−0.88147	C2 s (22.65%), p 3.41 (77.16%)
			C1 s (43.93%), p 1.27 (55.98%)
BD(1) C1-N1	1.99 e^-	−0.82358	C1 s (19.16%), p 4.21 (80.66%)
			N1 s (20.21%), p 3.94 (79.72%)
BD*(1) C1-N1	0.26 e^-	−0.12976	C1 s (19.16%), p 4.21 (80.66%)
			N1 s (20.21%), p 3.94 (79.72%)
BD(1) C1-O1	2.00 e^-	−1.43141	C1 s (37.26%), p 1.68 (62.62%)
			O1 s (45.05%), p 1.20 (54.19%)
BD*(1) C1-O1	0.02 e^-	0.47551	C1 s (37.26%), p 1.68 (62.62%)
			O1 s (45.05%), p 1.20 (54.19%)
BD(2) C1-O1	1.99 e^-	−0.64604	C1 s (0.00%), p 1.00 (99.77%)
			O1 s (0.00%), p 1.00 (99.43%)
BD*(2) C1-O1	0.07 e^-	−0.20634	C1 s (0.00%), p 1.00 (99.77%)
			O1 s (0.00%), p 1.00 (99.43%)
LP(1) O1	1.98 e^-	−0.93211	O1 s (54.73%), p 0.82 (45.07%)
LP(2) O1	1.70 e^-	−0.50655	O1 s (0.13%), p 99.99 (99.38%)

[a] Calculated on the B3LYP/aug-cc-pVTZ level of theory.

Table S8. Selected NBOs (BD = 2-center bond; LP = 1-center valence lone pair; BD* = 2-center antibond) of the *O*-protonated species of *β*-propiolactam together with calculated values for occupancy and s- and p-character.[a]

Bond	Occupancy	Energy	s-, p-character
BD(1) C3-C2	1.97 e^-	−0.77803	C3 s (25.89%), p 2.86 (73.94%)
			C2 s (23.94%), p 3.17 (75.81%)
BD(1) C3-N1	1.98 e^-	−0.91098	C3 s (19.45%), p 4.13 (80.38%)
			N1 s (30.65%), p 2.26 (69.19%)
BD(1) C2-C1	1.97 e^-	−0.84572	C2 s (22.95%), p 3.35 (76.82%)
			C1 s (35.84%), p 1.79 (64.04%)
BD(1) C1-N1	2.00 e^-	−1.10674	C1 s (33.01%), p 2.03 (66.89%)
			N1 s (35.52%), p 1.81 (64.17%)
BD*(1)C1-N1	0.03 e^-	0.28658	C1 s (33.01%), p 2.03 (66.89%)
			N1 s (35.52%), p 1.81 (64.17%)
BD(2) C1-N1	1.97 e^-	−0.59417	C1 s (0.00%), p 1.00 (99.65%)
			N1 s (0.00%), p 1.00 (99.82%)
BD*(2) C1-N1	0.31 e^-	−0.25520	C1 s (0.00%), p 1.00 (99.65%)
			N1 s (0.00%), p 1.00 (99.82%)
BD(1) C1-O1	2.00 e^-	−1.25812	C1 s (31.23%), p 2.20 (68.63%)
			O1 s (36.36%), p 1.74 (63.19%)
BD*(1) C1-O1	0.04 e^-	0.20163	C1 s (31.23%), p 2.20 (68.63%)
			O1 s (36.36%), p 1.74 (63.19%)
LP(1) O1	1.96 e^-	−0.83045	O1 s (41.54%), p 1.40 (58.25%)
LP(2) O1	1.76 e^-	−0.56886	O1 s (0.00%), p 1.00 (99.62%)

[a] Calculated on the B3LYP/aug-cc-pVTZ level of theory.

Table S9. Comparison of selected NBOs together with electron occupancies (occ.) and s- and p-character of *β*-propiolactam, the *N*-protonated species and the *O*-protonated species of *β*-propiolactam.[a]

Bond	*β*-propiolactam		*N*-protonated species of *β*-propiolactam		*O*-protonated species of *β*-propiolactam	
	Occ.	s- and p-character	Occ.	s- and p-character	Occ.	s- and p-character
C1–O1 (σ)	2.00	C1 s (36.42%), p 1.74 (63.45%)	2.00	C1 s (37.26%), p 1.68 (62.62%)	2.00	C1 s (31.23%), p 2.20 (68.63%)
		O1 s (41.04%), p 1.42 (58.28%)		O1 s (45.05%), p 1.20 (54.19%)		O1 s (36.36%), p 1.74 (63.19%)
C1–O1 (σ*)	0.02	C1 s (36.42%), p 1.74 (63.45%)	0.02	C1 s (37.26%), p 1.68 (62.62%)	0.04	C1 s (31.23%), p 2.20 (68.63%)
		O1 s (41.04%), p 1.42 (58.28%)		O1 s (45.05%), p 1.20 (54.19%)		O1 s (36.36%), p 1.74 (63.19%)
C1–O1 (π)	2.00	C1 s (0.00%), p 1.00 (99.76%)	1.99	C1 s (0.00%), p 1.00 (99.77%)		
		O1 s (0.00%), p 1.00 (99.57%)		O1 s (0.00%), p 1.00 (99.43%)		
C1–O1 (π*)	0.28	C1 s (0.00%), p 1.00 (99.76%)	0.07	C1 s (0.00%), p 1.00 (99.77%)		
		O1 s (0.00%), p 1.00 (99.57%)		O1 s (0.00%), p 1.00 (99.43%)		
C1–N1 (σ)	1.99	C1 s (30.68%), p 2.25 (69.17%)	1.99	C1 s (19.16%), p 4.21 (80.66%)	2.00	C1 s (33.01%), p 2.03 (66.89%)
		N1 s (35.18%), p 1.84 (64.62%)		N1 s (20.21%), p 3.94 (79.72%)		N1 s (35.52%), p 1.81 (64.17%)
C1–N1 (σ*)	0.08	C1 s (30.68%), p 2.25 (69.17%)	0.26	C1 s (19.16%), p 4.21 (80.66%)	0.03	C1 s (33.01%), p 2.03 (66.89%)
		N1 s (35.18%), p 1.84 (64.62%)		N1 s (20.21%), p 3.94 (79.72%)		N1 s (35.52%), p 1.81 (64.17%)
C1–N1 (π)					1.97	C1 s (0.00%), p 1.00 (99.65%)
						N1 s (0.00%), p 1.00 (99.82%)
C1–N1 (π*)					0.31	C1 s (0.00%), p 1.00 (99.65%)
						N1 s (0.00%), p 1.00 (99.82%)

[a]Calculated on the B3LYP/aug-cc-pVTZ level of theory.

Table S10. Crystal data and structure refinement for $[C(O)F(CH_2)_2NH_3][SbF_6]$ (**1**), $[C(OH)_2(CH_2)_2NH_3][AsF_6]_2$ (**3**) and $[C(OH)_2(CH_2)_2NHSO][SbF_6]_2 \cdot HF$ (**4**).

	$[C(O)F(CH_2)_2NH_3][SbF_6]$ (**1**)	$[C(OH)_2(CH_2)_2NH_3][AsF_6]_2$ (**3**)	$[C(OH)_2(CH_2)_2NHSO][SbF_6]_2 \cdot HF$ (**4**)
Empirical formula	C3 H7 F7 N O Sb	C3 H9 F12 N O2 As2	C3 H8 F13 N O3 S Sb2
M_r	327.85	468.95	628.66
Crystal system	triclinic	monoclinic	triclinic
Space group	$P\bar{1}$	$P2_1/n$	$P\bar{1}$
a [Å]	5.4383(4)	8.1022(2)	7.8845(8)
b [Å]	7.4689(6)	11.6917(4)	8.6948(9)
c [Å]	10.7243(13)	12.7565(5)	12.0433(7)
α [°]	100.215(9)	90	83.250(7)
β [°]	103.362(9)	92.465(3)	73.866(8)
γ [°]	90.033(7)	90	69.580(9)
V [Å^3]	416.70(7)	1207.29(7)	743.07(13)
Z	2	4	2
ρ_{calcd} [gcm^{-3}]	2.613	2.580	2.810
μ[mm^{-1}]	3.394	5.693	3.929
$\lambda_{Moκα}$	0.71073	0.71073	0.71073
F(000)	308	896	584
T[K]	160(2)	126(2)	116(2)
hkl range	–7:6; –9:9;–12:14	–9:11; –16:16;–18:16	−9:10; −11:11;−16:15
refl. measured	3716	12429	6425
refl. unique	2063	3684	3686
R_{int}	0.0336	0.0379	0.0428
parameters	130	199	240
R(F)/*w*R(F^2)[a)]	0.0332/ 0.0634	0.0426/ 0.0703	0.0462/0.0879
weighting scheme[b)]	0.0245	0.0293	0.0303
S(GoF)[c)]	1.032	1.041	1.047
residual density [eÅ^{-3}]	0.857/ −0.848	0.806/ –0.677	1.950/ −1.308
device type	Oxford XCalibur	Oxford XCalibur	Oxford XCalibur
solution/refinement	SHELXT	SHELXT	SHELXT
CCDC	2062961	2062962	2062963

a) $R_1 = \Sigma||F_o|-|F_c||/\Sigma|F_o|$; b) $wR_2 = [\Sigma[w(F_o^2-F_c^2)^2]/\Sigma[w(F_o)^2]]^{1/2}$; $w = [\sigma_c^2(F_o^2)+(xP)^2+yP]^{-1}$; $P = (F_o^2+2F_c^2)/3$ c) GoF = $\{\Sigma[w(F_o^2-F_c^2)^2]/(n-p)\}^{1/2}$ (*n* = number of reflexions; *p* = total number of parameters).

Table S11. Cartesian coordinates of calculated minimum structure of $[C(O)F(CH_2)_2NH_3]^+ \cdot HF$ at the B3LYP/aug-cc-pVTZ level of theory.

Atom	x	y	z
F	4.603415	1.424747	4.811568
O	5.102853	0.394984	6.687191
N	3.106168	-0.074080	8.484731
C	2.385879	-0.321565	7.177724
H	1.318152	-0.287769	7.374816
H	2.656037	-1.327666	6.865649
C	2.780524	0.705409	6.121039
H	2.310227	0.441803	5.173530
H	2.415365	1.706041	6.369740
C	4.271656	0.797185	5.930506
H	2.808161	0.807548	8.919090
H	2.942973	-0.830739	9.148538
H	4.115599	-0.015276	8.270154
F	2.042938	2.481602	9.178240
H	1.905854	3.182375	9.775085

Table S12. Cartesian coordinates of calculated minimum structure of $[C(OH)_2(CH_2)_2NH_3]^{2+} \cdot 3HF$ at the B3LYP/aug-cc-pVTZ level of theory.

Atom	x	y	z
O	1.484897	5.474129	4.855161
O	3.000457	4.017730	5.466283
N	2.016381	1.405456	6.721071
C	1.288623	1.773755	5.447332
H	0.448802	1.087901	5.367172
H	1.973277	1.565340	4.628788
C	1.778577	4.296413	5.218152
C	0.760550	3.208926	5.399267
H	0.051557	3.274591	4.569861
H	0.173017	3.464182	6.289507
H	0.523761	5.666139	4.650520
H	3.645717	4.782190	5.336524
H	2.863632	1.961860	6.854449
H	1.429488	1.516010	7.551769
H	2.299261	0.408772	6.675438
F	-1.010999	5.869421	4.342791
H	-1.471643	6.626226	4.040522
F	4.568103	6.042419	5.205280
H	5.475217	6.203312	5.047001
F	2.581653	-1.225070	6.145449
H	2.848845	-2.093173	6.360860

Table S13. Cartesian coordinates of calculated minimum structure of the transition state and concurrently starting point for IRC calculations at the MP2/aug-cc-pVTZ level of theory.

Atom	x	y	z
C	-0.700793	1.069375	-0.156676
C	-1.299493	-0.303755	0.332876
H	-1.093296	1.315808	-1.141393
H	-0.675249	1.930613	0.502090
H	-1.355470	-0.411146	1.410180
N	-0.052788	-1.054960	-0.198715
H	1.233521	-1.039531	0.353584
C	0.532974	0.251275	-0.211879
O	1.668355	0.191597	0.272686
H	-2.200209	-0.621683	-0.178213
H	-0.202634	-1.538784	-1.085637

Table S14. Cartesian coordinates of calculated minimum structure of endpoint of IRC calculation (*O*-protonation) on MP2/aug-cc-pVTZ level of theory.

Atom	x	y	z
C	0.549342	1.070483	0.000089
C	1.514323	-0.150697	-0.000098
H	0.567269	1.688305	0.894278
H	0.567197	1.688667	-0.893842
H	2.102227	-0.286047	-0.901350
N	0.284797	-0.996837	0.000008
H	-2.283922	-0.693155	0.000003
C	-0.521115	0.032779	0.000015
O	-1.803382	0.153561	0.000022
H	2.102477	-0.286146	0.900974
H	0.127230	-1.999155	0.000033

Table S15. Cartesian coordinates of calculated minimum structure of endpoint of IRC calculation (*N*-protonation) on MP2/aug-cc-pVTZ level of theory.

Atom	x	y	z
C	-0.709294	0.996584	0.018536
C	-1.484711	-0.330860	0.077228
H	-0.883785	1.618029	-0.859315
H	-0.759210	1.622485	0.909110
H	-2.008566	-0.517729	1.007554
N	-0.230310	-1.173454	-0.006555
H	-0.021944	-1.744909	0.814004
C	0.604948	0.270831	-0.071491
O	1.758972	0.392680	-0.153904
H	-2.131501	-0.524372	-0.770761
H	-0.137535	-1.752049	-0.843167

Table S16. Cartesian coordinates of calculated minimum structure of *β*-propiolactam on the B3LYP/aug-cc-pVTZ level of theory.

Atom	x	y	z
C	-0.656253	-0.845432	0.000427
C	0.894473	-0.768356	0.000038
H	-1.098157	-1.291023	-0.890421
H	-1.096967	-1.287204	0.893870
H	1.385374	-1.154041	-0.890139
H	1.385086	-1.153129	0.890788
C	0.706632	0.765037	-0.000714
N	-0.657427	0.622852	-0.002377
H	-1.399099	1.305676	0.000673
O	1.428260	1.726693	-0.000054

Table S17. Cartesian coordinates of calculated minimum structure of the *N*-protonated species of *β*-propiolactam on the B3LYP/aug-cc-pVTZ level of theory.

Atom	x	y	z
C	0.344468	1.144977	-0.000093
C	1.446234	0.066240	0.000035
H	0.292441	1.783374	0.882969
H	0.292253	1.783723	-0.882872
H	2.065343	0.034417	-0.889476
N	0.444484	-1.078323	-0.000032
H	0.447384	-1.673981	-0.828378
C	-0.739445	0.104531	0.000019
O	-1.878624	-0.079239	0.000048
H	2.064851	0.034665	0.889907
H	0.447798	-1.674517	0.827933

Table S18. Cartesian coordinates of calculated minimum structure of the *O*-protonated species of *β*-propiolactam on the B3LYP/aug-cc-pVTZ level of theory.

Atom	**x**	**y**	**z**
C	1.518485	-0.153337	0.000295
C	0.549257	1.070691	-0.000098
H	2.111846	-0.288340	-0.898342
H	2.111017	-0.288224	0.899416
H	0.567204	1.694345	-0.891356
H	0.567091	1.694772	0.891027
C	-0.523415	0.030312	-0.000247
O	-1.803928	0.145416	0.000032
N	0.283116	-0.996307	-0.000286
H	0.128080	-1.997811	-0.000145
H	-2.301585	-0.689921	0.001445